ABSTRACT

Title of thesis: AN ANALYSIS OF HEAT FLUX-INDUCED ARC FORMATION IN RESIDENTIAL ELECTRICAL CABLES

Cameron James Novak, Master of Science, 2011

Thesis directed by: Professor Stanislav I. Stoliarov
Professor James G. Quintiere
Department of Fire Protection Engineering

The mechanisms by which fire environments may trigger electrical arcs in household wiring are often misunderstood. A thorough knowledge of these mechanisms may assist fire investigators to determine whether a given arcing event was the cause or result of a fire. In this study, both unenergized and energized cables were tested under a variety of conditions to observe the behavior and breakdown of cable insulation. This research may have applications for the fire protection community and, in particular, the field of fire investigation. The data collected during testing indicates that electrical cables must be exposed to minimum heating conditions before a fault will occur, aiding in the analysis of the electrical system and tracing the progression of a fire.

AN ANALYSIS OF HEAT FLUX-INDUCED ARC FORMATION IN RESIDENTIAL ELECTRICAL CABLES

by

Cameron James Novak

Thesis submitted to the Faculty of the Graduate School of the
University of Maryland, College Park in partial fulfillment
of the requirements for the degree of
Master of Science
2011

Committee:

Professor Stanislav Stoliarov, Chair
Professor Christopher Davis
Professor James Quintiere
Dr. David Sheppard

Acknowledgements

I wish to thank the many individuals who have assisted, encouraged, and believed in me throughout this research project. Without all of you, this project would not have come to fruition. I would first like to thank my committee: Dr. Christopher Davis, Dr. James Quintiere, and Dr. Stanislav Stoliarov of the University of Maryland; and Dr. David Sheppard of the ATF Fire Research Laboratory for your personal time commitment and efforts to see this project through to the end.

University of Maryland – Department of Fire Protection Engineering

I would like to thank Dr. Stoliarov and Dr. Quintiere, for without your continued guidance, wisdom and support this project would not have materialized.

Bureau of Alcohol, Tobacco and Firearms (ATF)

I would like to thank the ATF for granting me access to their Fire Research Laboratory and its equipment. More specifically, I would like to acknowledge and thank Mr. John Allen, Mr. Brian Grove, and Mr. Jason Ouellette, whose backing was instrumental in the implementation and progression of this endeavor. A special thanks to Mrs. Leanora Bender, Mr. Jamie Lord, Mr. Jeremy Neagle, and Mr. Michael Keller. Their time, expertise, and much-needed assistance were a major factor in the development and success of the research.

I would like to extend a special thank you to Michael Keller for taking this project, and ultimately me, under his care and supervision. You have been a great inspiration and mentor, and now too, I call you a friend.

Experts in the Field

Many thanks go to the experts that I consulted with before and over the course of this project for advice and ideas. I hope you benefit from this project as much as I have.

Family and Friends

Many thanks go to my friends and family who have provided tremendous support over the course of the project. Without them I may not have had the willpower to keep at it.

To Mom and Dad – Thank you for your help and encouragement over the years. You've raised me to take responsibility for my life and to work hard for the things I desire. It has finally paid off. I'm proud to be your son, and I hope I've made you proud as well. I love you both.

To Mandy Boo – thank you for your patience and support while I continued my academic journey. Although it hasn't been easy, knowing I had your support gave me the strength to see this project through to the end. I love you.

Table of Contents

List of Figures

List of Tables

1. Introduction

1.1 Electrical Fires

Electrical fires are often the result of several factors coming together to cause the failure of one or several components. Most investigations are initially conducted by fire department personnel who may not have the time or resources to fully investigate all fires and may lack a working knowledge of electricity. This may lead to false origin and cause determinations. The National Fire Incident Reporting System (NFIRS) lists the causes of electrical ignition as follows [1]:

- Cords/Plugs
- Lamps/Lighting
- Power Transfer
- Electrical Wiring
- Electrical Distribution/ Power Transfer
- Heating Related
- Other Equipment

Electrical wiring was cited as the cause for 46.8% of all electrical fires from 2003 to 2005. One issue with this determination is that fixed wiring is a robust component when compared to the many connections in the system [2]. Although possible, it is unlikely to find a fire that originates in the middle of a wire in a circuit.

Researchers in Japan have conducted several studies related to electricity and fire, but few have been translated into English. Electrical fires and the degradation of

polyvinylchloride (PVC) insulation have been the focus of some scrutiny in the United States, however none of these studies discuss the process of arcing through char in detail [3], [4], [5], [6], [7], [8].

1.1.1 Causes of Electrical Fires

While electrical fires can be caused by a variety of things, the majority of these causes can be grouped into a few basic categories. The most basic and common forms of electrical ignition can be classified as:

- Resistive heating
- Overloads
- Arcs/Sparks
- Faults

1.1.1.1 Resistive Heating

Resistive heating is best described as localized heating to the point where nearby combustible materials ignite. Resistive heating most often occurs at electrical connections, either the result of a poor connection or the formation of oxides on the metals. These connections can become so hot that they begin to glow (Figure 1). Common examples of resistive heating are screw or push-in wire connections on household outlets and crimp connections for electronics [9], [10], [11], [12], [13].

Figure 1 - Glowing electrical connection on a residential receptacle [Photo courtesy of James Novak – used with permission].

1.1.1.2 Faults

Faults occur when current flows outside of the intended circuit. This can result in failure of the circuit and potentially lead to ignition. A bolted fault (also called a short-circuit or short) occurs when there is little resistance at the fault location. A ground fault occurs when a conductor or an energized portion of the circuit makes contact with a grounded object, allowing current to flow to earth.

During a fault, the short-circuit current is the maximum available current at the "worst" conditions possible. These conditions produce the highest short-circuit current and usually include the voltage difference and the impedance of the entire system at the fault location [14].

1.1.1.3 Overloads

There are two types of overloads in electrical systems: current overloads and voltage overloads. A current overload is characterized by a current flow that exceeds that which the system was designed for. This excessive current flow can be caused by faults in the system, bypassing circuit protection devices, or using too many appliances on one branch circuit. A current overload generates heat along the entire length of the conductor due to the inherent resistance of the wire. This heat causes the insulation of the conductors to melt and fail, potentially leading to a fault. In order for a fire to start from a current overload, a sustained current of 3-7 times the rated current is required [15]. Installing a circuit protection device rated higher than what the circuit is capable of handling may allow an overload to continue undetected; however this does not cause the overload itself. Figure 2 illustrates the effects of a current overload on an electrical cable.

Figure 2 - Insulation failure due to current overload.

A voltage overload occurs when excessive voltage is applied to the system, such as a lightning strike or voltage surge. A voltage overload may also be caused by an open or floating neutral. An open neutral is created when the neutral conductor in a system is disconnected, resulting in the system's reference to ground being lost. The loss of the neutral allows voltages in the system to vary from nearly zero to twice the line-to-neutral voltage (depending on the load at the time). In the United States, this maximum voltage can be as high as 240 volts in residential circuits. As circuit breakers only detect excessive currents, a voltage overload can go unnoticed until a fire or electrical failure occurs. A surge protection device may be used to limit the damage caused by a voltage overload.

1.1.1.4 Arcs/Sparks

Electric arcs and electric sparks are electric discharges across a gap or through a semi-conductive medium between two conductors [16]. An arc is a sustained event while sparks are generally short-lived. NFPA 921: Guide for Fire and Explosion Investigations [17] classifies sparks as solid particles that emit heat and light, while Babrauskas has deemed these mechanical sparks [16]. Mechanical sparks are created by processes such as welding and grinding. Molten metal may be ejected when a make-and-break arc is created as two conductors come into contact and separate. It is possible that these arcs and sparks can ignite nearby combustibles if enough energy is released. While arcs are created easily by conductor contact, they do not spontaneously occur at normal household voltages. It is has been found that in order for an arc to spontaneously occur across a one-inch air gap, a voltage potential of 76.2kV (or 30kV for a gap of one centimeter) must exist [18]. Therefore it is unlikely that an arc will spontaneously establish itself across an

air gap under normal residential voltages and conditions. Figure 3 shows an arc produced on an electrical cable as it experienced thermal degradation.

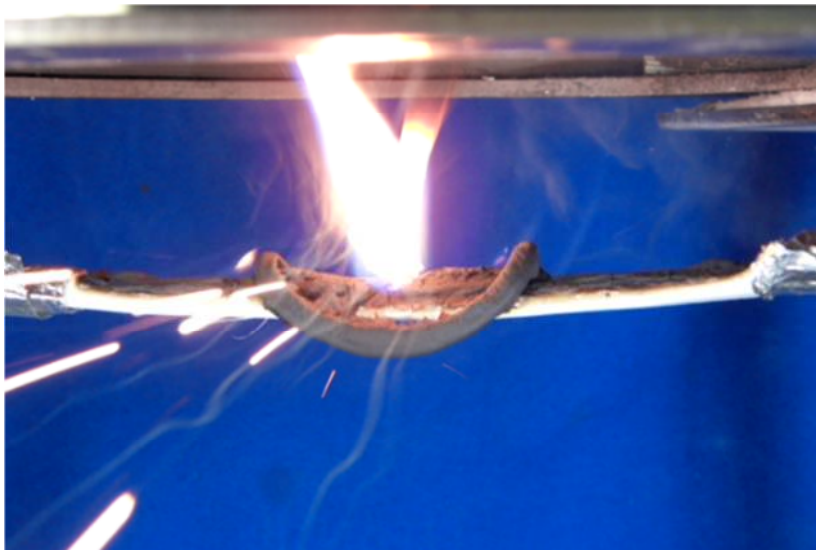

Figure 3 - Arcing from a 120 VAC Circuit.

Another form of ignition related to arcing is arc (or carbon) tracking. This process occurs when contaminants form a conductive path across an insulating material, allowing the flow of current. The heating caused by this current leads to further charring or carbonization and consequently, more current to flow. Figure 4 illustrates how electricity flows through a block of wood after it has been wet with water. Two nails were driven into the wood and connected to a neon sign transformer with a voltage potential of 6kV. Arc tracking can occur on electrical cables as well. In many formulations of PVC insulation, calcium carbonate ($CaCO_3$) is used as a filler. Studies have shown that when cables are heated, the calcium carbonate attracts water, which can conduct electricity and cause arc tracking [19].

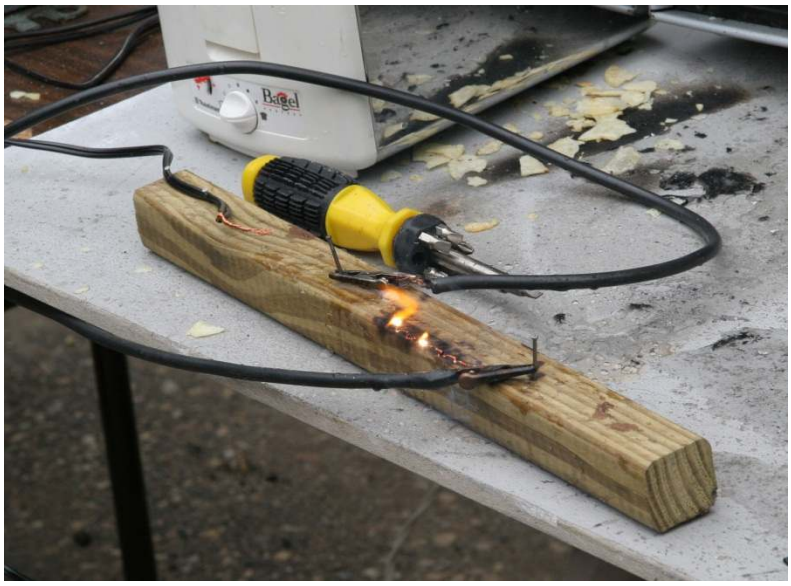

Figure 4 - Arc tracking on a block of wood [Photo Courtesy of James Novak – used with permission].

1.2 Breakdown of Electrical Insulation

The degradation of PVC, while a complicated process, occurs in a relatively predictable way. Its high chlorine content makes pure PVC inherently fire retardant. However, additives used to achieve the desired properties for cable insulation (fillers, plasticizers, etc.) counteract this effect, making the final product more flammable and thus, additional fire retardants must be added. Degradation may occur due to exposure to elevated temperatures, radiation, chemicals, biological substances and electric potential. Exposure to water may cause water-soluble flame-retardants to leach out of PVC, further increasing its flammability. PVC can breakdown over an extended period of time when exposed to sunlight or elevated temperatures (in excess of 100°F/38°C) [20].

Babrauskas has conducted extensive research on the properties of electrical wiring, insulation and the factors leading to their failure [2], [15], [16], [19], [21], [22], [23]. He notes that loss of the plasticizer occurs at moderate temperatures (100°C) with

detectable degradation around 120℃. The use of calcium carbonate as a filler can cause wet tracking (arc tracking due to moisture) to occur at temperatures around 110℃. In his submission to the SFPE Handbook [16], Babrauskas states that of the three ways an arc can be formed across a carbonized path (arc tracking, overheating, and fire impingement), extensive research has only been conducted on the process of arc tracking. The Ignition Handbook [19] is a comprehensive literature on fire and fire causes, including research from all over the world, providing valuable insight into fires involving electricity. While exploring the existing research, Babrauskas found that PVC products fail as a result of the following factors:

- Errors in the formulation during manufacture
- Faults in the extrusion process during manufacture
- Contamination during manufacture
- Entrapment of moisture during manufacture
- Excessive current
- Excessive thermal insulation
- Localized heating due to staples, nails or other objects
- Localized heating due to strand breakage
- Failed terminations/connections
- Dielectric breakdown of PVC
- Arcing across a carbonized path
- Creep of insulation
- Chemical degradation
- Voltage surges

Otani [24] found that electrical plugs that used calcium carbonate ($CaCO_3$) as a filler failed after moderate heating. In these tests the plugs were heated to 110-120℃ for ten days and then cooled to room temperature. The results show that over time (on the order of days), the resistance of the insulation can drop to a sufficient level whereby current can flow and cause ignition.

Kemal et al. ran two series of tests; one in which PVC cables were exposed to elevated temperatures and one in which the cables were exposed to both elevated temperatures and a saltwater solution [25]. Kemal's results show that under elevated temperatures, the leakage current of the cables increased with increasing temperatures. His testing also shows that the degradation of PVC materials that use calcium carbonate as a filler follows this general progression:

- HCl is released from PVC (known as dehydrochlorination).
- Calcium chloride is formed from the reaction between HCl and calcium carbonate.
- Moisture is attracted to the calcium chloride, inducing swelling and increasing conductivity.
- Internal and surface scintillations (electrical discharges) begin.
- Charring occurs and carbonized paths form.

Using thermogravimetry in both air and nitrogen, Benes et al. [26] determined that the thermal degradation of PVC insulation occurred in three different temperature ranges. The greatest mass loss occurred temperatures between 200 and 340℃. This period is also characterized by the breakdown of the PVC backbone, the release of HCl,

H_2O, CO_2 and benzene, and the formation of a char layer. From 360-530℃, this char layer was burned off and the total degradation of the PVC backbone took place. In the last step (530-770℃), only CO_2 was released due to the degradation of the filler $CaCO_3$.

Armstrong et al. [27] studied the thermally-induced chemical and electrical breakdown of electrical cables. No breakdown was observed until temperatures of 240℃ were reached, with rapid degradation occurring near 328℃. The resistance of the insulation remained constant up to 260℃. Data was collected through the use of thermogravimetric analysis (TGA) and differential scanning calorimetry (DSC) to obtain the breakdown characteristics of the insulation material as it was heated. Temperature data was drawn from tests in which the cables were loaded above their rated current capacity to further define this behavior. The studies by Armstrong and Benes produced temperature criteria for the degradation of PVC that were similar to those found in this study.

Beland has written several papers regarding electrical fires [28], [29], [30], [31]. In one study, Beland discusses the difficulty in creating an arc under normal conditions and what is required to ignite a fire by electrical means [28]. Through the use of experiments he provides a methodology to interpret arcing evidence and apply it to fire investigations by concluding that a visual inspection can, in most cases, prove whether an arc was the cause or result of a fire. It is discussed further in [30] how difficult it is for an arc to start a fire, even in conditions that provide a better-than-average chance. Beland also conducted tests in which different cables experienced current overloads until failure. His tests show that arcing occurs in plastic-sheathed cables at temperatures between 150

and 250℃. Beland asserts that the life of cable insulation is decreased by a factor of two for every increase in temperature of 8-10℃.

The formation of a char layer plays a large role in the decomposition of PVC. As the material begins to degrade, a porous, low density char is formed on the surface. This char influences the rest of the decomposition process by acting as a thermal insulator and slowing down the rate of degradation [32].

David Dini of Underwriters Laboratories (UL) conducted a study on the aging of electrical wiring systems to investigate the increasing frequency of electrically-related fires in older homes in the United States [33]. Hoffmann et al. [34] studied the effects of thermal degradation of electrical wiring by conducting tests with 713 power cords utilizing six heating conditions. As power cords are present on most, if not all, electronic appliances in our homes, it is likely that arcing evidence will be found during the fire investigation.

The behavior of PVC insulation while experiencing thermal degradation has been the focus of several other studies [20], [23], [25], [35], [36]. Karayildirim et al. explored the interactions between various filler materials and the degradation process [36]. These results show that when carbonates are used as fillers, the peak temperature at which dehydrochlorination occurs is shifted to a higher temperature and a lower mass loss rate is achieved.

Similar to the tests in this study, Hagimoto et al. conducted tests using a cone calorimeter to induce arcing on Japanese cables and cords [37]. In these tests, the samples were backed with gypsum board and exposed to heat fluxes of 10, 20, 30, and 40 kW/m^2.

Using a power cable composed of PVC insulation and two current-carrying wires, it was found that the lowest heat flux required to induce arc-tracking was 40 kW/m^2.

In a separate study, PVC-insulated cables were subjected to external (from an applied heat flux) and internal (from excessive current flow) heating conditions to determine the time at which electrical breakdown occurred [38]. In these tests electrical cables were subjected to various heat fluxes from a radiant panel in various configurations. These cables were tested while backed with a marinate board, a 2”x8” pine board, and in open air. The time to electrical breakdown was found to be dependent on variables such as the applied heat flux, the backing material (or lack thereof), and the method by which the cable was mounted.

Significant variations in the temperatures that induce the breakdown of PVC insulation can be seen in the previously mentioned studies and can be attributed to several factors. The various test methods and apparatus that were used can have a significant effect on these temperatures. The samples themselves may also play a role as the chemical and physical make-up of the insulation can vary between manufacturers.

There are several resources available covering topics such as the manufacture, processing, and uses of PVC [32], [39], [40], [41]. These references provide insight into the processing and manufacture of many plastic products, covering subjects such as additives and fillers, material properties, and behavior while experiencing thermal degradation.

1.3 Arc Mapping

According to NFPA 921 [17], arc mapping is a technique used to aid in the determination of the origin of a fire using the identification of arc locations within an electrical system. The relationship of these artifacts with respect to the building as well as each other can help pinpoint the area of origin. The methodology is based on the premise that as fire attacks an electrical cable, an arc is likely to form. If the arcing event trips the circuit protection device, the circuit will be de-energized and no further arcing will occur. In cases where the circuit protection device does not cut off power to the circuit, multiple arcs may be formed on the same branch circuit. In most cases, when an arc occurs on a branch circuit conductor, the electricity downstream of the arc site will be cut off and no more arcs will occur. However, the circuit upstream between the arc site and the power source (electrical panel) will still be energized (assuming the circuit protection device did not activate). If the fire continues to move towards the power source, multiple arcs may be formed on the same circuit (assuming the circuit protection device still does not trip). By observing these artifacts, it can be hypothesized that the arcs furthest downstream from the power source were formed first, and are therefore closest to the origin of the fire.

Through an analysis of the branch circuits within a structure and creating a diagram (an arc map) of the arc locations, the fire investigator can form a hypothesis as to the fire's origin and its progression over time [42], [43]. The results presented in this thesis have great implications on the process of arc mapping and the analysis of the electrical system of a structure during the fire investigation.

1.4 Goals

It was the goal of this research to provide a greater understanding of electricity as it relates to fire investigation and electrical phenomena by conducting tests that initiate the arcing through char process. By analyzing how cable insulation degrades under radiant heat, we were able to approximate the point at which the insulation becomes a semi-conductive material. An investigation was conducted into the artifacts and electrical waveforms created as a result of the arcing process in order to determine if any patterns existed that may assist in the analysis and understanding of arcing through char. This information may benefit engineers and fire investigators alike by providing the knowledge of what is required to form an arc and aid in the arc mapping process.

2. Background Information

2.1 The Basics of Electricity

Electricity is caused by the flow of electrons through materials or matter. Electrons are negatively charged particles that surround the nucleus of atoms. Materials such as metals have electrons that are free to move with little resistance, making them conductors. Wood, paper, plastic, and rubber are examples of insulators; materials that have electrons held tightly within the atom. Insulators are used to prevent the unsafe or unnecessary flow of current out of a circuit and to isolate the circuit from its surroundings.

Voltage (V) is defined as a difference in electric potential between two points. It is the equivalent to varying pressures in a hydraulic system. Voltage is measured in units of volts. An electric current (I), measured in amperes (or amps), is the rate at which

electrons flow, per unit time, and is created when electrons are allowed to flow between two points of different voltage potential. This electric flow is similar to the rate at which a fluid flows in a hydraulic system.

Resistance (R) is the opposition to the flow of electrons and is measured in units of ohms. It can be likened to the resistance water encounters while trying to flow through a pipe. An interesting relationship was formed by Georg Ohm that relates all of these values, called Ohm's Law. With Ohm's Law, if two of four values - power (P), resistance (R), voltage (V), or current (I) are known, it is possible to calculate the other two. The basic equation of Ohm's Law is:

$$V = I * R \qquad (1)$$

Power companies use the kilowatt-hour (1000 W-hr = 1kW-hr) as a standard measure of power consumption and charge their customers according to the amount of power used each month. Many appliances found in the home are rated based on the power they consume (i.e. 100W light bulbs, 1000W microwave).

2.1.1 Alternating Current

Alternating current (AC) is the most widely used form of electricity in the United States. This form of electricity is created when the current oscillates (or alternates) from zero to a maximum value, through zero to a minimum value and back to zero again. This entire process makes up one cycle and occurs many times in one second. The number of cycles per second, or frequency, is measured in Hertz (Hz). The standard frequency in the United States is 60 Hz, where the current alternates 60 times per second. In many other countries the standard frequency is 50 Hz with varying voltage levels. Due to these

differences, appliances used in one country may require an adapter in order to operate in another country.

An important aspect of alternating current systems is that the voltage or current levels can be increased or decreased in magnitude based upon the requirements of the end user. These voltage changes can be induced using transformers.

2.2 Electrical Systems

The vast majority of residential wiring in the United States consists of nonmetallic (NM) sheathed cable. This NM cable comes in a range of sizes, the most common for residential construction being 12/2 and 14/2. These designations refer to the size and number of conductors in the cable; the first number (12 or 14) referring to the size or diameter of the conductors based on the American Wire Gauge (AWG) system and the second number (2) referring to the number of current-carrying conductors in the cable. For example, in a 14/2 system, the conductors are 14 AWG with two current-carrying conductors and a grounding conductor. The grounding conductor is not included in the designation as, under normal circumstances, it does not carry any current.

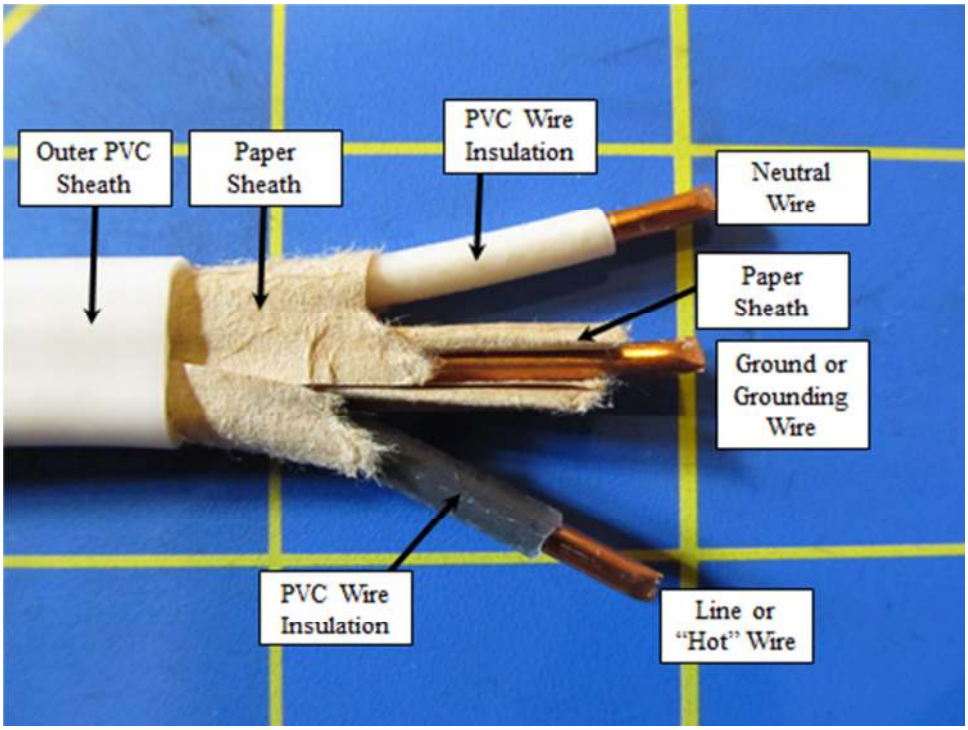

Figure 5 - Nonmetallic (NM) sheathed cable configuration.

The wires that make up the NM cables used in this research are insulated with polyvinylchloride (PVC) insulation. The line or "hot" conductor can be identified by black insulation as required by NFPA 70: The National Electrical Code (NEC) [44]. The "neutral" or grounded conductor is designated with white insulation. The equipment grounding conductor or "ground" conductor will either have green insulation or no insulation at all. In a typical NM cable, the ground conductor is wrapped with only a layer of paper and no PVC insulation. The conductors are laid parallel to each other and wrapped with another layer of paper, followed by the outer PVC sheath (Figure 5). Both the line and neutral conductors have a clear, thin nylon jacket surrounding the PVC insulation. Common sizes of cables and their ampacities (the maximum allowable currents), as allowed by the NEC, can be found in Table 1.

Table 1 - Wire sizes and allowable ampacities, as outlined by the NFPA 70: The National Electrical Code [44]**.**

Wire Size (AWG)	Wire Diameter (in/mm)	Ampacity (Amperes)
18	.04/1.02	6
16	.051/1.3	8
14	.064/1.62	15
12	.081/2.05	20
10	.102/2.6	30
8	.162/4.11	40

The ampacities listed in Table 1 are the highest allowable values at a given temperature while operating at full load in free air. If the ambient temperature in the installation setting will be higher than that specified for a given rating, the ampacity must be lowered to account for the rise in temperature. Overheating becomes an issue when cables are stacked on top of each other or covered with insulation in void spaces [45].

2.3 Cable Insulation

The use of polyvinylchloride (PVC) insulation became more frequent during World War II due to the shortage of rubber. Prior to this, electrical cables insulated with rubber had the tendency to allow fire to spread along their length; a major disadvantage on naval ships where fires traveled from one compartment to the next using the cables as fuel. This expedited the development of PVC as an insulating material due to its inherent fire retardant behavior. PVC saw its first use in residential wiring in 1939 [32] and is now estimated to account for two-thirds of the wiring used in buildings in the United States [15].

PVC is a synthetic polymer that has thermoplastic properties, meaning that once formed (by a machine or by heat and pressure), it can be reformed using the same process [20]. PVC exists in its raw form as either rigid PVC (RPVC) or flexible PVC (FPVC), and any product made of this material will have properties somewhere in between those of RPVC and FPVC.

The composition of electrical insulation varies from manufacturer to manufacturer, but the main components generally remain the same [20]. Because PVC degrades when exposed to heat and light, stabilizers are added to prevent excessive deterioration. Plasticizers are added to make the final product more flexible, fillers are added to lower costs, and flame retardants are added for safety. Colors are created using dyes or pigments. The following are typical formulations for NM sheathing and wire insulation, as identified by Grossman [40]:

Table 2 - Typical Formulations for NM Sheathing and Cable Insulation [40]**.**

NM Sheath		**Wire Insulation**	
Ingredient	**%**	**Ingredient**	**%**
PVC	46-48	PVC	56-59
Plasticizer	25-29	Plasticizer	28-30
Calcium Carbonate	23-24	Calcium Carbonate	2.8-5.9
Stabilizer	.8-1.2	Misc. Fillers	5.6-5.9
Misc. Additives	.1	Stabilizer	2.3-4.1
Lubricants	0-2.4		

3. Testing

3.1 Methodology

A cone heater was used to apply a uniform radiant heat flux in an attempt to collect data regarding the time-to-failure for unenergized and energized cables. These tests were repeated over a range of heat fluxes to observe the relationship between the time-to-failure and heat flux, the waveforms produced by the arcing faults, and the artifacts left behind as a result of these faults.

The focus of the first set of tests was to find the approximate time-to-failure of unenergized cables, eliminating the variable of electricity and simplifying the testing procedure and subsequent analysis. These tests formed the groundwork for the testing of energized cables that followed in the next series of tests, where an emphasis was placed on finding the time at which an arcing fault occurred. This allowed the study of how electricity affected the time-to-failure of the cables as well as the arc marks and waveforms produced as a result of this phenomena. An attempt was then made to determine what effect, if any, a reduced-oxygen environment would have on the process of arcing through char by conducting several tests of energized cables in a chamber filled with nitrogen. Lastly, tests were conducted at various voltages to determine how this would influence the time-to-failure of the cable.

3.2 Materials

The materials used in this research were chosen based on their widespread use in today's market and the ease with which they can be obtained in nearly all home improvement stores across the country. The cable used for this project is classified by UL

(Underwriter's Laboratories) as a nonmetallic (NM) sheathed cable. Size 14 AWG wire was used as it is one of the most widely used wire sizes in residential and commercial construction. A new roll of cable is shown in Figure 6.

Figure 6 - The cable used for testing, as purchased from a local home improvement store.

3.3 Preliminary Testing

In order to gain an understanding of how the wire insulation might behave under heating conditions, several preliminary tests were conducted. To explore the relationship between the resistance of the insulation and temperature, a small sample of insulation was stripped off of a wire, flattened, and placed between two electrodes. The samples were approximately 10 mm long, 5.1 mm wide, and .4 mm thick. For the first set of tests, the sample was placed between two bolts and heated with a gas-fueled burner (Figure 7). The flame was applied and removed at one-minute intervals to illustrate the temperature dependence of the insulation. This setup was tested with and without a sample of insulation to ensure that the flame itself was not causing current to flow between the

electrodes. In this test it was assumed that the insulation sample was small enough that there were no thermal gradients within the sample. The temperature was measured using a Type-K thermocouple that was placed between the surface of one bolt and the insulation sample. A small indentation was ground into the surface of one bolt to provide depression for this thermocouple to sit, allowing the insulation sample to lay flat across the surface of the bolt.

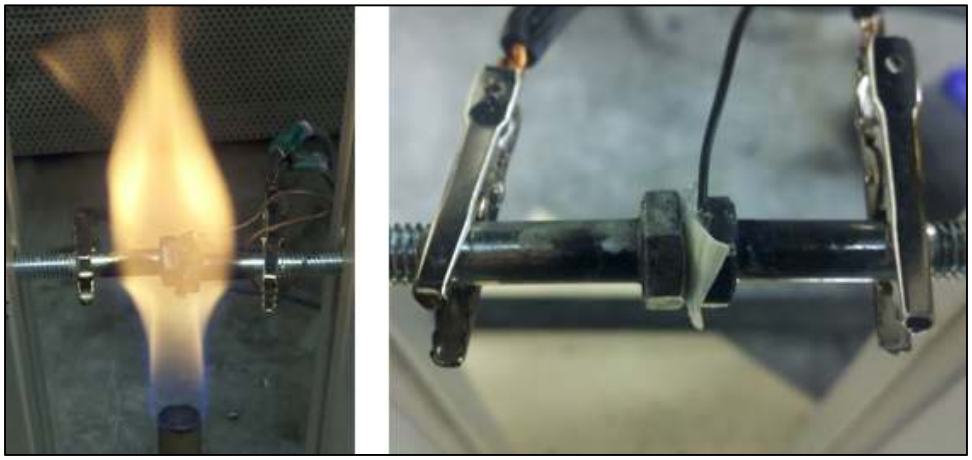

Figure 7 - Wire-insulation test using hexagonal bolts and a gas-fueled flame.

To better regulate the temperature of the sample, this test was repeated in a laboratory convection oven, where the sample was flattened and placed between two copper electrodes (Figure 8). The temperature of one alligator clip was measured using a Type-K thermocouple. It was assumed that the insulation sample and the electrodes/alligator clips were approximately the same temperature throughout the test. The sample was heated at a rate of 10℃ per minute. In order to create fluctuations in the temperature of the sample, the door to the oven was opened. The door was kept open until the sample had cooled to a point where the resistance was seen to increase and return to an infinite value. Figure 9 shows the resistance and temperature data for one of

the oven tests, illustrating the relationship between these two values. The resistance in each test was observed to drop from its initial value to a value between 10,000 and 100,000 ohms. While this drop in resistance is noticeable, it is not of sufficient magnitude to cause a failure of the cable by itself.

Figure 8 – The test configuration used in the oven tests to determine the temperature dependence of the PVC wire insulation.

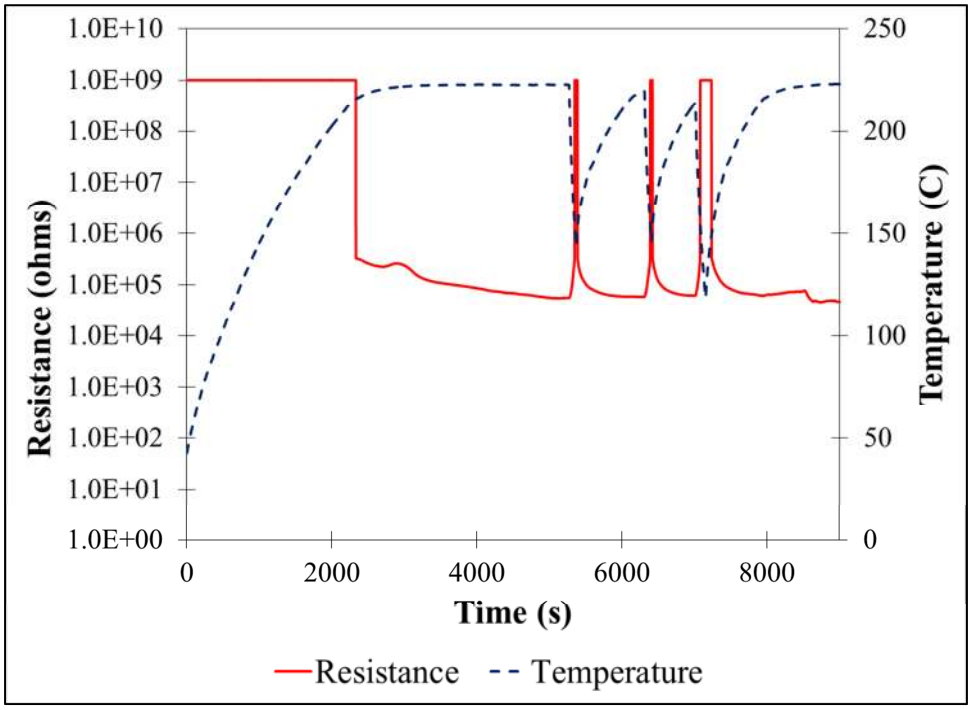

Figure 9 - The resistance of the wire insulation was found to be inversely dependent to the fluctuations in temperature.

As shown in Figure 9, the resistance of the PVC sample fluctuated with temperature. It is believed that the first drop in the resistance corresponds to the conversion of the PVC into char, which was found in both of these tests. This char was porous and brittle, crumbled easily when handled, and was black in color. The fluctuations in the resistance of this char following the first drop are believed to be due to the heating (or cooling) of the char causing a decrease (or increase) in the resistance of the sample. In order to understand these fluctuations in resistance, a literature research was conducted into the resistivity of carbon and its dependence on temperature [46], [47]. Powell and Schofield [46] demonstrated that for several types of carbon and graphite the thermal and electrical conductivities varied with changes in temperature, however these fluctuations were not significant. These findings, coupled with the results of the

preliminary tests of the wire insulation, show that a failure of the insulation will not occur by heating alone.

3.4 Tests of Unenergized Cables

3.4.1 Setup for the Testing of Unenergized Cables

In order to simulate the effects of fire conditions on electrical cables, a radiant cone heater was used to apply a uniform heat flux to one side of an electrical cable. The cable was suspended under the heater to provide convective cooling to the bottom of the cable.

For the testing of unenergized cables, a data acquisition unit was used to collect heat flux measurements and measure the resistance between the line and ground wires as well as between the neutral and ground wires. Connections were made using 18 AWG wires with alligator clips soldered on the ends. These connections can be seen in Figure 10. The heat flux was calculated from the voltage readings produced by a water-cooled heat flux transducer.

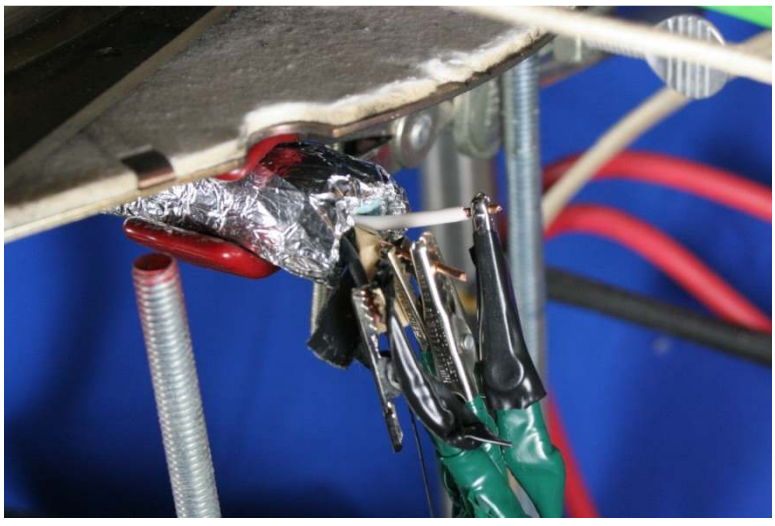

Figure 10 - Connections used to measure the resistance during the tests of unenergized cables.

In order to place the cable sample in the same position for each test, a simple device was made to hold the cable in place. This holder was constructed using a 5.1 cm (2 inch) long piece of 1.3 cm (.5 inch) diameter copper pipe. The holder was made by rolling a cable sample in a paper towel to insulate it from the copper pipe. The roll was inserted into the pipe so that both ends of the cable/paper towel stuck out of the pipe. The pipe was flattened along its length in order to provide slight pressure on the insulated roll. It was then wrapped with more insulation, followed by a layer of aluminum foil to protect the entire assembly from the heat produced by the cone heater. This assembly allowed a new cable sample to be easily inserted for each test through the hole formed in the paper towel, shown in Figure 11. A picture of the holder in its final form can be seen in Figure 12. The holder was placed in a ring stand clamp and attached to a platform under the cone heater. The holder was placed on the side closest to the power source, which will be referred to as the "source side." The end furthest away from the power source will be known as the "load side." The final test setup is shown in Figure 13.

Figure 11 - End view of the holder assembly showing where a new cable was inserted for each test.

Figure 12 - The final device used to hold and shield the cable during testing.

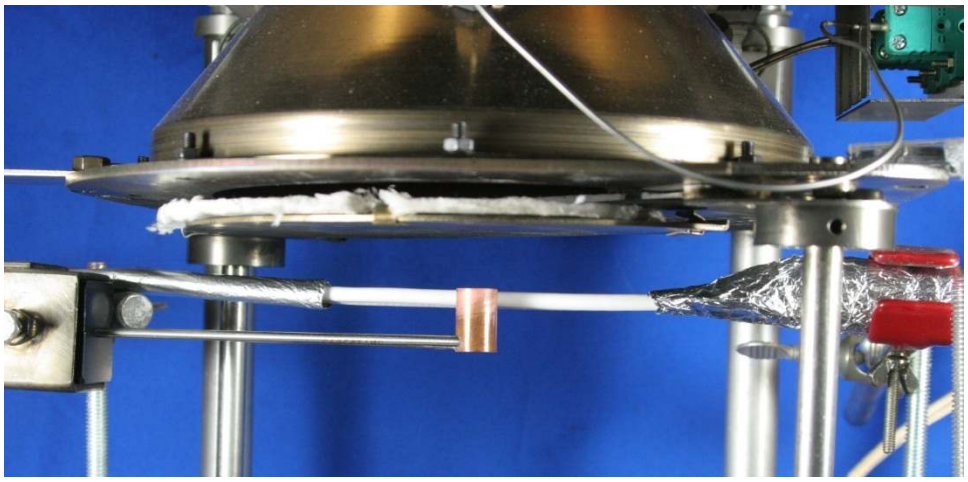

Figure 13 - Setup for the testing of electrical cables to simulate fire exposure.

3.4.2 Procedure for the Tests of Unenergized Cables

Tests were conducted such that a 10.2 cm (4 inch) long section of cable was subjected to a uniform radiant heat flux from a cone heater. The cable was suspended 2.5 cm (1 inch) below the heater and placed in the same plane as the top surface of the heat flux gauge. The ends of the cable were thermally insulated to provide a well-defined area that was exposed to a uniform heat flux. The load end of the cable was left unsecured to ensure that any expansion or movement along the length of the wires would not lead to physical contact between them. However, the cable was supported such that it would lay flat and level under the heater.

The heat flux was varied by adjusting the temperature on the cone heater to obtain the desired output. Once the heat flux was reached, the heater was allowed to stabilize for five minutes and the protective shutter was closed. The test sample was then positioned under the heater and the data acquisition equipment started and allowed to record measurements for one minute. After this one minute period, the shutter was opened and each test was conducted for up to two hours or until the resistance between any two wires (line and ground or neutral and ground) had dropped below 100 kΩ (100,000 ohms). When the test was finished, the shutter was closed and the sample was removed. The sample was then marked with the test number and heat flux.

3.4.3 Results for the tests of Unenergized Cables

Criteria for the failure were arbitrarily chosen for the results of the unenergized cables in order to gain an understanding of the breakdown of cable insulation. Resistances of 100k, 50k, 30k, and 20k ohms were used to define a failure of the cables. The time-to-failure of unenergized cables is presented in Table 3. A graph of the changes in resistance with time at a constant applied heat flux of 26 kW/m^2 is shown in Figure 14. This data suggests that it may be possible to estimate the failure of energized cables based on criteria derived from the tests of unenergized cables.

Table 3 - Time-to-failure of unenergized cables under various heat fluxes.

	Time-to-Failure (seconds)			
Heat Flux (kW/m^2)	**100,000 Ohms**	**50,000 Ohms**	**30,000 Ohms**	**20,000 Ohms**
55	41	43	168	190
53	88	161	309	-
50	132	138	150	154
48	132	139	146	150
48	106	290	-	-

46	398	-	-	-
43	163	175	183	190
41	206	215	240	256
40	322	-	-	-
38	211	238	292	354
37	200	211	225	236
35	603	-	-	-
34	325	350	386	-
32	404	473	560	-
31	409	445	505	-
30	968	-	-	-
29	3447	-	-	-
29	468	631	761	855
28	792	-	-	-
27	1422	1534	1670	1789
26	2233	-	-	-
26	681	894	1240	-
26	6889	-	-	-
25	1624	-	-	-
24	7128	-	-	-
24	7475	-	-	-
22	7835	-	-	-
20	5398	-	-	-

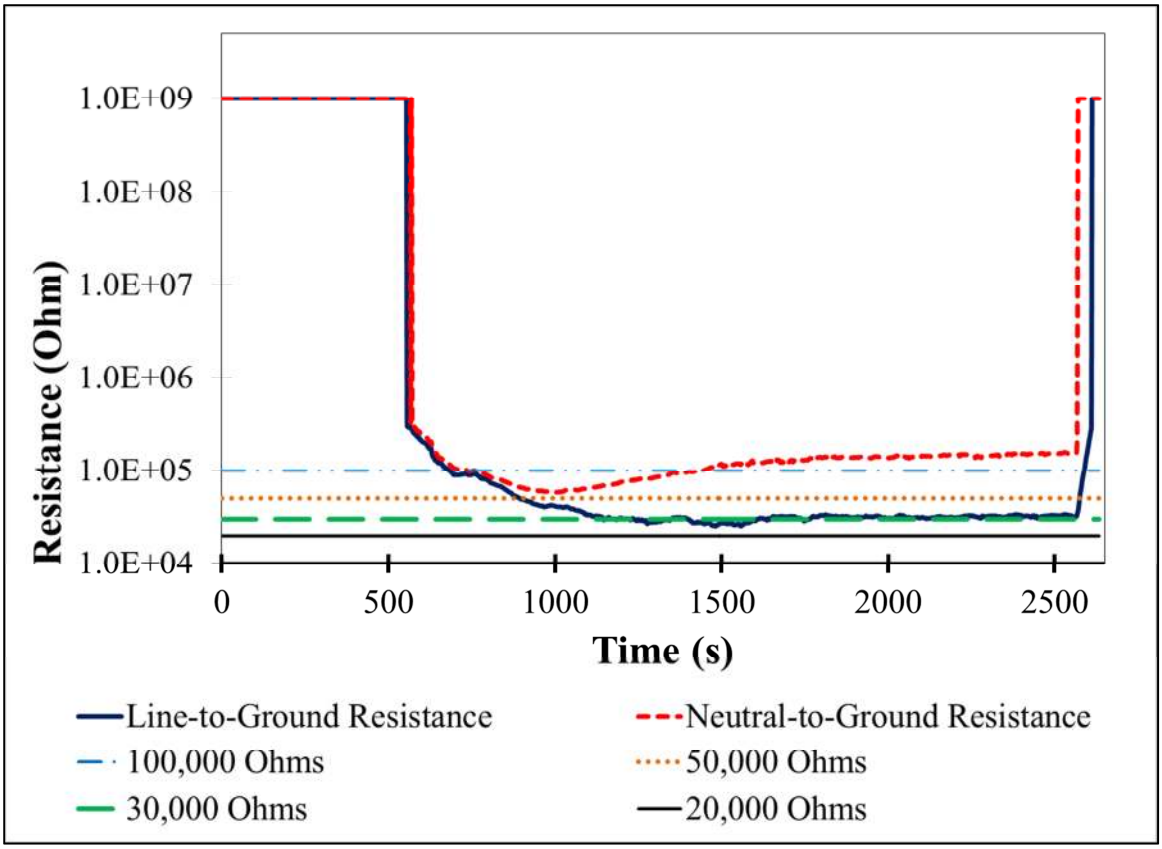

Figure 14 - At 26 kW/m^2 the resistance of the wire insulation is seen to drop to approximately 30,000 ohms.

3.5 Fire Behavior of Electrical Cables

The overall behavior of the cable and its insulation during testing was consistent from test to test. In most tests the outer sheath of the cables tended to swell and contract, forming a 'C' shape, as shown in Figure 15. While not seen in every test, ignition generally occurred at heat fluxes between 50 and 55 kW/m^2. The discoloration of the insulation and the production of gases and smoke were indicators that degradation may be occurring. These signs were often visible within the first 10 to 20 seconds after the protective shutter was opened. The char created during these tests was found to be very porous and brittle. It broke when handled and was easily removed by hand.

Figure 15 - 'C' shape formed by the swelling insulation as it charred.

3.6 Testing of Energized Cables

3.6.1 Setup for the Testing of Energized Cables in an Ambient Environment

The apparatus used in these tests was identical to that used in the tests of unenergized cables. However, instead of resistance measurements, the voltage and current were measured in an attempt to capture the electrical waveforms of the arcing faults. The currents on all three legs of the circuit (line, neutral, and ground) as well as the line-to-neutral and neutral-to-ground voltages were measured using a power quality analyzer (replacing the data acquisition unit previously used). The heat flux was measured before each test to ensure that the proper setting had been reached. The heat flux was not monitored throughout the test as it was a concern that molten copper from the arcs may damage the transducer surface or that the cables would fault to the transducer itself.

Test power was obtained from a 120/240 VAC panel and protected by a 40 ampere-rated fuse at the main cutoff switch. A 10 AWG extension cord was run from this

panel to the testing station and connected to a remote breaker panel. At the testing station, a 15 ampere-rated thermal/magnetic circuit breaker was used to provide primary circuit protection of the test apparatus. The ends of the cable were thermally insulated to provide a well-defined area that was exposed to a uniform radiant heat flux. The load end of the cable was supported to keep it level under the heater and was not restrained longitudinally, allowing expansion of the wires.

3.6.2 Procedure for the Testing of Energized Cables in an Ambient Environment

The heat flux of the cone heater was set and allowed to stabilize for approximately five minutes, after which the protective shutter was closed and the cable sample was inserted under the heater. The heat flux transducer was removed after ensuring the cable was placed in the correct position. Data acquisition was allowed to record for one minute and then the protective shutter was opened. Tests were conducted until a failure occurred or two hours had elapsed, whichever came first. Two hours was chosen as the cutoff for the testing as it was believed this was ample time for a structure fire (commercial or residential) to burn before being extinguished under normal circumstances. Several tests were conducted for longer periods in order to determine when the cables would fail outside of the period of investigative interest (i.e. minutes versus hours).

After testing, a thorough analysis of the cables was conducted to locate and identify any artifacts that may have been left behind by the arcing phenomena observed. Once a test was completed, the cable was cut just outside of the holder on the source side,

leaving approximately 9.5 cm (3.75 inches) of clean insulation on the cable. The cables were marked with the test number and heat flux on the load side and a distinct mark was placed on the source side. Before any destructive analysis was performed, any important external features were photographed. The degraded insulation was then removed from the cable using gloved hands and a bamboo skewer. The locations of any arc marks were noted and photographed under a microscope. Once the majority of the insulation was removed, the cables were placed in an ultrasonic water bath for one hour to further clean and polish the wire surface. The cables were allowed to dry and any loose insulation remaining on the wires was carefully removed using gloved hands and a small painter's brush. The artifacts left by the arcing faults were again photographed under the microscope for further analysis. Care was taken not to dislodge or disturb any artifacts left on the wires.

3.6.3 Results of the Energized Cable Tests

The failure of an energized cable resulted in the formation of an electric arc, characterized by a flash of light and the ejection of molten copper (See Figure 3). A sharp increase in the current was observed, causing the activation of the circuit breaker cutting off power to the circuit. The time-to-failure at various heat fluxes for the tests of energized cables is shown in Table 4. The time-to-failure can be seen to increase with decreasing heat flux, and becomes infinite in the vicinity of 25 kW/m^2. As in the tests of unenergized cables discussed previously, signs of degradation were often observed within the first 10 to 20 seconds after the shutter was opened. The physical appearance of the cables was consistent throughout the range of tests and similar charring behaviors were

observed. It was noticed that the insulation was often ignited upon the initiation of the arc with the flames being sustained for up to one minute.

Table 4 - Time-to-failure of cables in an ambient environment as it relates to heat flux.

Heat Flux kW/m^2	Time (s)	Arc? (Y/N)	Heat Flux kW/m^2	Time (s)	Arc? (Y/N)
55	107	Y	32	1353	Y
53	200	Y	31	458	Y
53	240	Y	30	493	Y
52	180	Y	29	503	Y
52	218	Y	28	739	Y
51	209	Y	27	605	Y
50	276	Y	27	951	Y
50	162	Y	26	8422	N
49	274	Y	26	1554	Y
48	237	Y	26	1330	Y
47	317	Y	25	3439	Y
45	470	Y	25	2729	Y
44	318	Y	25	4790	Y
43	5404	N	25	873	Y
43	306	Y	25	858	Y
42	295	Y	25	925	Y
41	364	Y	25	4433	Y
40	360	Y	25	7244	N
39	397	Y	24	4488	N
38	314	Y	24	4724	Y
38	332	Y	24	7244	N
37	7235	N	24	12259	N
37	565	Y	24	977	Y
36	429	Y	24	1125	Y
35	654	Y	24	8594	N
34	537	Y	23	11530	N
34	1511	Y	23	11194	N
33	854	Y	23	18303	N
32	889	Y	22	7215	N
32	594	Y	22	14587	N

The voltage and current waveforms were captured in order to observe the electrical behavior of the arcing events. These waveforms generally occurred in approximately one-half of a cycle (1/120th of a second) and were found to be nearly identical from test-to-test. Representative waveforms are presented in Figures 16, 17, and 18 below, with the remainder of the waveforms located in the appendix.

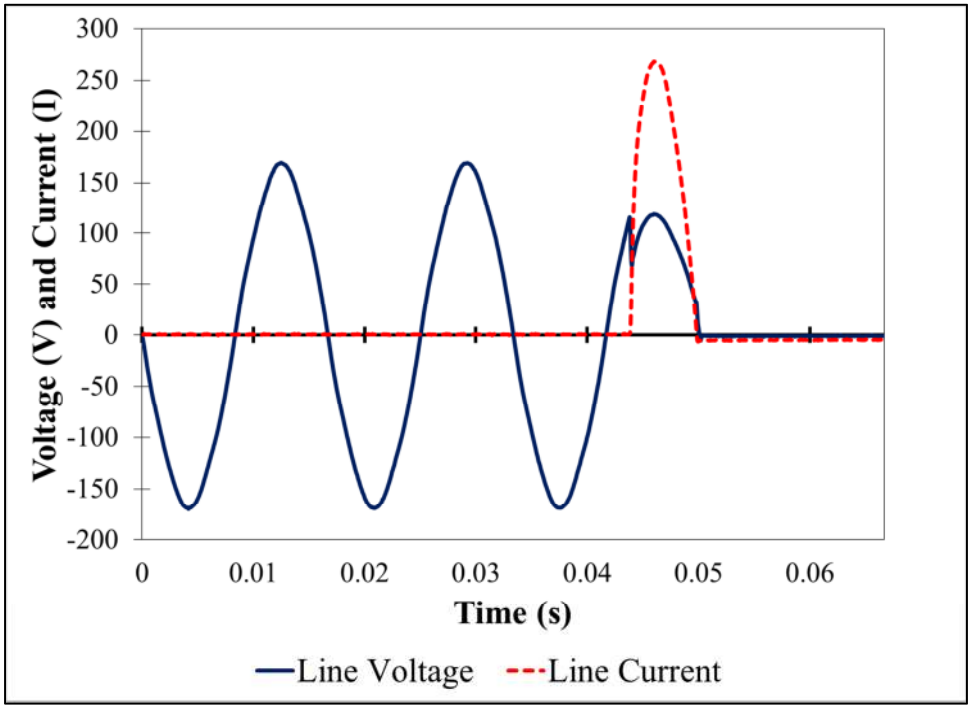

Figure 16 - Waveforms produced during test 2-6. A total of four cycles (1/15 of a second) is shown.

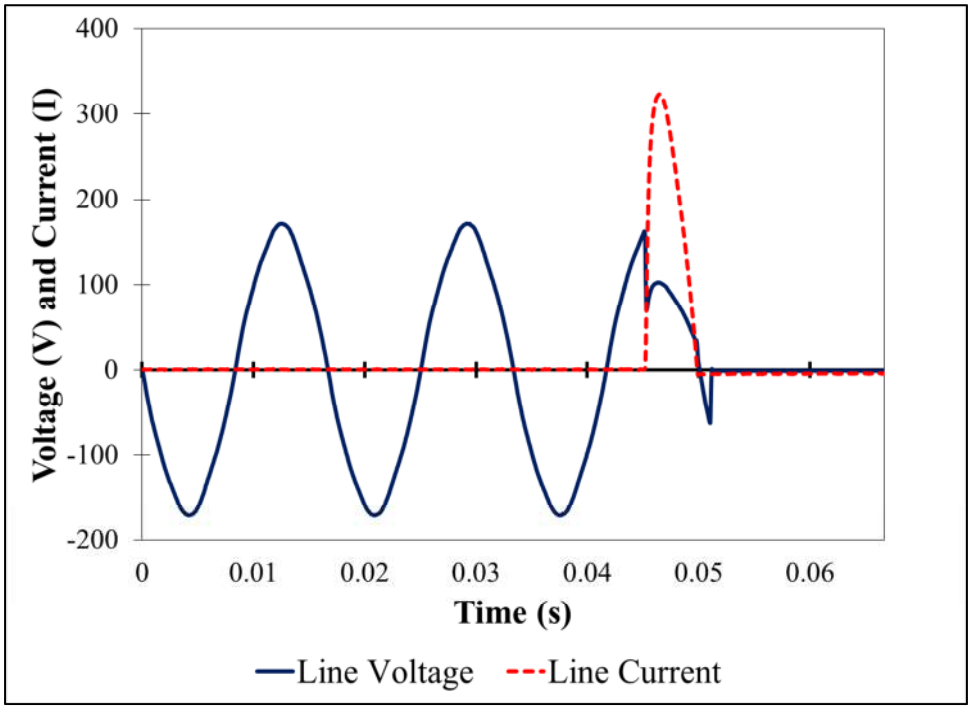

Figure 17 - Waveforms produced during test 2-30. A total of four cycles (1/15 of a second) is shown.

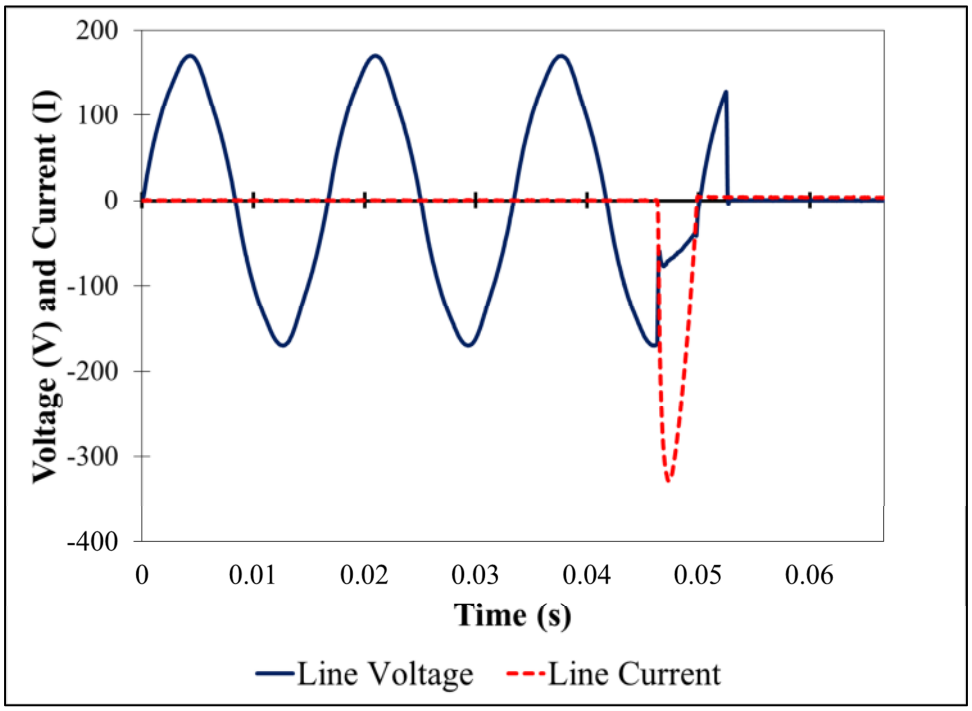

Figure 18 - Waveforms produced during test 2-51. A total of four cycles (1/15 of a second) is shown.

As part of the analysis of the arc beads created in these experiments, photographs were taken under a microscope to better observe the artifacts created by the fault. High dynamic range (HDR) photography [48] was utilized to enhance the photographs taken under the microscope. The cables were photographed so that the line or "hot" conductor was in the top of each picture. Photographs of the arc beads can be found in the appendix, with a select few shown below.

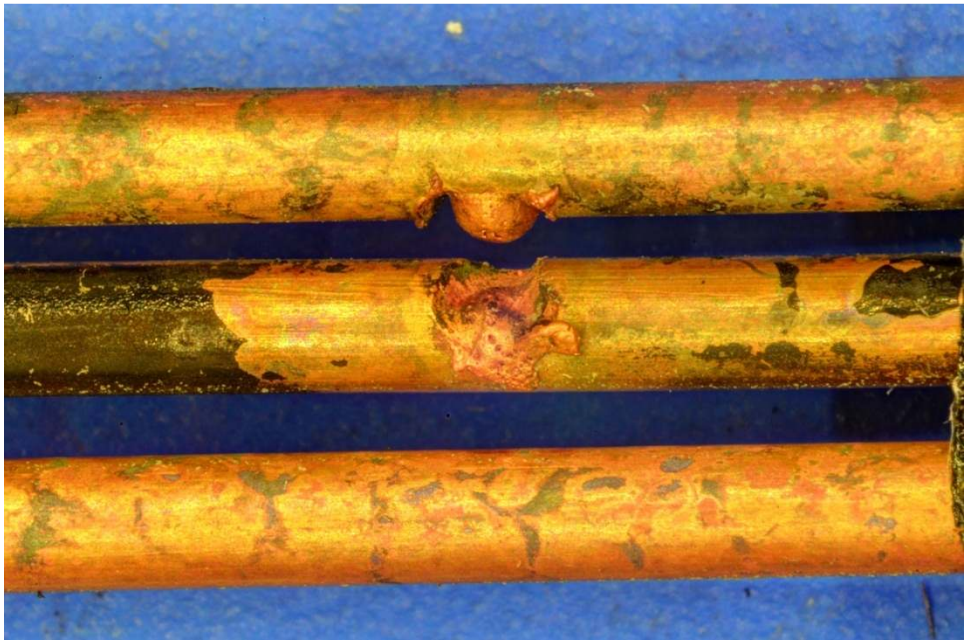

Figure 19 - Arc 2-7 from the tests of energized cables in an ambient environment (16x magnification).

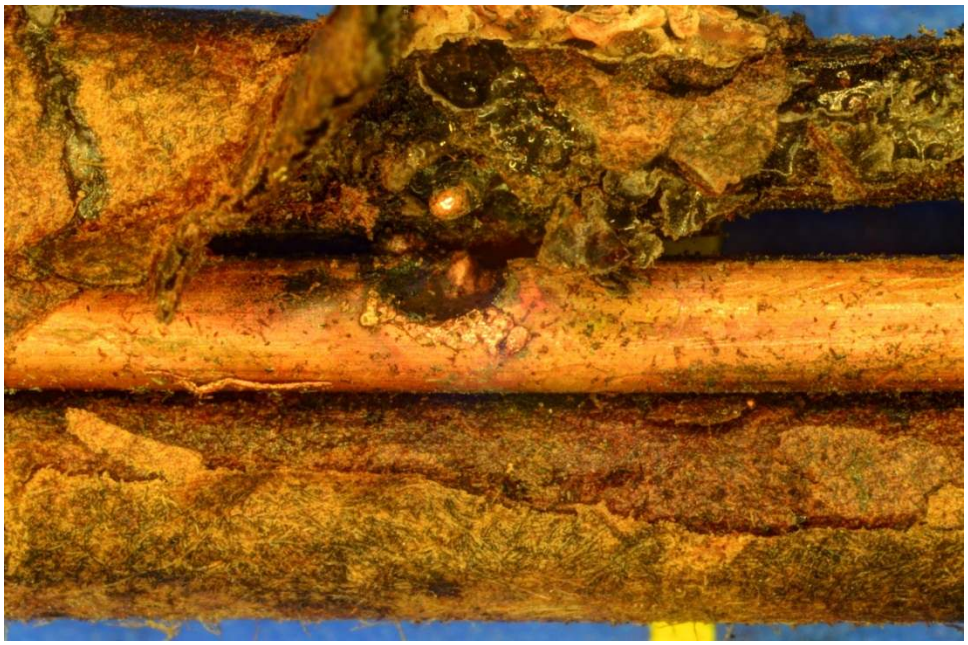

Figure 20 - Arc 2-5 from the tests of energized cables in an ambient environment (16x magnification).

Figure 21 - Arc 2-57 from the tests of energized cables in an ambient environment (16x magnification).

A select number of tests were chosen for analysis using the scanning electron microscope/energy dispersion spectroscopy (SEM/EDS) apparatus available. The goal of this study was to take a photograph utilizing the SEM and recreate the same picture on the microscope. This picture was then turned into an HDR photograph in order to better visualize the arcing damage on the conductors. Below are the results of these actions, with a normal microscope photograph, HDR photograph, and SEM photograph of each arc presented for clarity.

Figure 22 - Arc 2-48 from the tests of energized cables in an ambient environment (27x magnification).

Figure 23 - Arc 2-6 from the tests of energized cables in an ambient environment (22x magnification).

Figure 24 - Arc 2-7 from the tests of energized cables in an ambient environment (27x magnification).

These photographs show that the arcing damage created as a result of these tests is consistent with current descriptions of arcing damage presented in the literature and that all artifacts exhibited similar physical characteristics across the range of heat fluxes. All of the arc marks produced in these tests were easily identified as such by visual inspection. The microscopic and SEM analyses provided further proof of the consistency in arcing damage and allowed further identification of the arcing characteristics.

3.7 Tests of Energized Cables in a Nitrogen Environment

Tests of energized cables were conducted in a nitrogen environment to determine what effect, if any, a reduced-oxygen environment would have on the arcing process. Similar to the testing of energized cables in ambient air, these tests were conducted on energized cables that were placed within a controlled-atmosphere chamber (Figure 25). This chamber was used to lower the amount of oxygen in the surrounding environment. The chamber was flooded with nitrogen, lowering the concentration of oxygen and reducing or eliminating the effects of the oxidation process from the reaction. This testing used the same test setup as that used for the unenergized and energized cables previously discussed. The use of a controlled-atmosphere chamber has been the subject of several studies, and is becoming more popular in the study of degradation of materials [49], [50].

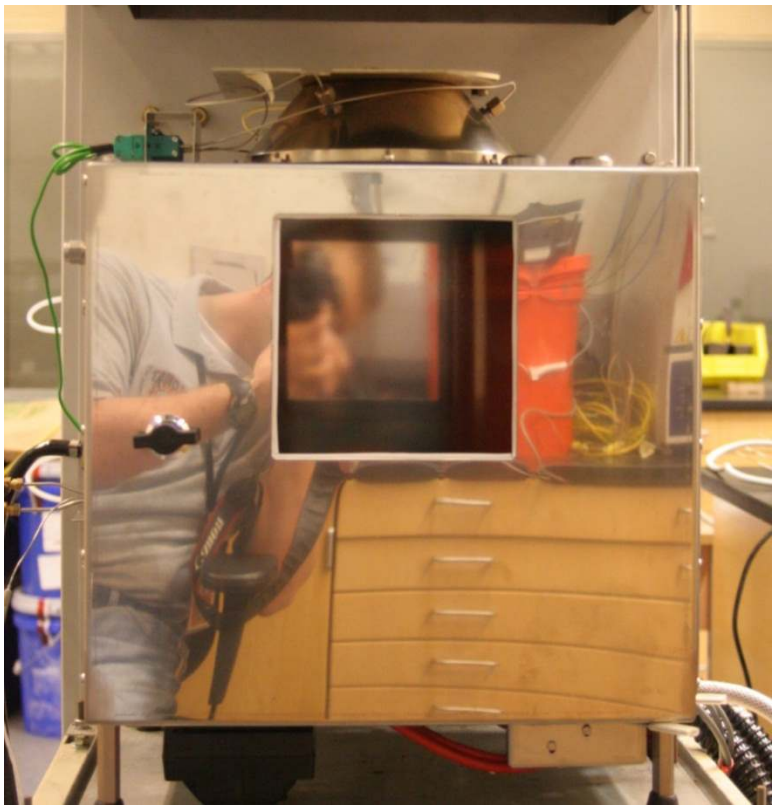

Figure 25 - Controlled-atmosphere chamber used in the testing of energized cables in a reduced-oxygen environment.

3.7.1 Setup for the Tests of Energized Cables in a Nitrogen Environment

A maximum flow rate between 150 and 180 liters per minute was recommended by the manufacturer to reduce the oxygen concentration within the chamber [51]. A bank of four cylinders was used to supply the necessary nitrogen. Two cylinders were used at one time to reach this flow rate and the remaining cylinders were in place in the event that one or both of the primary cylinders ran out of product. A four-valve manifold was used to control which tanks were supplying the chamber at any given time.

In order to route the electrical cables into the chamber, a port used for gas analysis during normal operation was removed. Both ends of the cable were thermally insulated to provide a well-defined area that was exposed to a uniform radiant heat flux. This also protected the cable on the source side from being heated such that that it would arc to the chamber itself at the entry point. The load side of the cable was supported by an insulated bar within the chamber, allowing the cable to be suspended approximately 2.5 cm (1 inch) below the heating coil. The power analyzer and power supply used in the previous tests of energized cables were also utilized in these tests.

3.7.2 Procedure for the Tests of Energized Cables in a Nitrogen Environment

Using a water-cooled heat flux transducer, the heat flux was set at the desired level and allowed to stabilize for approximately five minutes. At this point the protective shutter was closed and the cable sample was routed through a port in the side of the chamber. Once the sample was in place within the chamber, the door was closed and the nitrogen turned on so gas was flowing through the chamber at the specified rate (150-180 liters per minute). The power to the cable was then turned on and all recording instruments started and allowed to record data for one minute. After this one minute period, the protective shutter was opened and the test was conducted until an arcing fault occurred or two hours had elapsed, whichever came first. It was assumed that any oxygen trapped within the cable was either displaced during the initial one-minute start-up period or was soon evacuated after the cable began to char.

3.7.3 Results for the Tests of Energized Cables in a Nitrogen Environment

Tests in the reduced-oxygen environment were conducted at heat fluxes of 48, 50, and 54 kW/m^2 with a minimum of two tests conducted at each flux. In these tests, the time-to-failure was observed to be slightly less than those of the energized cables. A comparison of these times is provided in Table 5. Similar behaviors were observed during the degradation of the insulation in each test when compared to the prior tests. The behavior of the cable insulation was identical to that of the cables tested previously. Of special note is that no ignition of the insulation was observed in any of the tests conducted in a nitrogen environment, even at higher heat fluxes.

Table 5 - Time-to-failure of energized cables in nitrogen and ambient environments.

Nitrogen Tests		Energized Tests	
Heat Flux (kW/m^2)	**Time (s)**	**Heat Flux (kW/m^2)**	**Time (s)**
54	77	55	107
54	94	53	200
50	112	53	240
50	122	52	180
48	205	52	218
48	182	51	209
-	-	50	276
-	-	50	162
-	-	49	274
-	-	48	237

Photographs were taken under a microscope to better observe the arcing damage left behind after the fault. For the analysis of the arc beads, any loose insulation was removed from the wires and the cable was placed in an ultrasonic water bath for one hour. Any remaining insulation was removed using gloved hands or a painters brush. The

cables were photographed such that the line or “hot” conductor was at the top of each picture. Photographs of the arc beads can be found in the appendix, with a select few shown below. No differences in the shape or appearance of the arc beads were observed when compared with those formed in an ambient environment.

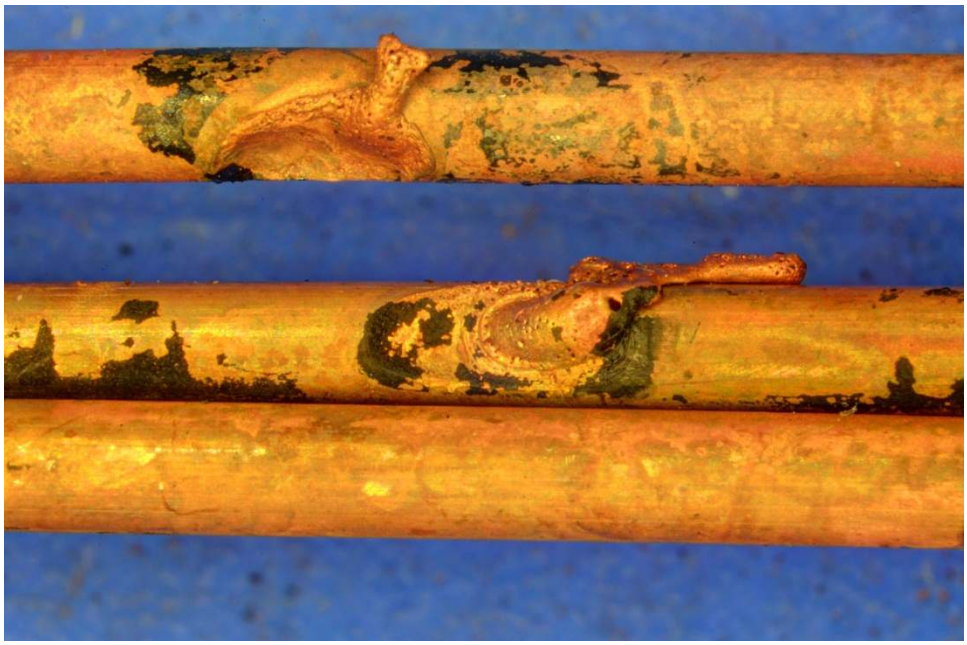

Figure 26 - Arc 3-6 from the tests of energized cables in a nitrogen environment (16x magnification).

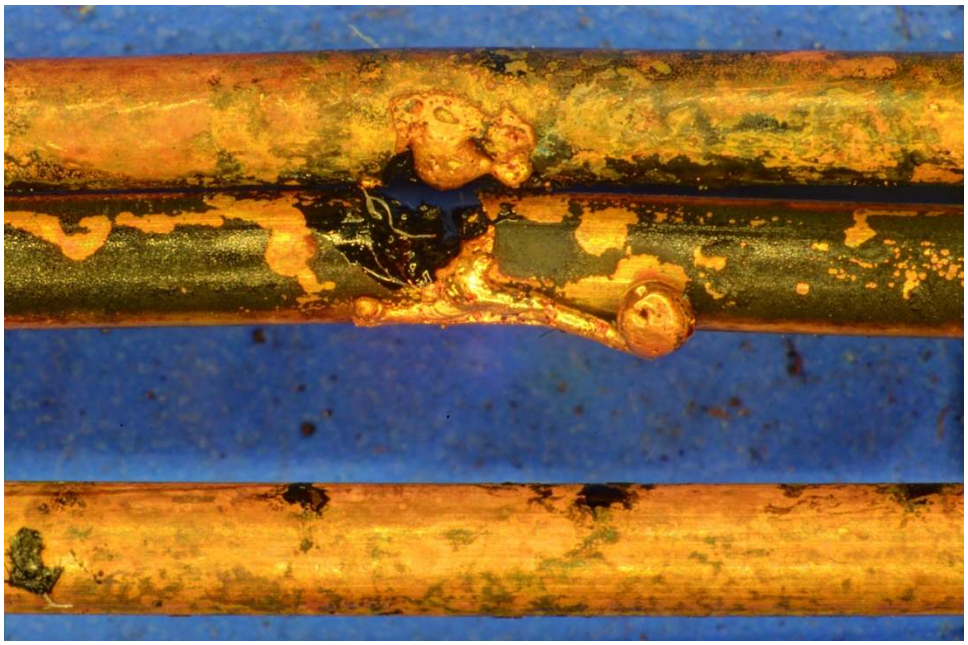

Figure 27 - Arc 3-4 from the tests of energized cables in a nitrogen environment (16x magnification).

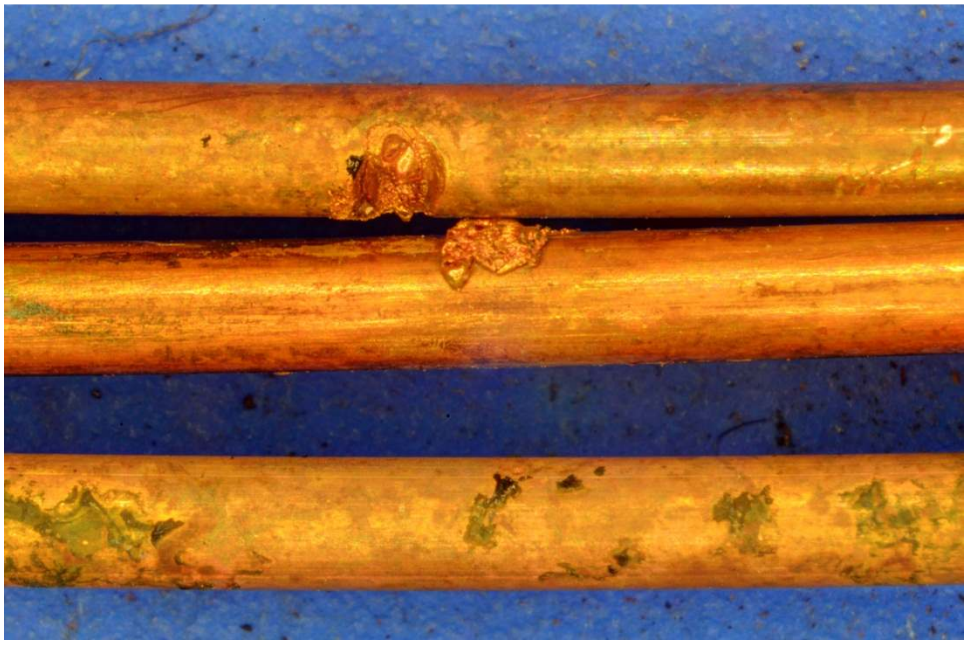

Figure 28 - Arc 3-3 from the tests of energized cables in a nitrogen environment (16x magnification).

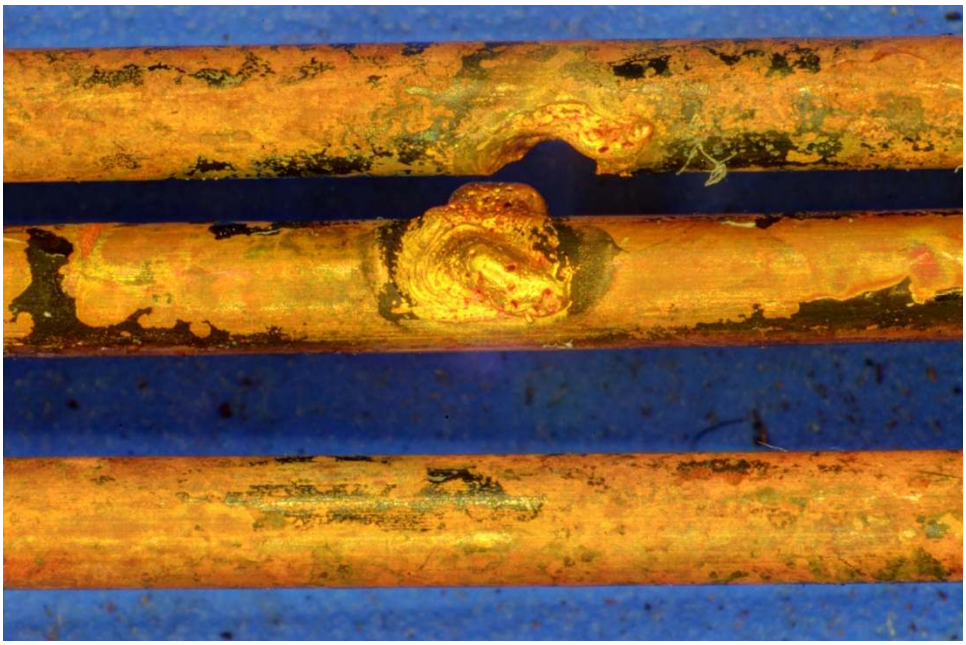

Figure 29 - Arc 3-2 from the tests of energized cables in a nitrogen environment (16x magnification).

Five test samples were examined using scanning electron microscope/energy dispersion spectroscopy (SEM/EDS) and high dynamic range (HDR) photography [48]. The SEM picture was recreated using the microscope and converted into an HDR photograph. The results of these actions are shown below, with a microscope photograph, HDR photograph, and SEM photograph of each arc presented for clarity.

Figure 30 - Arc 3-1 from the tests of energized cables in a nitrogen environment (27x magnification).

Figure 31 - Arc 3-2 from the tests of energized cables in a nitrogen environment (30x magnification).

Figure 32 - Arc 3-3 from the tests of energized cables in a nitrogen environment (33x magnification).

Figure 33 - Arc 3-6 from the tests of energized cables in a nitrogen environment (33x magnification).

These photographs show that the arcing damage created as a result of these tests is consistent with current descriptions of arcing damage presented in the literature and that all artifacts exhibited similar physical characteristics across the range of heat fluxes. All of the arc marks produced in these tests were easily identified as such by visual inspection. The microscopic and SEM analyses provided further proof of the

consistency in arcing damage and allowed further characterization of the arcing characteristics.

3.8 Variable Voltage Experiments

To test the dependence of the time-to-failure on the applied voltage, the voltage was varied between 0 and 140 VAC with the use of an autotransformer. A test apparatus identical to that used in the tests of energized cables was utilized for these tests, which were conducted at a constant heat flux (50kW/m^2). By conducting a minimum of two tests at each voltage, the time-to-failure was observed to vary with the applied voltage, the data of which is shown in Table 6.

Table 6 - Time-to-failure of energized cables under varying voltages.

Voltage (VAC)	Heat Flux kW/m^2	Time (s)	Arc? (Y/N)	Voltage (VAC)	Heat Flux kW/m^2	Time (s)	Arc? (Y/N)
140	50	190	Y	50	50	5263	N
140	50	150	Y	50	50	6275	N
140	50	155	Y	50	50	385	Y
120	50	276	Y	50	50	626	Y
120	50	162	Y	40	50	6299	Y
100	50	168	Y	40	50	1398	Y
100	50	239	Y	40	50	465	Y
100	50	145	Y	40	50	1263	Y
80	50	149	Y	30	50	1890	Y
80	50	214	Y	30	50	507	Y
80	50	383	Y	30	50	4231	N
60	50	469	Y	30	50	3427	Y
60	50	333	Y	30	50	6765	Y
60	50	387	Y	30	50	919	Y
60	50	311	Y	30	50	4736	Y
60	50	614	Y	20	50	10593	Y
60	50	260	Y	20	50	10868	N
50	50	7529	N	25	50	12859	N

It is can be seen from Table 6 that the applied voltage has an effect on the time-to-failure of the cables, where an increased voltage causes a decrease in time. The appearance of the cables after testing was similar to that of previous tests in which the insulation had charred. The damage caused by the arcing events exhibited varying characteristics across the voltage range. Above 60 VAC, the arc marks were consistent with descriptions of arcing damage presented in the literature and with the artifacts previously examined. Below 60 VAC, however, the arc marks occasionally had the appearance of melting. An example of this "melting" characteristic is shown in Figure 34. An interesting observation was made of tests at 60VAC, where significant sections of the cables were arced away, as seen in Figure 35. Further testing at lower voltages must be conducted to fully understand this behavior.

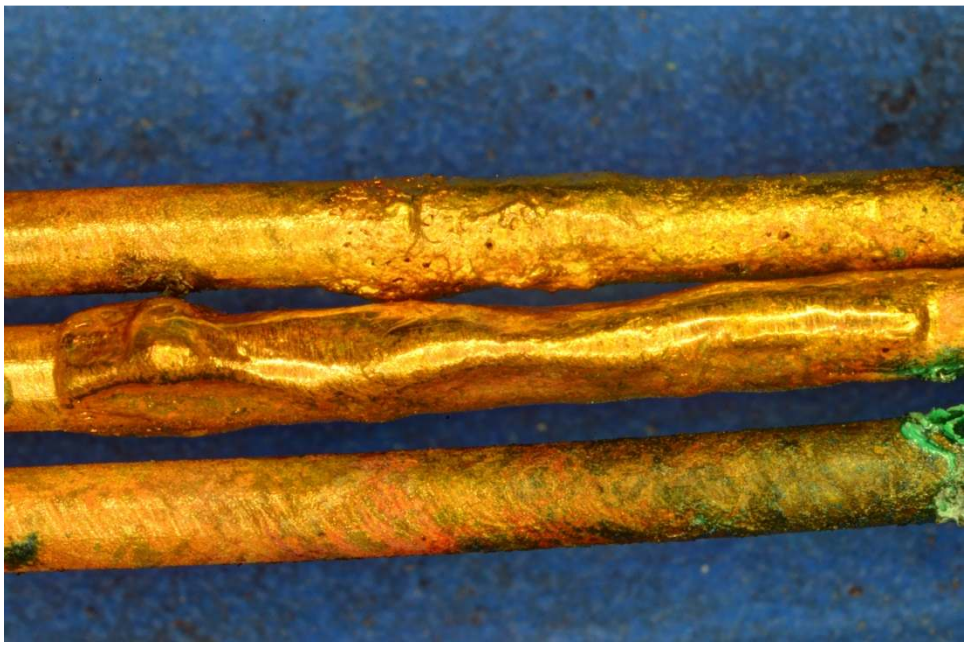

Figure 34 - Arc 20-1 produced during the variable voltage tests(12.5x magnification).

Figure 35 - Arc 60-2 of the variable voltage experiments. One square equals 2.5 cm (1 inch).

3.9 Failure Time Analysis

In an effort to analyze and predict the failure of an energized cable, the data collected was plotted as a function of one divided by the time-to-failure ($1/t_{fail}$). An 80% confidence interval was used to provide constraints on the reciprocal time prediction of cable failure.

For the tests in which no failure occurred, these times were summed with a single test that did fail, creating one data point that would represent several tests. This enabled every test to be considered a failure, with some tests exhibiting extended failure times. The reciprocal time-to-failure data for the test of energized cables in an ambient environment are shown in Figure 36. The raw data, which exhibited a linear appearance, was fitted with a linear trend line. The dashed lines represent the 80% confident interval used to provide constraints on the data.

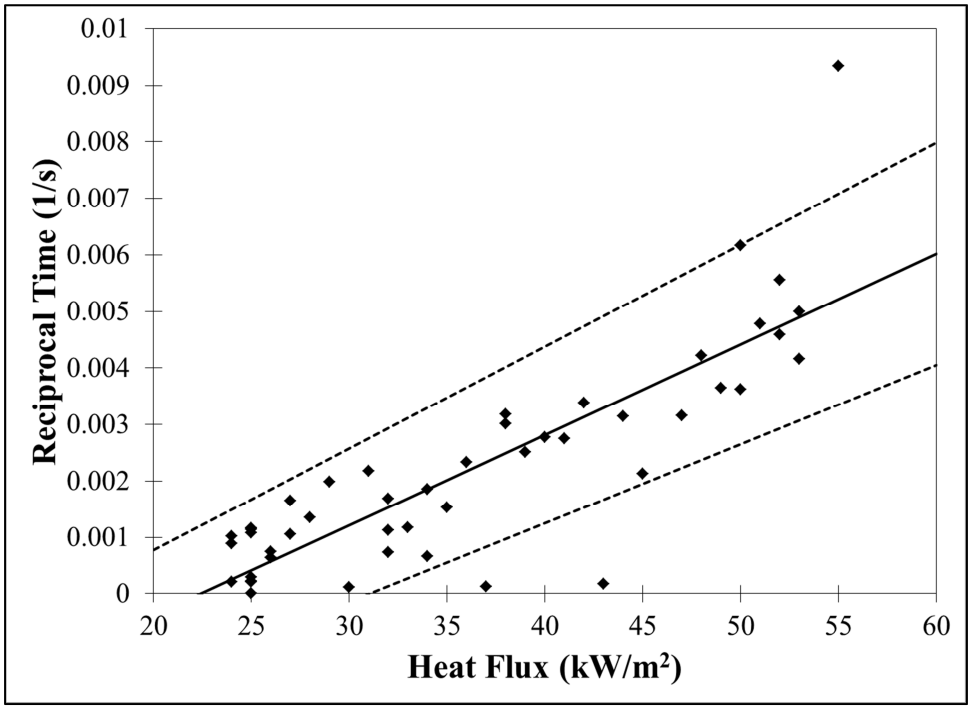

Figure 36 – Analysis of the reciprocal time-to-failure of energized cables.

Using the data from the tests of energized cables, an estimate of reciprocal time-to-failure can be made using the linear trend line presented in Figure 36. The linear trend line, expressed by Equation 3, suggests that a critical heat flux for this type of cable may exist at the point where it crosses the axis. This critical heat flux describes the minimum heating conditions required to induce a failure on the electrical cable, below which no failure will occur. The critical heat flux for this cable can be calculated using Equation 2, and is approximately 22 kW/m^2.

$$\frac{1}{t_{fail}[s]} = Heat\ Flux\ [kW/m^2] * (1.6 * 10^{-4}) - .0036 \qquad (2)$$

In order to find a criterion for failure of the unenergized cables, the data from this test series was compared to the linear trend line produced by Figure 36. In these plots the raw data for the reciprocal time-to-failure of the unenergized tests was plotted with the

linear trend line (Equation 2, represented by the solid line). The 80% confidence intervals were plotted using the dashed lines. A linear curve fit for each set of unenergized test data (50k, 30k, and 20k ohms) is used to show the linear trends of each data set, and is represented with a dotted line. The results of this analysis show that the 30k ohm failure criteria provide the closest match to that of the energized tests. These graphs of these comparisons are shown in Figures 37, 38, and 39. This may allow the use of unenergized tests to approximate the time-to-failure of an electrical cable, simplifying the testing procedure for future studies.

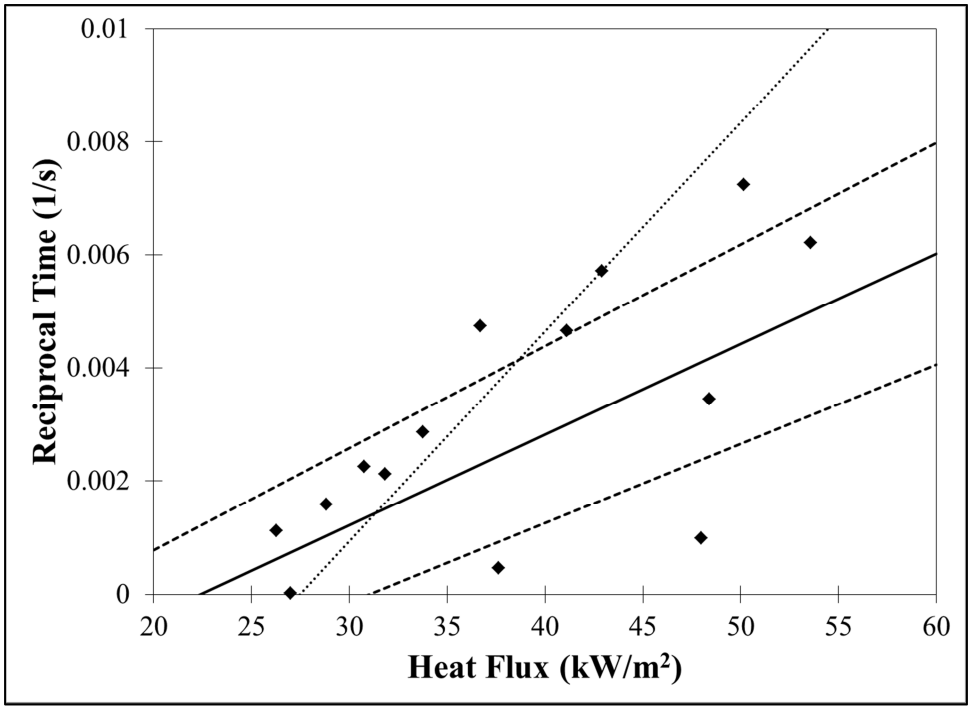

Figure 37 - Comparison of the 50k ohm unenergized test data to the linear data of produced from the tests of energized cables.

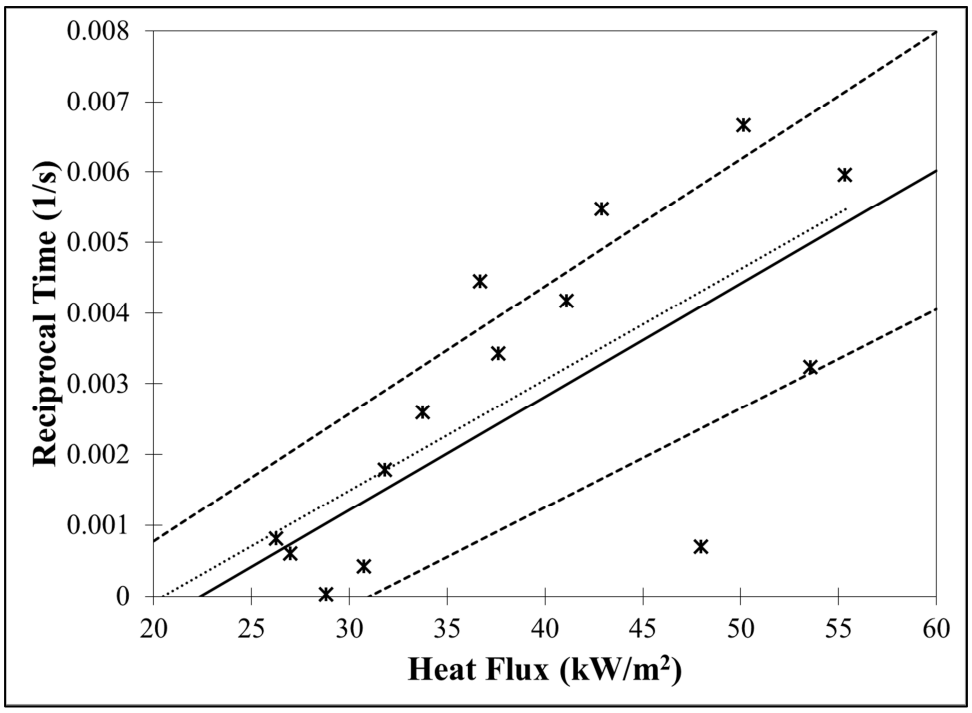

Figure 38 - Comparison of the 30k ohm unenergized test data to the linear data of produced from the tests of energized cables.

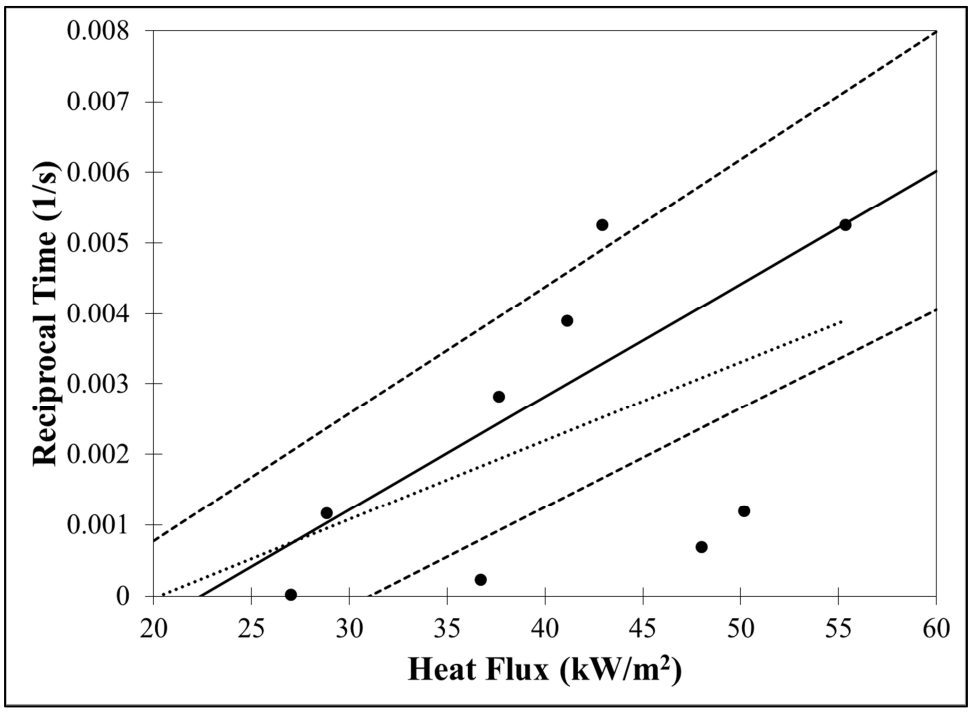

Figure 39 - Comparison of the 20k ohm unenergized test data to the linear data of produced from the tests of energized cables.

A comparison of the reciprocal time-to-failure data from the tests of cables in a reduced-oxygen environment to that of the energized tests in an ambient environment and was conducted in order to determine if similar failure times were encountered. As stated previously, the time-to-failure of tests in a reduced-oxygen environment was less than that observed in tests of energized cables in ambient conditions, which is further exemplified by Figure 40. The raw data for the reciprocal time to failure is plotted against the linear trend line of the energized test data (represented by the solid line) and the 80% confidence limits (represented by the dashed lines). It is possible that the char formed in ambient air is less conductive than that formed in an oxygen-deficient atmosphere, causing a longer time-to-failure. It is also possible that there was increased heat transfer from the walls of the chamber to the sample, causing a quicker failure time of the cable. Further testing in an oxygen-deficient environment is needed to fully understand this.

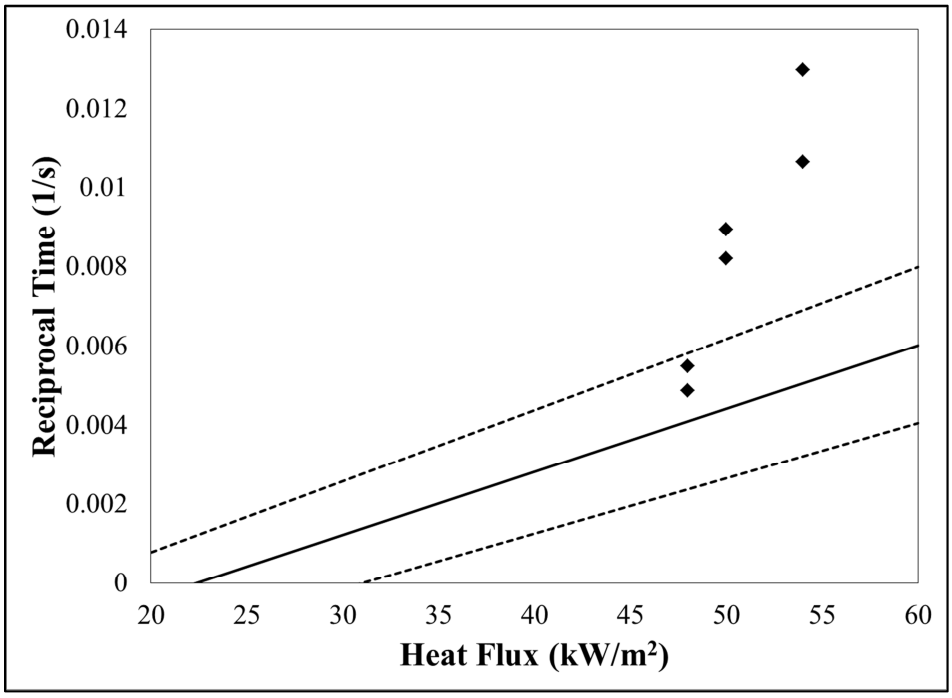

Figure 40 - The reciprocal time-to-failure of energized cables in a reduced-oxygen environment.

The frequency of the failure of an energized cable was estimated using both energized and unenergized (30k ohm) test data. To approximate this frequency, failure times were lumped into groups based on the heat flux at which the tests were conducted. For the energized tests, groups of 5 kW/m^2 were used. Due to the smaller amount of test data available, a grouping of 10 kW/m^2 was used for the unenergized tests. The frequency was calculated by taking the number of failures in each grouping and dividing by the sum of the test times. A plot of the frequency is shown in Figure 41. As a result of this the frequency of an electrical failure can be approximated using an exponential curve fit, described by Equation 3. The frequency is calculated in units of 1/s, and the heat flux represented in units of kW/m^2.

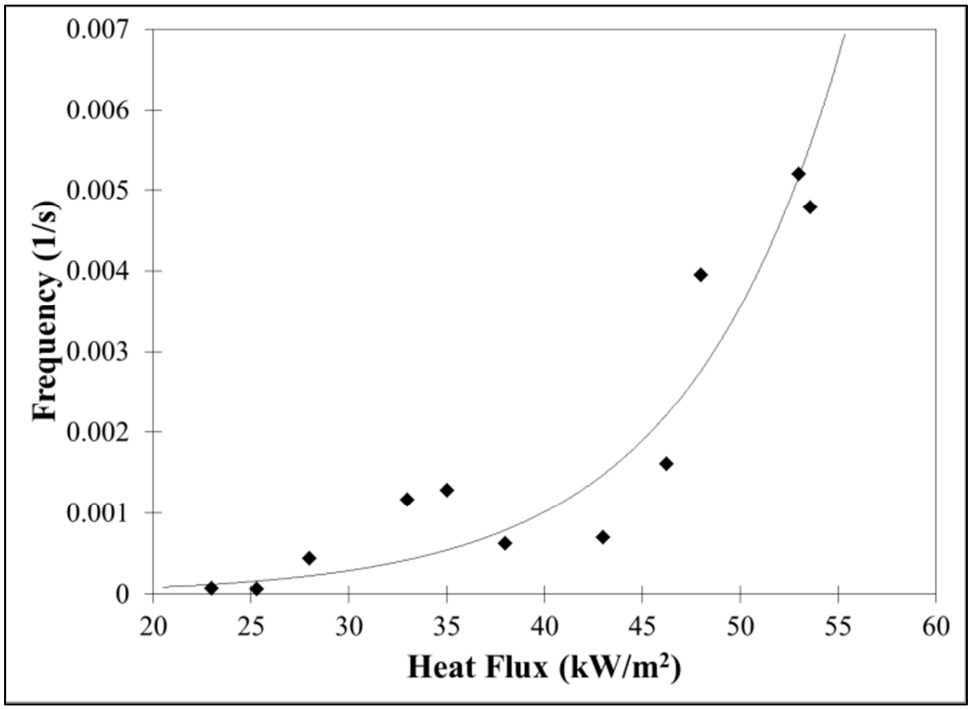

Figure 41 - The frequency of the overall failure of NM cable.

$$Frequency\ [1/s] = (7x10^{-6})e^{(.1253 * Heat\ Flux\ [kW/m^2])} \qquad (3)$$

3.10 Failure Mode

Two failure mechanisms were considered to determine how electrical arcs were formed on an electrical cable: thermal runaway and dielectric failure. The concept of thermal runaway has long been used to describe the arcing through char process. In this failure mode, as the insulating material chars and degrades, it starts to allow the passage of current. This current flow causes resistive heating of the char, further degrading the material, which in turn allows more current to flow. This process exhibits a growth in the current flow over time, which has been observed in tests of older cloth and rubber-insulated NM cables [52]. This growth in current can be seen in Figure 42, where small fluctuations in the current correspond with the fluctuations of the voltage, leading up to the arc on the cable.

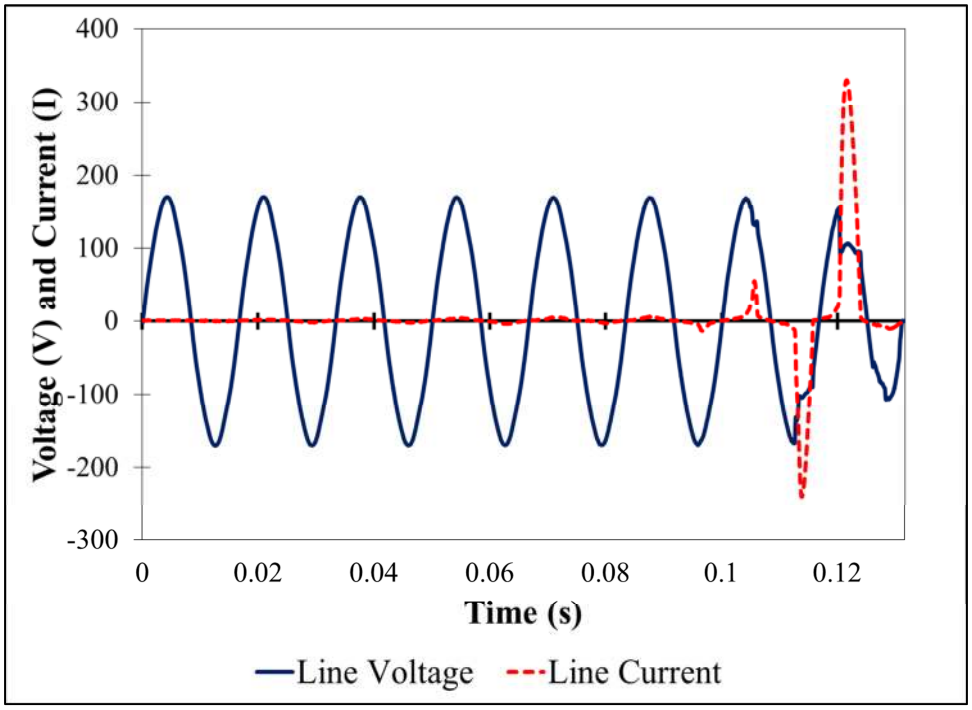

Figure 42 – Voltage and current waveforms produced by a cloth/rubber-insulated NM cable.

A dielectric failure is characterized by the nearly instantaneous failure of an insulating material, allowing an arc to propagate. In this case, the cable insulation is degraded to such a degree that the voltage present has the capability of arcing through the last bit of charred material. The dielectric strength of a material is highly dependent on the applied voltage. Babrauskas states that a typical "handbook value" for the dielectric strength of PVC is 350 MV/m [15]. These handbook values are often higher than what is actually found in real-world applications as the samples and test methods are tailored to obtain the best results. Tests of PVC wire formulations under conditions specified in ASTM D149 [53] have been found to produce results in the area of 24-36 MV/m.

The dependence of time on the applied voltage and the nearly instantaneous failure of the cables (as evidenced by the waveforms captured) together suggest the presence of a dielectric breakdown mechanism for the charred material left behind after thermal degradation of the cable insulation, which should have a lower dielectric threshold than that of PVC. The dielectric mode of failure is best portrayed by the current waveforms captured during these tests, in which the rise in current is nearly instantaneous (see Figures 43 and 44). The reciprocal time-to-failure can be seen in Figure 45, where the data exhibits a linear dependence on the applied voltage.

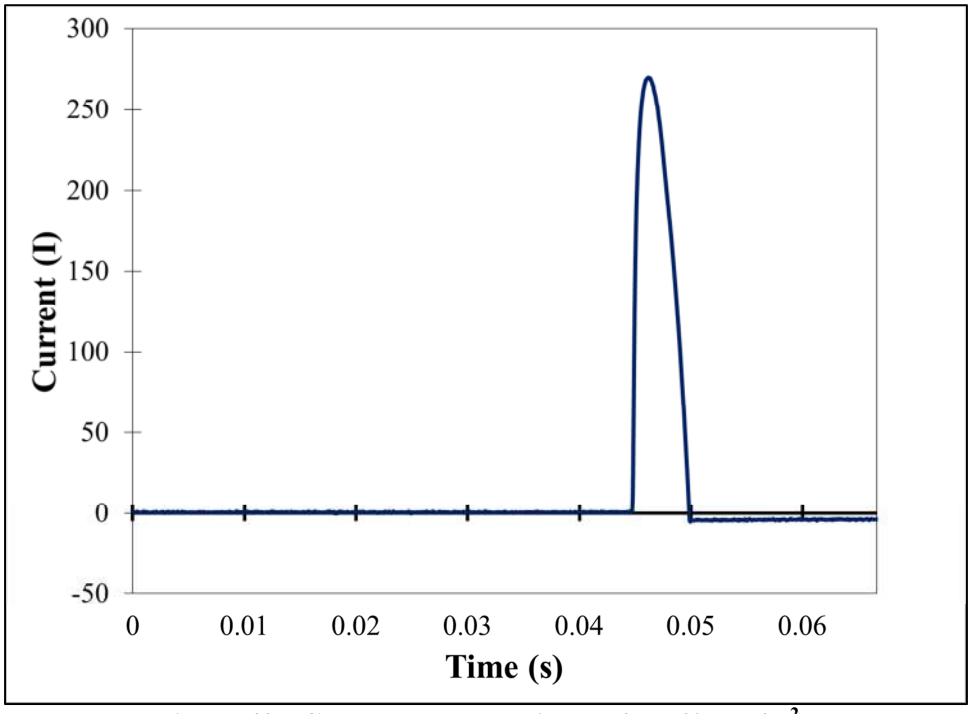

Figure 43 - Current produced in test 2-7 (49 kW/m^2).

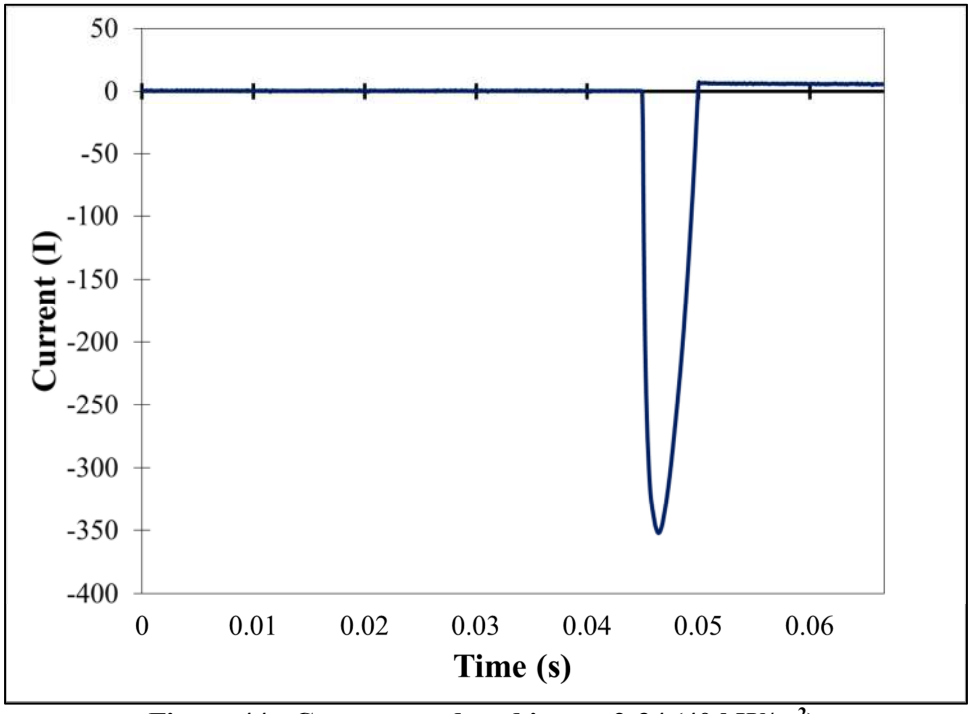

Figure 44 - Current produced in test 2-34 (40 kW/m^2).

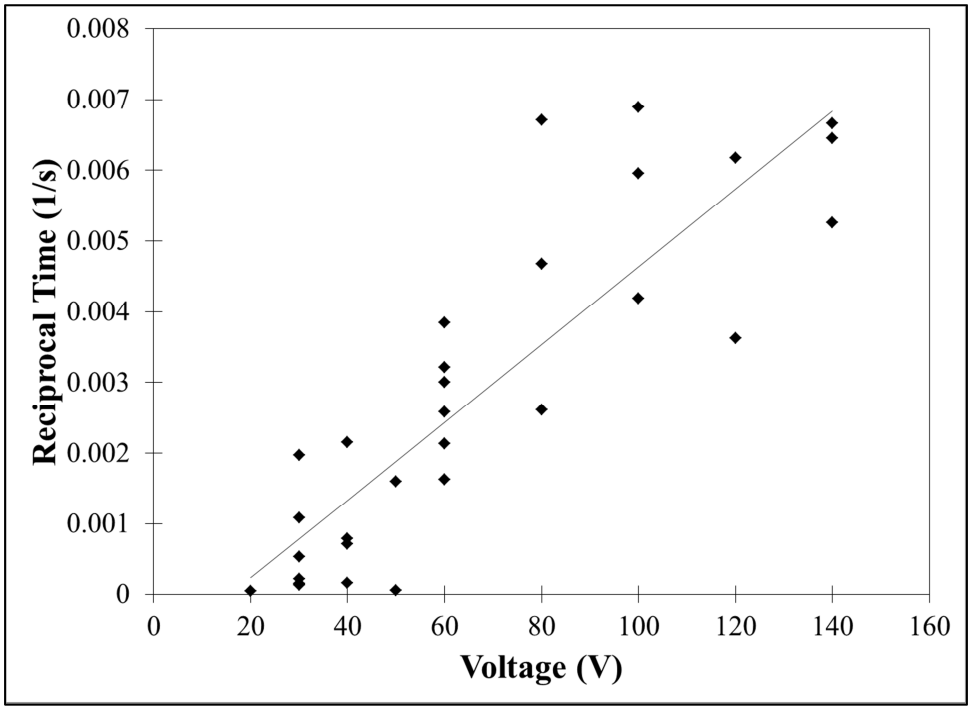

Figure 45 - The reciprocal time-to-failure of an energized cable as it relates to the applied voltage. The heat flux was kept constant at 50 kW/m^2 for all tests.

Thus, according to our hypothesis in which a dielectric failure mode causes the creation of an arc on an electrical cable, three conditions must be met:

1) The cable must be thermally degraded such that a significant fraction of the insulation is converted to char,
2) A sufficient temperature of the char must be reached, and
3) A sufficient voltage must be applied to the cable

This testing seems to rule out the concept of a thermal runaway as no buildup of current was observed as in the testing of older cloth/rubber insulated cables. Instead, a nearly instantaneous failure occurs in which the current jumps from zero to its maximum value in less than half a cycle. The absence of large reductions in resistance of the

insulation in the tests of unenergized cables support this theory, as the resistances reached would not produce current levels of sufficient magnitude to cause thermal runaway.

An equation of the approximate reciprocal time-to-failure can be derived from the linear curve fit of energized tests at 50 kW/m^2 (from Figure 45) is shown below in Equation 4. This reciprocal time-to-failure is dependent on the applied voltage, measured in volts.

$$\frac{1}{t_{fail\,[s]}} = Voltage[VAC, RMS] * (6 * 10^{-5}) - .0009 \qquad (4)$$

3.11 Thermakin Model

To aid in the understanding of the processes by which these cables fail, a computer pyrolysis model was used to find and estimate failure criteria. Developed at the Federal Aviation Administration (FAA), Thermakin is a one-dimensional model created to predict the behavior of materials experiencing thermal decomposition [54]. By solving energy and mass conservation equations, Thermakin can describe the transport of energy, chemical reactions, transportation of gases, and charring and intumescent behavior of materials exposed to external heat.

To perform these calculations, the material is broken up into components that have the ability to react both chemically and physically. The governing equations used in Thermakin are shown below:

$$\sum_{c}^{comp} \xi_c c_c \frac{\partial T}{\partial t} = \frac{\partial}{\partial x}\left(k_M \frac{\partial T}{\partial x} \right) + \sum_{r}^{reac} r_r h_r - \sum_{g}^{gases} J_g \frac{\partial}{\partial x}\left(\int_0^T c_g dT \right) + \alpha_M I \left(1 - \frac{\sigma T^4}{I_S} \right) \qquad (5)$$

$$\frac{\partial \xi_g}{\partial t} = \sum_{r}^{reac} \theta_r^g r_r - \frac{\partial J_g}{\partial x} \qquad (6)$$

$$r_r = A_r \exp\left(-\frac{E_r}{RT}\right)\xi_r \qquad (7)$$

$$J_g = -\rho_g \lambda_M \frac{\partial}{\partial x}\left(\frac{\xi_g}{\rho_g}\right) \qquad (8)$$

The first equation (Equation 5) is the energy conservation statement and Equation 6 represents the mass balance for any gaseous component. While second order reactions can be defined within the framework of Thermakin, Equation 7 represents the first order reaction rate, *r*. The gaseous mass flux of a component (J) is defined in Equation 8. Thermakin assumes that only gaseous components are mobile. This implies that for a liquid or solid component, the last right-hand-side term in the mass balance equation is zero [55].

In these equations, the variables ξ, *c* and ρ represent the concentration, heat capacity and density of any component used in the model. *T* is temperature; *t* is time; and *x* is the Cartesian coordinate used to denote the depth of the material. *h* is the heat of reaction and θ is a stoichiometric coefficient. This stoichiometric coefficient is negative when the corresponding component is a reactant and positive when it is a product. *A* and *E* are the Arrhenius parameters; and *R* is the gas constant. *k*, λ and α are thermal conductivity, gas transfer and radiation absorption coefficients, respectively. I_S is the flux of infrared radiation from an external source incident onto the material surface. *I* represents the flux of the radiation inside the material, which is computed using a generalized form of Beer-Lambert law and corrected for the material reflectivity. σ is the Stefan-Boltzmann constant. Subscript or superscript *g* is used to refer to a gaseous component; subscript *c* is used for all types of components (including gaseous). The

subscript *r* is used to refer to a reaction and the corresponding reactant. Subscript *M* indicates a property of a mixture (rather than that of an individual component).

In this analysis, Thermakin was used to model the rate of char formation within a pure PVC block under various heat fluxes. The time to reach a critical char fraction at various depths of the block was monitored. Assumptions made in this analysis included:

- The test sample was represented by a 4mm thick solid block of pure PVC
- No air gaps or paper wraps were present in this block
- The heat flux was constant
- No ignition of the cable occurred

In order to fully describe the materials used in the model, a components file (included in the appendix) is created. The components file for this simulation included the various "components" used to model the PVC block. These included pure PVC, intermediate forms of PVC, a PVC char, and two gaseous products of PVC. Thermakin allows the user to set the desired boundary conditions required for that simulation. For this analysis, it was assumed that the sample was initially at room temperature and was exposed to a constant heat flux. Natural convection was used with a convective heat transfer coefficient of 10 W/m^2k. At the bottom boundary there was no externally applied heat flux and natural convection was used with a convective heat transfer coefficient of 10 W/m^2k. These conditions closely simulated the tests performed under the radiant cone heater. The thermal and chemical properties for PVC were obtained from previous studies, and are included in the appendix [56]. A comparison of TGA data for a sample of PVC insulation obtained in this study and from this prior work is shown in Figure 46. The ambient temperature in these simulations was assumed to be 300K (27℃).

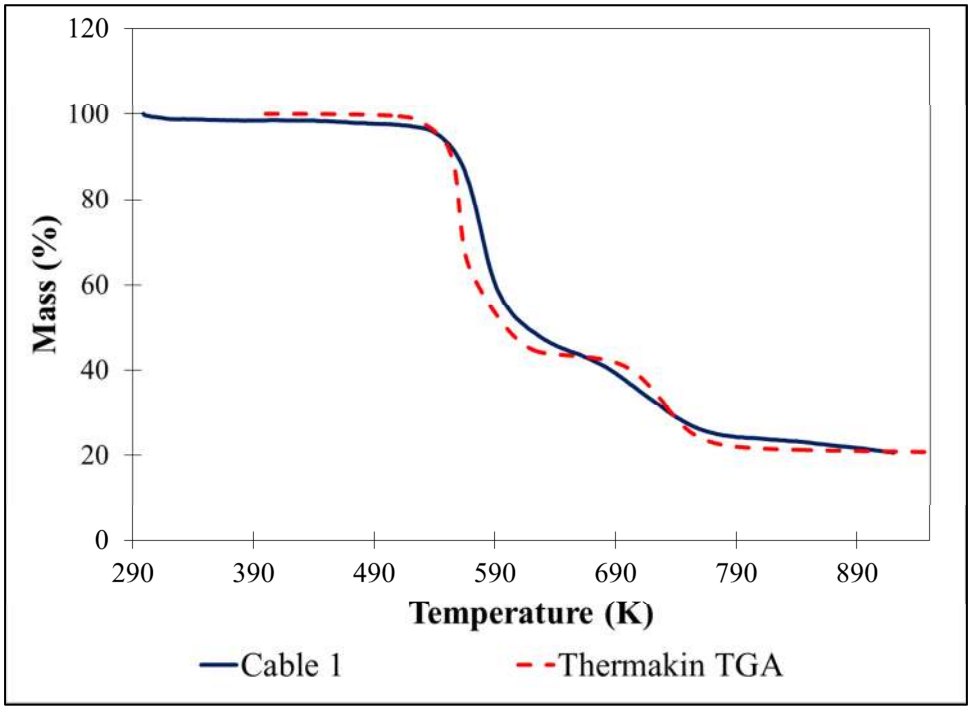

Figure 46 - A comparison of TGA data for wire insulation used in this study and a PVC sample used to obtain properties for the Thermakin model.

The variables that contributed to the failure of an electrical cable and the formation of an arc were considered, including the temperature and composition of the cable insulation at various depths. It was decided upon that the char fraction would provide a sufficient criterion for failure, which was calculated by dividing the concentration of char by the sum of the concentrations of solid, charred, and gaseous PVC. The concentrations of pure and charred PVC, the intermediate PVC constituents, and the gases produced by the degraded PVC were calculated by Thermakin. Char fractions of 10, 25, 50, 60, 70, 80 and 90 percent were used as failure criteria. Data was collected at depths of 1.03, 1.23, 1.43, 1.63, 1.83, and 2.03 mm below the top surface of the PVC block. A depth of 1.03 mm is approximately equivalent to the top of the wires within the cable assembly, while 2.03 mm is approximately in the middle of the two wires.

Using the data calculated by the Thermakin model, an reciprocal time analysis was conducted and compared with the data found from the energized tests. Based on this analysis, a 10% char fraction was found to produce results that closely matched those of the energized test data. Figure 49 (below) illustrates the agreement between these two analyses, which exhibit a similar linear slope. It was found that the concentration of pure PVC had dropped to zero by the time a 10% char fraction was reached, indicating that the PVC was either in a gaseous, charred, or intermediate form at the time of "failure." A temperature criterion was also required in order to characterize the cable failure, which was estimated to be between 200 and 250℃ based upon the preliminary tests discussed previously. The lowest temperature calculated by Thermakin at which a failure occurred was 384℃, far exceeding these temperatures.

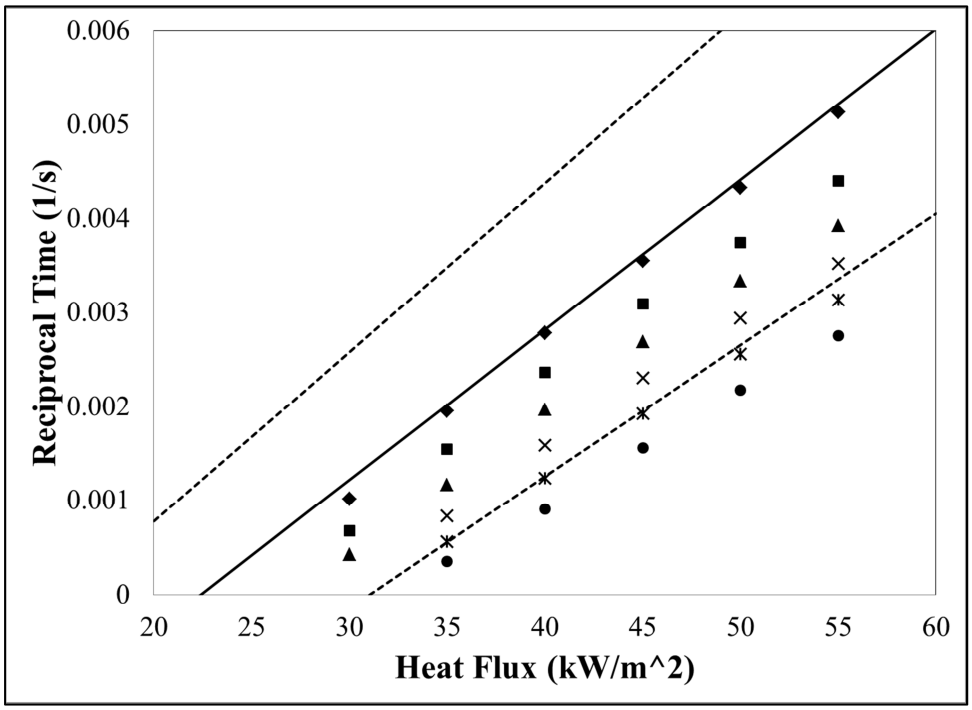

Figure 47 – Comparison of the Thermakin reciprocal time-to-failure and the linear regression data from the tests of energized cables.

3.11.1 Fire Scenario Analysis

In order to further explore the failure criteria created using Thermakin, the model was used to simulate fire conditions before and during flashover in a semi-realistic cable configuration. In the simulated environment, a PVC cable was installed above a ceiling made of gypsum board. Literature data reports that common upper layer gas temperatures at the onset of flashover are in the area of 600°C, which, using $T_{rad} = \sigma\varepsilon T^4$, would produce a radiant heat flux of 33 kW/m^2 at the ceiling. Average temperatures at the ceiling during flashover are approximately 1000°C, producing heat fluxes of nearly 150 kW/m^2.

With this data, Thermakin simulations were conducted at constant heat fluxes of 150, 100, 60, 50, and 33 kW/m^2 impinging on the ceiling, which were kept constant throughout the simulation. In this analysis, the worst-case conditions were simulated to find the fastest time at which a failure would occur. Under these conditions, the cable was laid flat on top of the gypsum board ceiling, which was 9.5 mm (3/8 inch) thick. It was assumed no air gaps existed between the cable and the gypsum board, providing the largest surface area for heat to be transferred. It should be noted that under normal circumstances electrical cables are mounted on a wooden framing member and are required by the NEC [44] to be offset from the gypsum board to prevent damage from fasteners such as nails or screws. It was assumed that the smoke in the upper gas layer was a perfect blackbody (i.e. $\varepsilon = 1$). A depth of 10.5 mm from the surface would correspond to the top surface of the wires within the cable package, while 11.5 mm would approximately be the middle of the cable package.

In this simulation the top boundary (i.e. the gypsum ceiling) was subjected to a constant heat flux without any convective heat transfer. Constant convective cooling took

place on the bottom boundary (the location of the PVC cable) with a convective heat transfer coefficient of 10 W/m^{2}k. The ambient temperature above the ceiling was 300K (27°C). The properties of the gypsum board were obtained from Karlsson and Quintiere [57]. The results of this analysis are shown in Table 7.

Table 7 - Time-to-failure during simulated "fire" conditions.

Depth from Top Surface (mm)	150 kW/m^2	100 kW/m^2	60 kW/m^2	50 kW/m^2
	Time (s)	Time (s)	Time (s)	Time (s)
10.4	380	505	836	1109
10.6	411	545	937	1295
10.8	438	587	1066	1564
11.0	466	634	1239	1964
11.2	496	690	1480	2601
11.4	529	756	1839	-
11.6	568	835	2414	-

Of special interest in this analysis are the times at which the earliest possible failure can occur. No failure was recorded over a one hour period at 33 kW/m^2. Heat fluxes of 150 kW/m^2 would have to be maintained for a minimum of 6.3 minutes (380 seconds) in order to induce a failure in the cable. Times of 8.4 minutes (505 seconds), 13.9 minutes (836 seconds), and 18.5 minutes (1109 seconds) are needed at heat fluxes of 100, 60, and 50 kW/m^2. These results suggest that under pre-flashover conditions (temperatures less than or equal to 600°C) arcing faults are highly unlikely to occur unless the ceiling or wall material has been breached. When flashover (temperatures greater than 600°C) has been reached, these conditions must be maintained for several minutes in order to induce a failure within the cable. At these conditions the gypsum

wallboard is also likely to fail, making it easier for these hot gases and flames to penetrate the wall or ceiling cavities.

3.12 Arcing Analysis

An investigation was conducted into the formation of the arc beads on the energized cables. As part of his analysis on arc mapping, Carey classified the recovered artifacts into several categories [58]. The arcs produced during testing were analyzed to determine if patterns could be found with respect to mass transfer between the wires and the waveforms produced during the arc. The arcing damage in this study was categorized using the following criteria:

- Bead
- Notch
- Bead within notch
- Notch with external bead
- Notch with internal and external beads
- Severed conductor

Each sample from the energized cables in ambient and nitrogen environments was inspected under a microscope to determine which of these characteristics were present. Only one characteristic was assigned to each wire. The result of this analysis is shown in Figure 48.

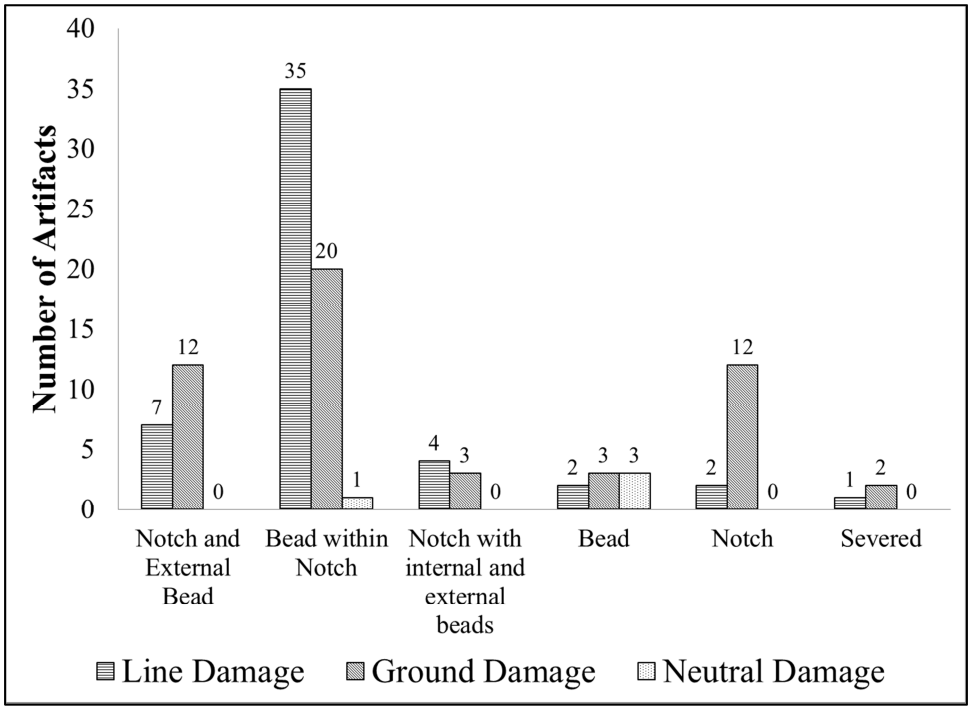

Figure 48 - Types of arcing damage observed on cable wires.

Based on the type of arcing damage, there is no clear pattern to determine whether mass is transferred from one conductor to another. The mass transfer from one energized conductor to another has been the subject of several studies [59], [60], [61]. During an arc, electrons move from the cathode to the anode while positive ions move from the anode to the cathode. Metal ions can only be transferred with the movement of atoms; therefore deposition can usually be seen on the cathode. In the case of alternating current, the anode and cathode change roles 60 times per second. If the arc is sustained over an even number of half-cycles, no net mass transfer should be observed. However, since the arcing in these tests often lasted for only half a cycle, a net mass transfer should be seen between the conductors.

The portion of the sine wave during which the arc occurs was also noted. Figure 49 shows that the majority of the arcs were initiated during the positive half of the sine

wave. On several occasions multiple "hits" or arc strokes were seen on the waveforms. While the arcs that contained multiple hits could be a "normal" occurrence, it is possible that they can be explained by the repeated abuse of the circuit breakers. As most circuit breakers are not manufactured to be used as switches or tripped multiple times, they can sustain damage that may affect their performance. It is believed that this is the case for several of the tests where long-term arcing waveforms were observed. The breakers were replaced if this type of behavior was observed, which reduced the occurrence of these events. From the current literature available, no pattern should exist as to the portion of the waveform at which the arc occurs.

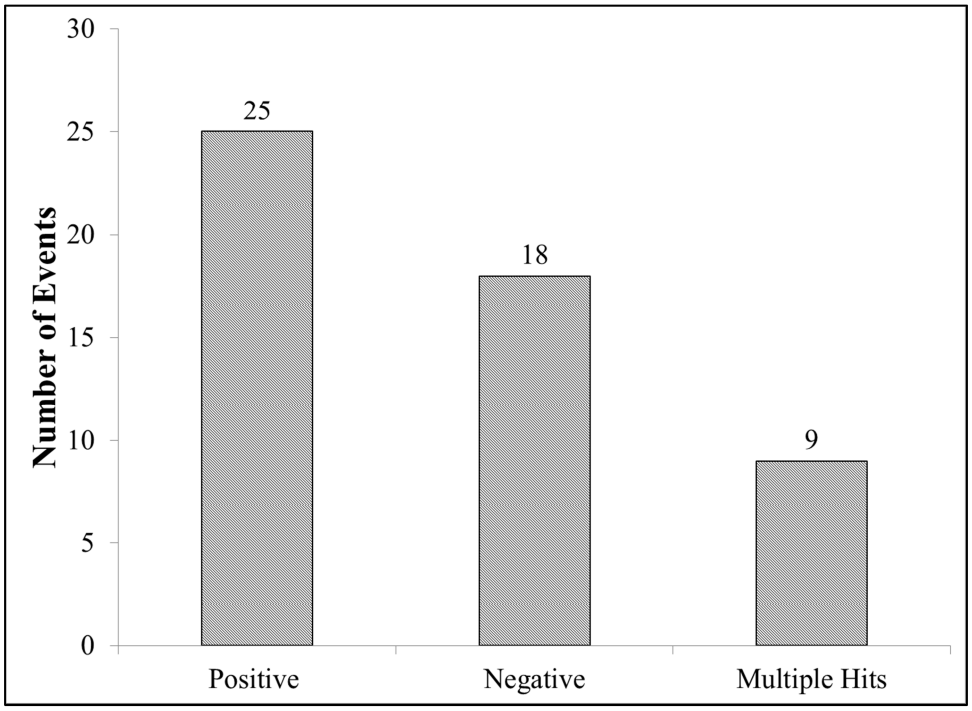

Figure 49 - Portion of the voltage sine wave where the arc was initiated.

The voltage at which the arc was initiated was observed to determine if a "threshold" voltage existed. Figure 50 shows the absolute value of the RMS voltages at which the arcing event started. The average value of these voltages is 112 VAC RMS. In

all tests the arc was found to initiate as the voltage was rising to its peak value, as can be seen in the graphs of the waveforms located in the appendix.

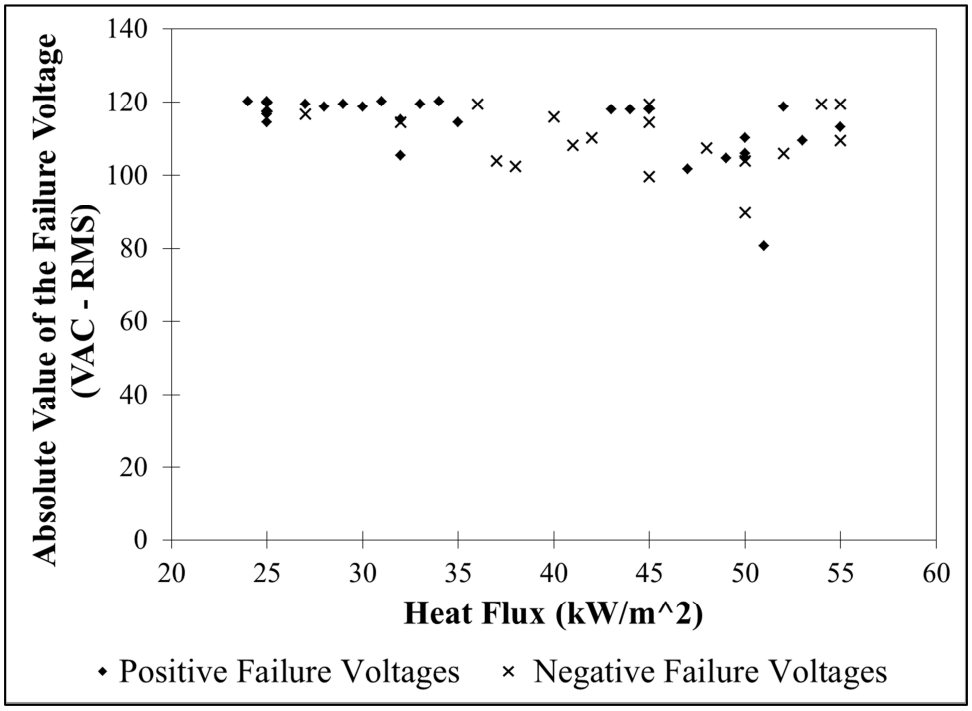

Figure 50 - Voltages at which the arc was initiated.

4. Cable Structure and Formula Variations

The data discussed previously was conducted using a single roll of cable, named Cable 1. A second roll of cable (Cable 2) of the same type and brand was purchased to determine if any variances existed between the failure times of different cables. The results of these tests revealed significant variations in the time-to-failure under similar conditions. These findings are important as they show the variability in the manufacture of a given product. Factors such as the chemical formulation of the insulation and the physical structure of the cable were investigated to determine what may be the cause of these variances.

In order to explore the differences that existed between these cables, energized tests were performed at heat fluxes of 55, 50, 45, 40 and 30 kW/m^2 with Cable 2. The

results of these tests are compared with the linear regression data of the previous energized tests (performed using Cable 1), as seen in Figure51.

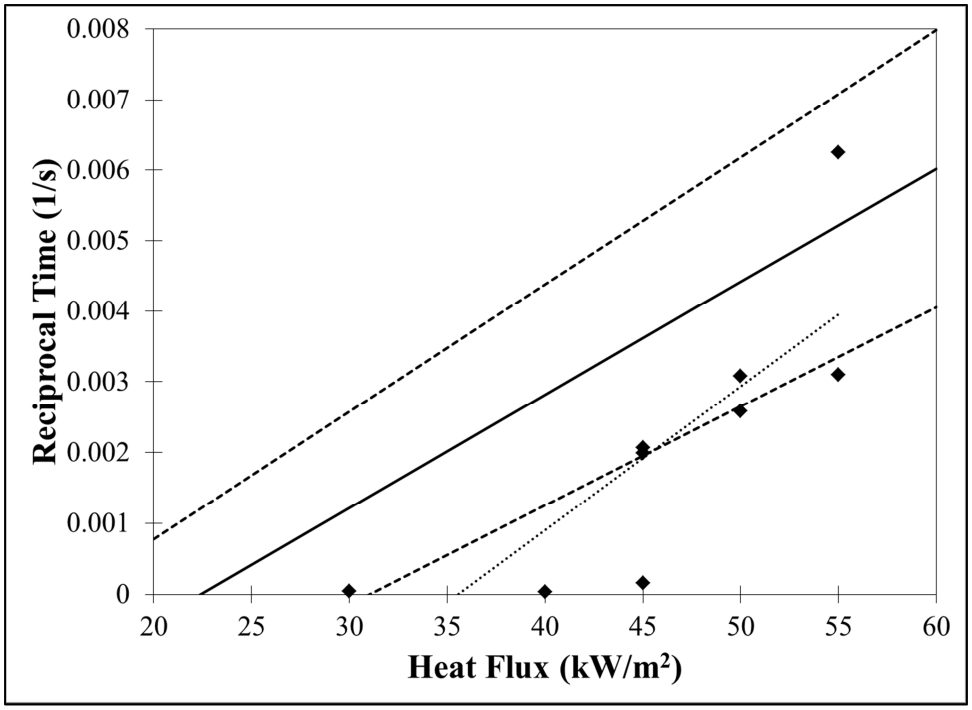

Figure 51 - The inverse failure time of Cable 2 compared to the linear regression from the energized tests of Cable 1.

Correspondence with the manufacturer confirmed no changes were made in the formulation of the cable or wire insulation. Despite this, differences may be due to slight defects or variations experienced during manufacture. To test the behavior of the PVC samples experiencing thermal decomposition, samples of the wire insulation were tested using thermogravimetric analysis (TGA). Tests were conducted on samples of the insulation stripped off of the neutral wire from each cable. The temperature of the TGA apparatus was increased from 300K (27℃) to 900K (627℃) at a rate of 10K per minute. The change in mass with respect to temperature for Cables 1 and 2 are shown in Figure 52. Data from both cables shows that while the degradation of the PVC is similar for both

samples over the temperature range presented, small variations exist that are unlikely to provide any explanation as to the differences in the time-to-failure.

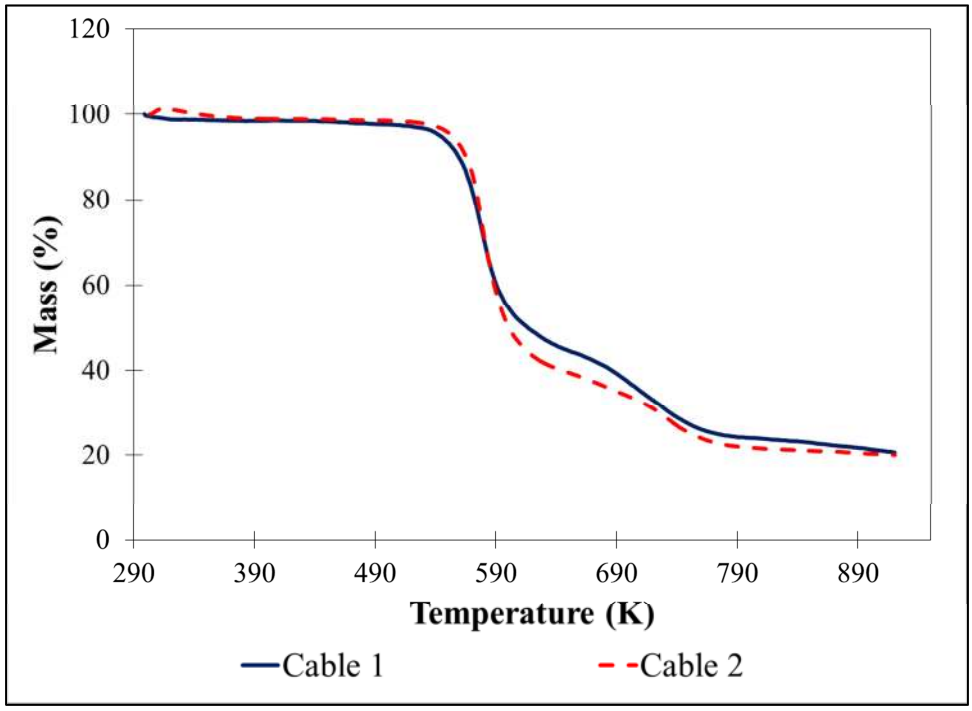

Figure 52 - Comparison of TGA data for two PVC samples.

The location of the paper sheath on the grounding wire was observed to change positions in each of the cables tested. In the "normal" or "ideal" manufacture of these cables, the grounding wire would be wrapped with paper, as shown in Figure 53. This wrapping is made up of one sheet of paper folded on either side along its length, creating a channel where the wire would sit. This forms one layer of paper on the underside and two layers on either side closest to the other wires. Figures 54 and 55 show this paper wrapping around the grounding conductor in the Cables 1 and 2, respectively. As evidenced in each of these photographs, as the position of the folds change the number of layers of paper insulation change. In Cable 1, there is only one layer of paper between the line and ground conductors. In Cable 2, this extra layer was on the "hot" or line side of the cable, putting three layers of paper between the line and grounding conductors.

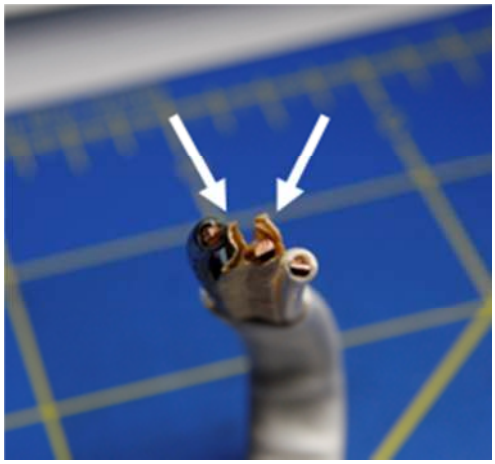

Figure 53 - Position of the paper sheath around the ground conductor in the “ideal” configuration. Note that there are two layers of paper on either side of the conductor.

Figure 54 – Position of the paper sheath around the ground conductor in Cable 1. Note that there is only one layer of paper on the side closest to the “hot” or line conductor (arrow).

Figure 55 - Position of the paper sheath around the ground conductor in Cable 2. Note that there are three layers of paper on the side closest to the "hot" or line conductor (arrow).

5. Conclusions

In order to study how fire environments can cause the failure of electrical cables, a testing strategy was developed that would induce the breakdown of PVC insulation by thermal and electrical means. To do this, tests were conducted on unenergized cables to measure the resistance of the insulation as it degrades, forming a set of criteria that was compared to data obtained later in the study. Tests were then conducted on energized cables in both ambient and reduced-oxygen environments to create electrical arcs on the cables and observe the arcing waveforms. The voltage was varied in another series of tests to explore the relationship between it and the time-to-failure of the cable. Based on experimental data of electrical cables, a one-dimensional pyrolysis model was used to develop failure criteria that can be extrapolated to various heating conditions. The failure of an electrical cable was found to be dependent on three factors: 1) the char produced during thermal degradation; 2) the temperature of the charred insulation; and 3) the voltage applied to the cable.

It was found that the time-to-failure of an electrical cable was directly related to the applied heat flux. This relationship shows that an increase in the applied heat flux will cause a decrease in the time-to-failure. An increase in the applied voltage of a cable will also cause the time-to-failure to decrease. Arcing was observed at voltages as low as 20 VAC (RMS) , and tests at lower voltages had the capability of producing arcing damage that resembled melting, evidenced by damage over a large (several millimeters) area. This type of damage is usually seen as a result of fire exposure. Tests conducted in a reduced-oxygen atmosphere exhibited shorter failure times than those conducted in an

ambient environment. The relationships between the applied voltage and ambient environment with the time-to-failure must be investigated further to gain a complete understanding of these phenomena.

The existence of a critical heat flux has also been discussed, suggesting that below this heat flux no failure will occur on an electrical cable. The Thermakin model aids in the prediction of this critical value, as well as the linear equation presented in Equation 2. This critical heat flux can be affected by many factors such as the absence or presence of a backing material and the heating conditions to which the cable is exposed to.

All arc beads created during these tests were identified as such based on a visual inspection of their physical appearance. This damage was consistent over the range of heat fluxes tested. A lack of oxygen was found to have no effect on the physical appearance of the arc beads when compared with those created in ambient environments. Microscopic and SEM analyses were used to confirm these observations.

The dependence of time on the applied voltage and the instantaneous rise in current suggest a dielectric failure mode. This precludes the concept of thermal runaway, where a gradual rise in current would be observed as the insulating material is thermally degraded. The results of this study provide insight into the role of electricity in fire investigations and lay the groundwork for further testing. A thorough and systematic analysis should be conducted in every fire investigation, and arc-fault mapping is an important tool that can and should be used in the investigation.

6. Future Work

While this study provides an indication of how and at what point an electrical cable can fail and lead to an electrical fault, there is still plenty of research to be done before a complete understanding can be reached. The use of different heat sources such as an open flame would provide further insight into the breakdown of the cable insulation and may provide a more realistic picture of fire damage. Also of investigative value are tests involving a longer span of cable, as this would replicate conditions found within a structure. As stated previously, the voltage applied to the cables and the environments in which the arcs are formed appear to play a role in the arcing process, however, they must still be investigated further to gain a complete understanding of their effects.

During the completion of this thesis, follow-up research was conducted at the ATF's Fire Research Laboratory to observe the effects of arc-fault circuit interrupters (AFCIs), ground-fault circuit interrupters (GFCIs), and thermal/magnetic breakers on the arcing waveforms, artifacts, and time-to-failure to determine if any differences existed. Ongoing research is being conducted on the differences between PVC-insulated cables and those insulated with cloth and rubber [52]. The ATF has plans to further explore the process and phenomena of arcing through char in order to provide a better understanding of it and its role in fire investigation and arc mapping.

The results of these tests reinforce the need for further testing. The testing completed in this study, while comprehensive in nature, is far too involved to characterize the behavior of different cables within a practical timeframe. To meet this need and reduce the amount of time required to gain a general understanding of the behavior of electrical cables under fire conditions, a revised test method is proposed here.

In this method, a test setup identical to that used in the testing of energized cables is required. The cable samples are placed under the cone heater for one to two hours based on a time criterion chosen by the researcher. Tests should be conducted at heat fluxes of 55, 50, 45, 40, 35, 30, and 25 kW/m^2 using a radiant heat source. Data should be collected using a power analyzer in order to capture the electrical waveforms created during arcing events. Three tests should be conducted at each heat flux in order to provide a statistical data set for the cable over this range of heating conditions. After each set of three tests (i.e. each time the heat flux is changed), the circuit breaker should be replaced to avoid over-stressing the breaker and obtaining erroneous results.

As it was unknown how many tests would need to be conducted in order to fully characterize this cable, tests were conducted at one to two kW/m^2 increments. This proposed method allows the researcher to perform a defined number of tests over a range of heat fluxes. This reduces the number of total tests necessary and eliminates the "guesswork" as to how the tests should be conducted.

7. Appendix

7.1 Arcing Artifacts – Energized Cables in an Ambient Environment

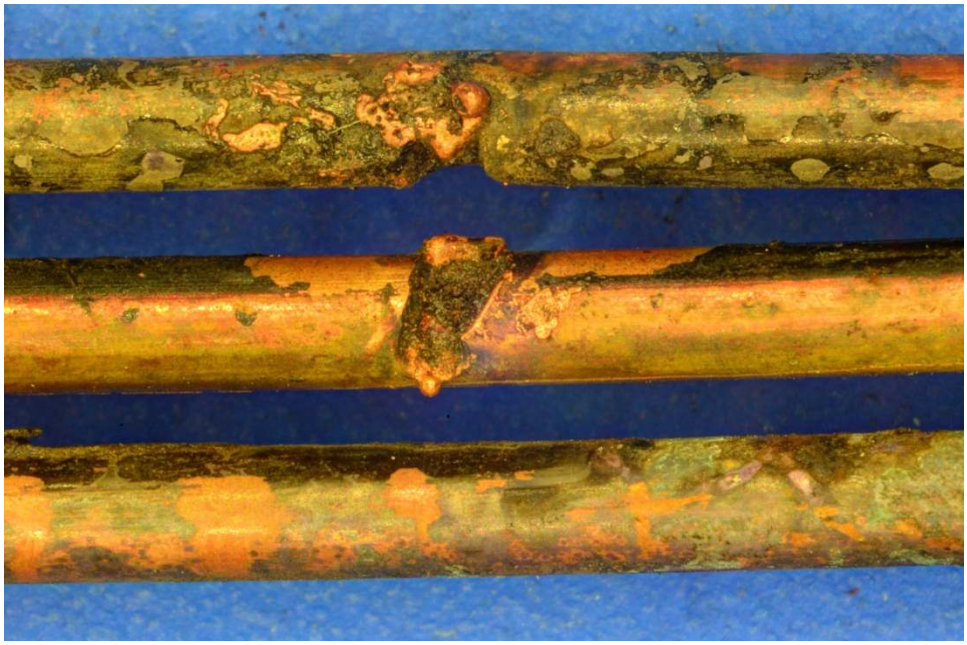

Figure 56 - Arc 2-4 (16x magnification)

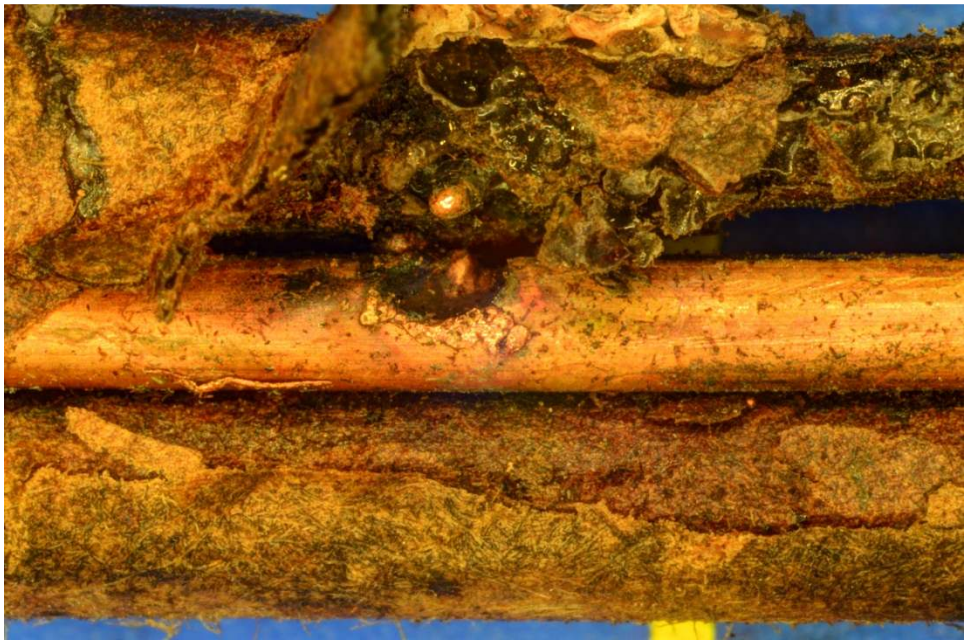

Figure 57 - Arc 2-5 (16x magnification)

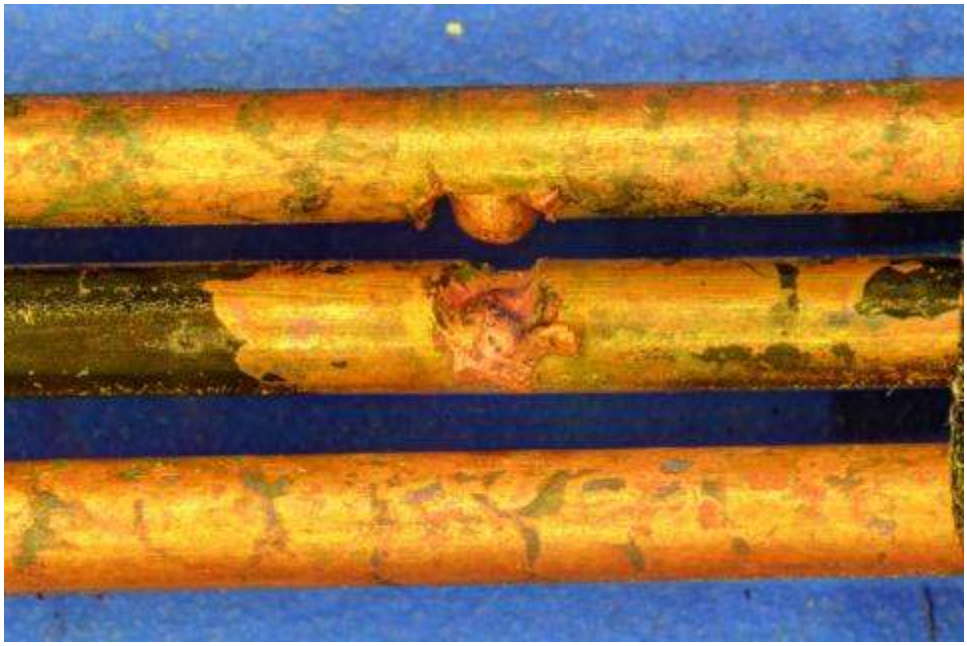

Figure 58 - Arc 2-6 (16x magnification)

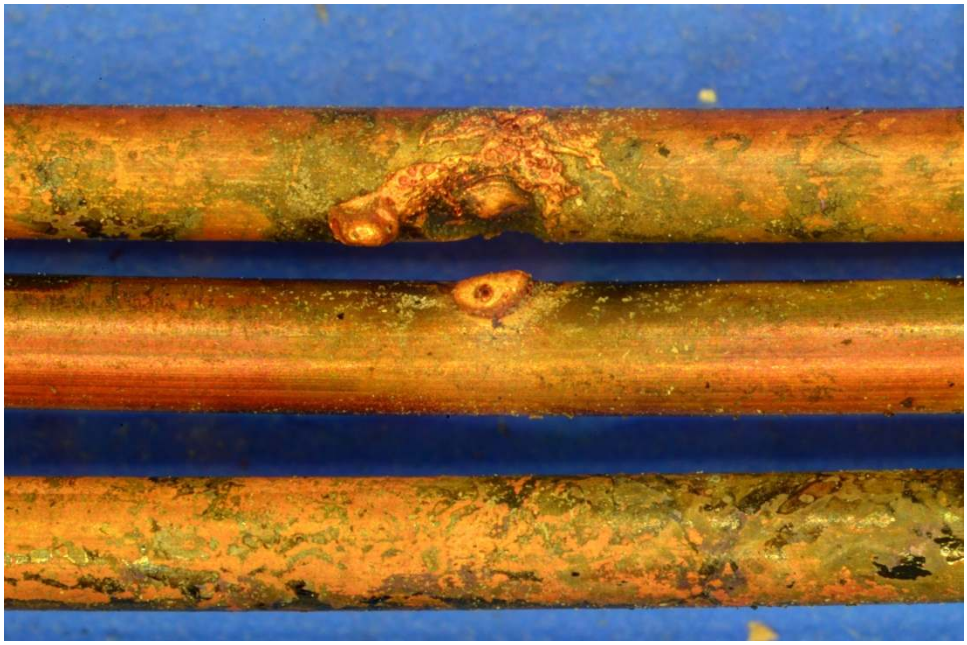

Figure 59 - Arc 2-7 (16x magnification)

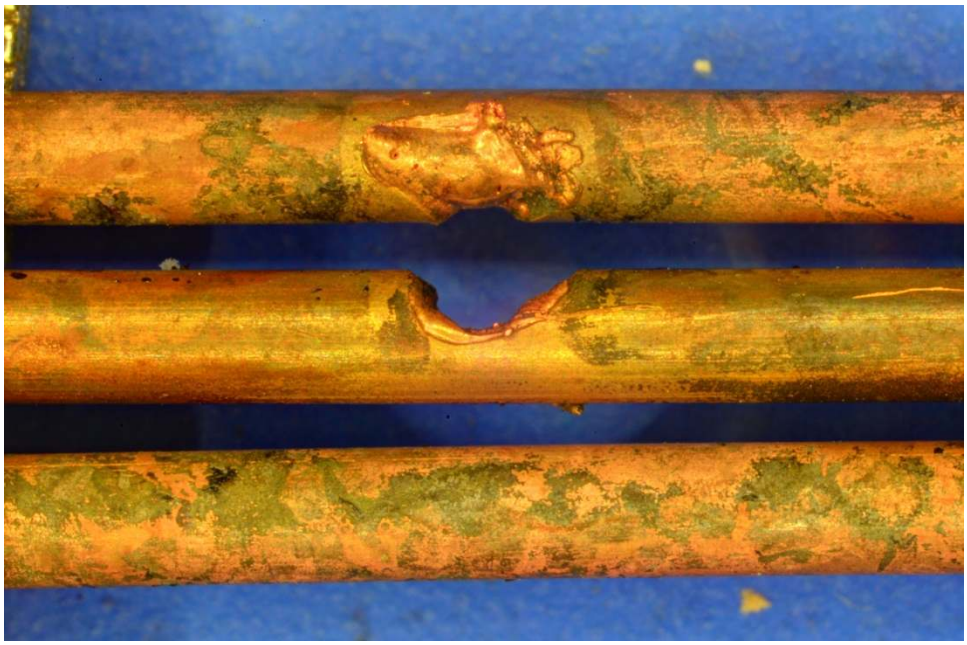

Figure 60 - Arc 2-8 (16x magnification)

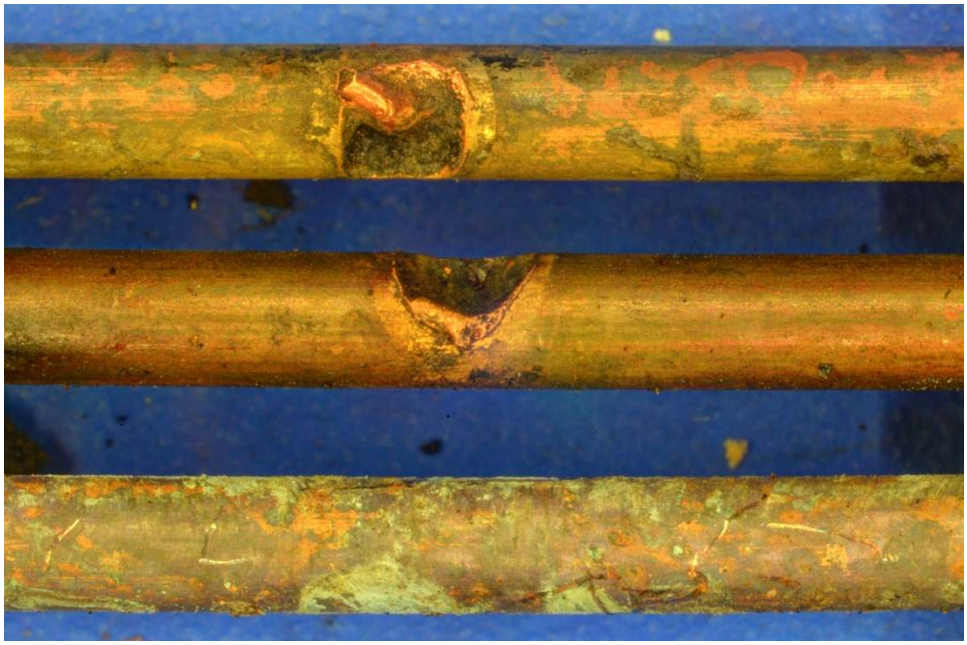

Figure 61 - Arc 2-9 (16x magnification)

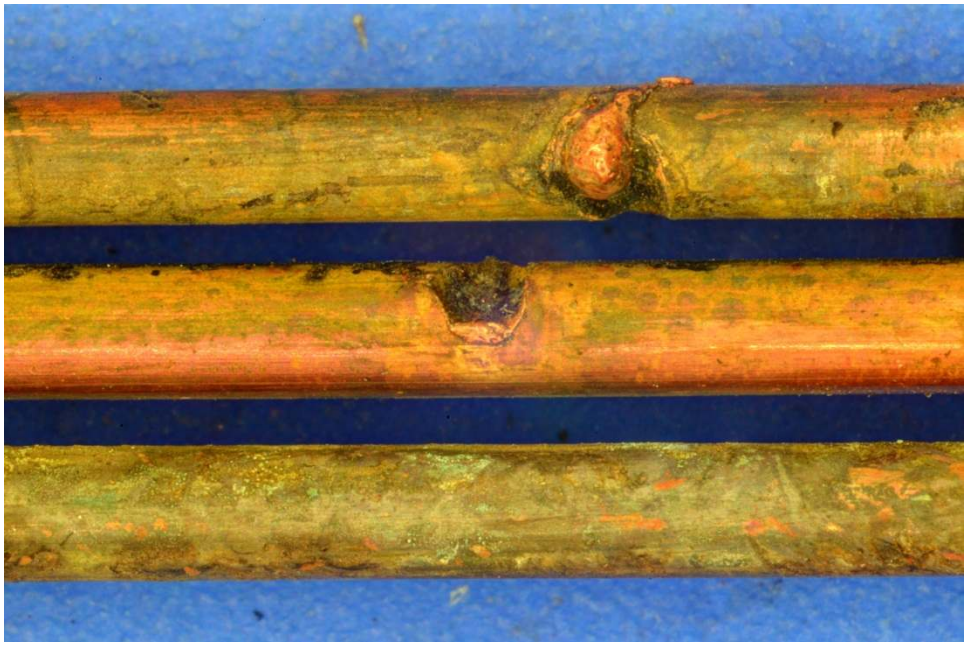

Figure 62 - Arc 2-11 (16x magnification)

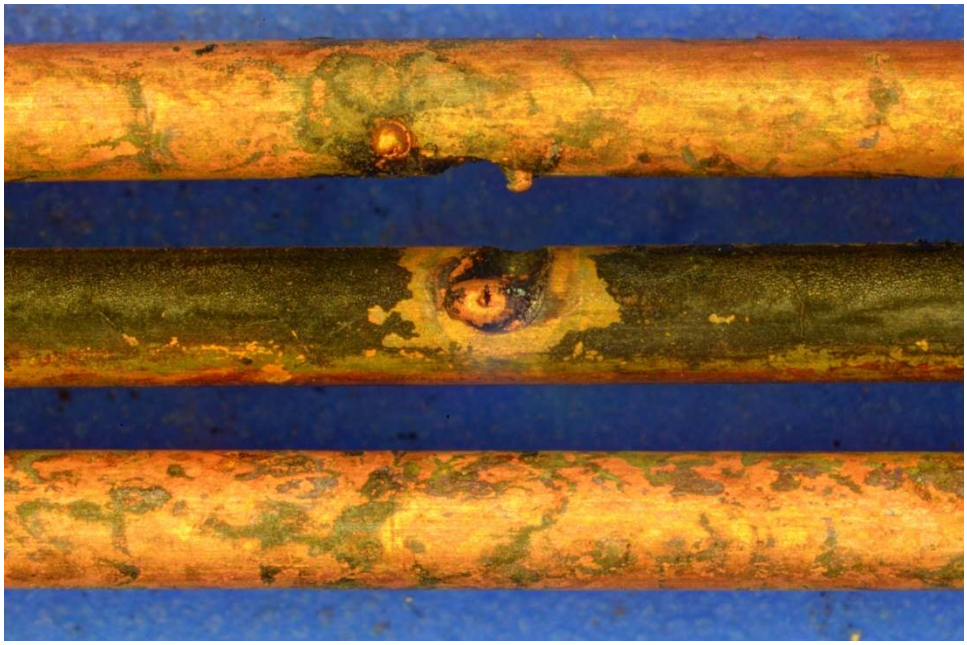

Figure 63 - Arc 2-12 (16x magnification)

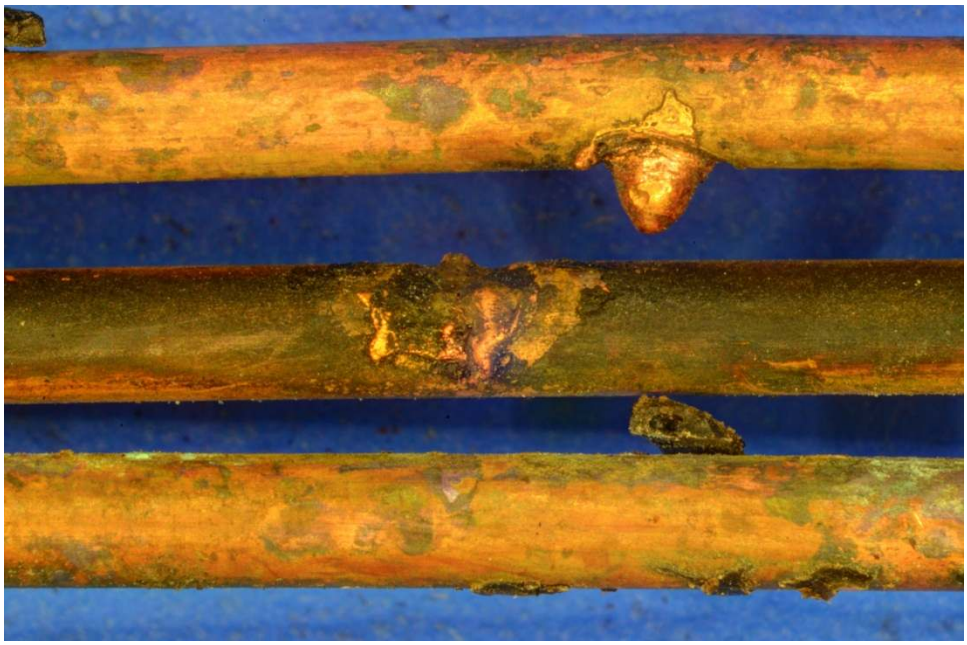

Figure 64 - Arc 2-13 (16x magnification)

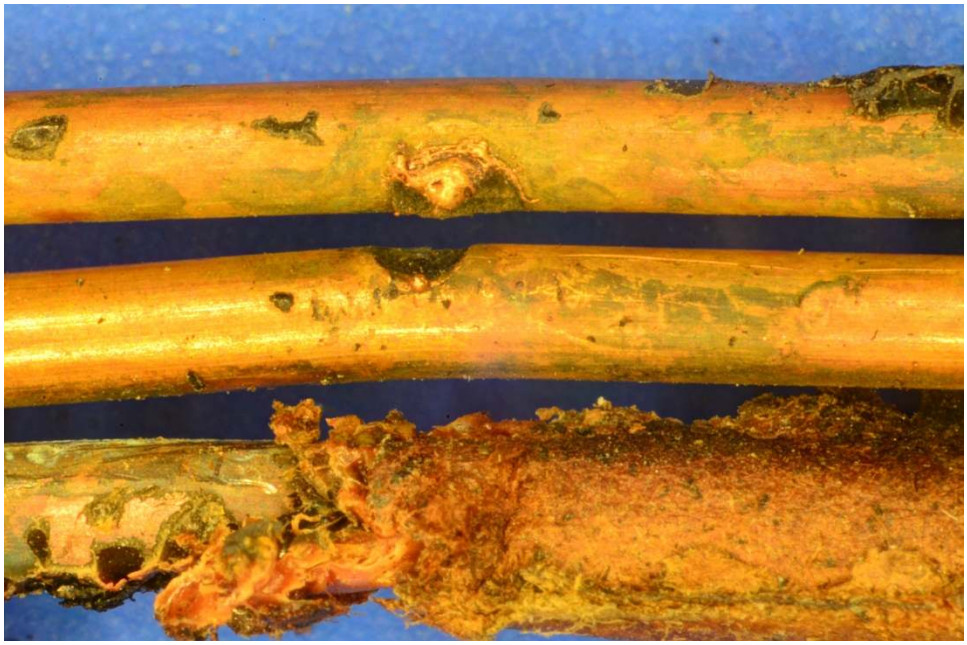

Figure 65 - Arc 2-14 (16x magnification)

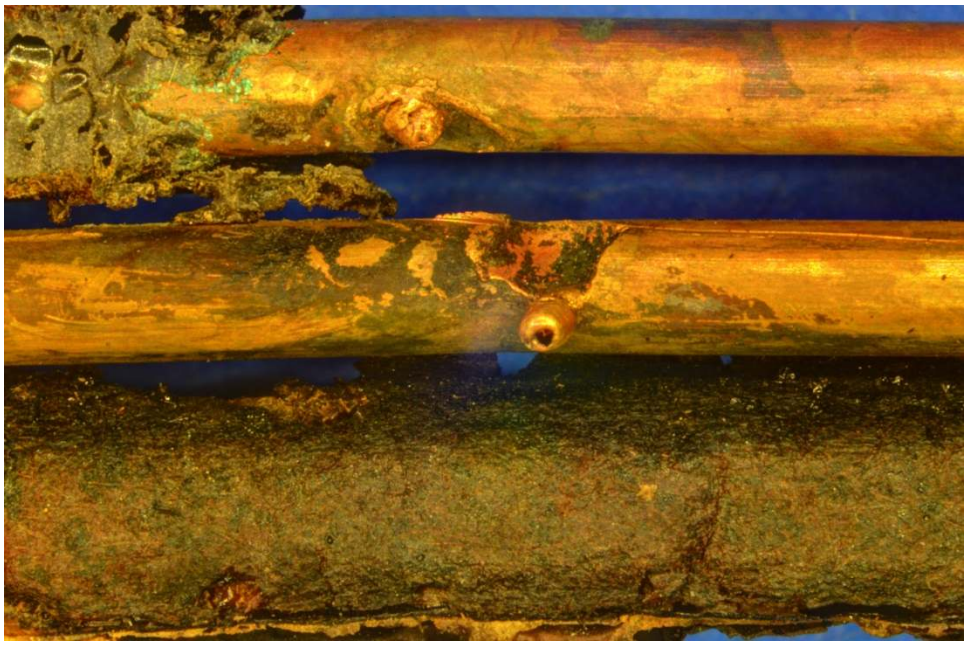

Figure 66 - Arc 2-15 (16x magnification)

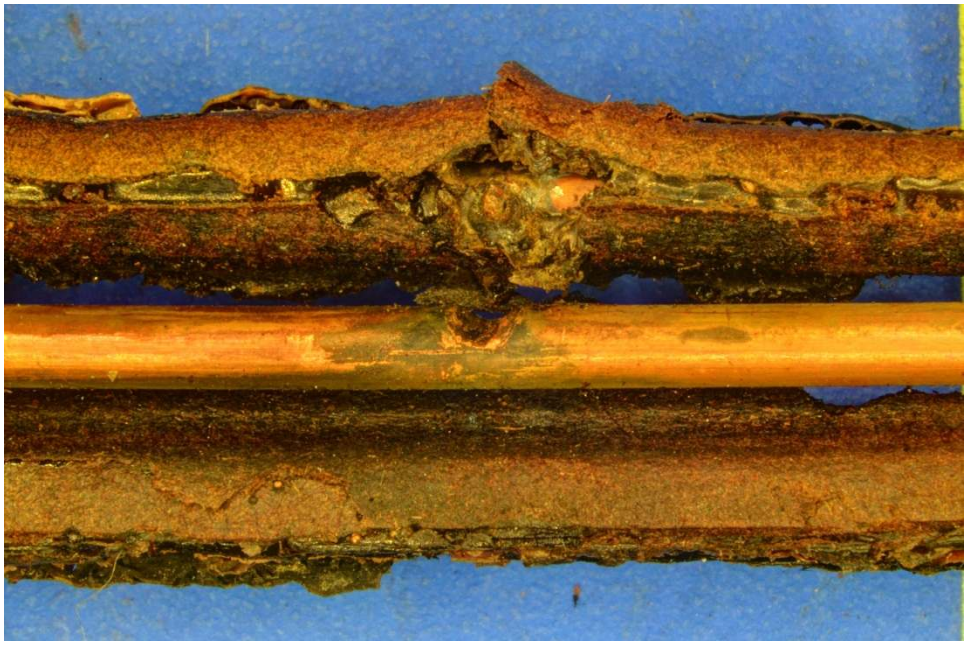

Figure 67 - Arc 2-16 (16x magnification)

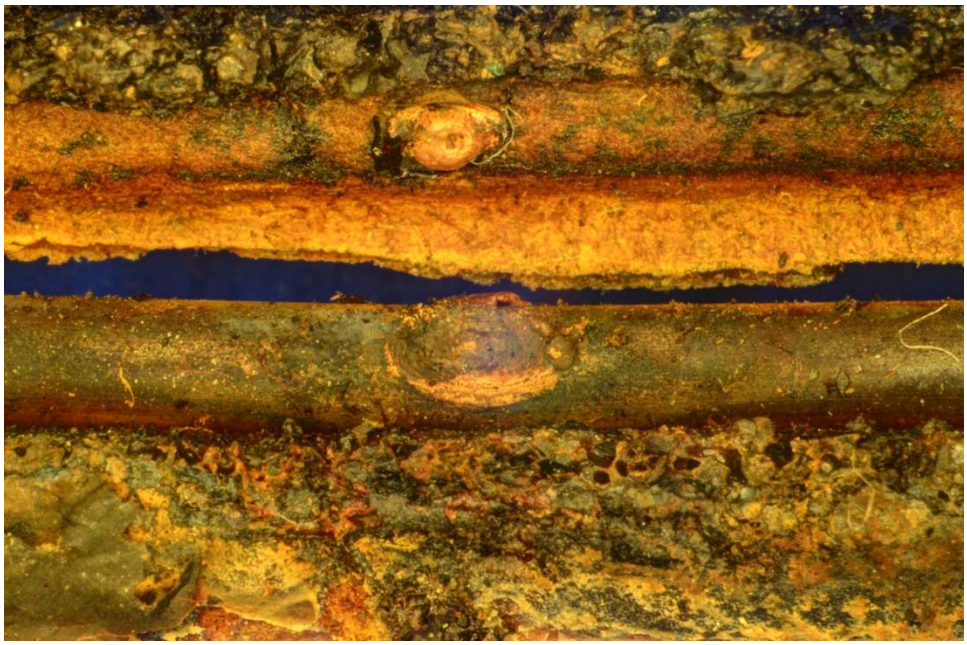

Figure 68 - Arc 2-17 (16x magnification)

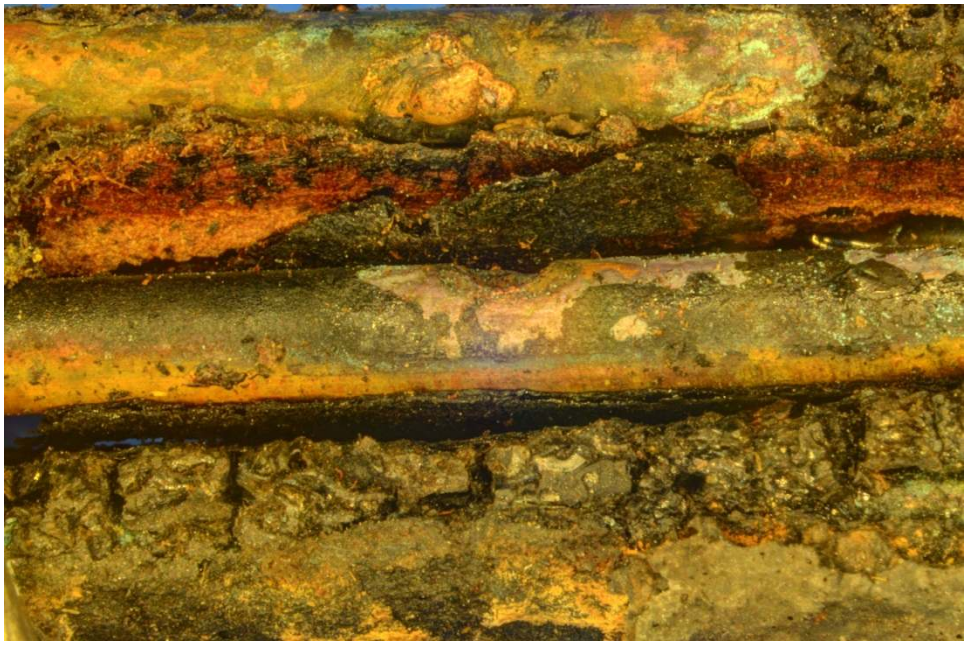

Figure 69 - Arc 2-18 (16x magnification)

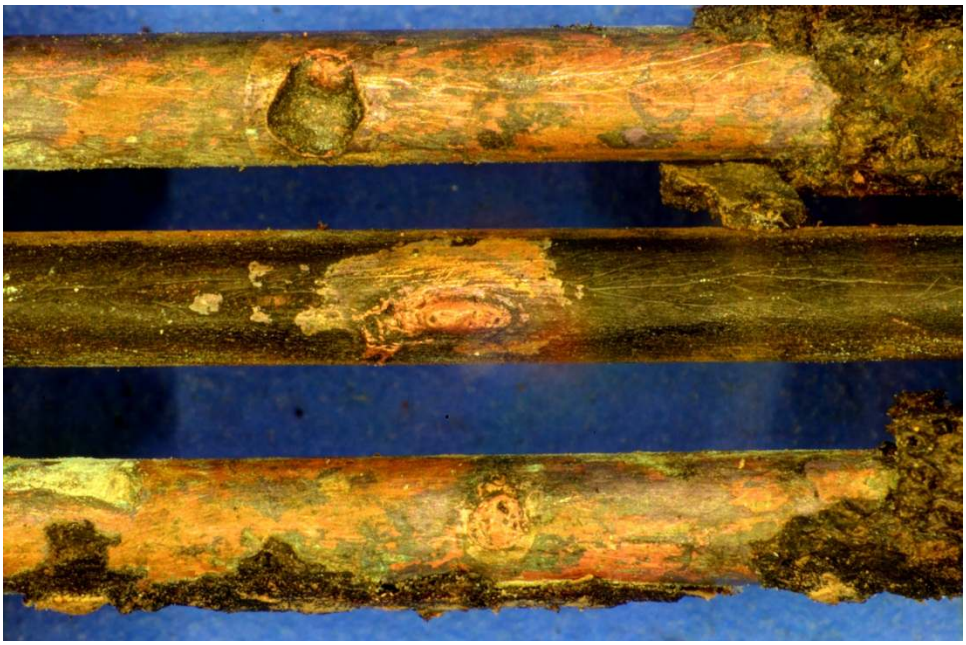

Figure 70 - Arc 2-20 (16x magnification)

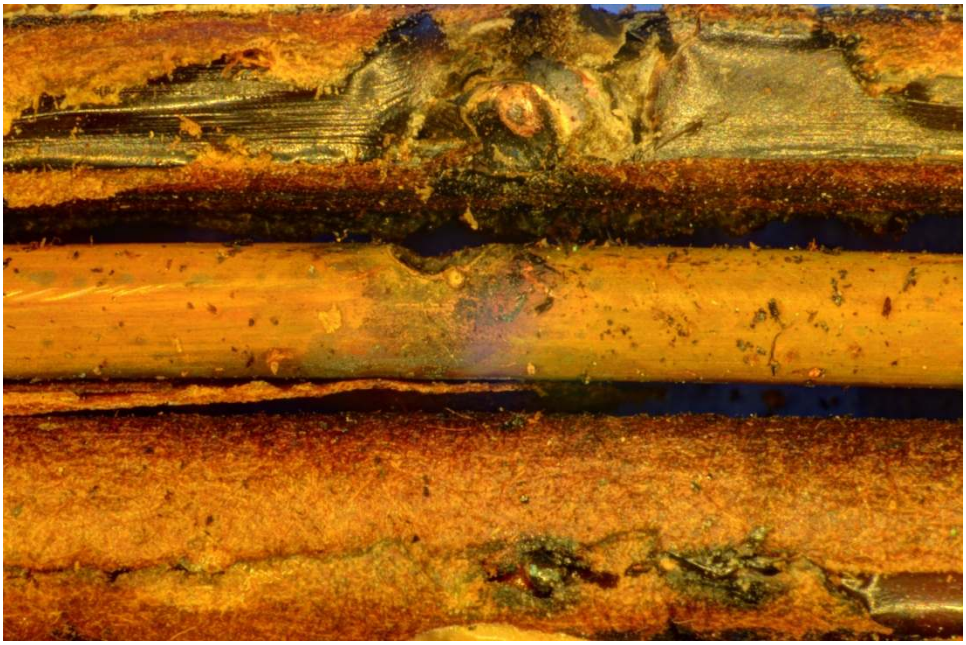

Figure 71 - Arc 2-21 (16x magnification)

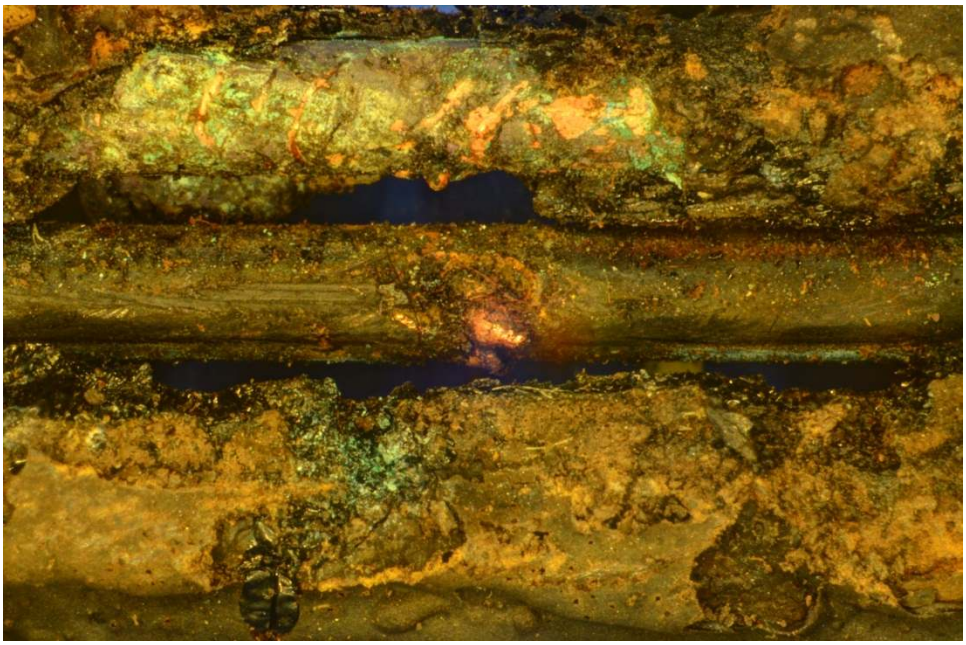

Figure 72 - Arc 2-23 (16x magnification)

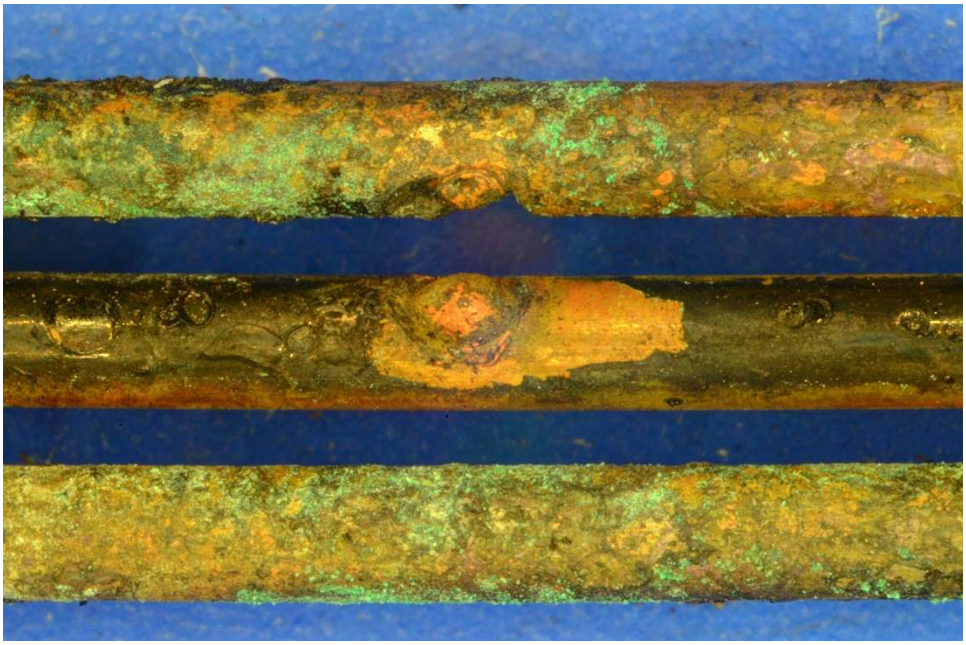

Figure 73 - Arc 2-26 (16x magnification)

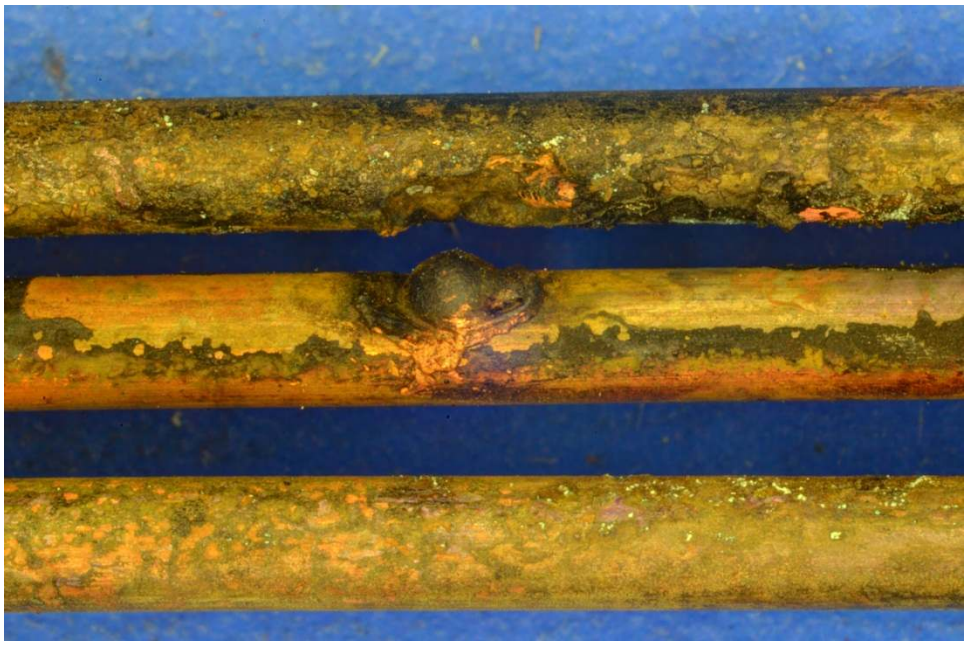

Figure 74 - Arc 2-27 (16x magnification)

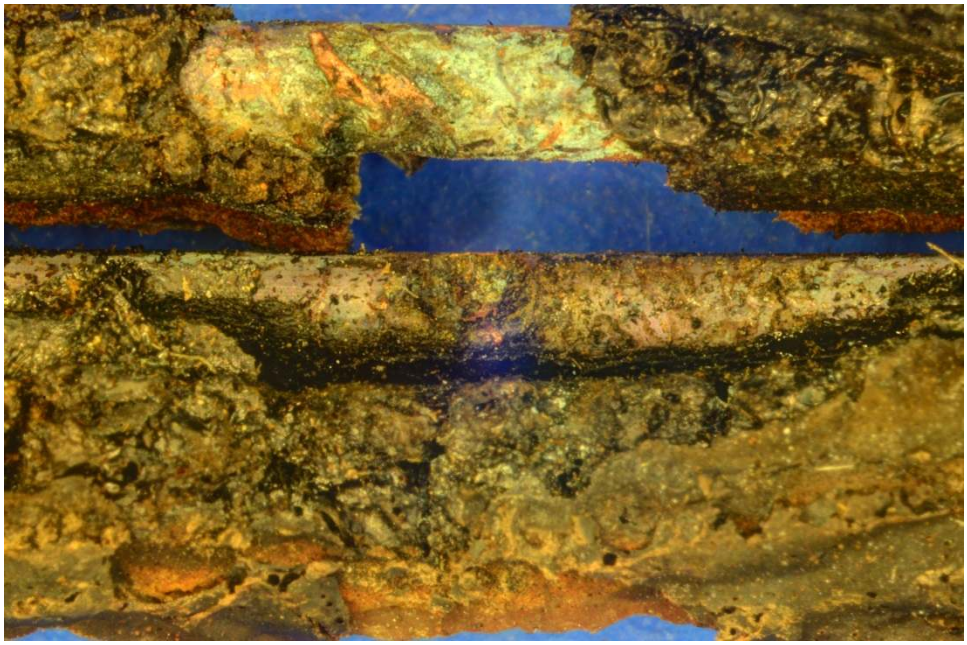

Figure 75 - Arc 2-28 (16x magnification)

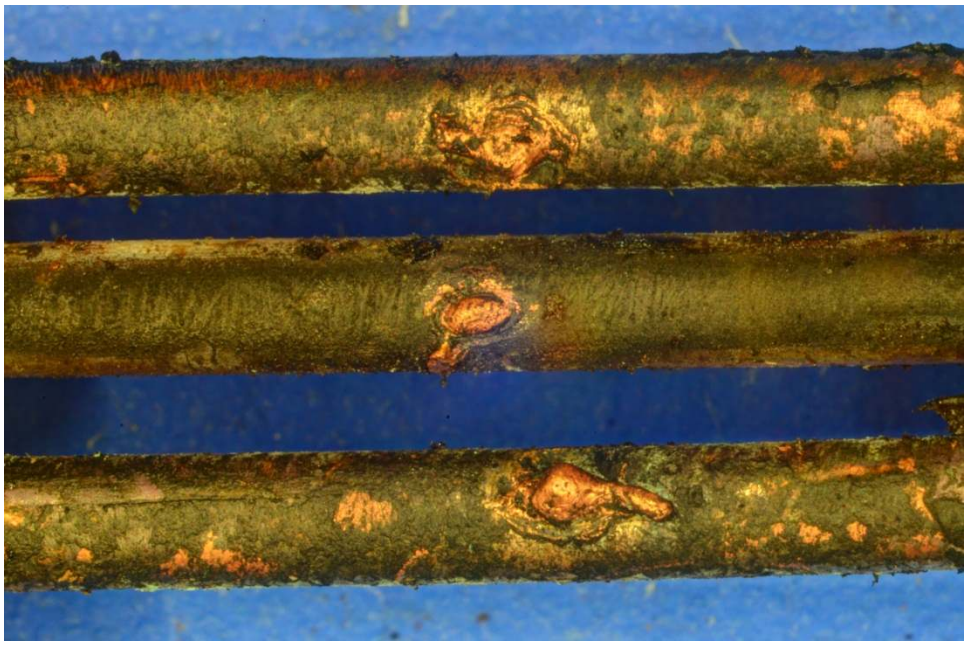

Figure 76 - Arc 2-29 (16x magnification)

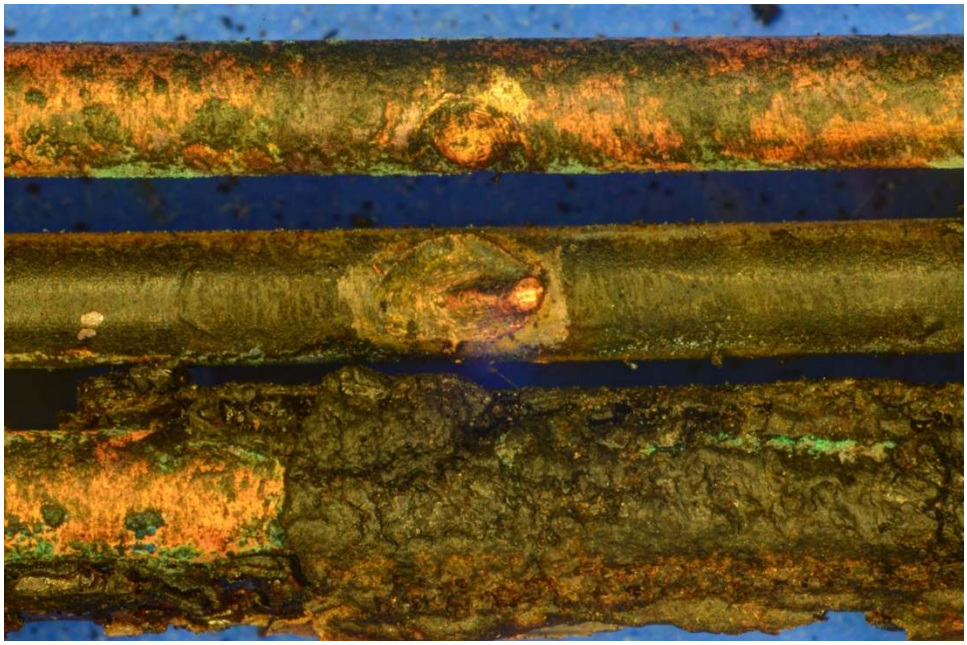

Figure 77 - Arc 2-30 (16x magnification)

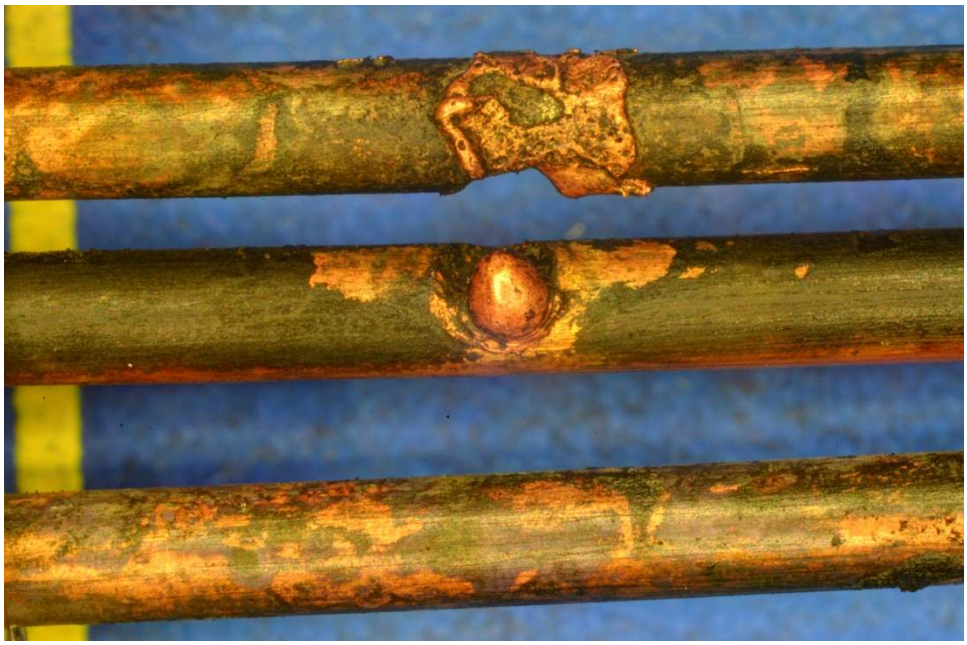

Figure 78 - Arc 2-34 (16x magnification)

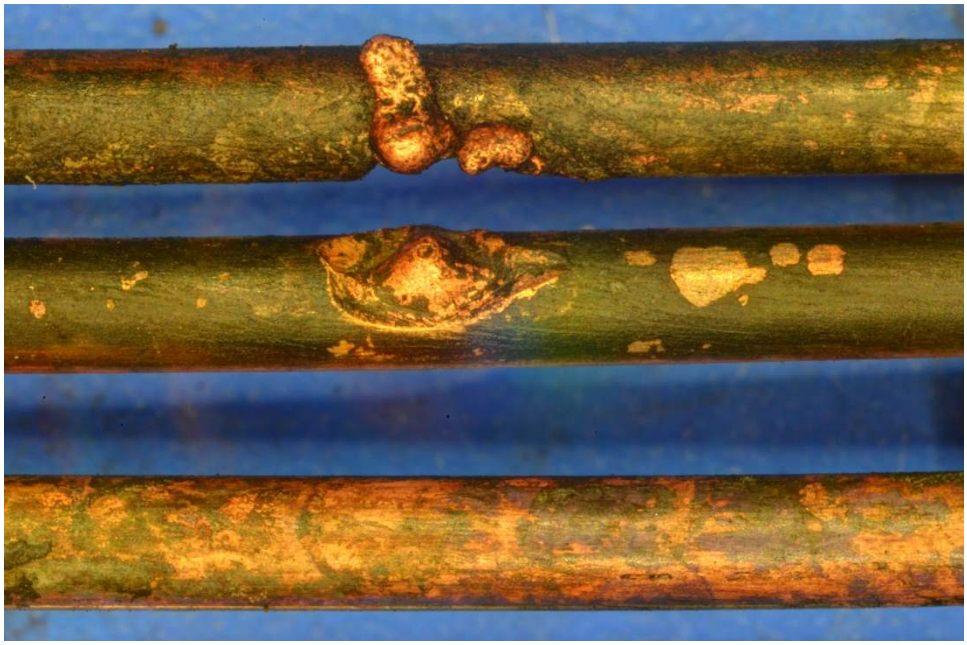

Figure 79 - Arc 2-35 (16x magnification)

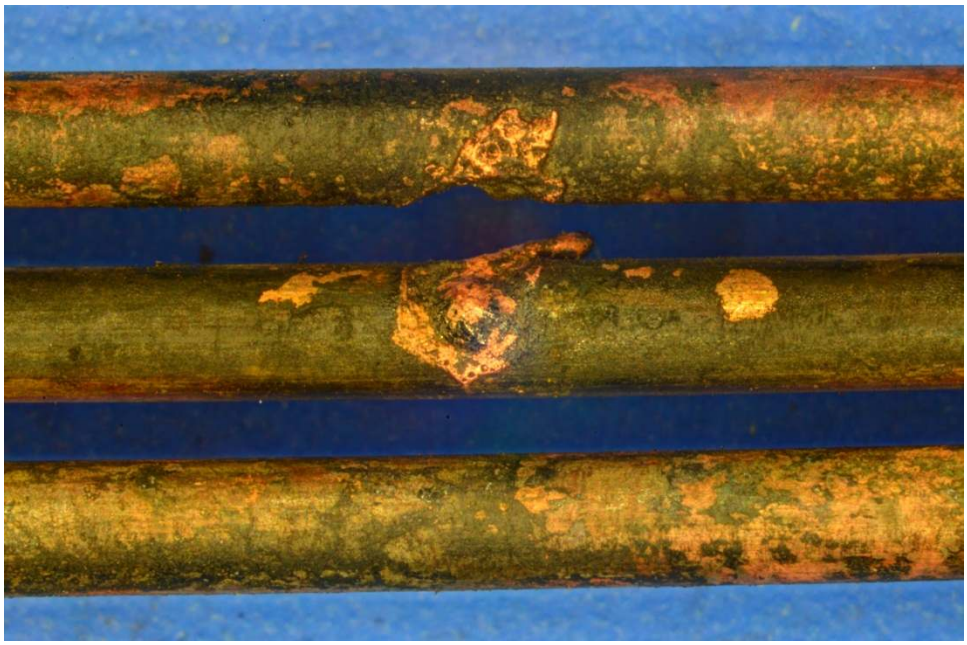

Figure 80 - Arc 2-36 (16x magnification)

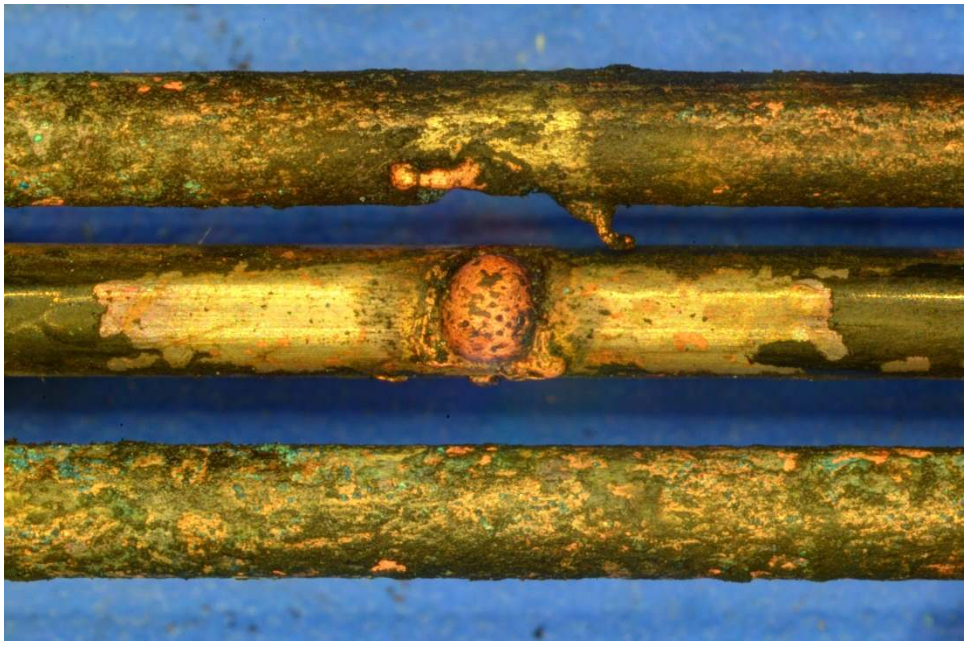

Figure 81 - Arc 2-37 (16x magnification)

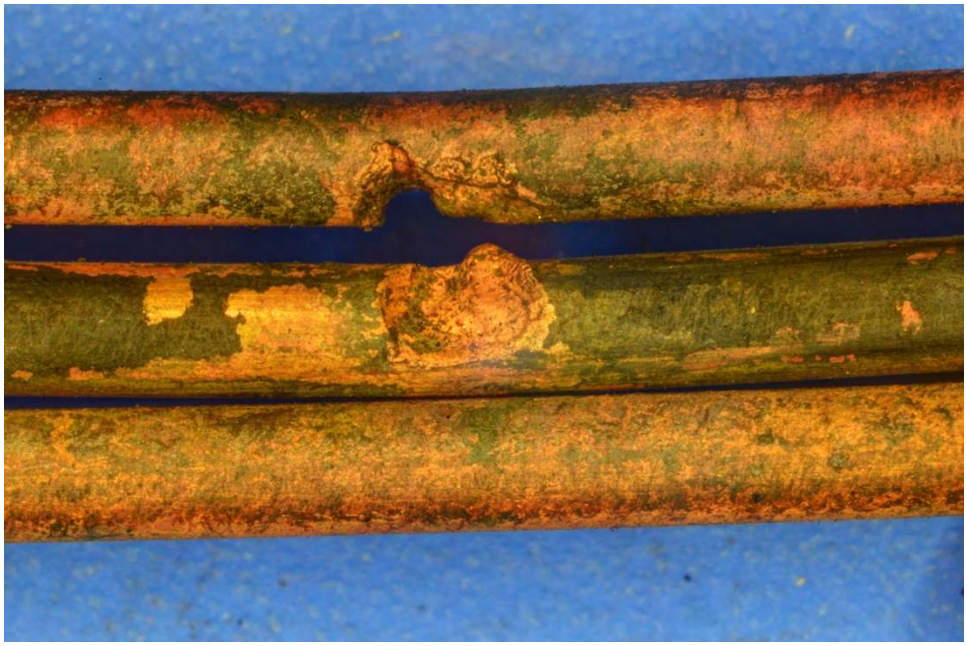

Figure 82 - Arc 2-38 (16x magnification)

Figure 83 - Arc 2-39 (16x magnification)

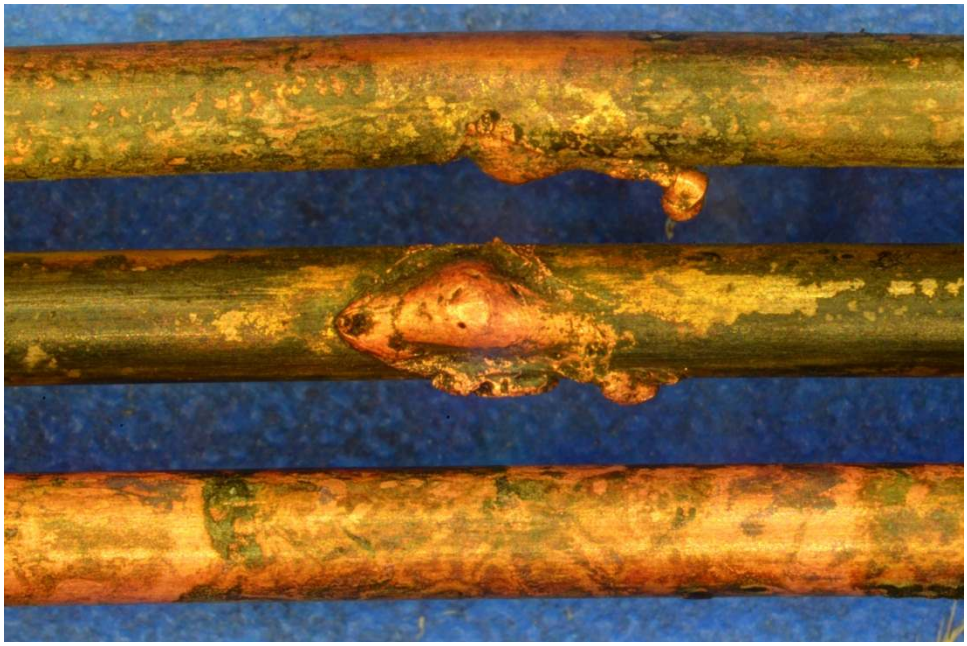

Figure 84 - Arc 2-40 (16x magnification)

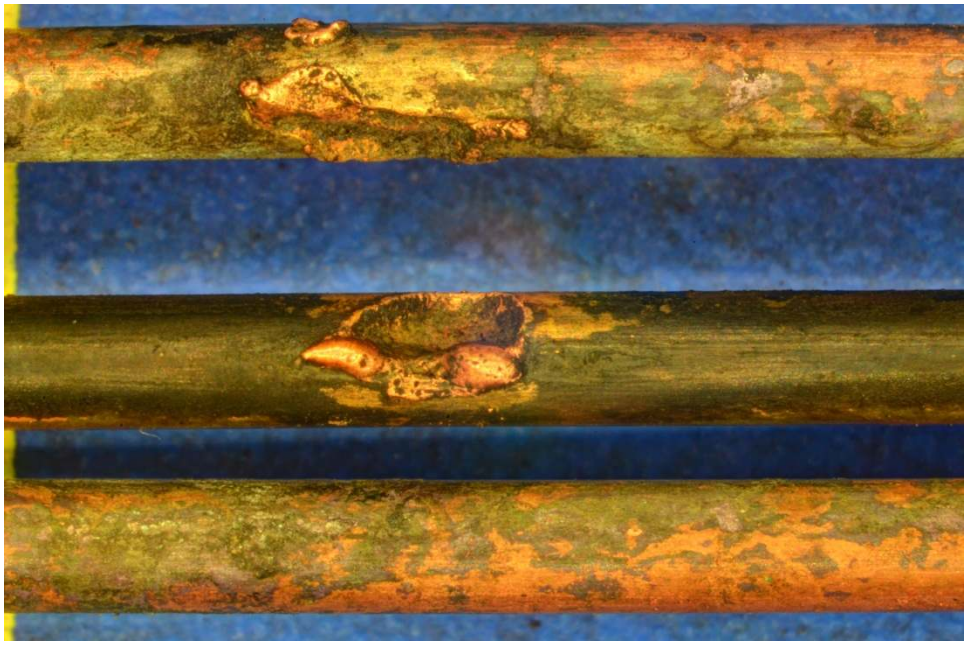

Figure 85 - Arc 2-42 (16x magnification)

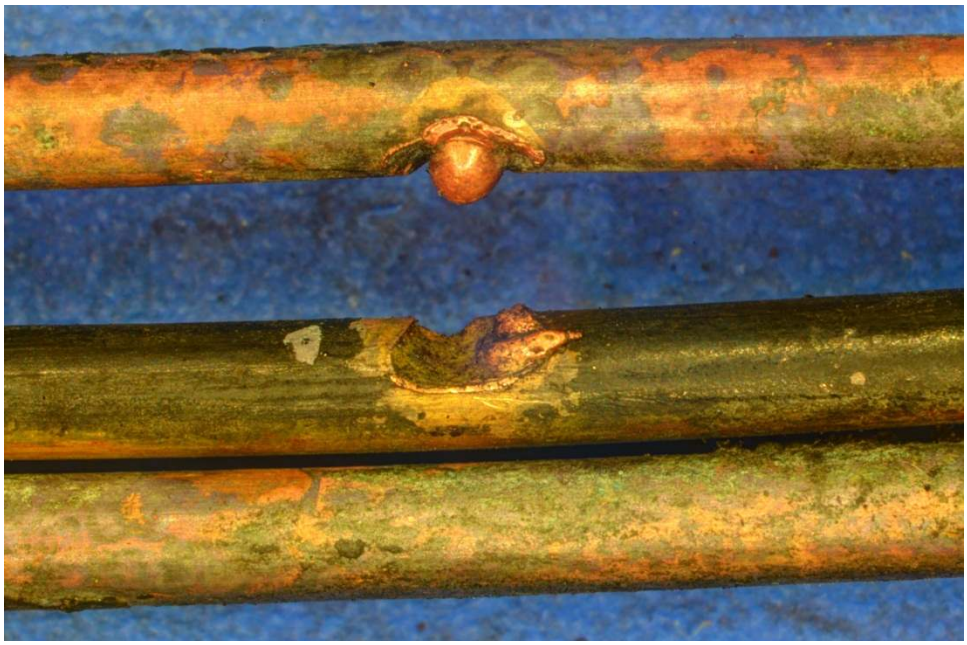

Figure 86 - Arc 2-43 (16x magnification)

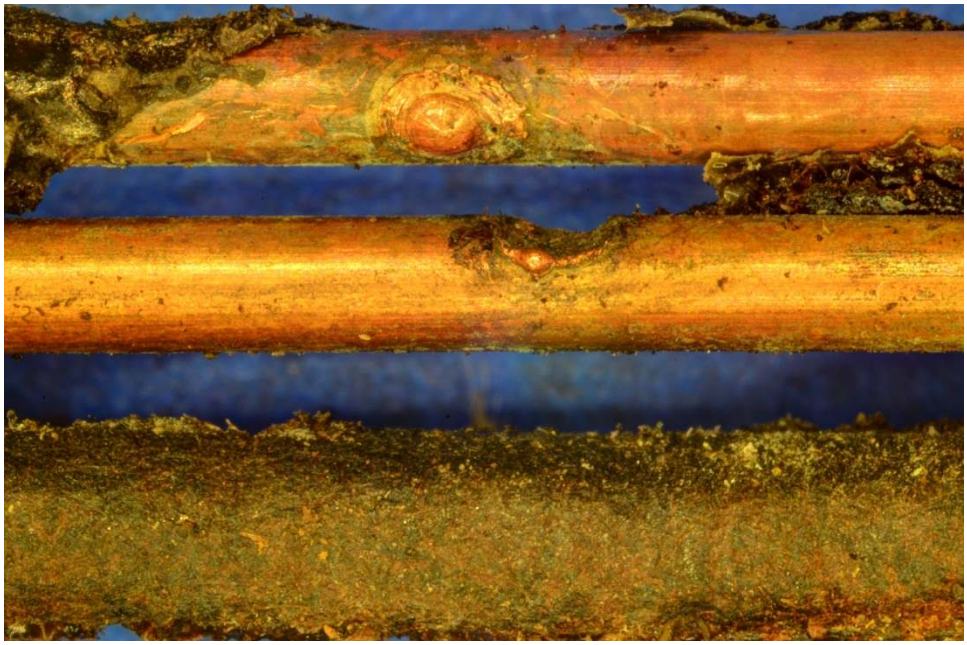

Figure 87 - Arc 2-44 (16x magnification)

Figure 88 - Arc 2-45 (16x magnification)

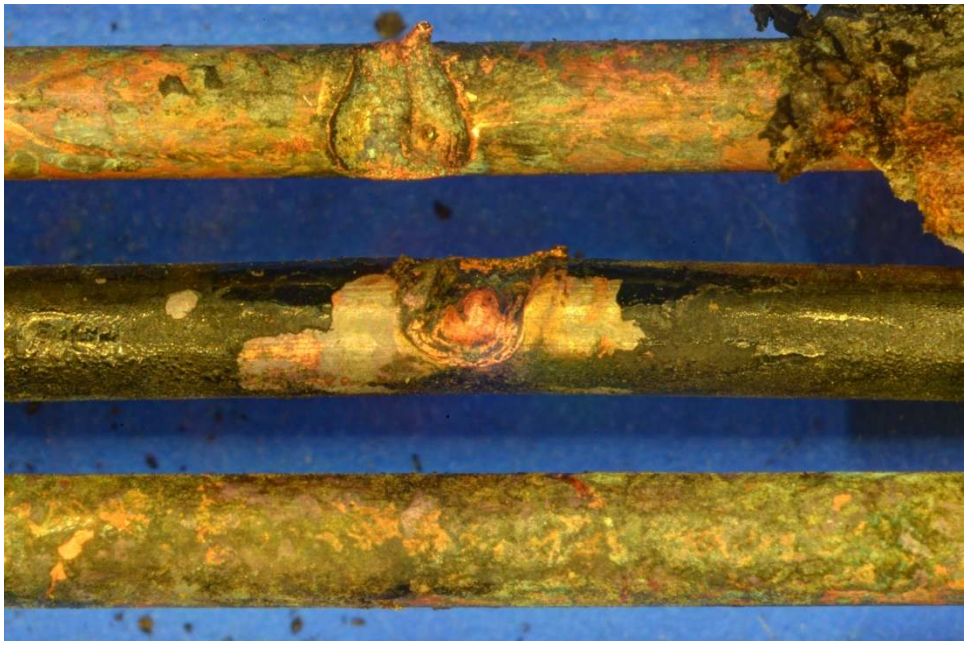

Figure 89 - Arc 2-46 (16x magnification)

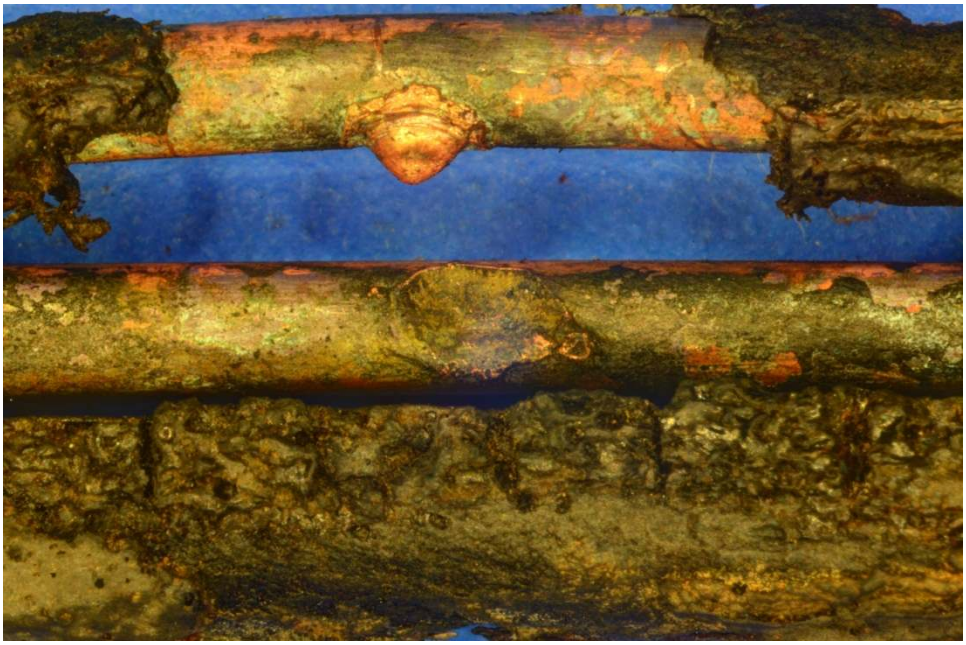

Figure 90 - Arc 2-47 (16x magnification)

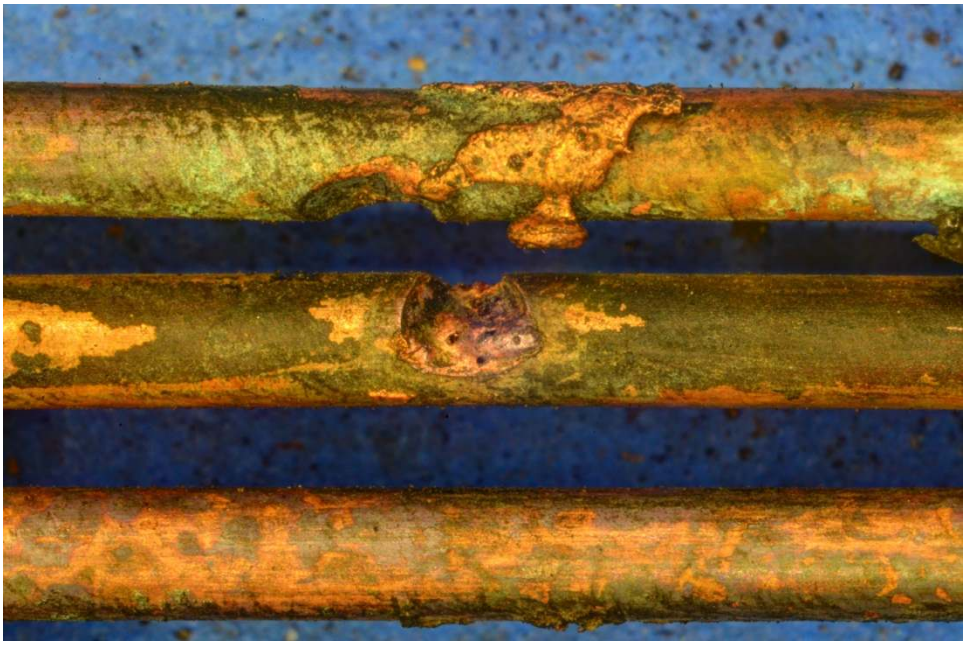

Figure 91 - Arc 2-48 (16x magnification)

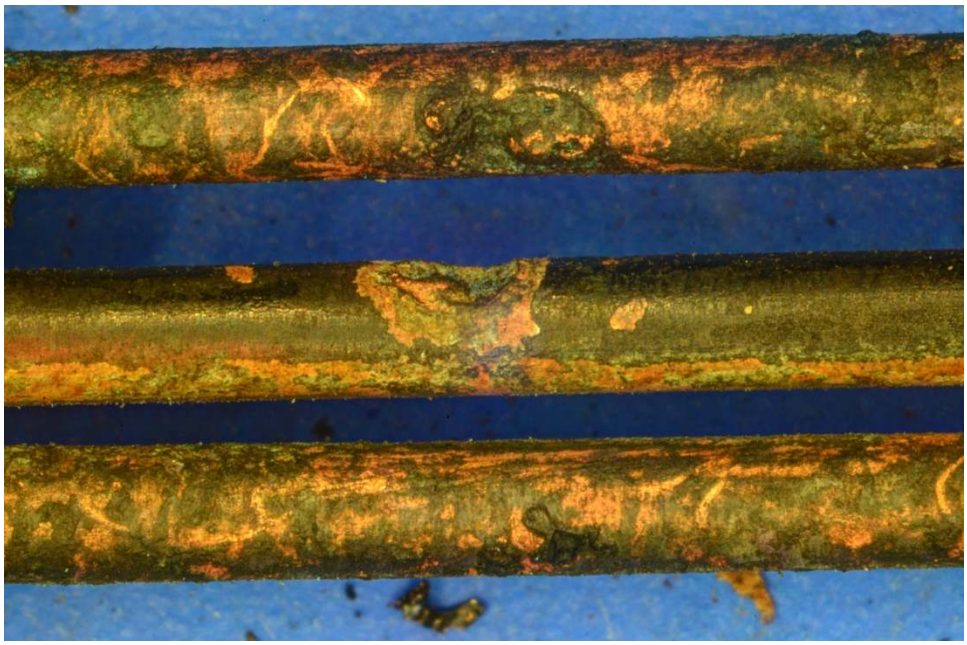

Figure 92 - Arc 2-49 (16x magnification)

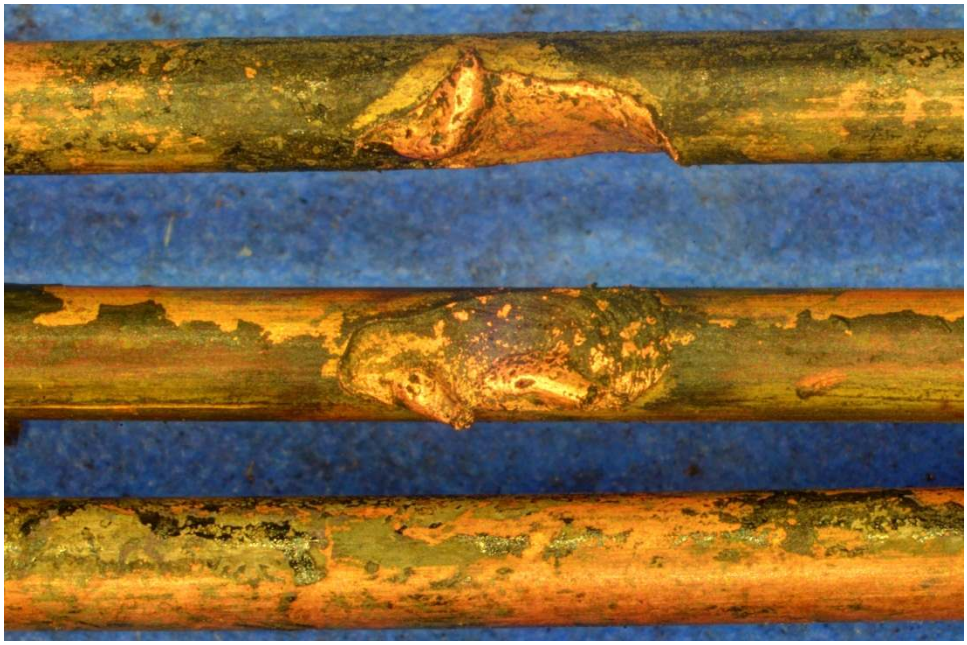

Figure 93 - Arc 2-50 (16x magnification)

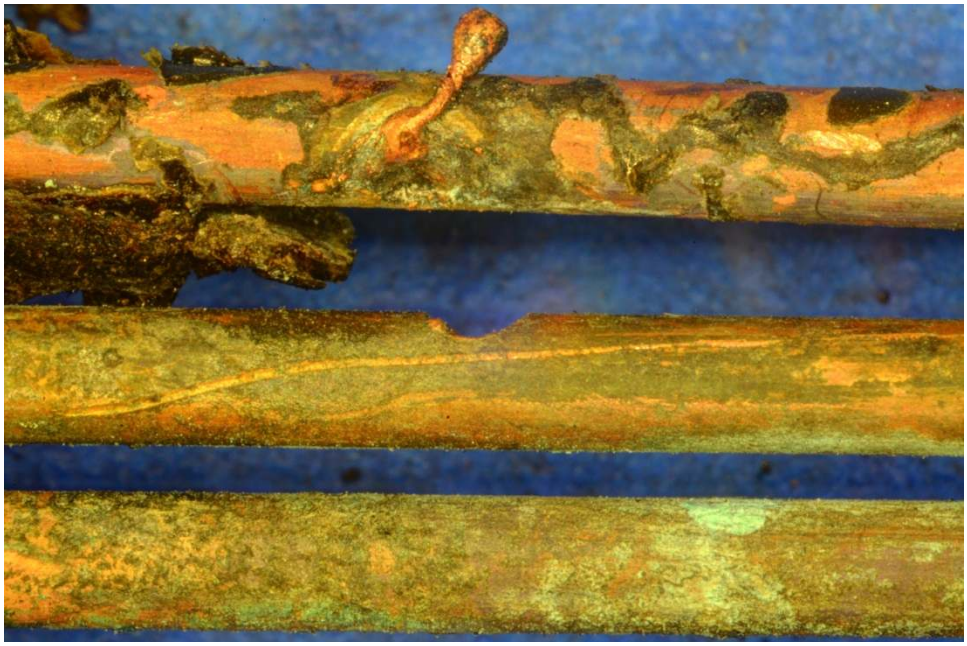

Figure 94 - Arc 2-51 (16x magnification)

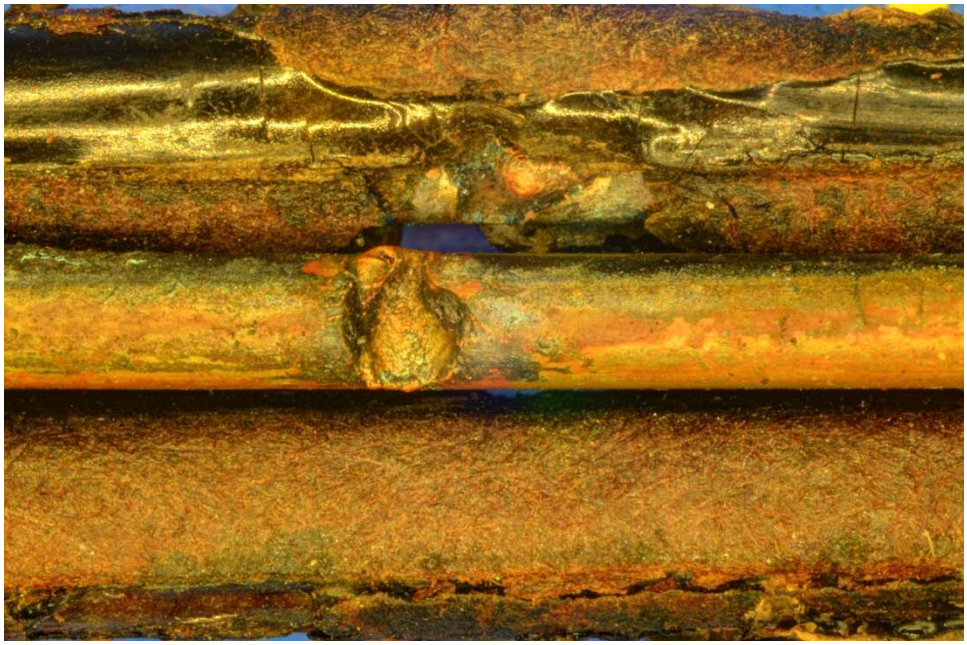

Figure 95 - Arc 2-54 (16x magnification)

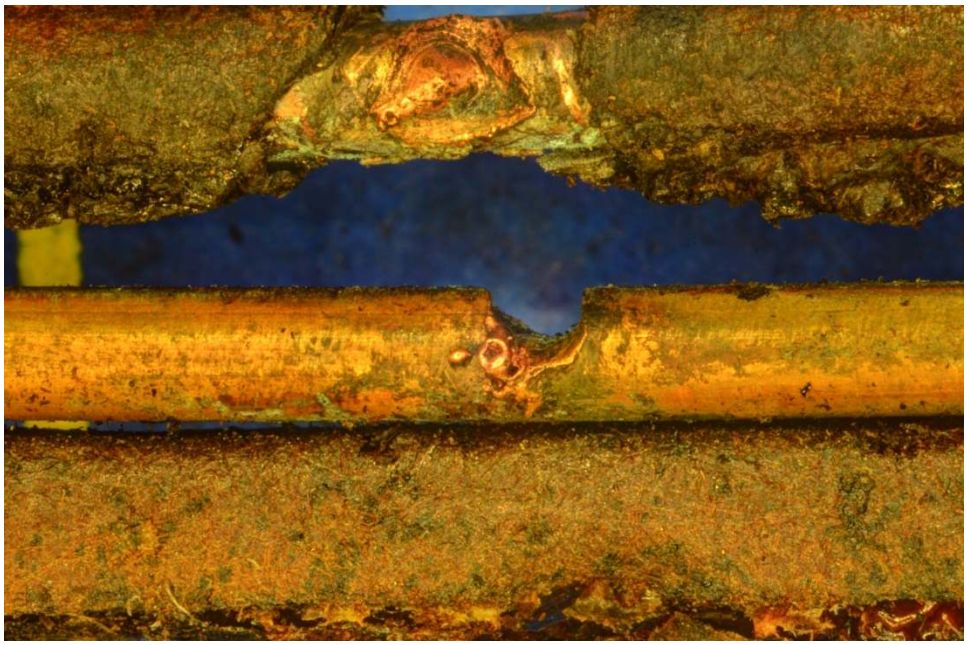

Figure 96 - Arc 2-55 (16x magnification)

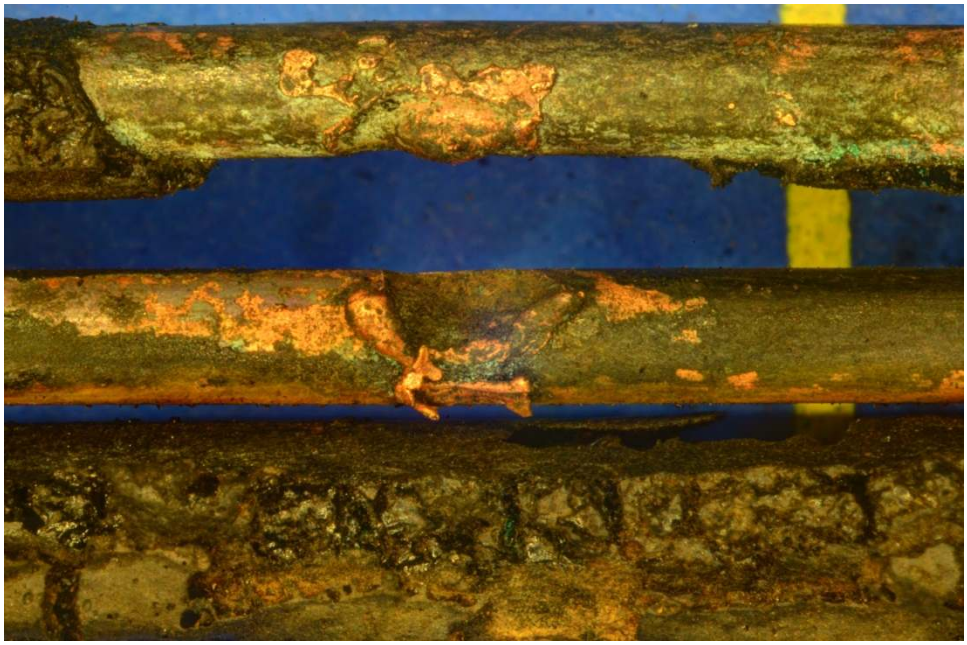

Figure 97 - Arc 2-56 (16x magnification)

Figure 98 - Arc 2-57 (16x magnification)

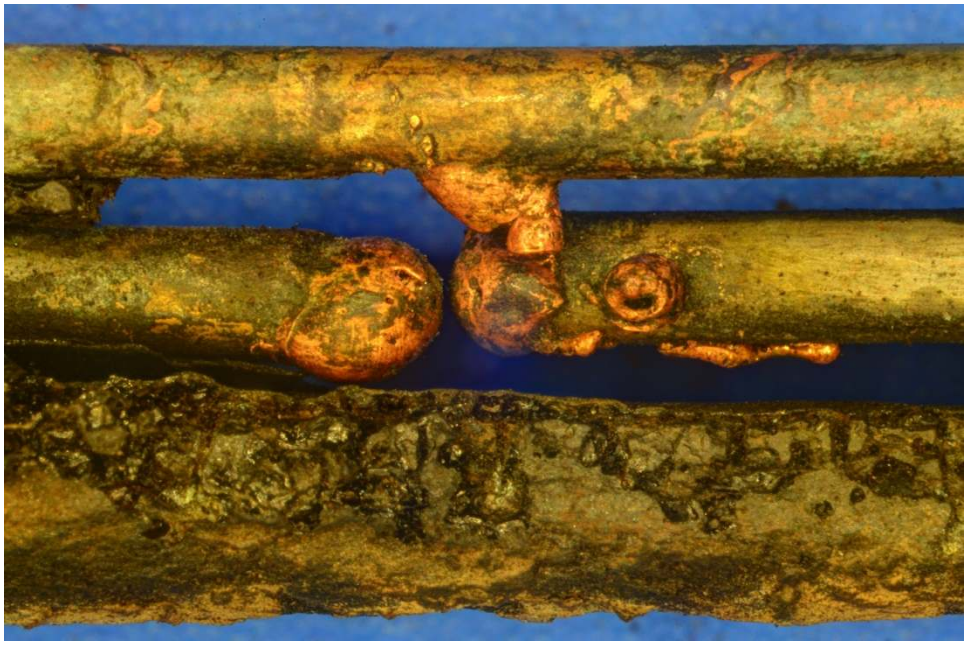

Figure 99 - Arc 2-58 (16x magnification)

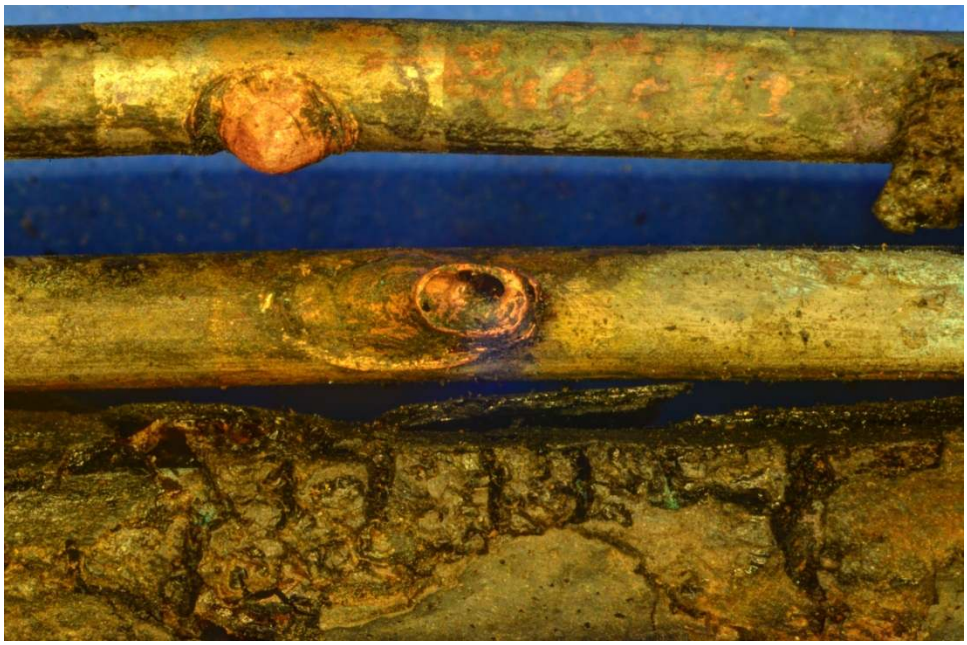

Figure 100 - Arc 2-60 (16x magnification)

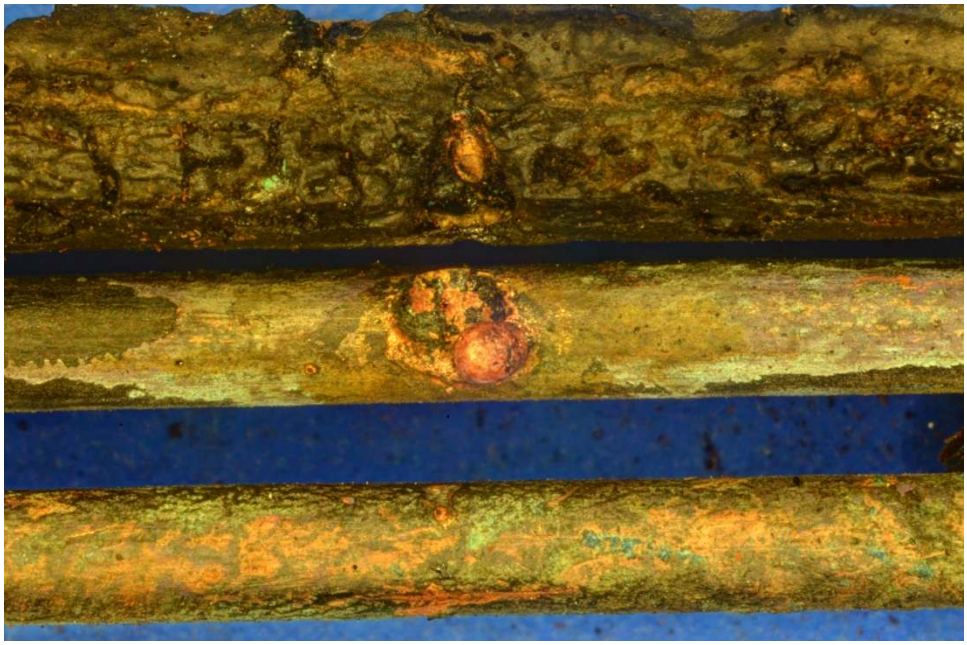

Figure 101 - Arc 2-61 (16x magnification)

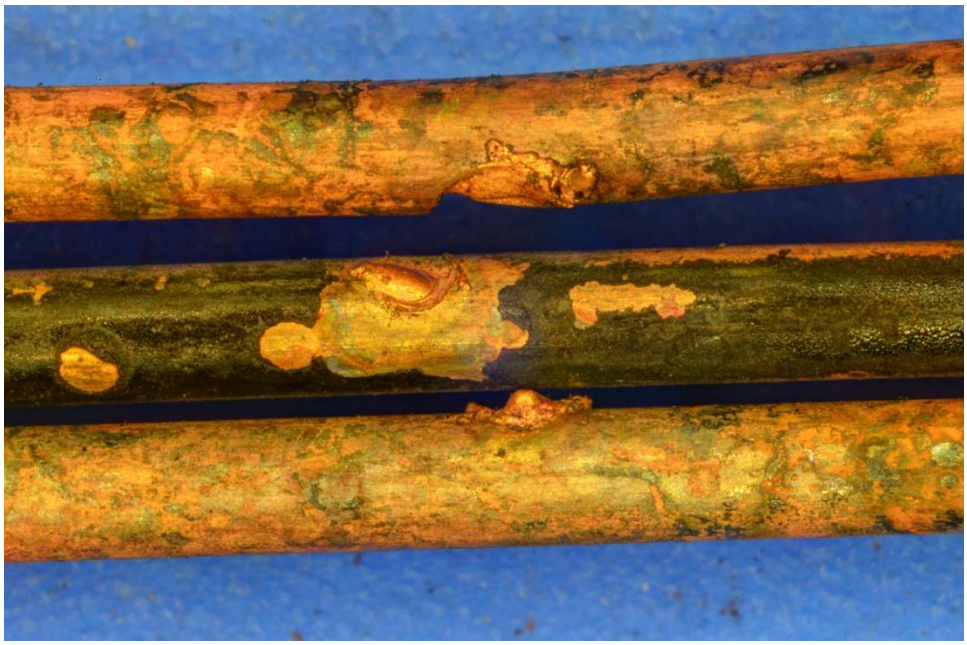

Figure 102 - Arc 2-64 (16x magnification)

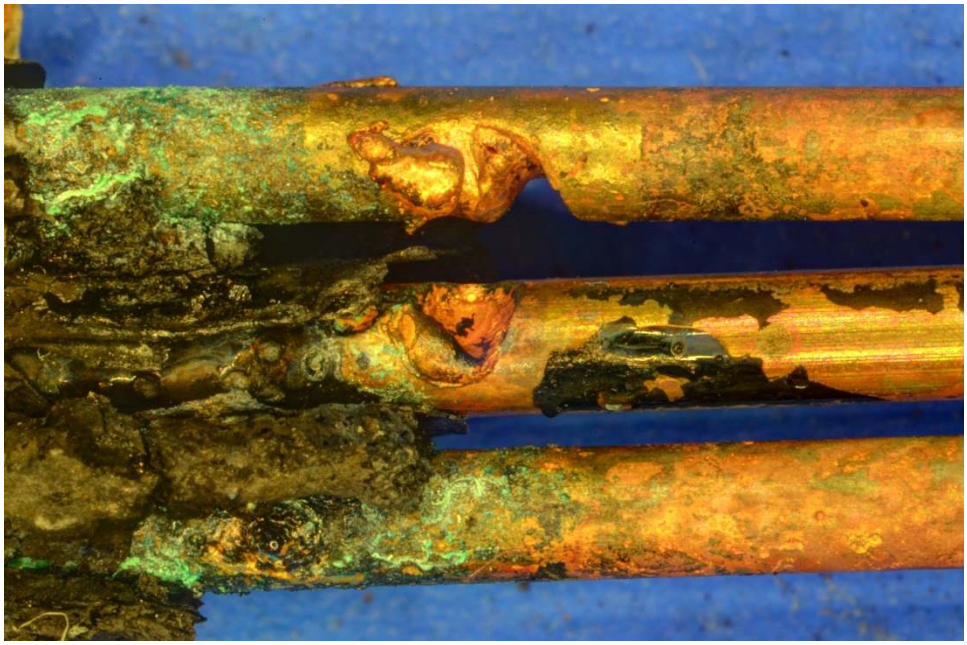

Figure 103 - Arc 2-68 (16x magnification)

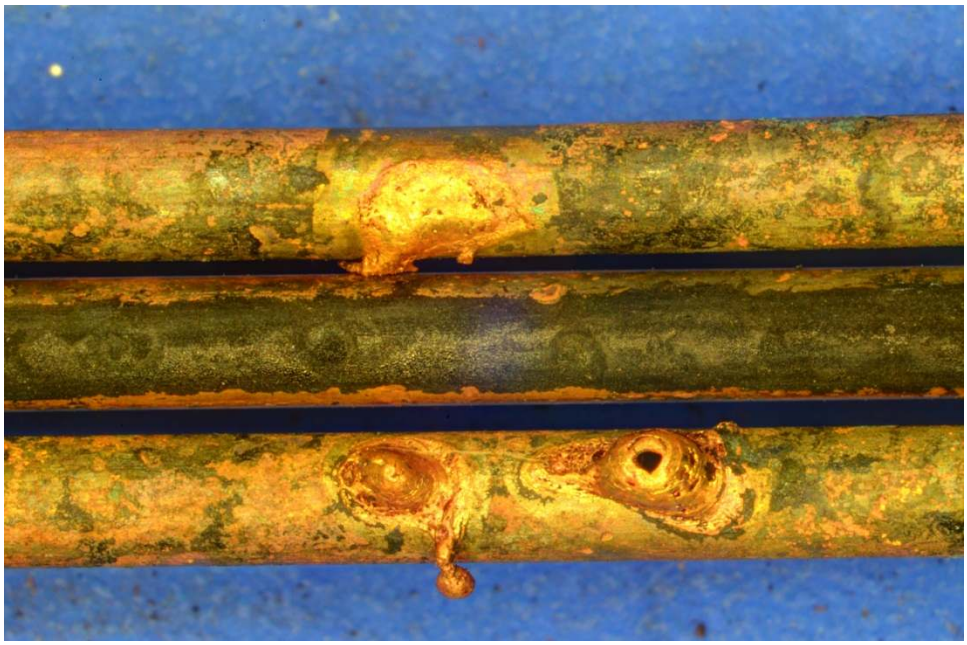

Figure 104 - Arc 2-69 (16x magnification)

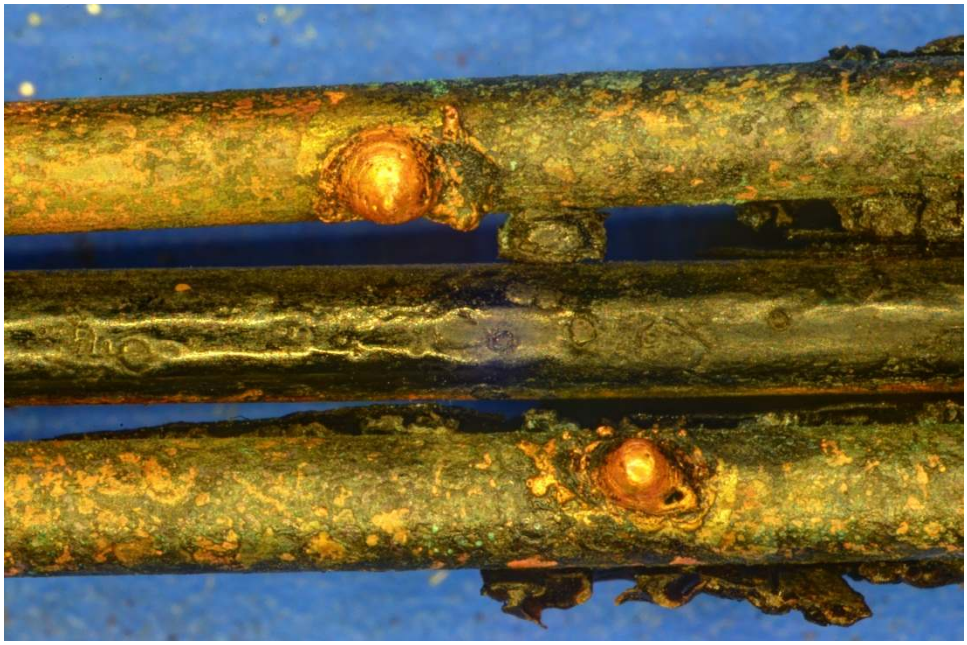

Figure 105 - Arc 2-70 (16x magnification)

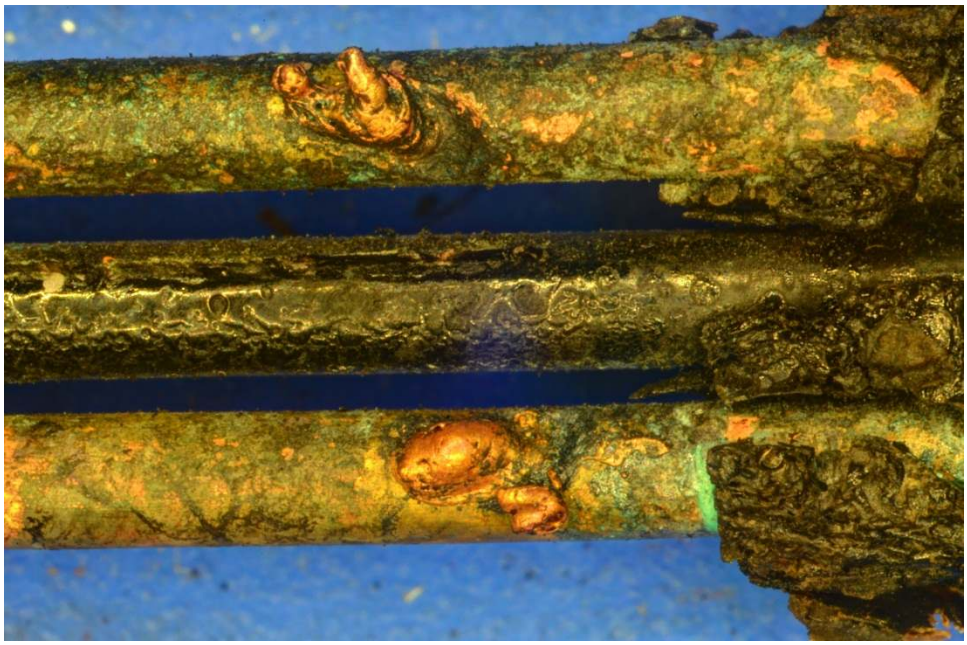

Figure 106 - Arc 2-71 (16x magnification)

7.2 Enhanced and SEM Photographs – Energized Tests in an Ambient Environment

Figure 107 - Arc 2-6 (22x magnification)

Figure 108 - Arc 2-7 (27x magnification)

Figure 109 - Arc 2-13 (27x magnification)

Figure 110 - Arc 2-14 (16x magnification)

Figure 111 - Arc 2-17 (27x magnification)

Figure 112 - Arc 2-26 (27x magnification)

Figure 113 - Arc 2-48.1 (27x magnification)

Figure 114 - Arc 2-48.2 (27x magnification)

Figure 115 - Arc 2-57.1 (25x magnification)

Figure 116 - Arc 2-57.2 (25x magnification)

Figure 117 - Arc 2-57.3 (27x magnification)

7.3 Arcing Waveforms – Energized Cables in an Ambient Environment

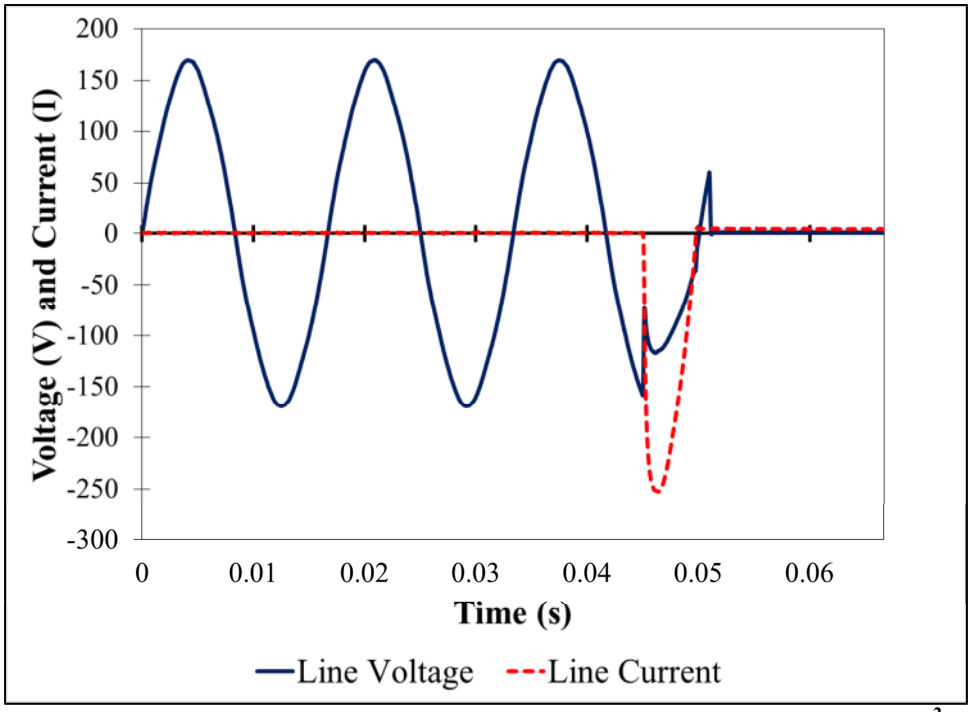

Figure 118 - Voltage and Current waveforms produced during test 2-4 (55 kW/m^2). A total of 4 cycles (1/15 of a second) is shown.

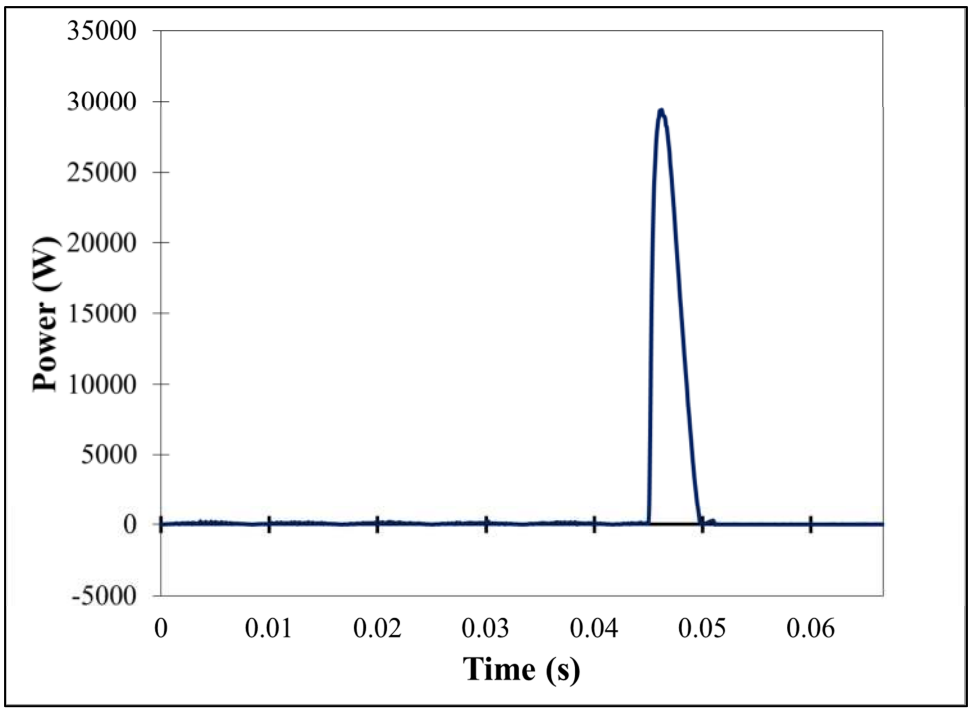

Figure 119 – Waveform of the instantaneous power produced during test 2-4 (55 kW/m^2). A total of 4 cycles (1/15 of a second) is shown.

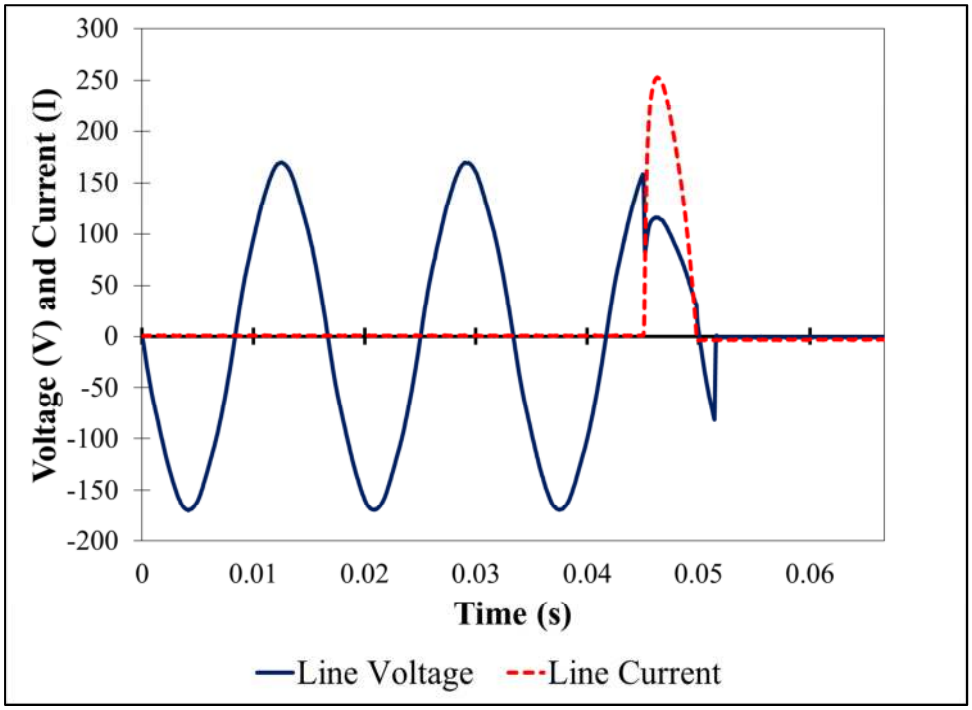

Figure 120 - Voltage and current waveforms from test 2-5 (53 kW/m^2). A total of 4 cycles (1/15 of a second) is shown.

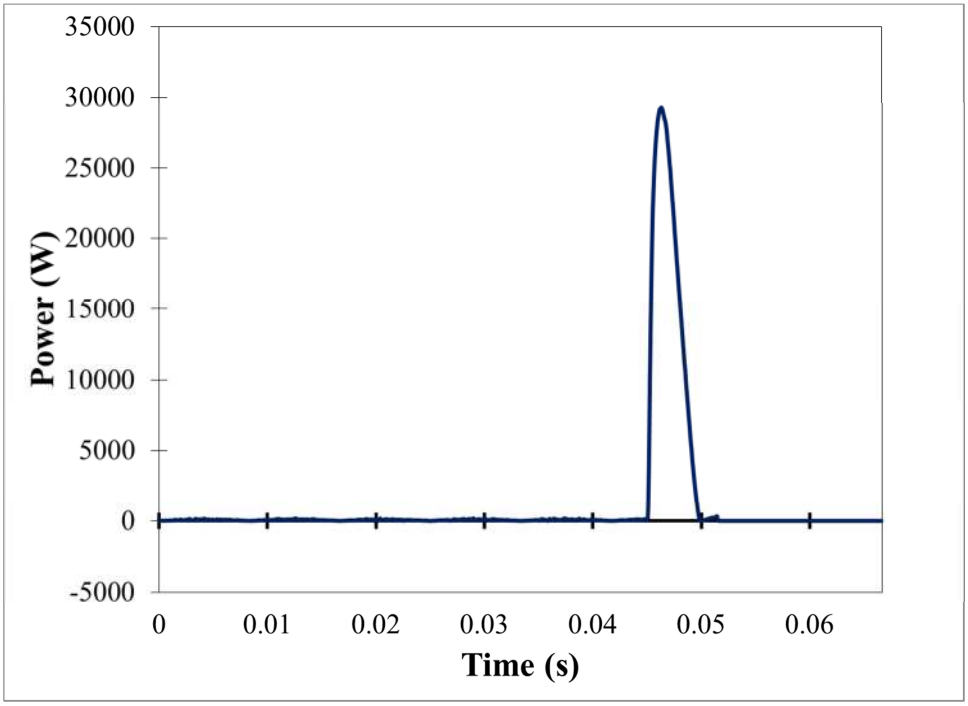

Figure 121 –Waveform of the instantaneous power produced during test 2-5 (53 kW/m^2). A total of 4 cycles (1/15 of a second) is shown.

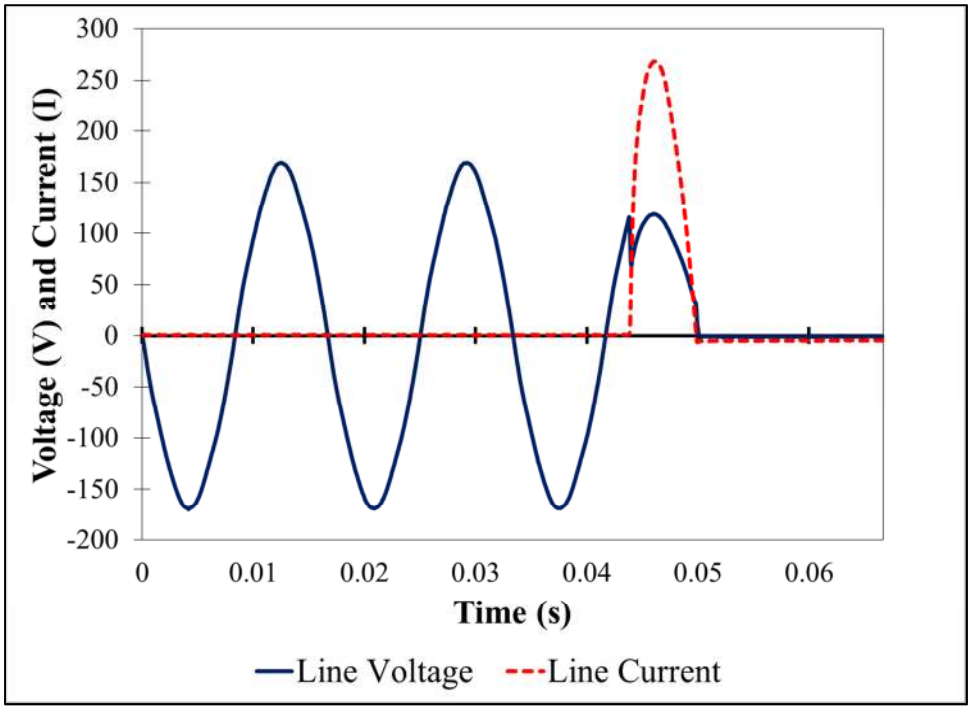

Figure 122 - Voltage and current waveforms produced during test 2-6 (51 kW/m^2). A total of 4 cycles (1/15 of a second) is shown.

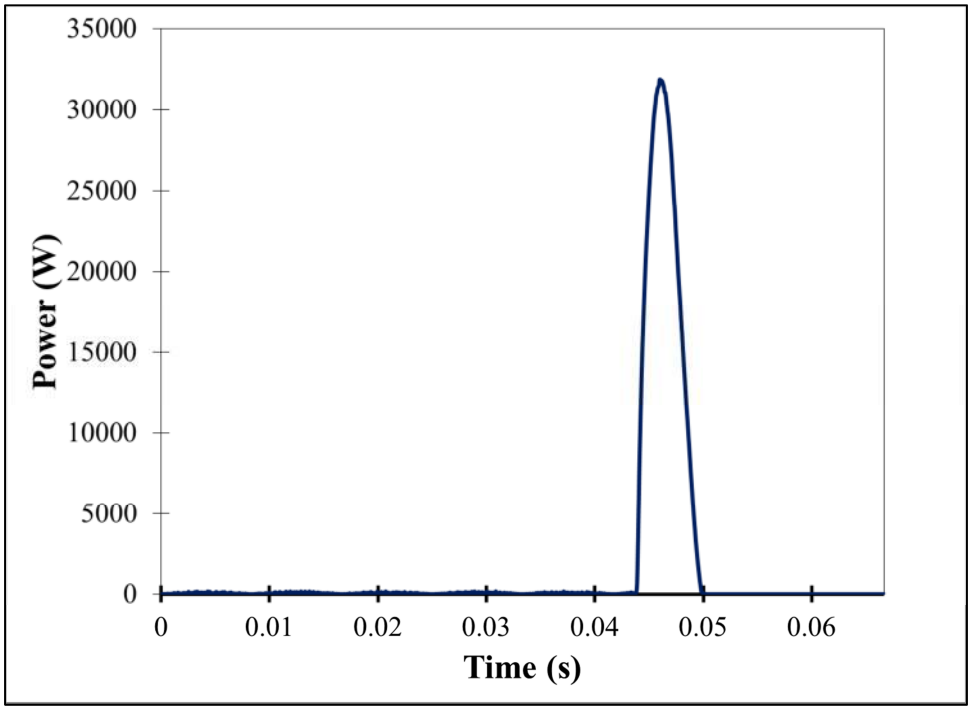

Figure 123 - Waveform of the instantaneous power produced during test 2-6 (51 kW/m^2). A total of 4 cycles (1/15 of a second) is shown.

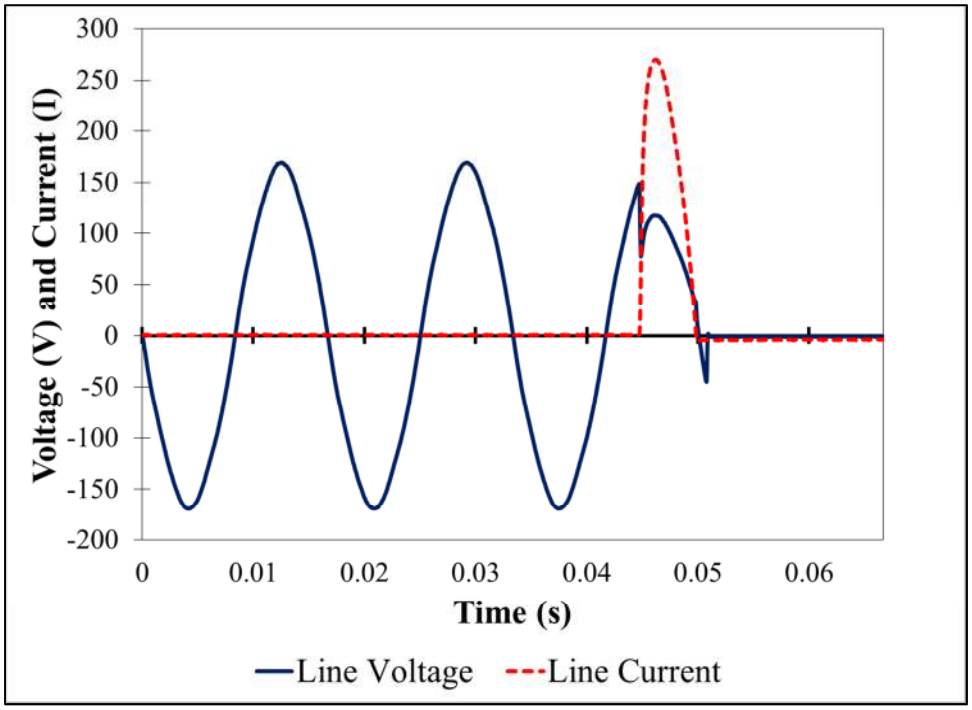

Figure 124 - Voltage and Current waveforms produced during test 2-7 (49 kW/m^2). A total of 4 cycles (1/15 of a second) is shown.

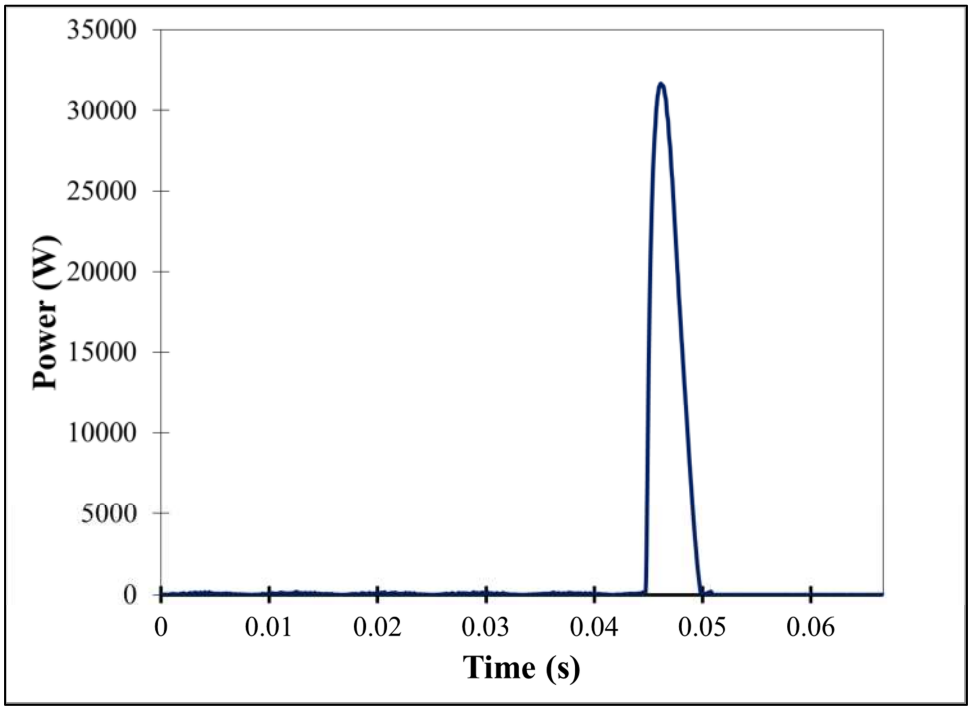

Figure 125 - Waveform of the instantaneous power produced during test 2-7 (49 kW/m^2). A total of 4 cycles (1/15 of a second) is shown.

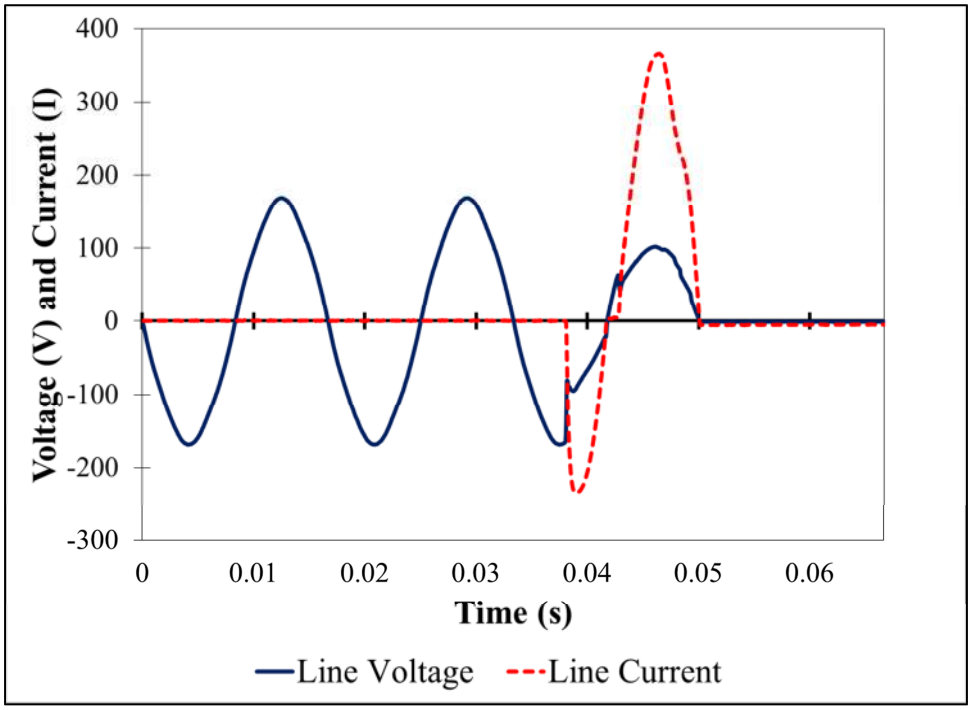

Figure 126 - Voltage and current waveforms produced during test 2-8 (47 kW/m^2). A total of 4 cycles (1/15 of a second) is shown.

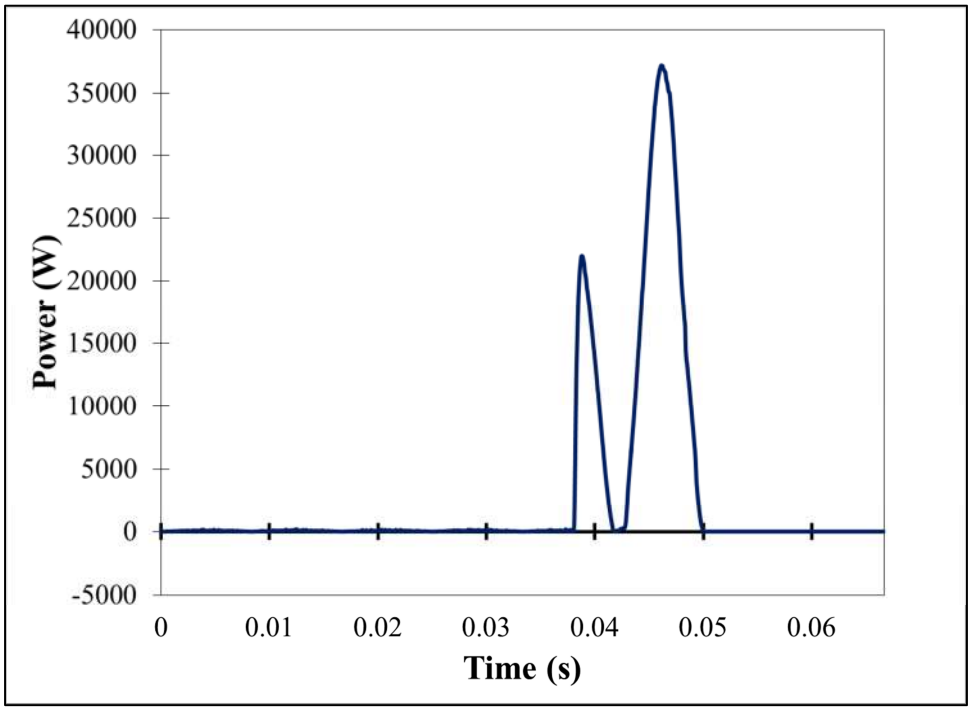

Figure 127 - Waveform of the instantaneous power produced during test 2-8 (47 kW/m^2). A total of 4 cycles (1/15 of a second) is shown.

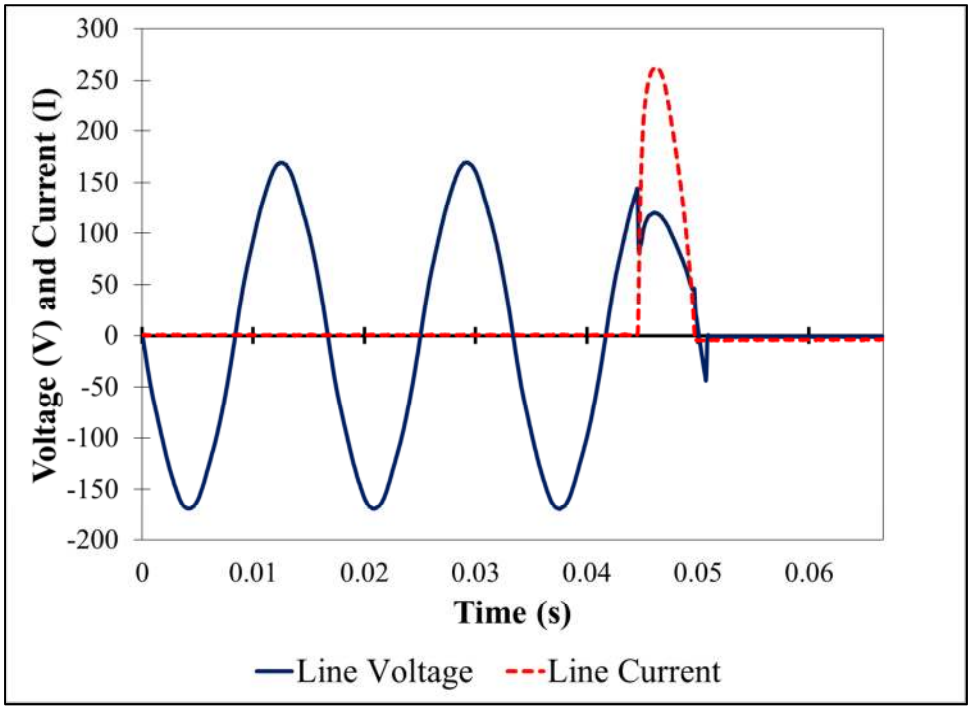

Figure 128 - Voltage and current waveforms produced during test 2-9 (45 kW/m^2). A total of 4 cycles (1/15 of a second) is shown.

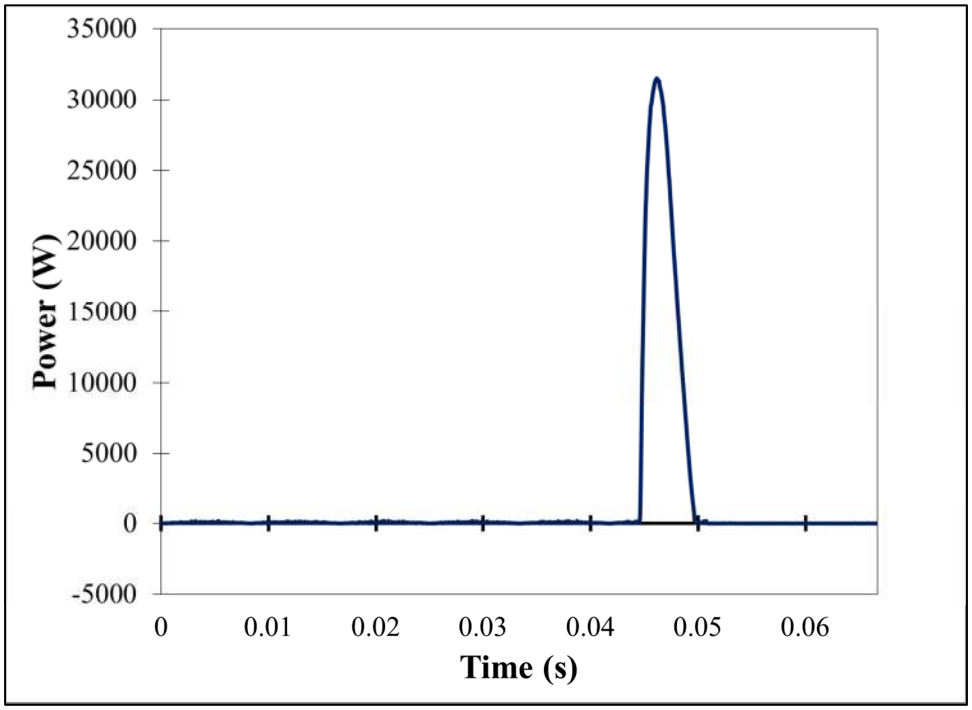

Figure 129 - Waveform of the instantaneous power produced during test 2-9 (45 kW/m^2). A total of 4 cycles (1/15 of a second) is shown.

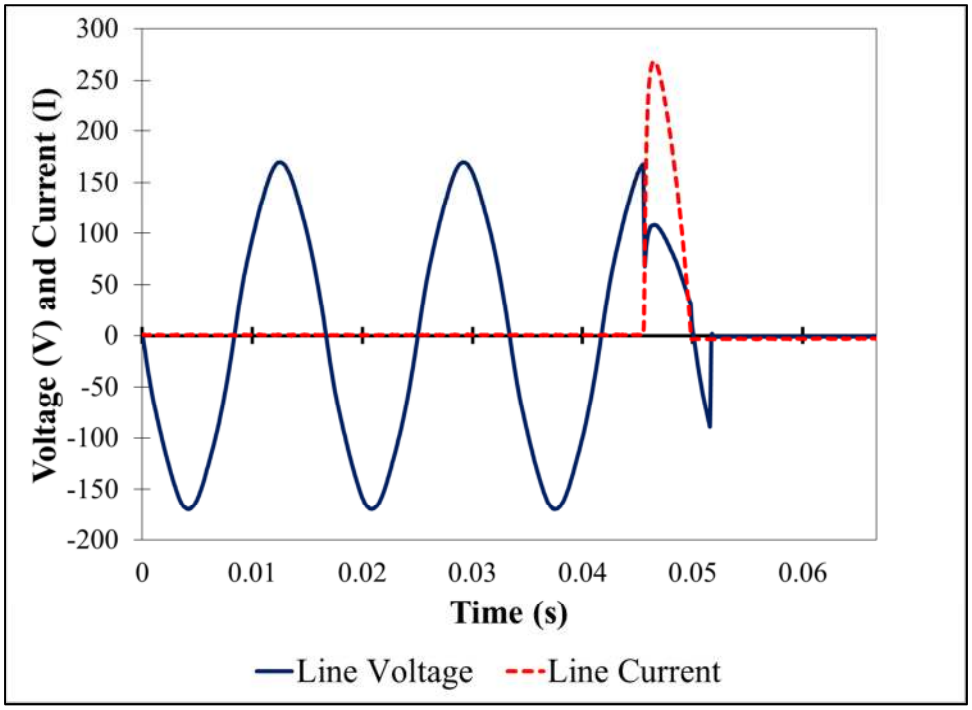

Figure 130 - Voltage and current waveforms produced during test 2-11 (43 kW/m^2). A total of 4 cycles (1/15 of a second) is shown.

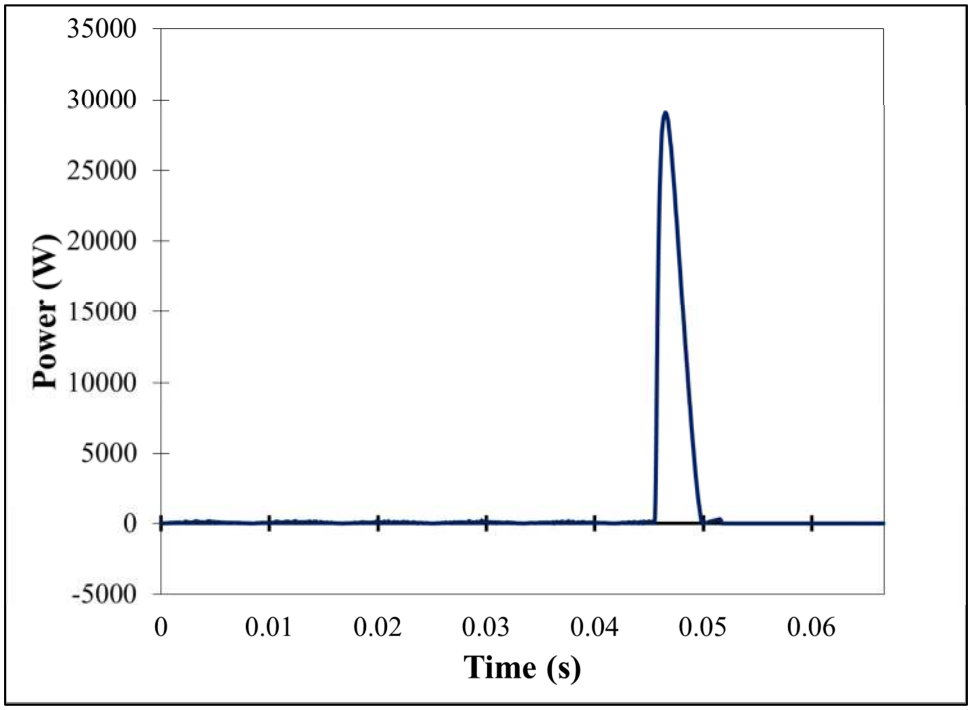

Figure 131 - Waveform of the instantaneous power produced in test 2-11 (43 kW/m^2). A total of 4 cycles (1/15 of a second) is shown.

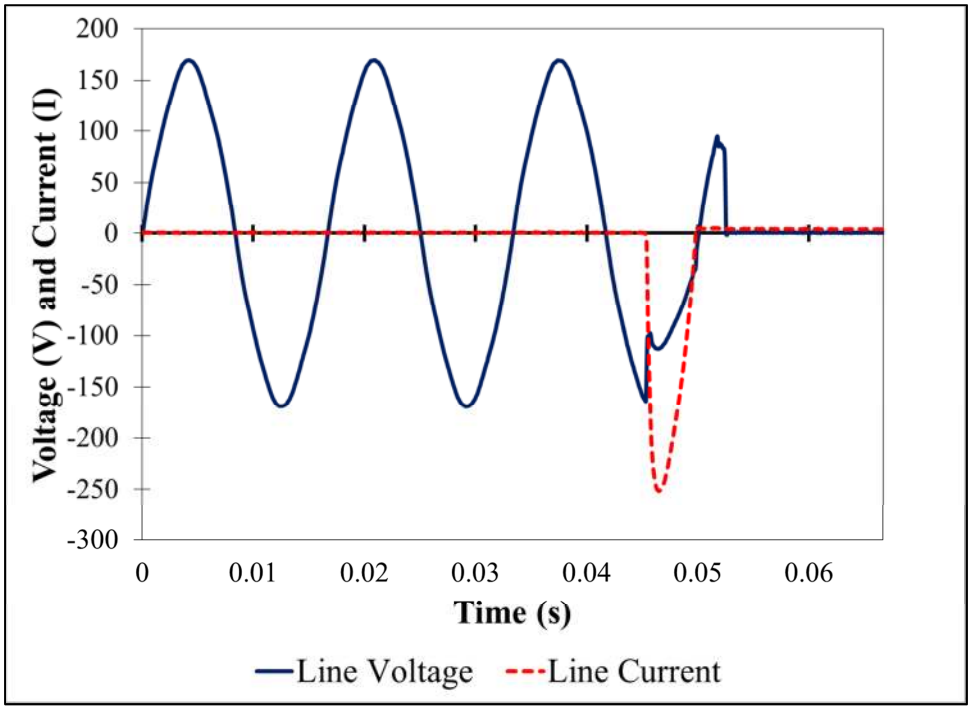

Figure 132 - Voltage and current waveforms produced during test 2-12 (40 kW/m^2). A total of 4 cycles (1/15 of a second) is shown.

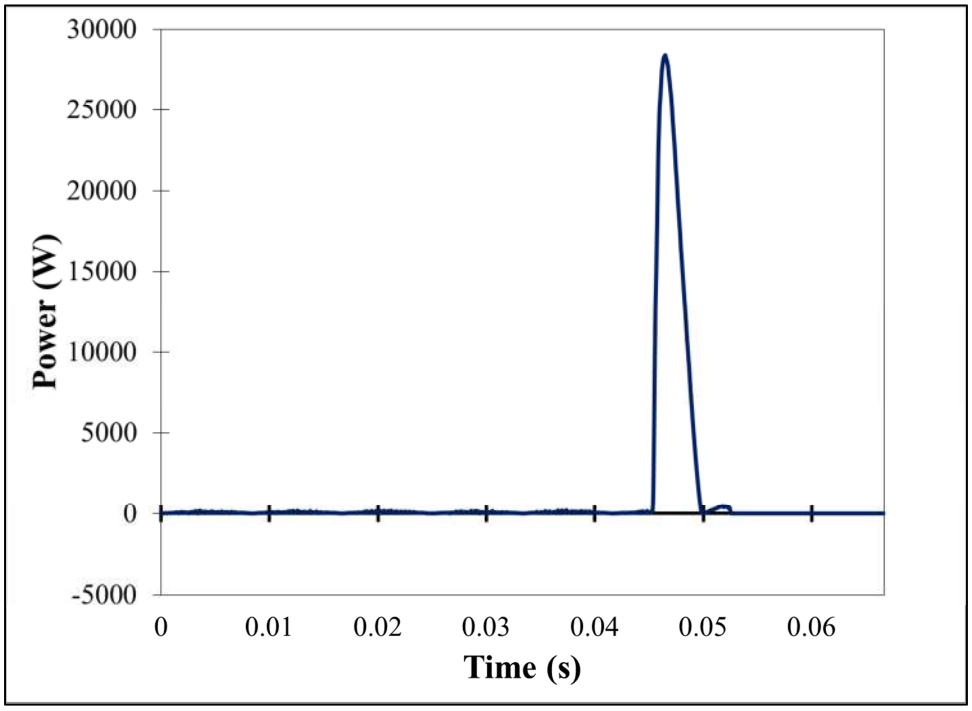

Figure 133 - Waveform of the instantaneous power produced during test 2-12 (40 kW/m^2). A total of 4 cycles (1/15 of a second) is shown.

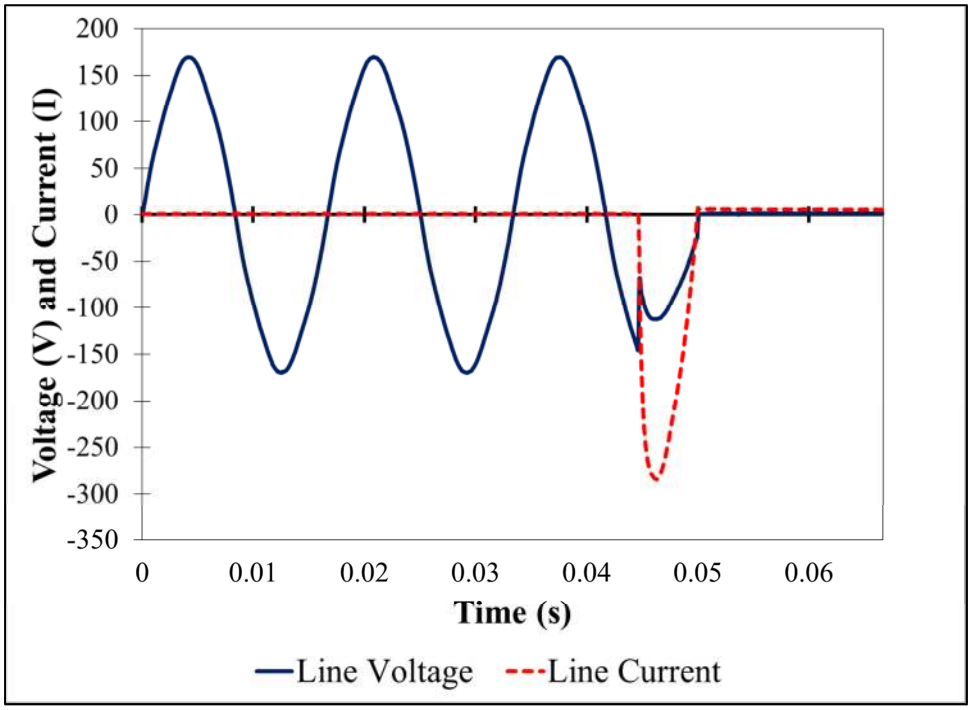

Figure 134 - Voltage and current waveforms produced in test 2-13 (38 kW/m^2). A total of 4 cycles (1/15 of a second) is shown.

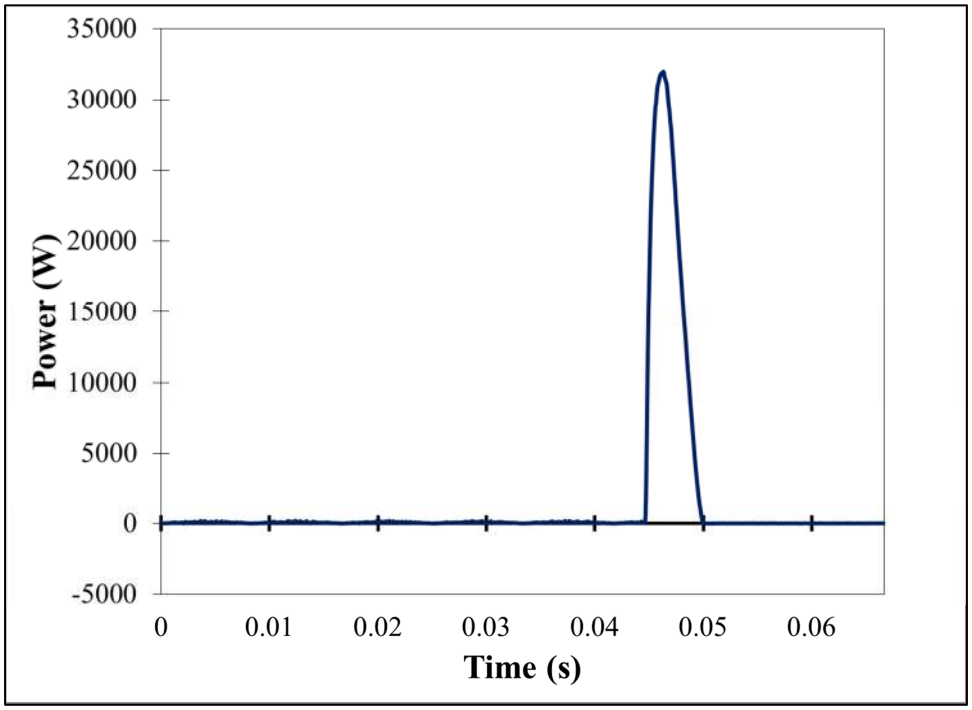

Figure 135 - Waveform of the instantaneous power produced in test 2-13 (38 kW/m^2). A total of 4 cycles (1/15 of a second) is shown.

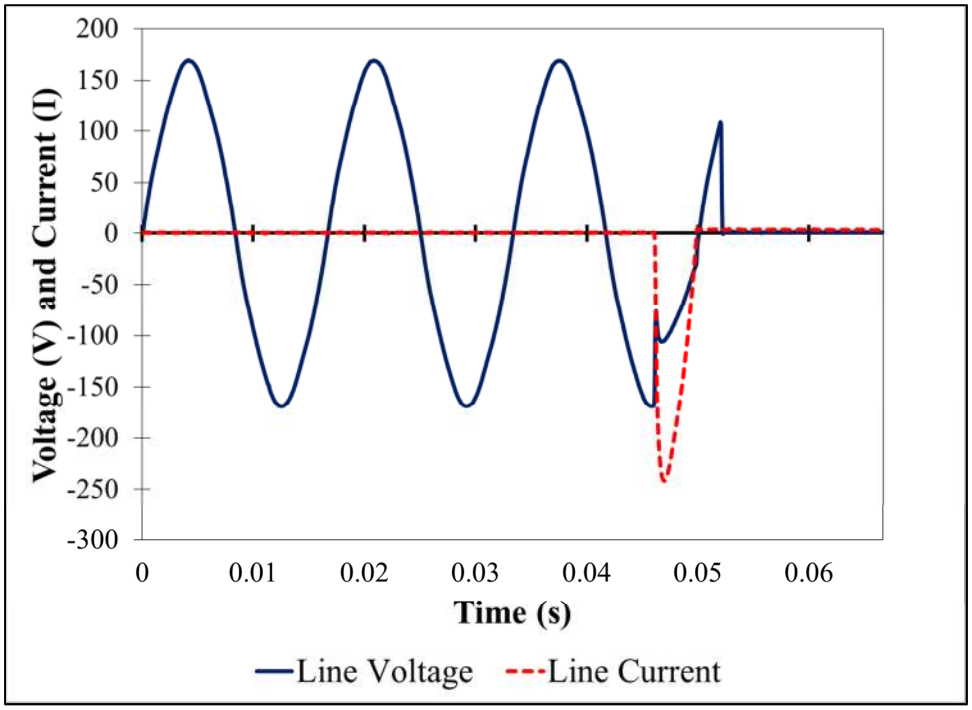

Figure 136 - Voltage and current waveforms produced in test 2-14 (36 kW/m^2). A total of 4 cycles (1/15 of a second) is shown.

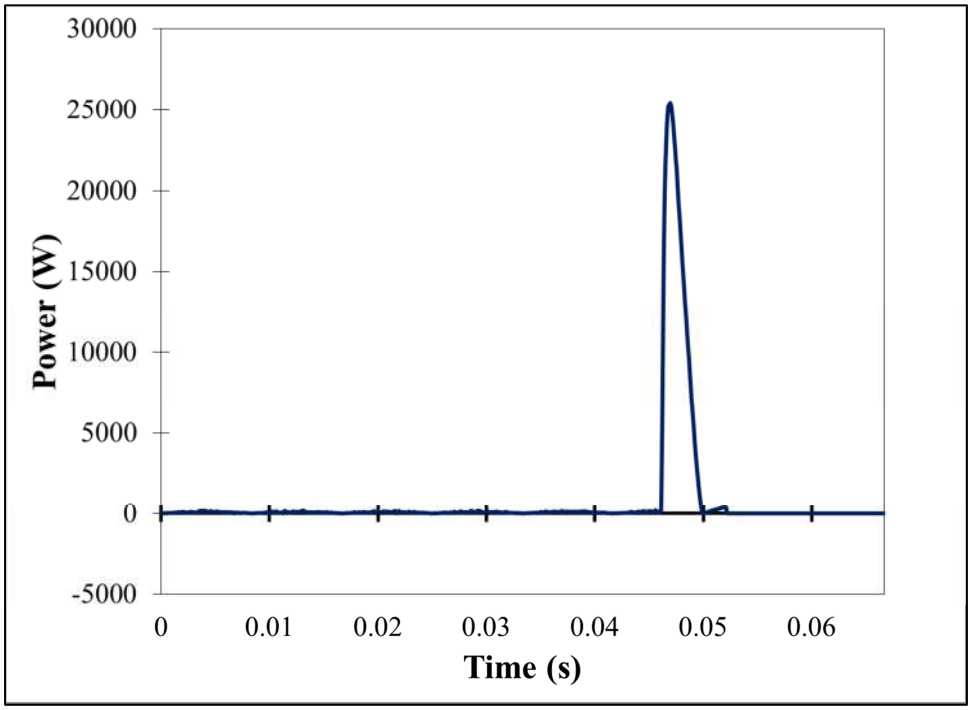

Figure 137 - Waveform of the instantaneous power produced in test 2-14 (36 kW/m^2). A total of 4 cycles (1/15 of a second) is shown.

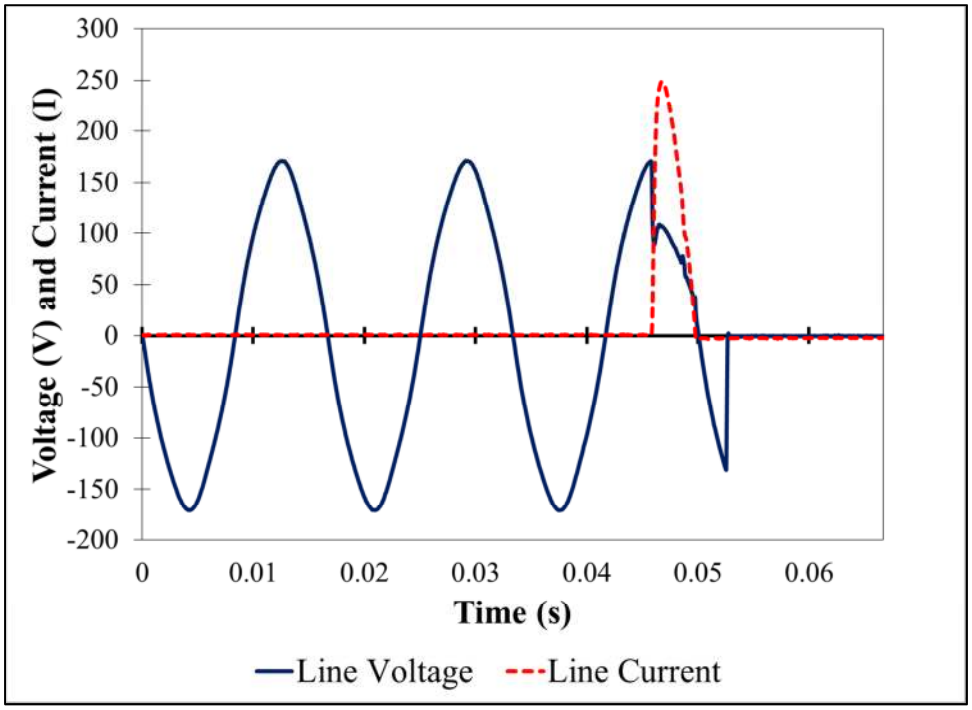

Figure 138 - Voltage and current waveforms produced in test 2-15 (34 kW/m^2). A total of 4 cycles (1/15 of a second) is shown.

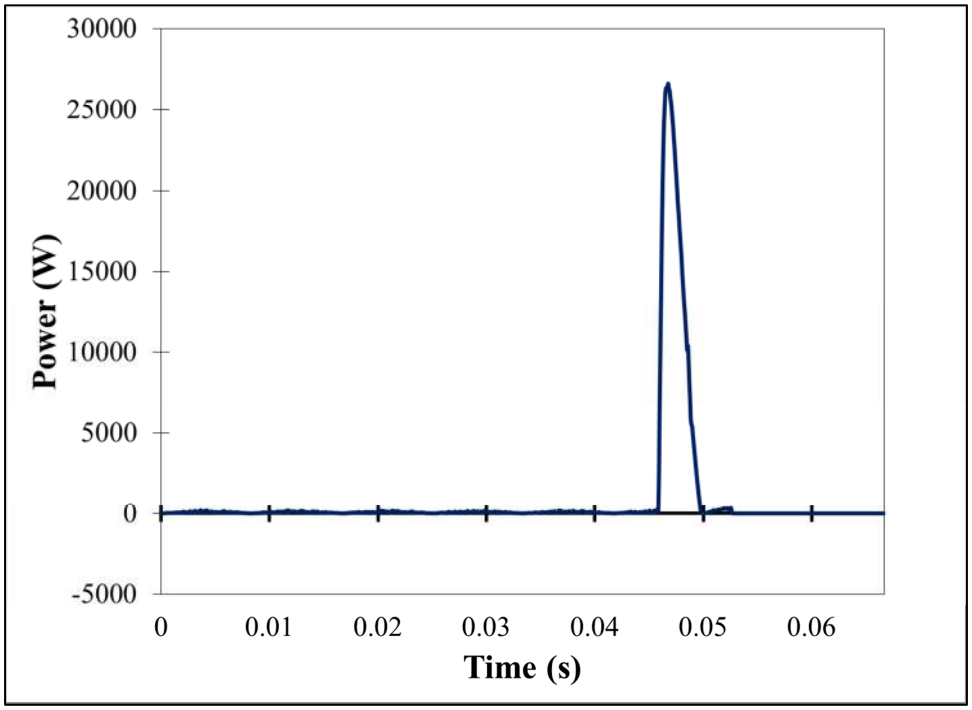

Figure 139 - Waveform of the instantaneous power produced in test 2-15 (34 kW/m^2). A total of 4 cycles (1/15 of a second) is shown.

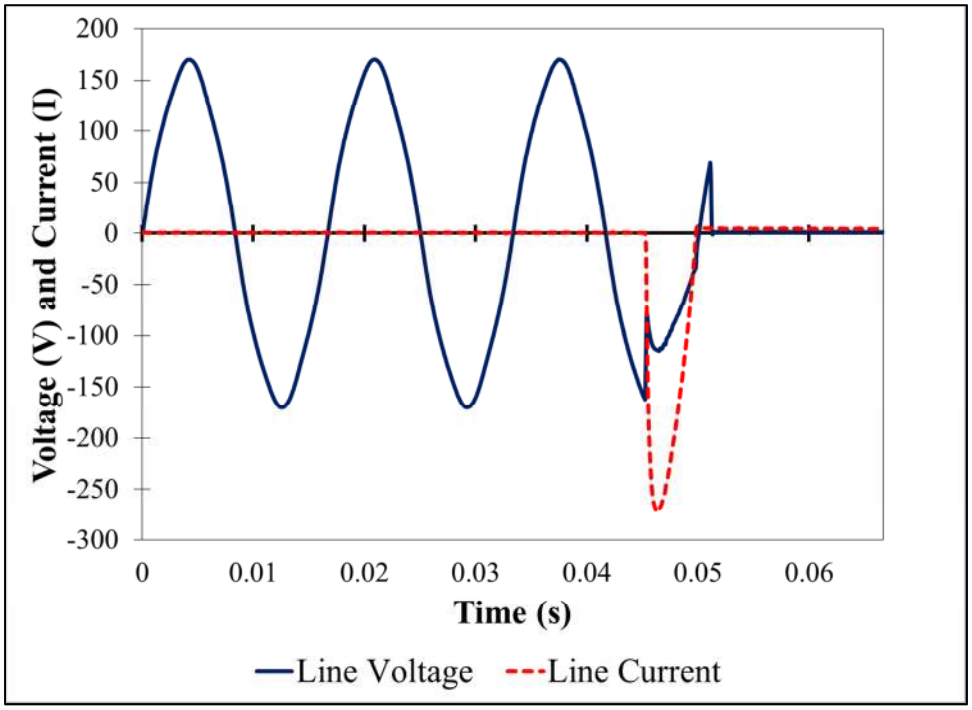

Figure 140 - Voltage and current waveforms produced in test 2-16 (32 kW/m^2). A total of 4 cycles (1/15 of a second) is shown.

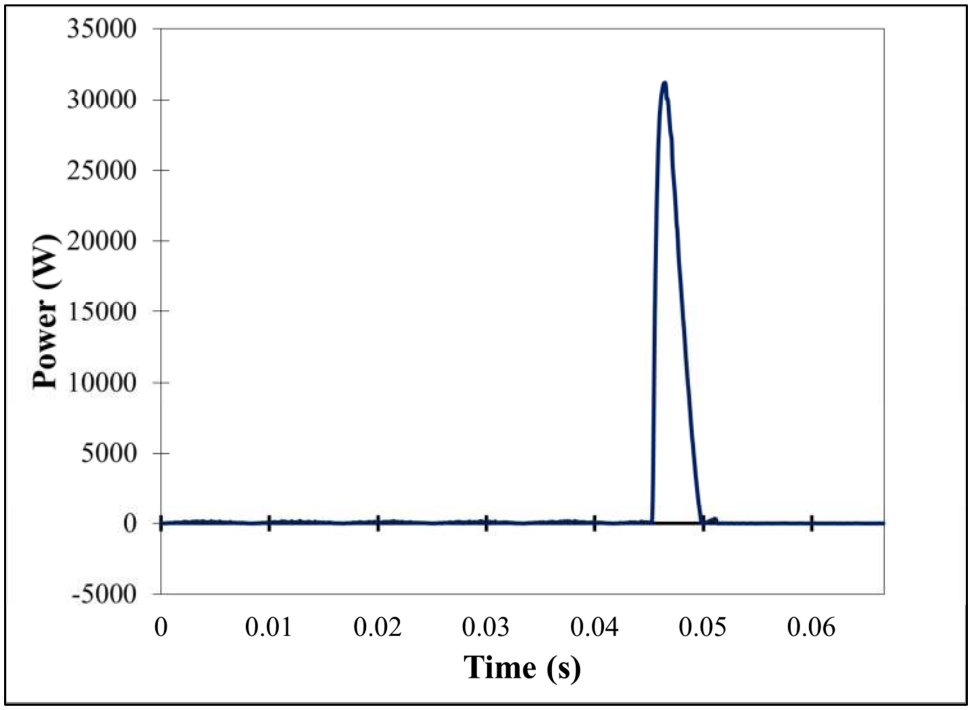

Figure 141 - Waveform of the instantaneous power produced in test 2-16 (32 kW/m^2). A total of 4 cycles (1/15 of a second) is shown.

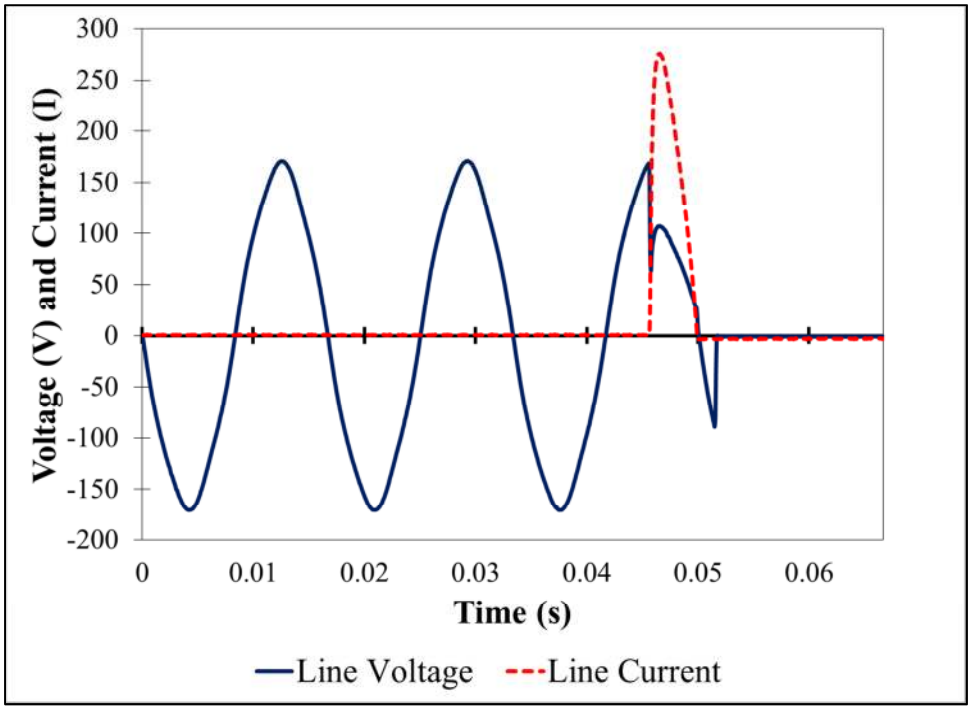

Figure 142 - Voltage and current waveforms produced in test 2-17 (30 kW/m^2). A total of 4 cycles (1/15 of a second) is shown.

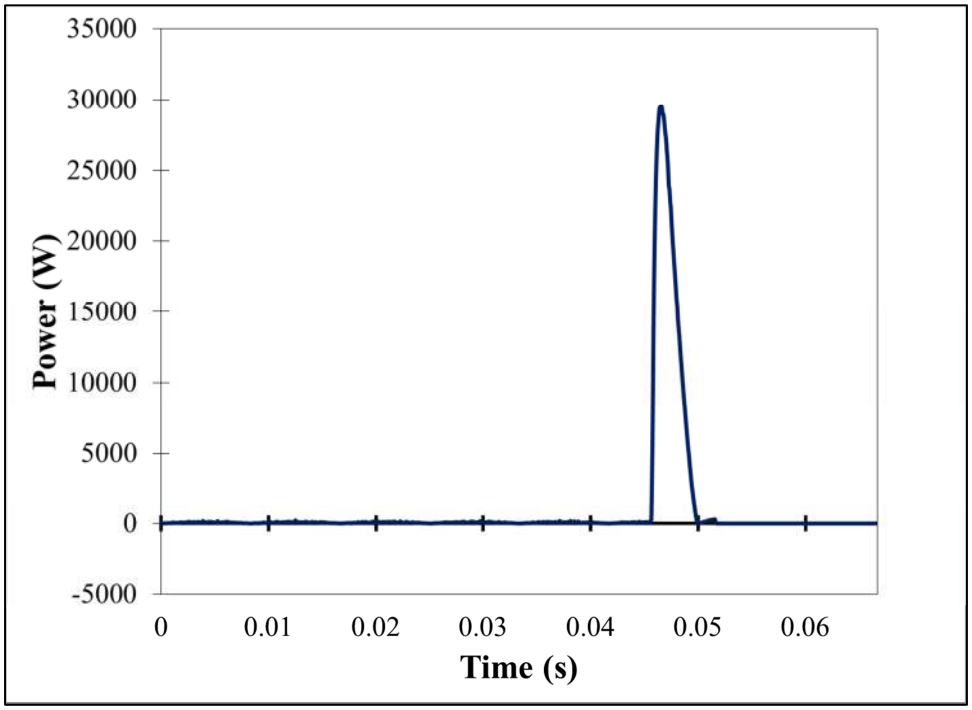

Figure 143 - Waveform of the instantaneous power produced in test 2-17 (30 kW/m^2). A total of 4 cycles (1/15 of a second) is shown.

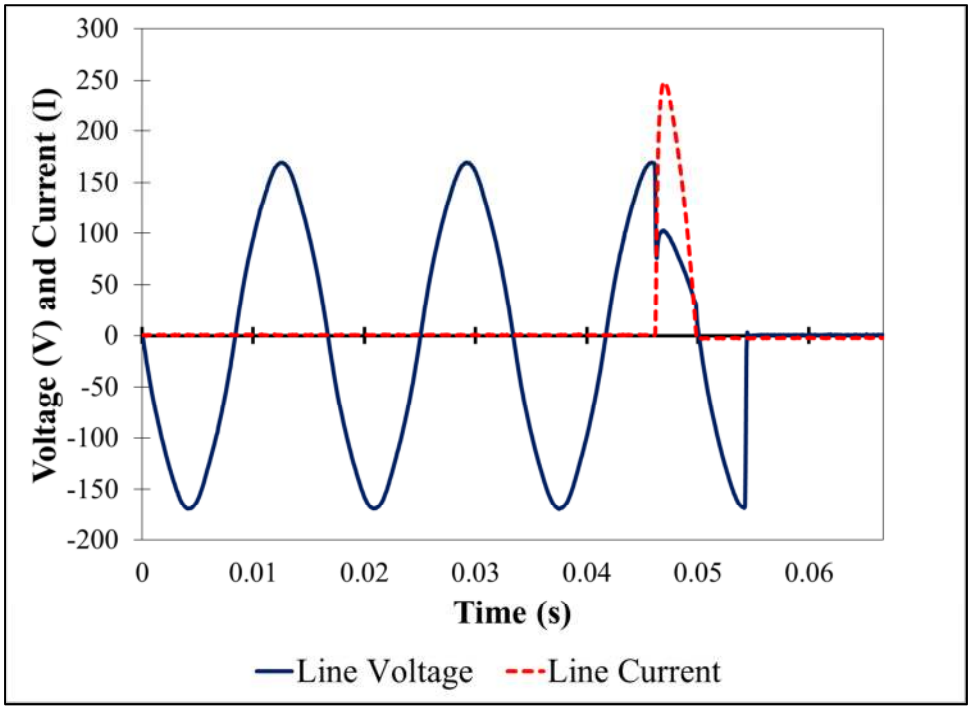

Figure 144 - Voltage and current waveforms produced in test 2-18 (28 kW/m^2). A total of 4 cycles (1/15 of a second) is shown.

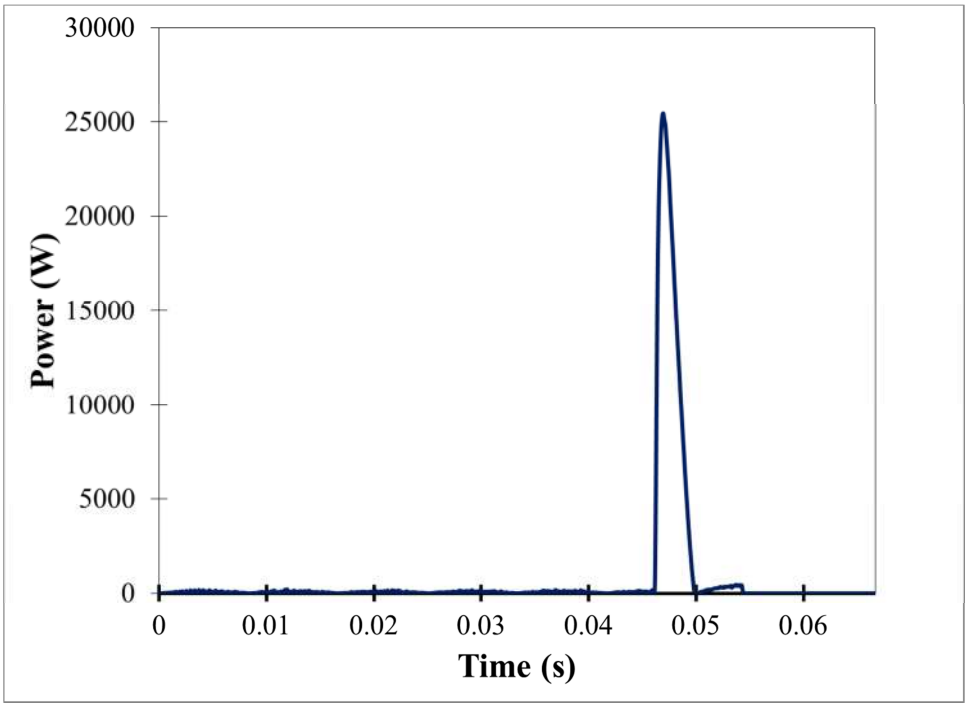

Figure 145 - Waveform of the instantaneous power produced in test 2-18 (28 kW/m^2). A total of 4 cycles (1/15 of a second) is shown.

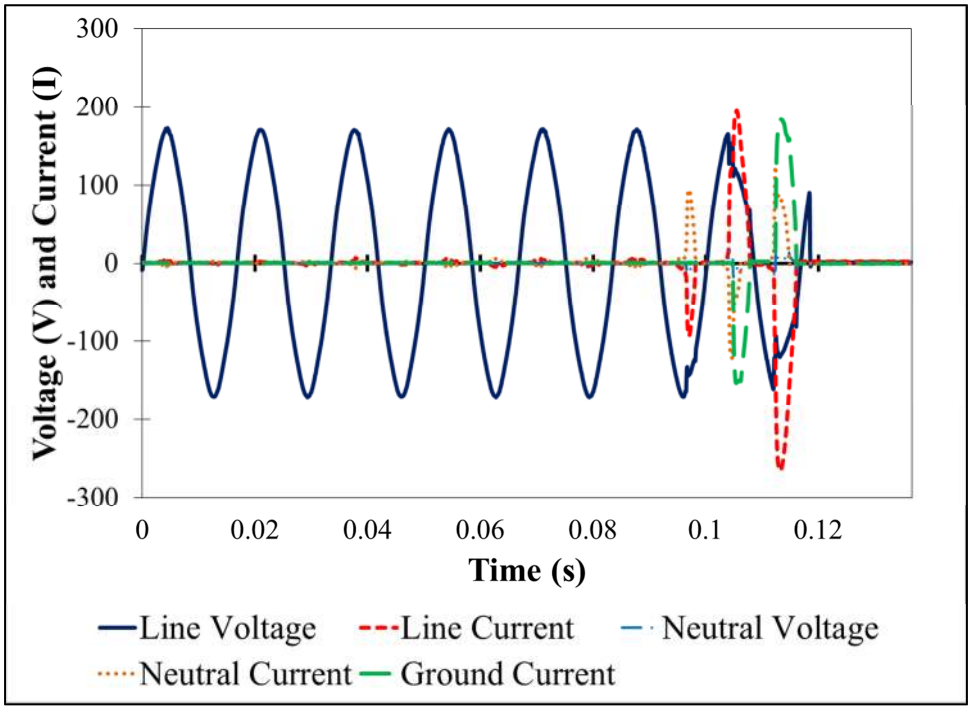

Figure 146 - Voltage and current waveforms produced in test 2-20 (26 kW/m^2). A total of 8 cycles (2/15 of a second) is shown.

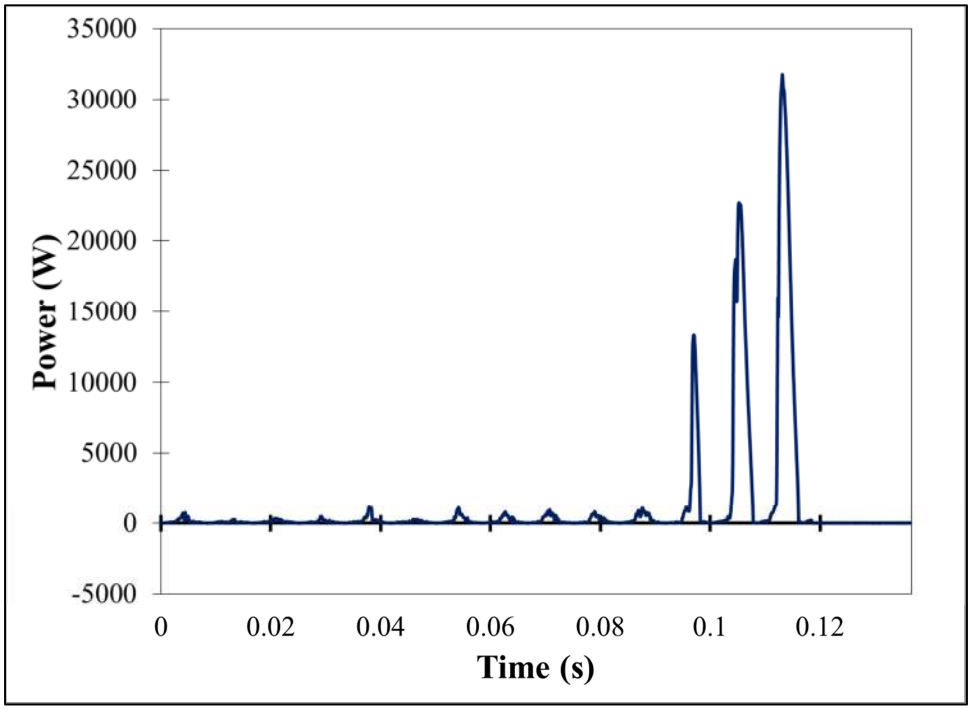

Figure 147 - Waveform of the instantaneous power produced in test 2-20 (26 kW/m^2). A total of 8 cycles (2/15 of a second) is shown.

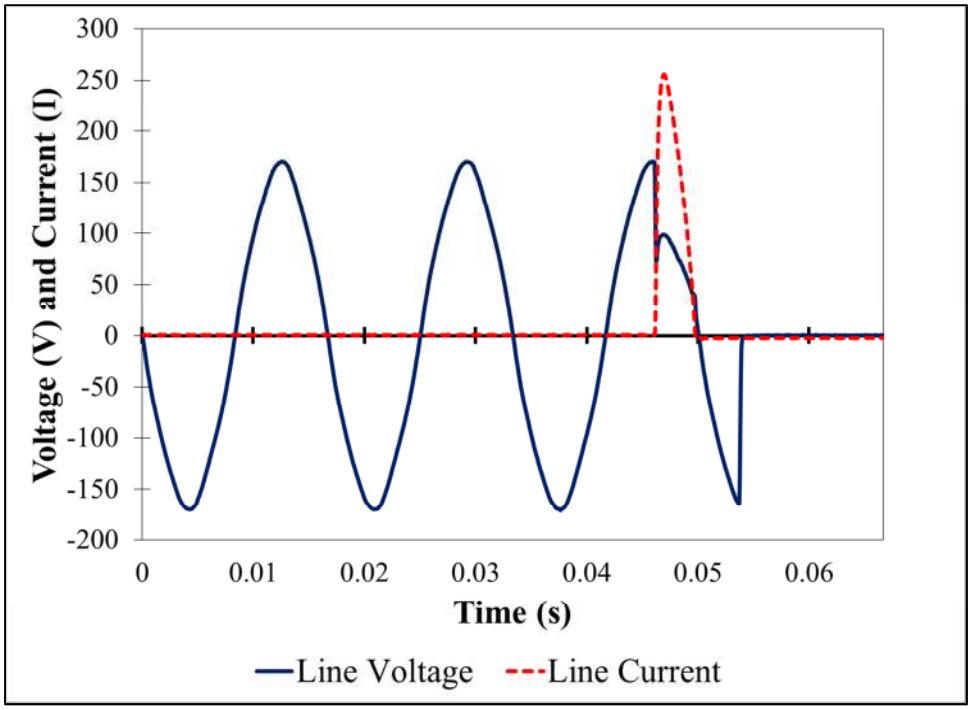

Figure 148 - Voltage and current waveforms produced in test 2-21 (26 kW/m^2). A total of 4 cycles (1/15 of a second) is shown.

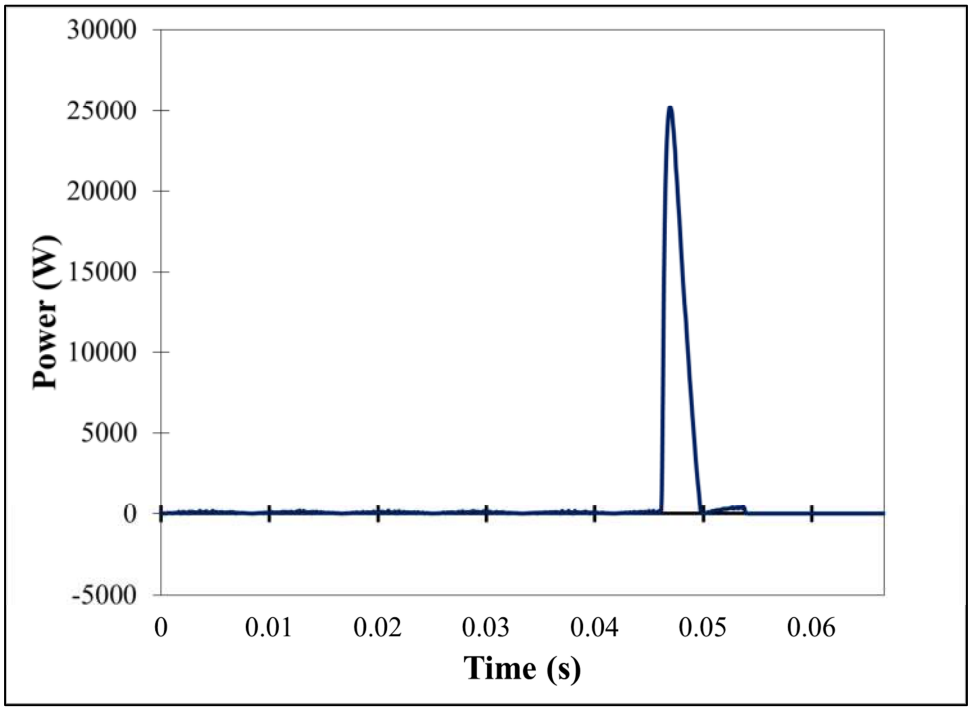

Figure 149 - Waveform of the instantaneous power produced in test 2-21 (26 kW/m^2). A total of 4 cycles (1/15 of a second) is shown.

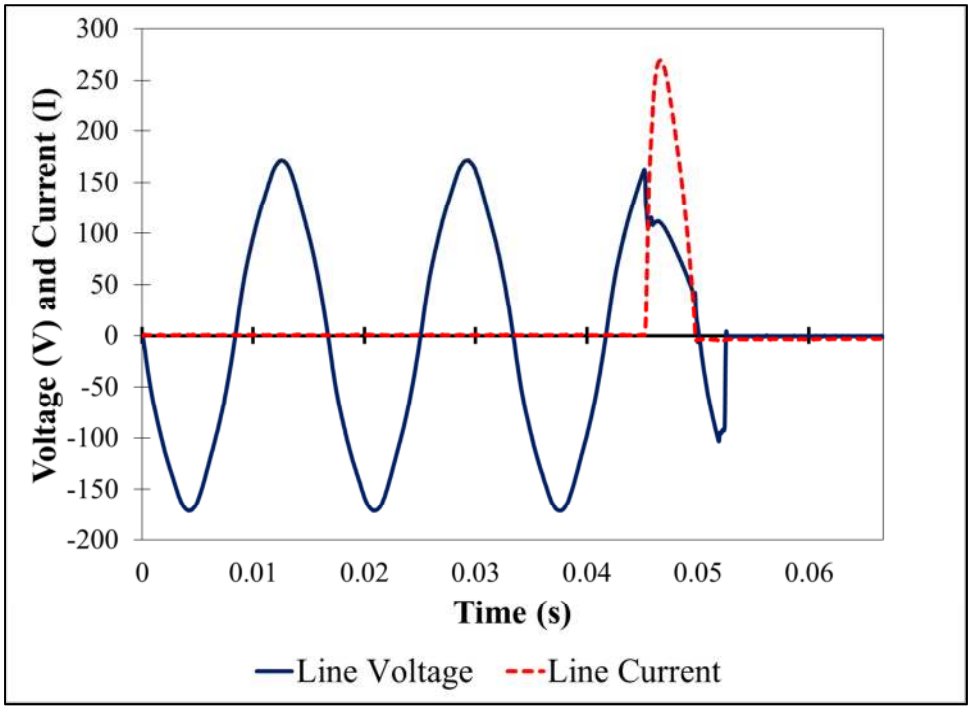

Figure 150 - Voltage and current waveforms produced in test 2-23 (24 kW/m^2). A total of 4 cycles (1/15 of a second) is shown.

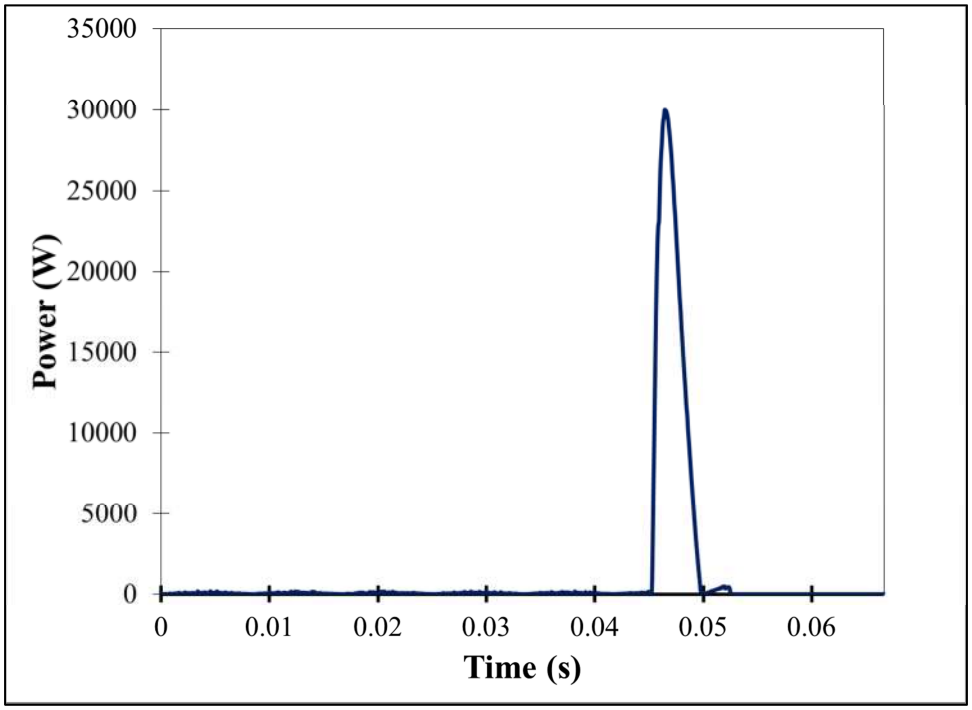

Figure 151 - Waveform of the instantaneous power produced in test 2-23 (24 kW/m^2). A total of 4 cycles (1/15 of a second) is shown.

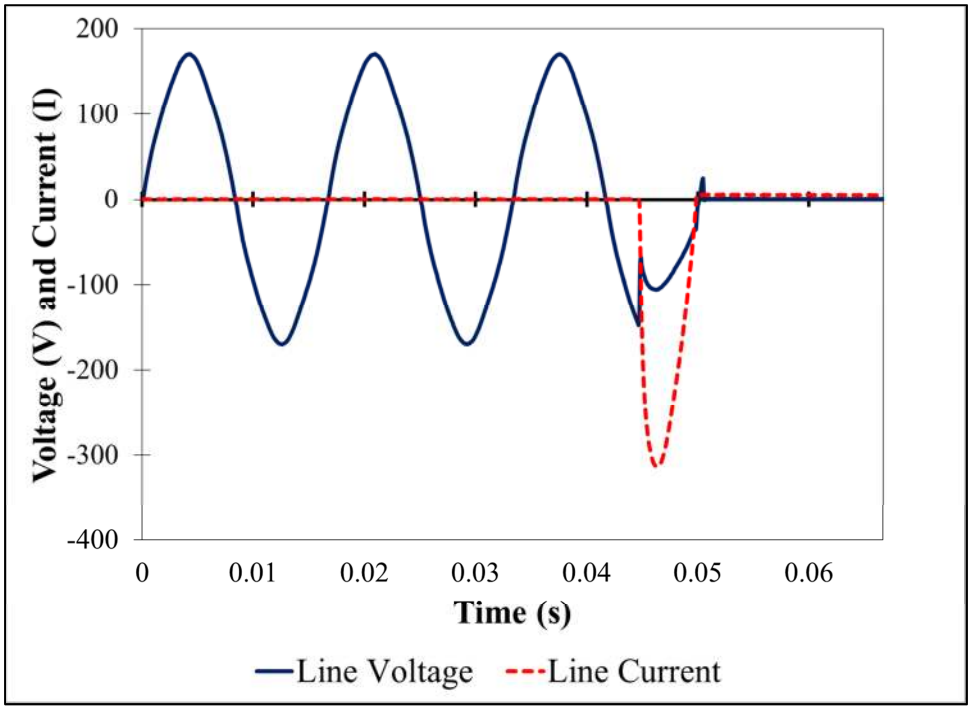

Figure 152 - Voltage and current waveforms produced in test 2-26 (50 kW/m^2). A total of 4 cycles (1/15 of a second) is shown.

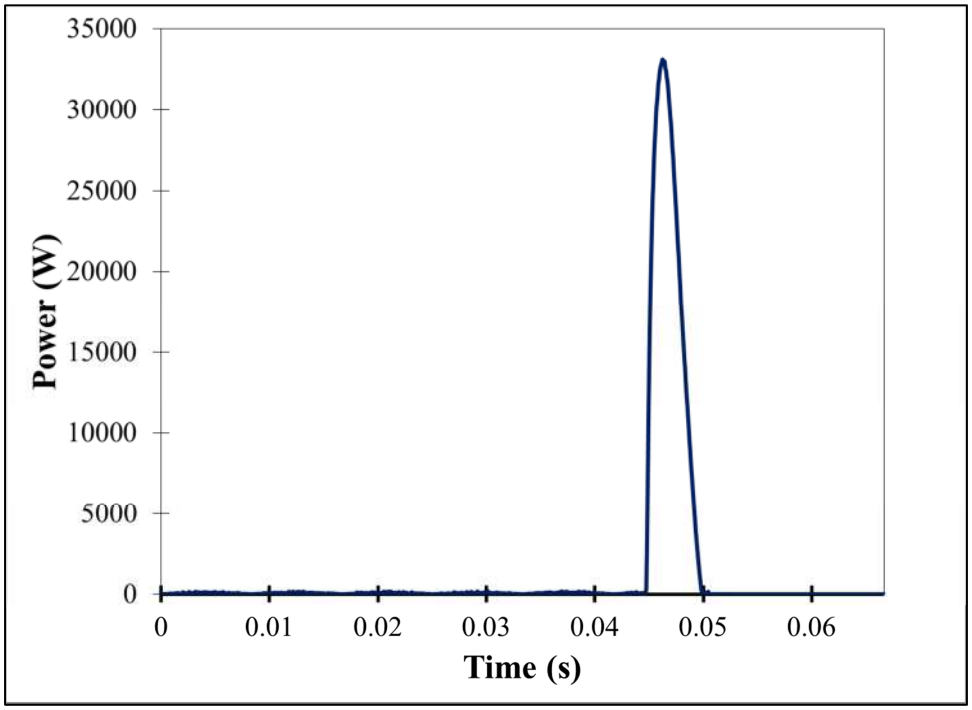

Figure 153 - Waveform of the instantaneous power produced in test 2-26 (50 kW/m^2). A total of 4 cycles (1/15 of a second) is shown.

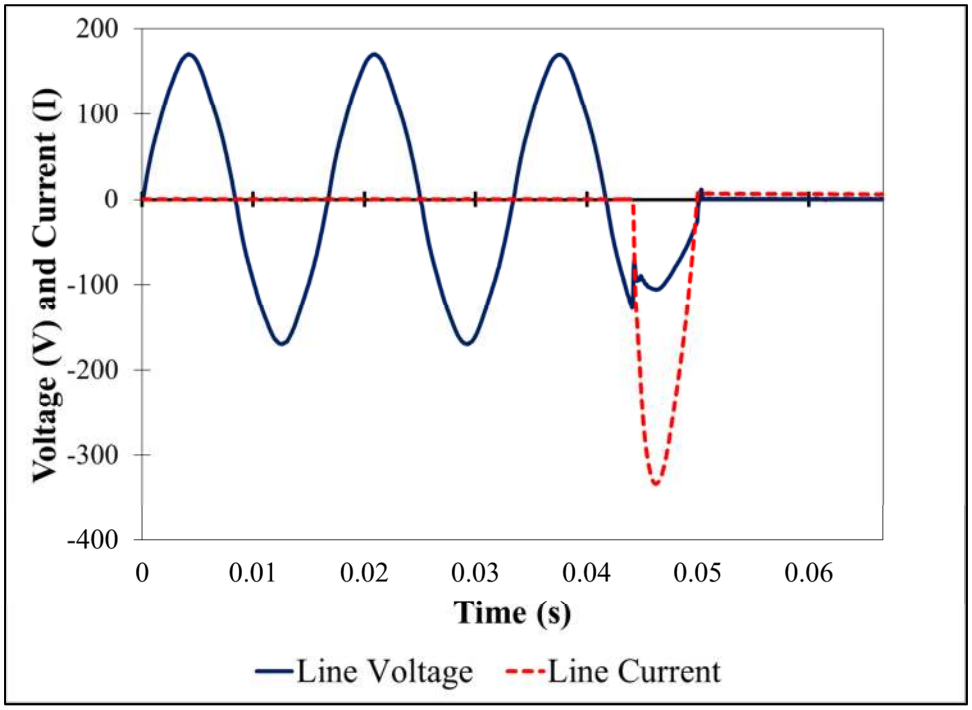

Figure 154 - Voltage and current waveforms produced in test 2-27 (50 kW/m^2). A total of 4 cycles (1/15 of a second) is shown.

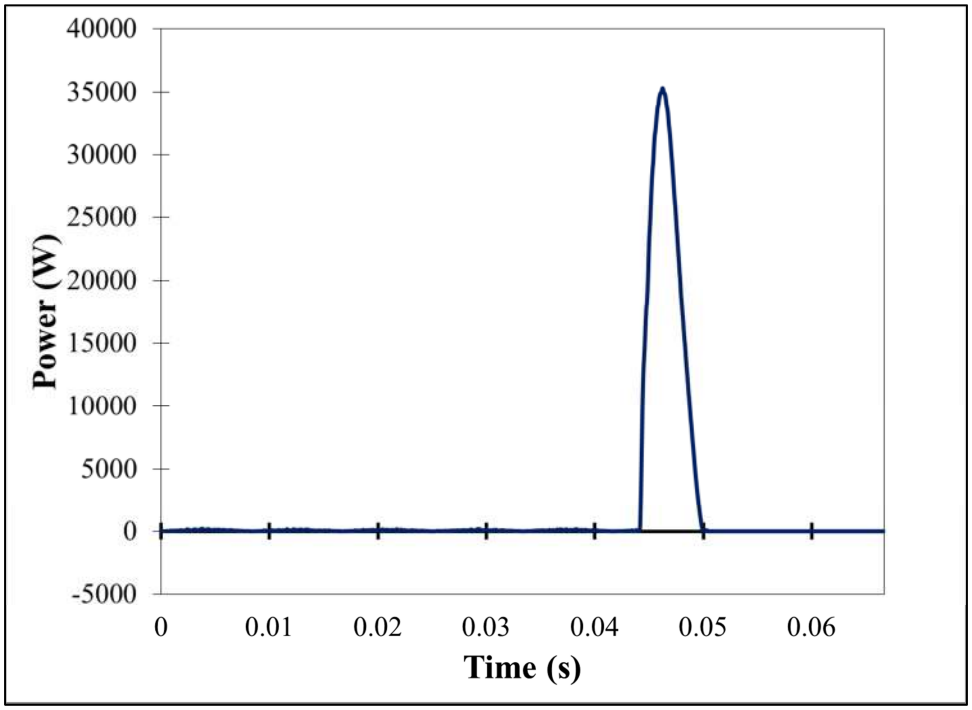

Figure 155 - Waveform of the instantaneous power produced in test 2-27 (50 kW/m^2). A total of 4 cycles (1/15 of a second) is shown.

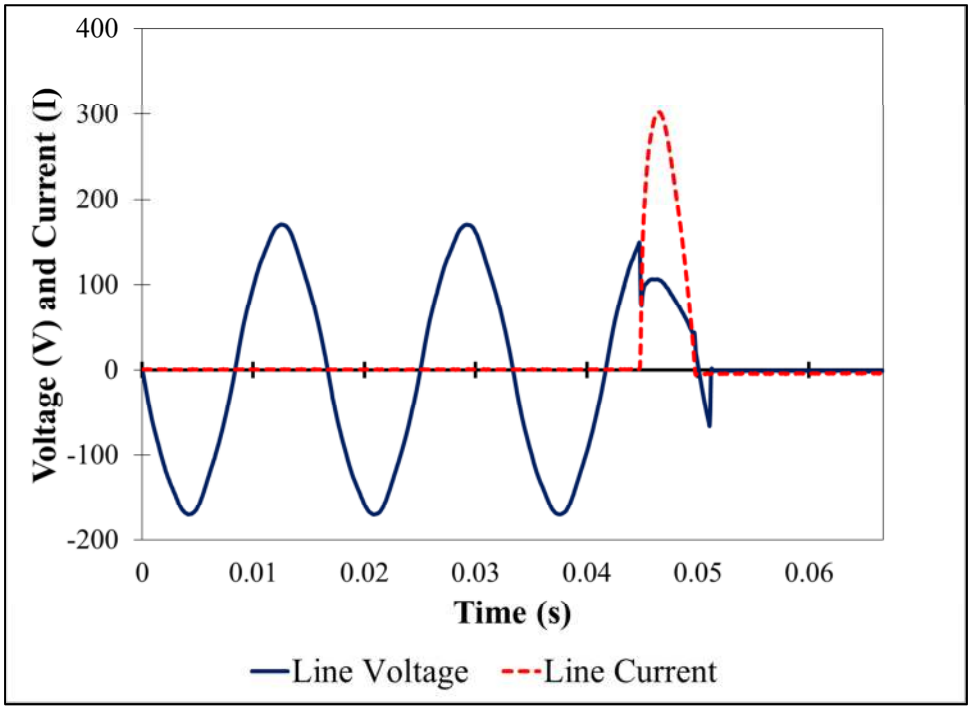

Figure 156 - Voltage and current waveforms produced in test 2-28 (34 kW/m^2). A total of 4 cycles (1/15 of a second) is shown.

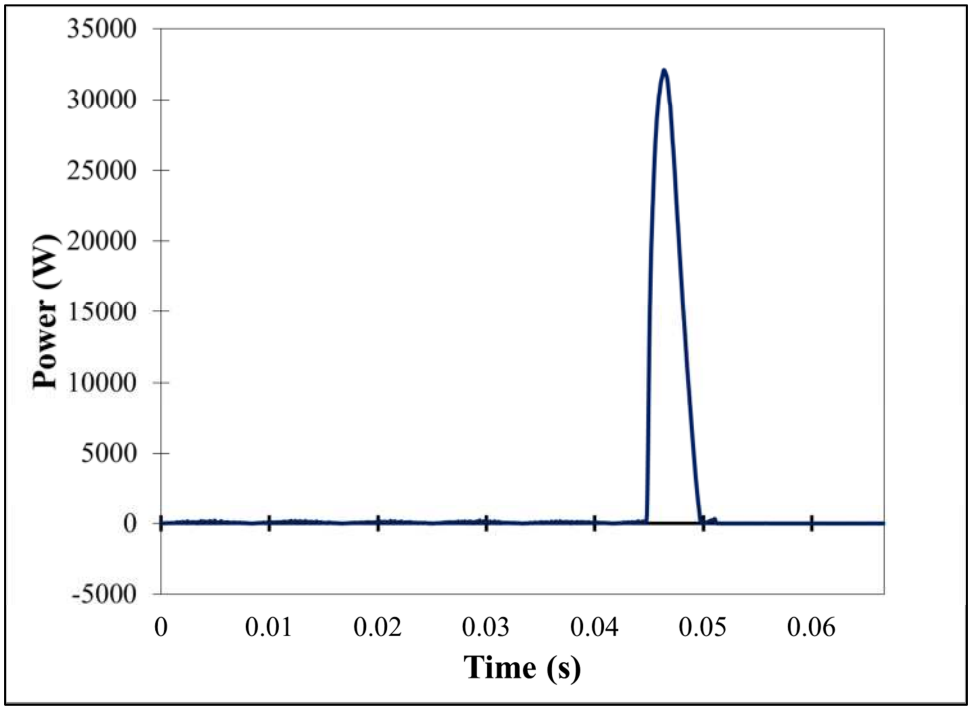

Figure 157 - Waveform of the instantaneous power produced in test 2-28 (34 kW/m^2). A total of 4 cycles (1/15 of a second) is shown.

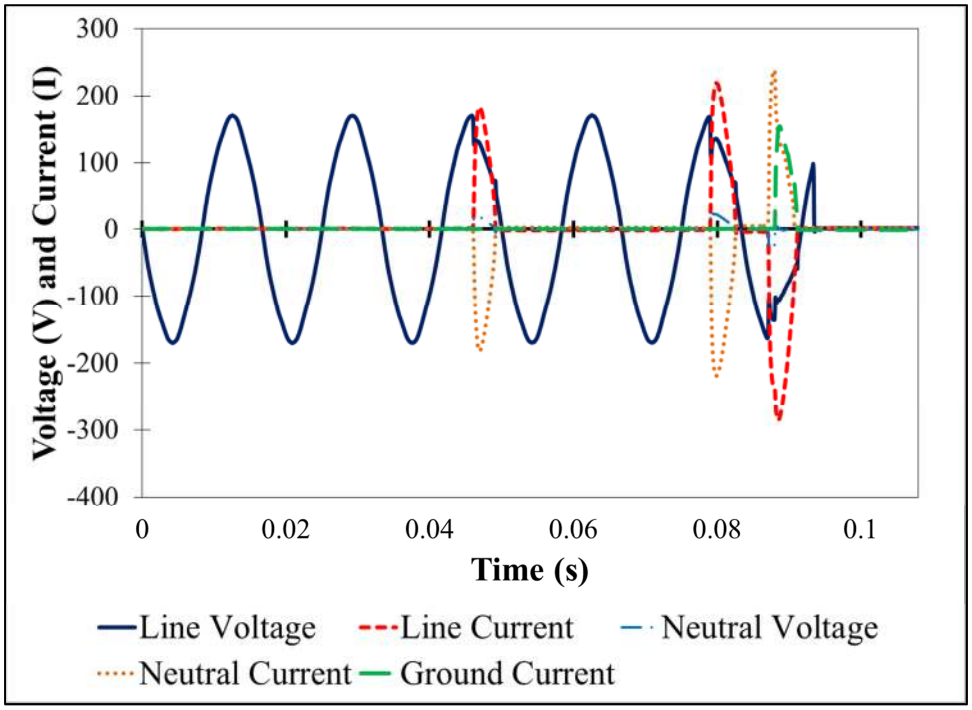

Figure 158 - Voltage and current waveforms produced in test 2-29 (32 kW/m^2). A total of 6 cycles (1/10 of a second) is shown.

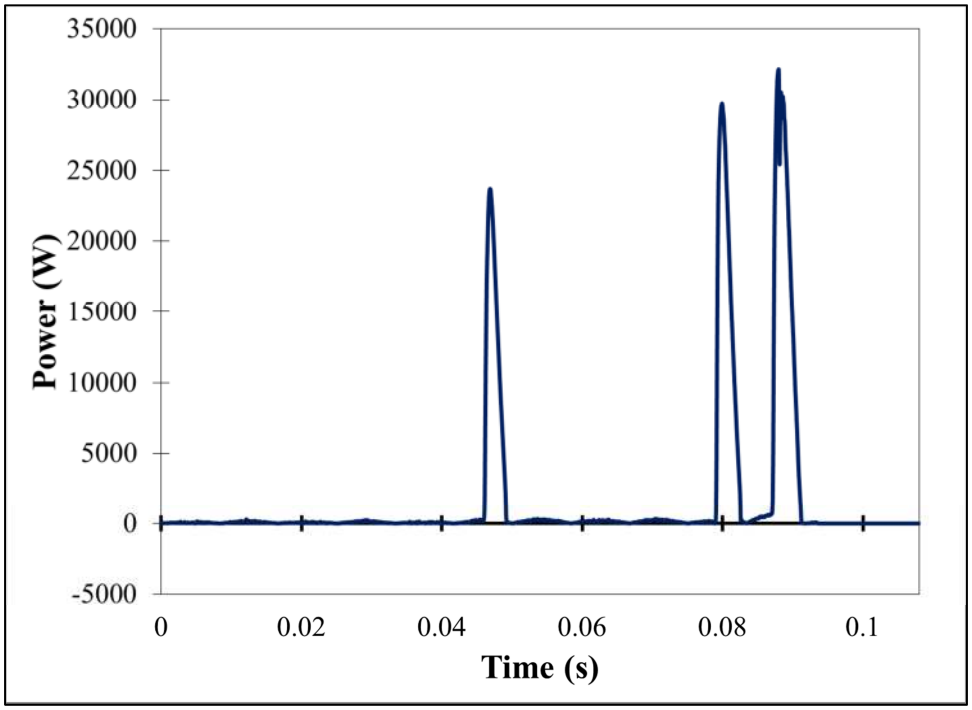

Figure 159 - Waveform of the instantaneous power produced in test 2-29 (32 kW/m^2). A total of 6 cycles (1/10 of a second) is shown.

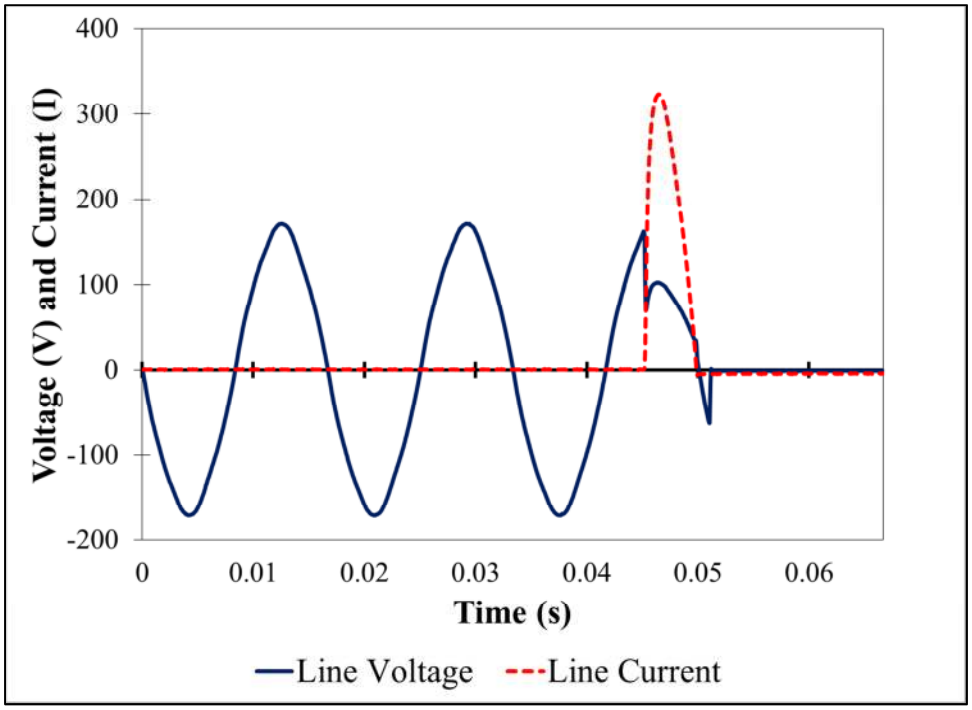

Figure 160 - Voltage and current waveforms produced in test 2-30 (32 kW/m^2). A total of 4 cycles (1/15 of a second) is shown.

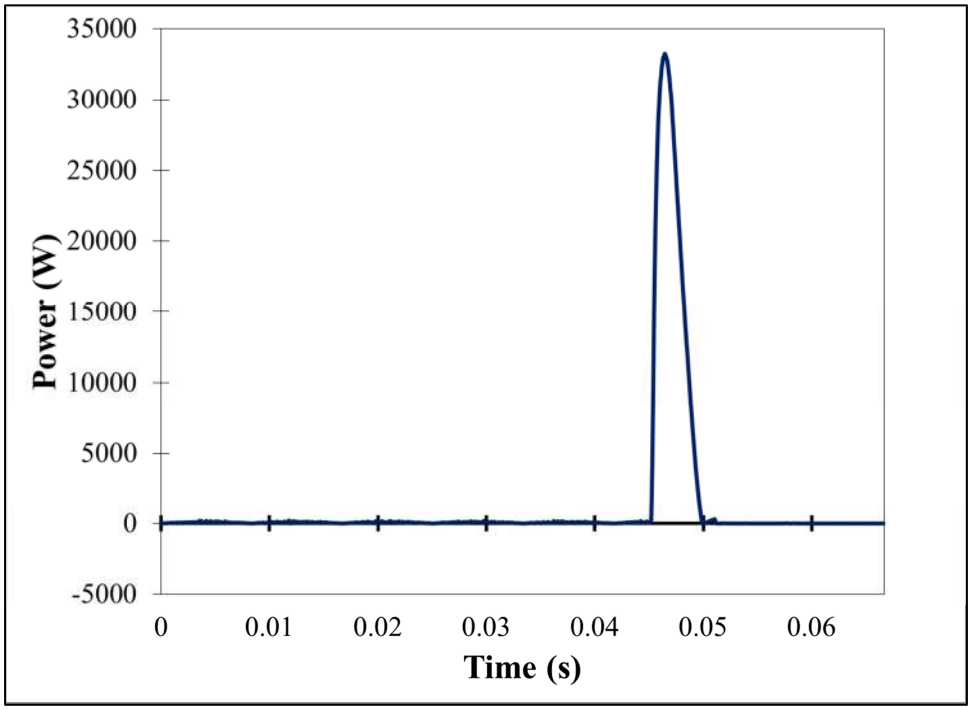

Figure 161 - Waveform of the instantaneous power produced in test 2-30 (32 kW/m^2). A total of 4 cycles (1/15 of a second) is shown.

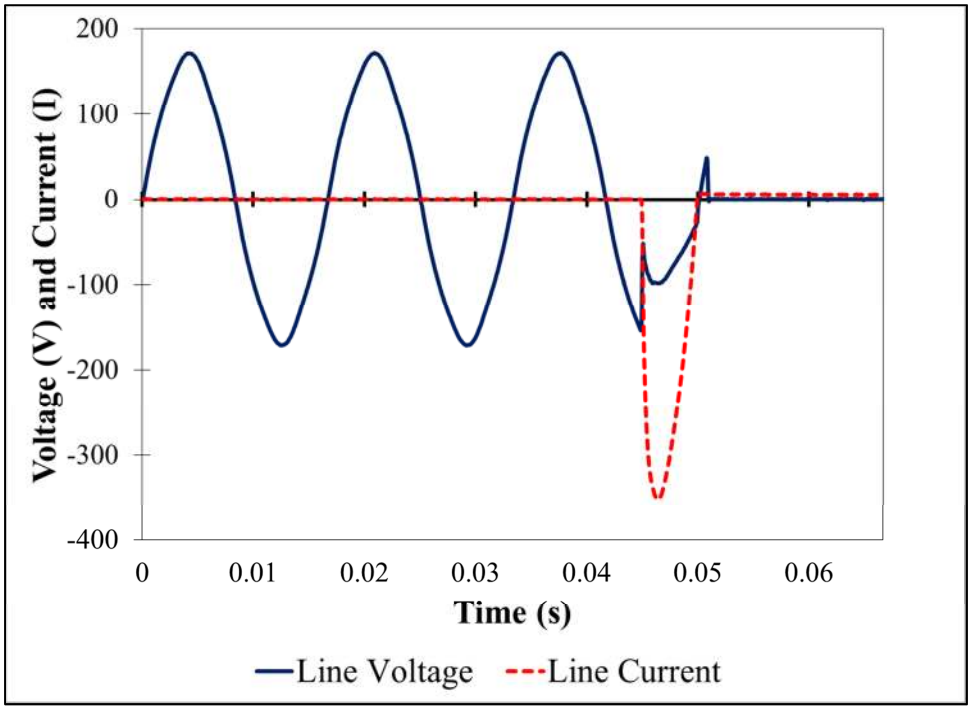

Figure 162 - Voltage and current waveforms produced in test 2-34 (40 kW/m^2). A total of 4 cycles (1/15 of a second) is shown.

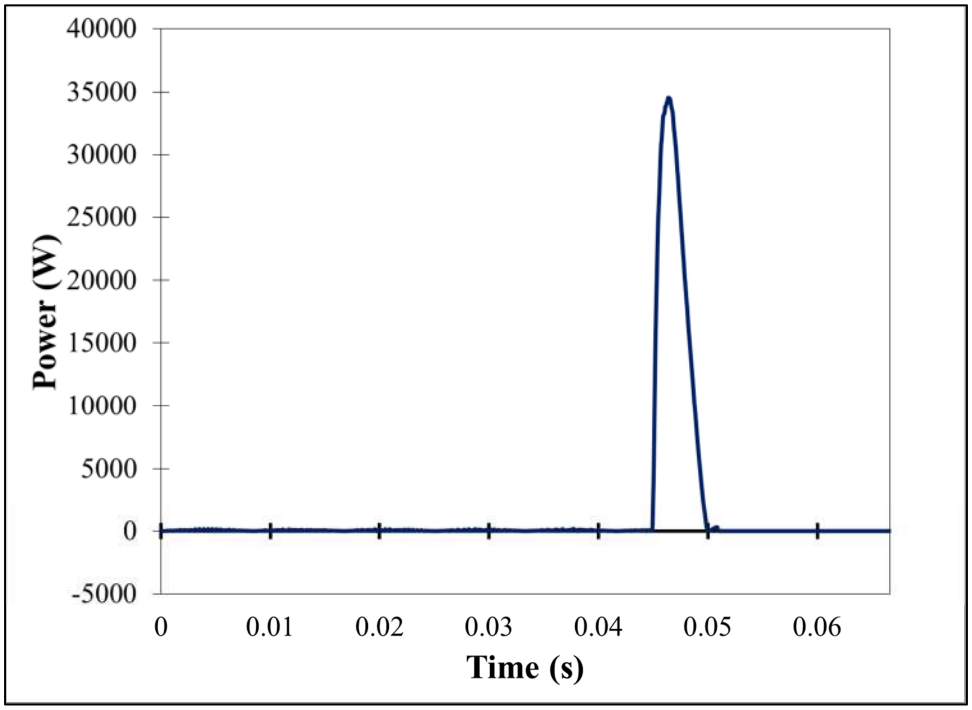

Figure 163 - Waveform of the instantaneous power produced in test 2-34 (40 kW/m^2). A total of 4 cycles (1/15 of a second) is shown.

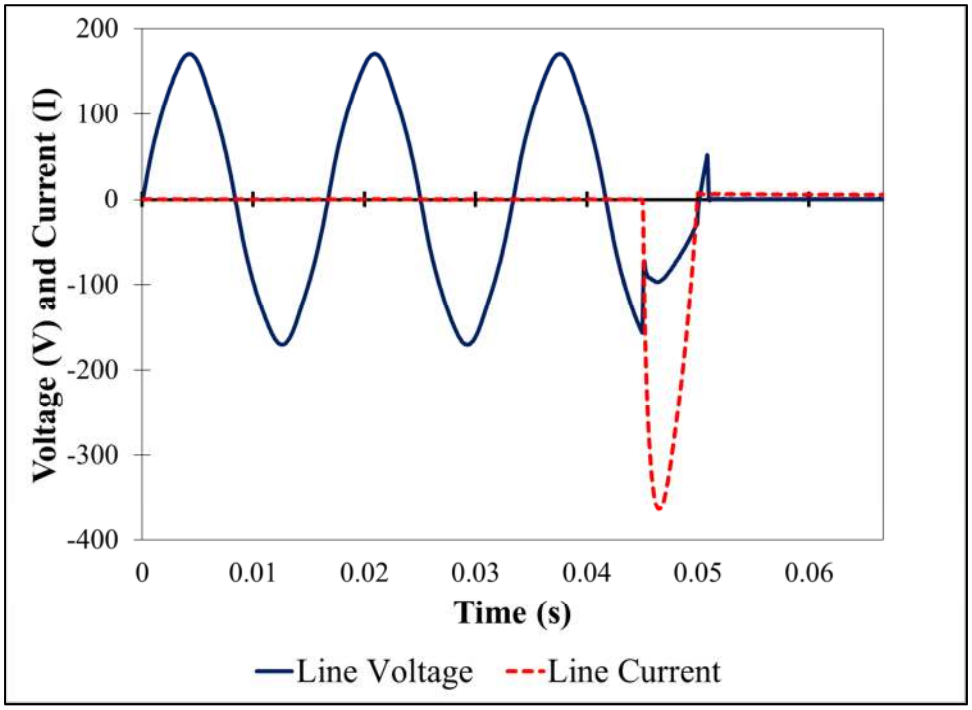

Figure 164 - Voltage and current waveforms produced in test 2-35 (42 kW/m^2). A total of 4 cycles (1/15 of a second) is shown.

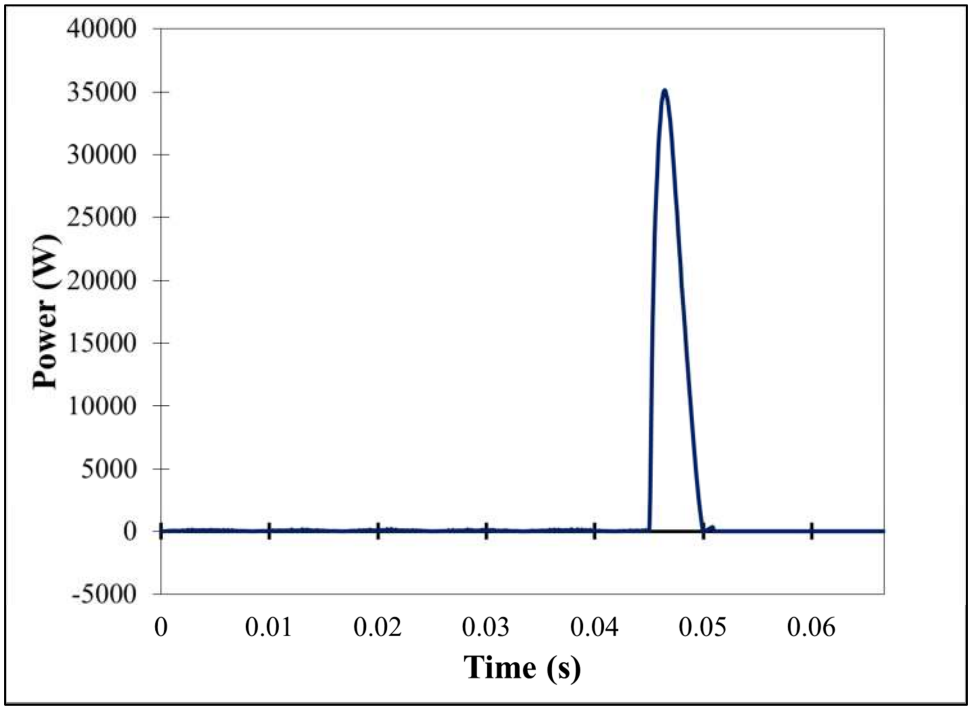

Figure 165 - Waveform of the instantaneous power produced in test 2-35 (42 kW/m^2). A total of 4 cycles (1/15 of a second) is shown.

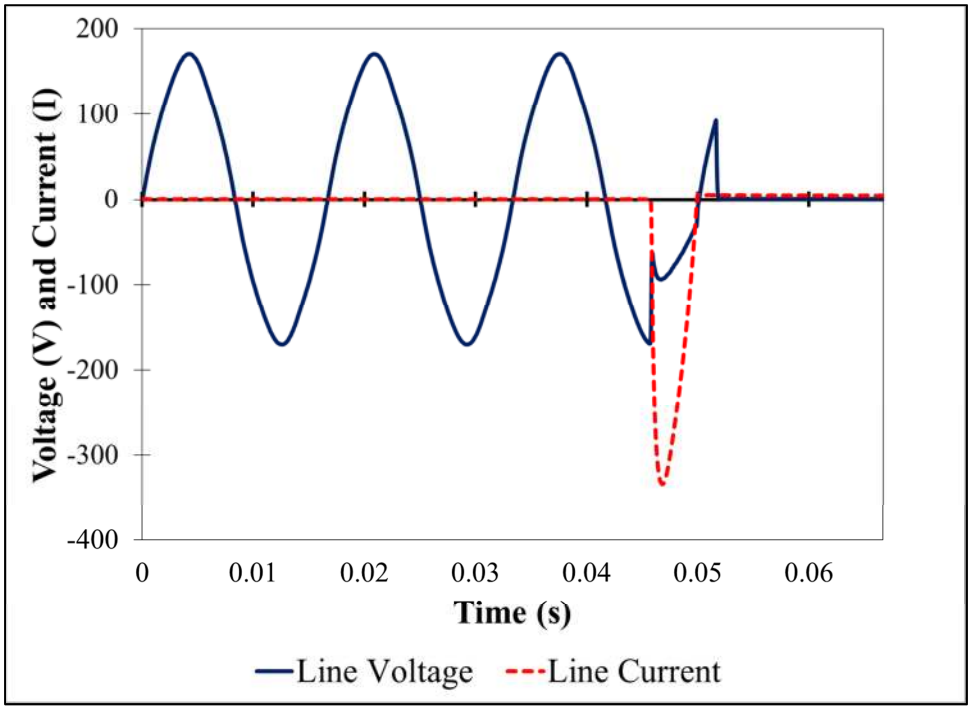

Figure 166 - Voltage and current waveforms produced in test 2-36 (53 kW/m^2). A total of 4 cycles (1/15 of a second) is shown.

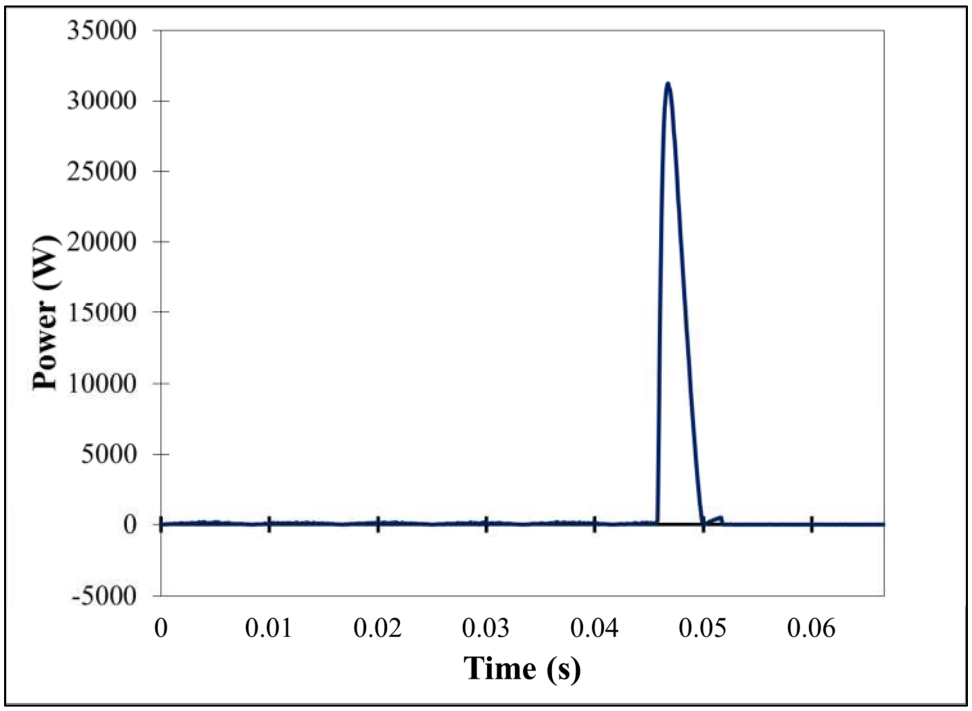

Figure 167 - Waveform of the instantaneous power produced in test 2-36 (53 kW/m^2). A total of 4 cycles (1/15 of a second) is shown.

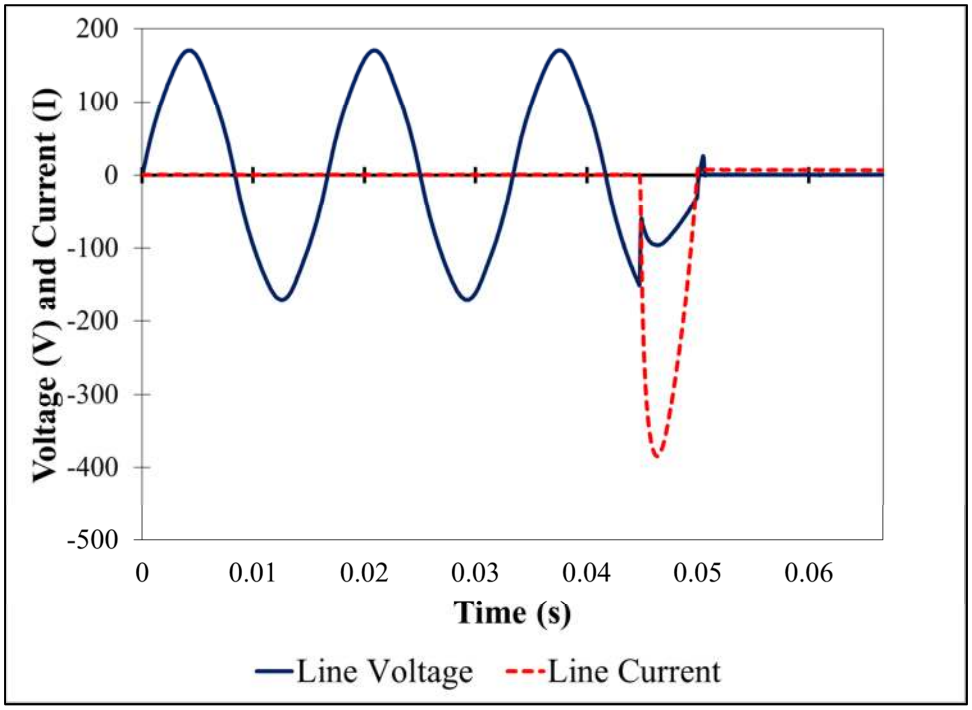

Figure 168 - Voltage and current waveforms produced in test 2-37 (52 kW/m^2). A total of 4 cycles (1/15 of a second) is shown.

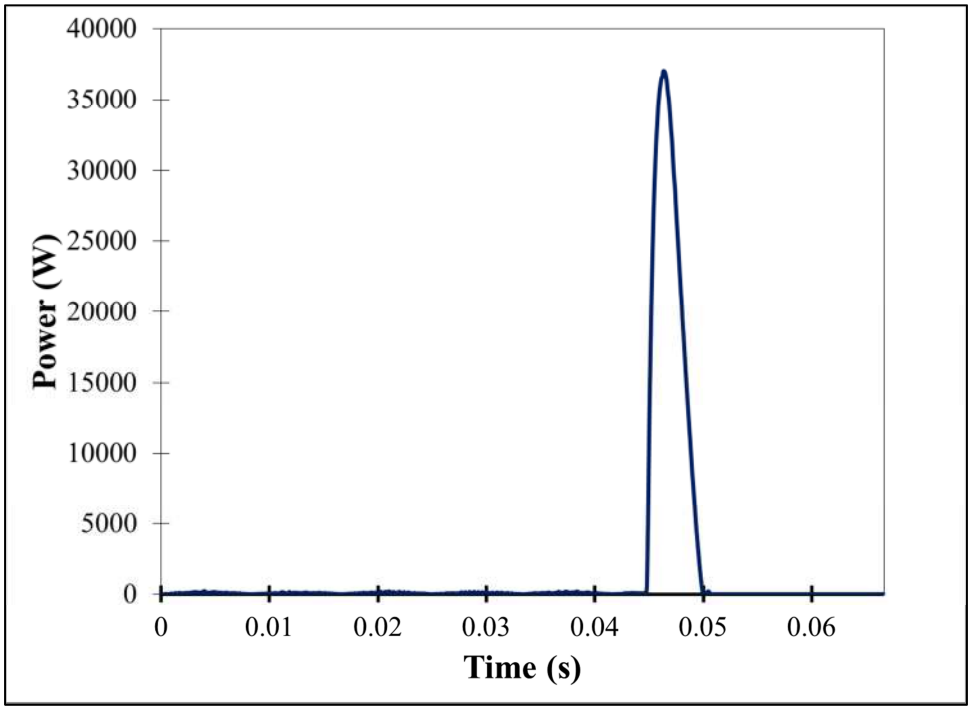

Figure 169 - Waveform of the instantaneous power produced in test 2-37 (52 kW/m^2). A total of 4 cycles (1/15 of a second) is shown.

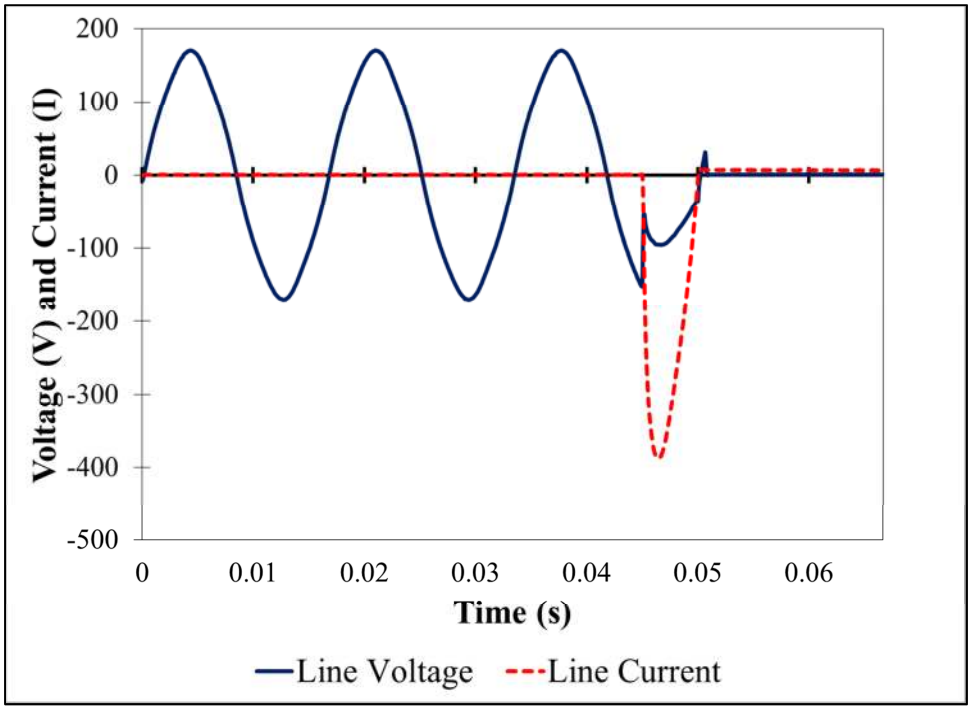

Figure 170 - Voltage and current waveforms produced in test 2-38 (48 kW/m^2). A total of 4 cycles (1/15 of a second) is shown.

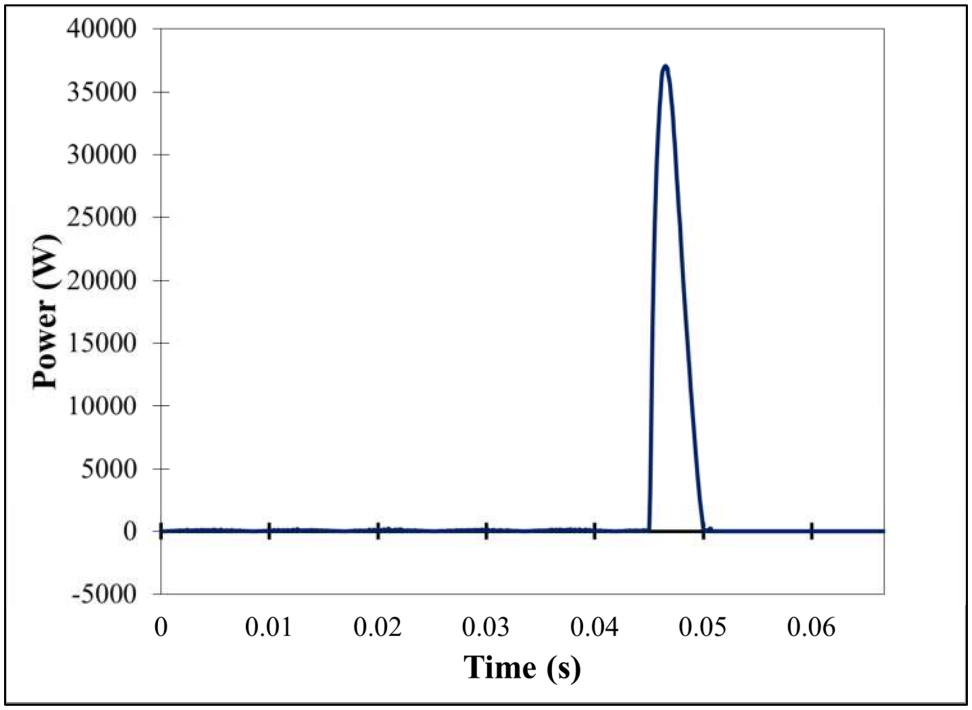

Figure 171 - Waveform of the instantaneous power produced in test 2-38 (48 kW/m^2). A total of 4 cycles (1/15 of a second) is shown.

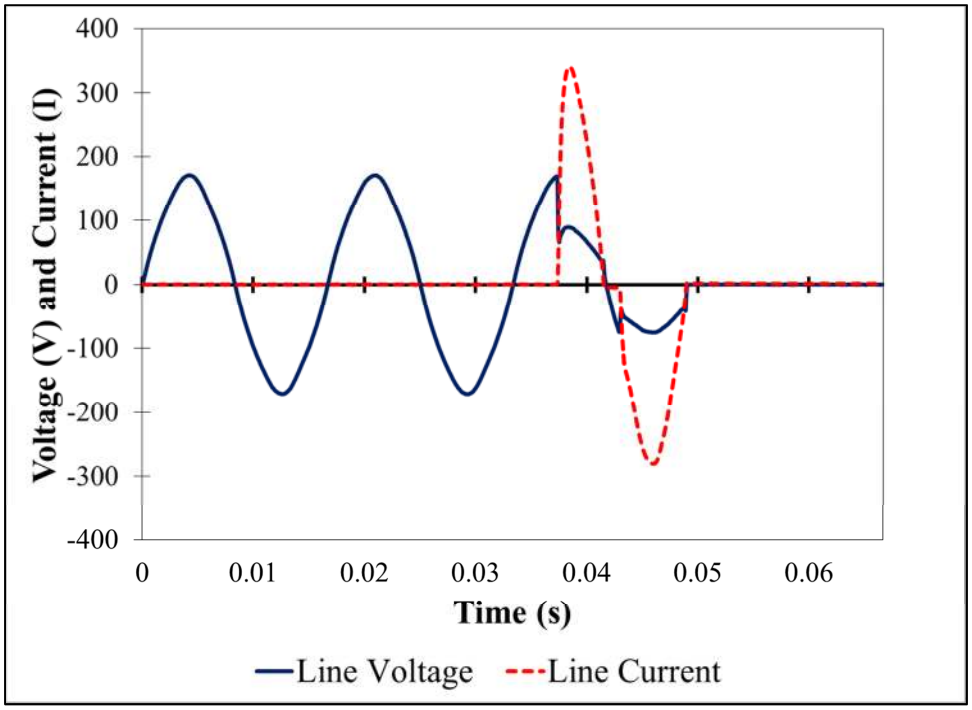

Figure 172 - Voltage and current waveforms produced in test 2-39 (44 kW/m^2). A total of 4 cycles (1/15 of a second) is shown.

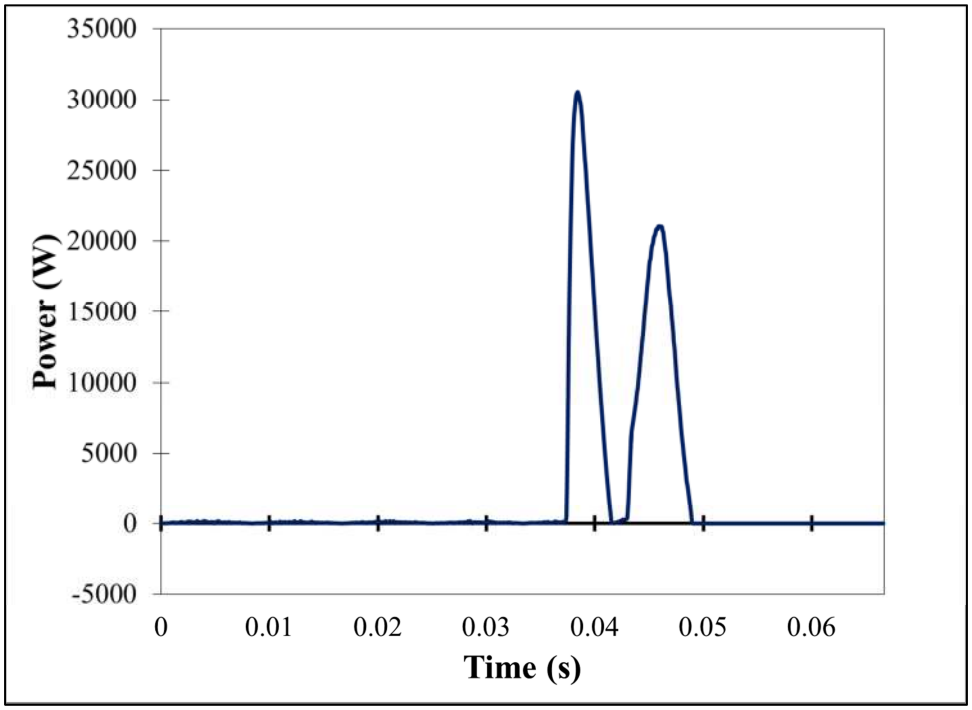

Figure 173 - Waveform of the instantaneous power produced in test 2-39 (44 kW/m^2). A total of 4 cycles (1/15 of a second) is shown.

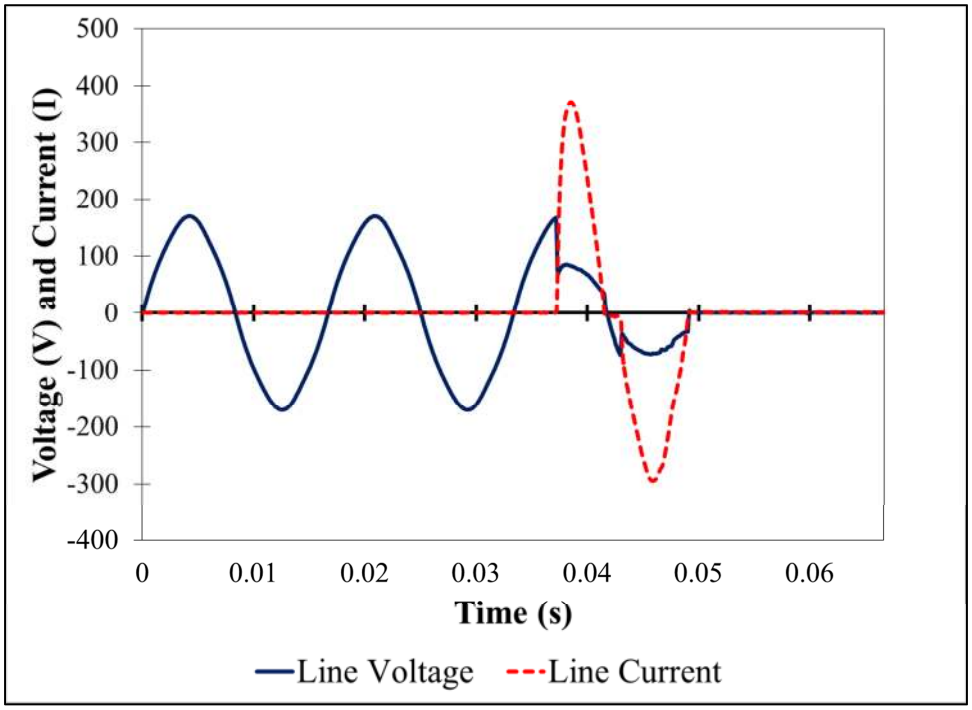

Figure 174 - Voltage and current waveforms produced in test 2-40 (39 kW/m^2). A total 4 cycles is (1/15 of a second) shown.

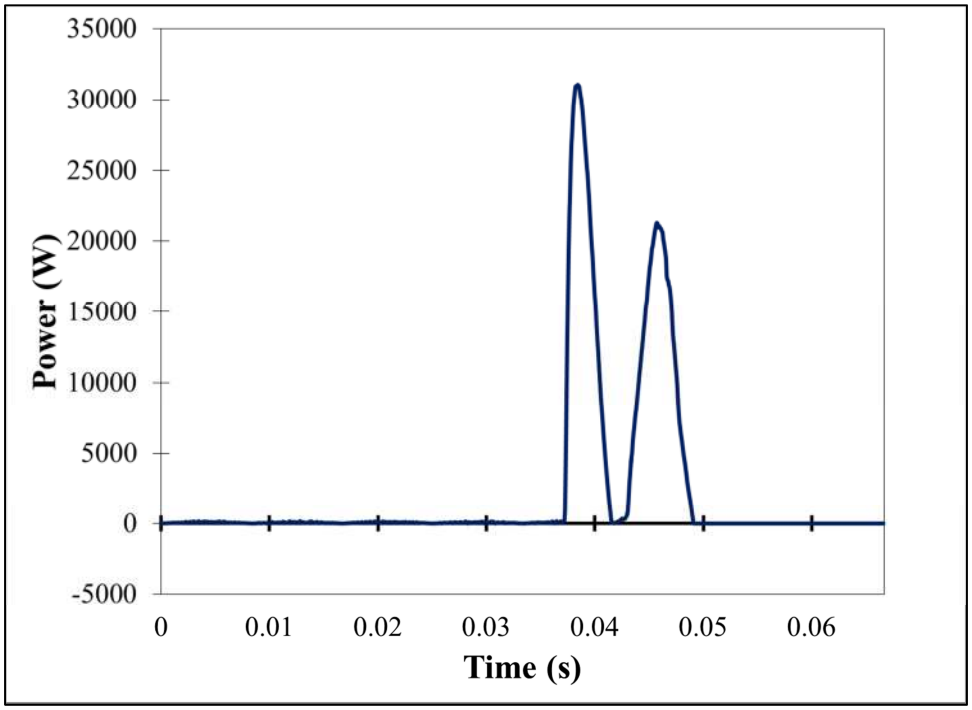

Figure 175 - Waveform of the instantaneous power produced in test 2-40 (39 kW/m^2). A total of 4 cycles (1/15 of a second) is shown.

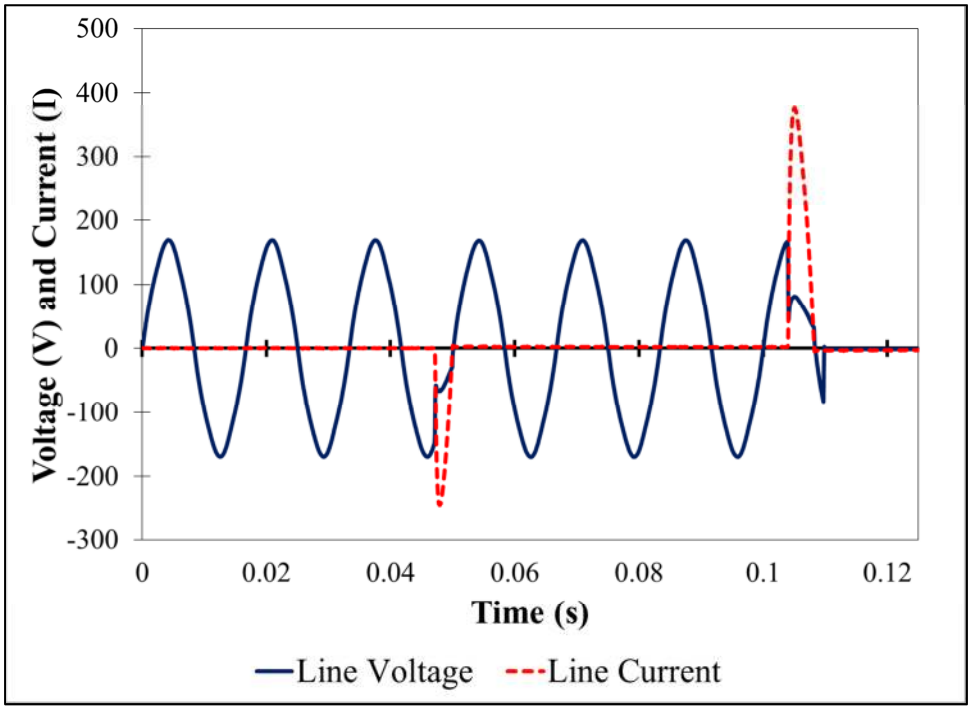

Figure 176 - Voltage and current waveforms produced in test 2-42 (37 kW/m^2). A total of 7.5 cycles (1/8 of a second) is shown.

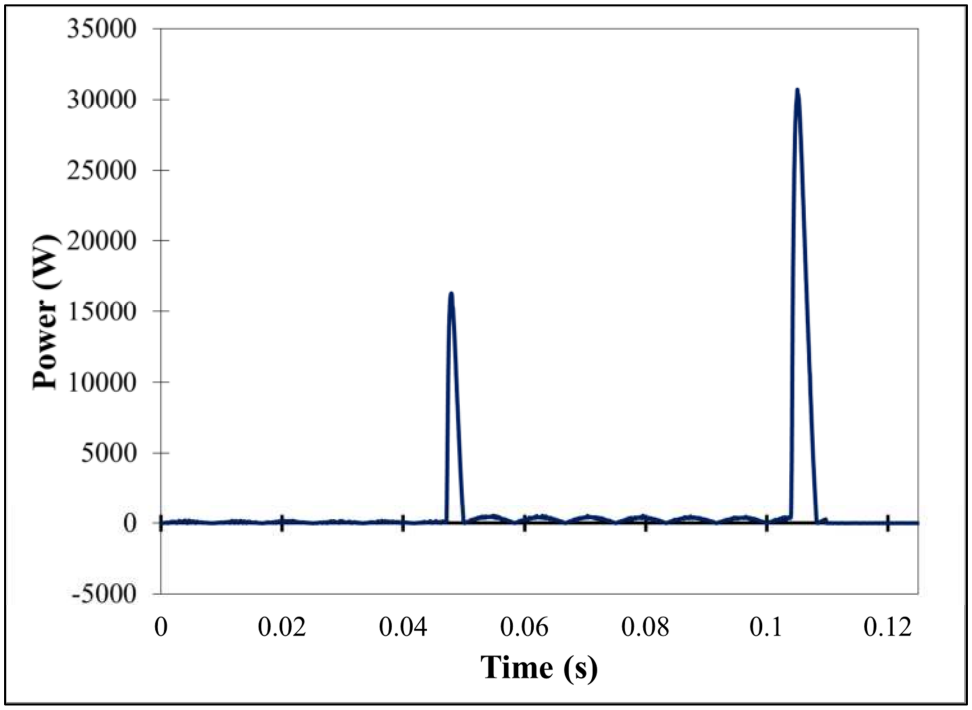

Figure 177 - Waveform of the instantaneous power produced in test 2-42 (37 kW/m^2). A total of 7.5 cycles (1/8 of a second) is shown.

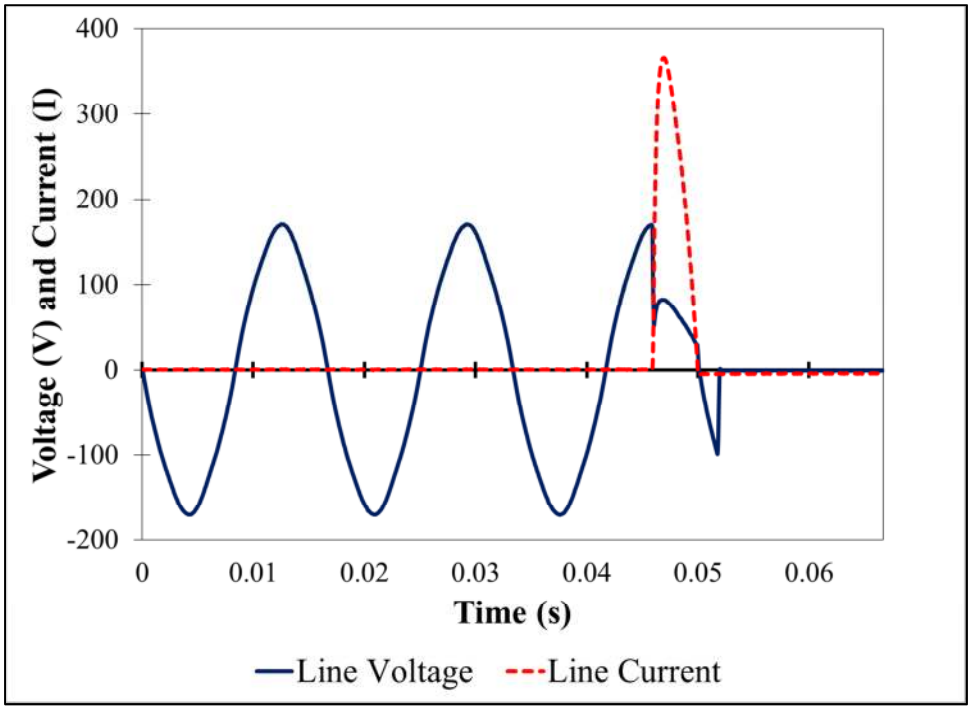

Figure 178 - Voltage and current waveforms produced in test 2-43 (35 kW/m^2). A total of 4 cycles (1/15 of a second) is shown.

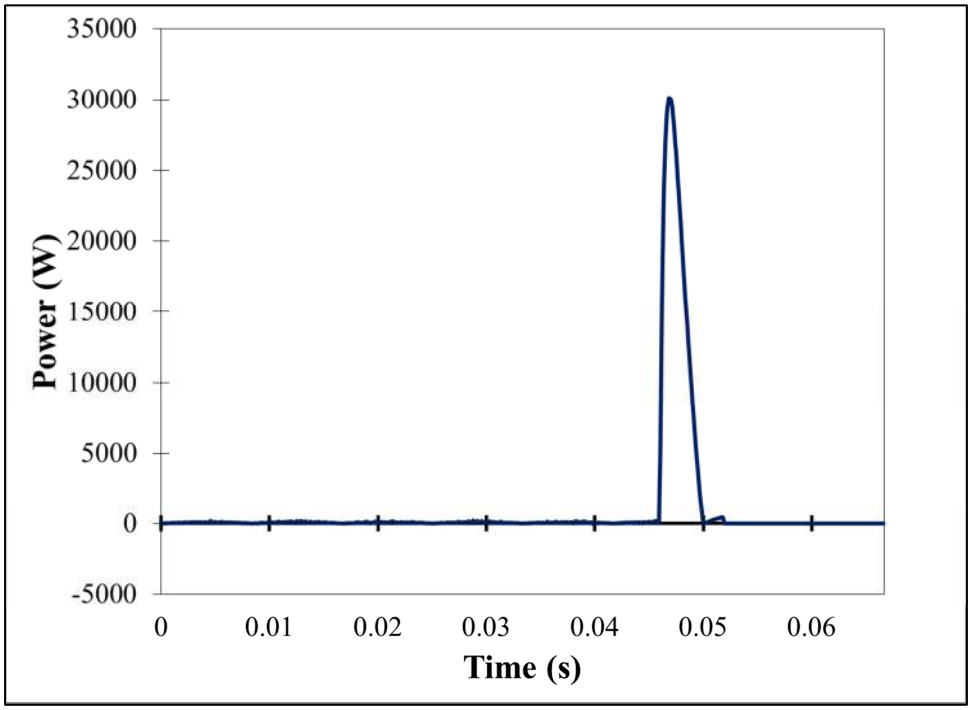

Figure 179 - Waveform of the instantaneous power produced in test 2-43 (35 kW/m^2). A total of 4 cycles (1/15 of a second) is shown.

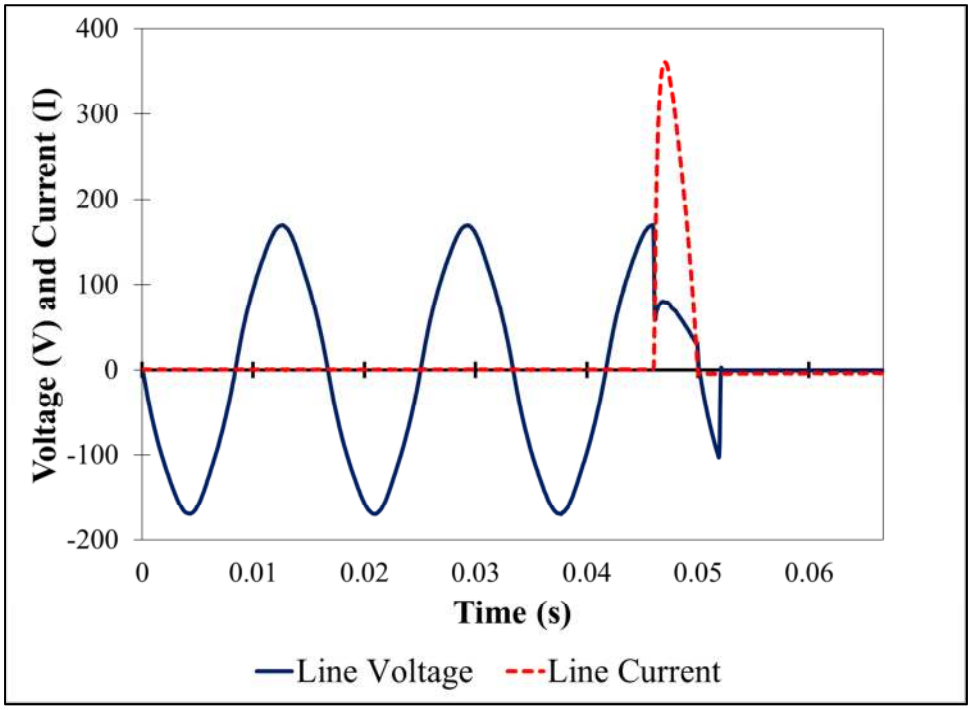

Figure 180 - Voltage and current waveforms produced in test 2-44 (33 kW/m^2). A total of 4 cycles (1/15 of a second) is shown.

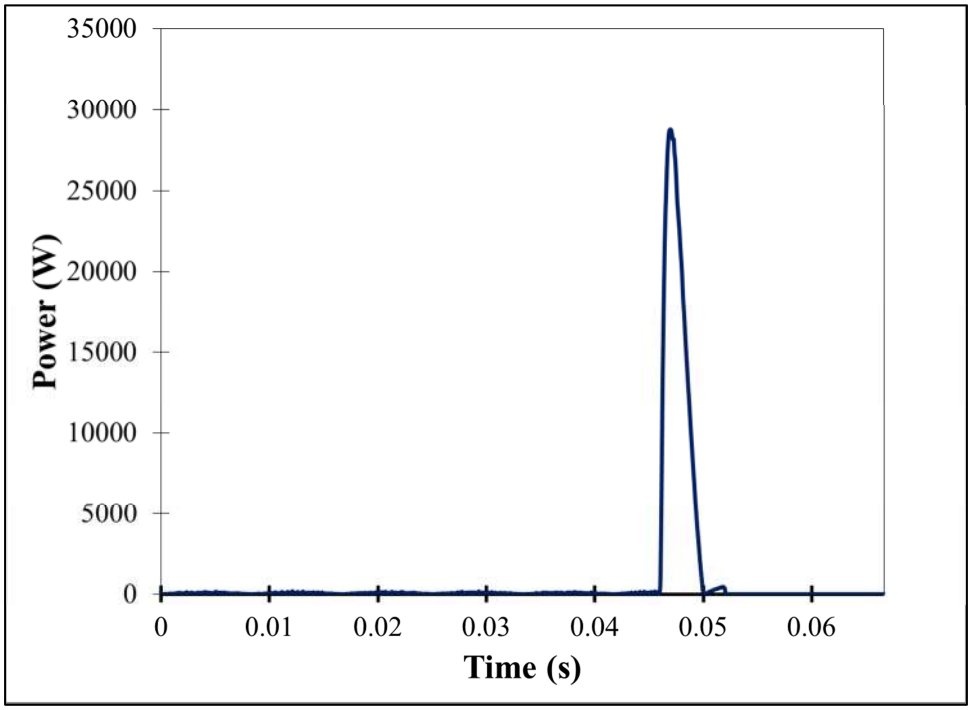

Figure 181 - Waveform of the instantaneous power produced in test 2-44 (33 kW/m^2). A total of 4 cycles (1/15 of a second) is shown.

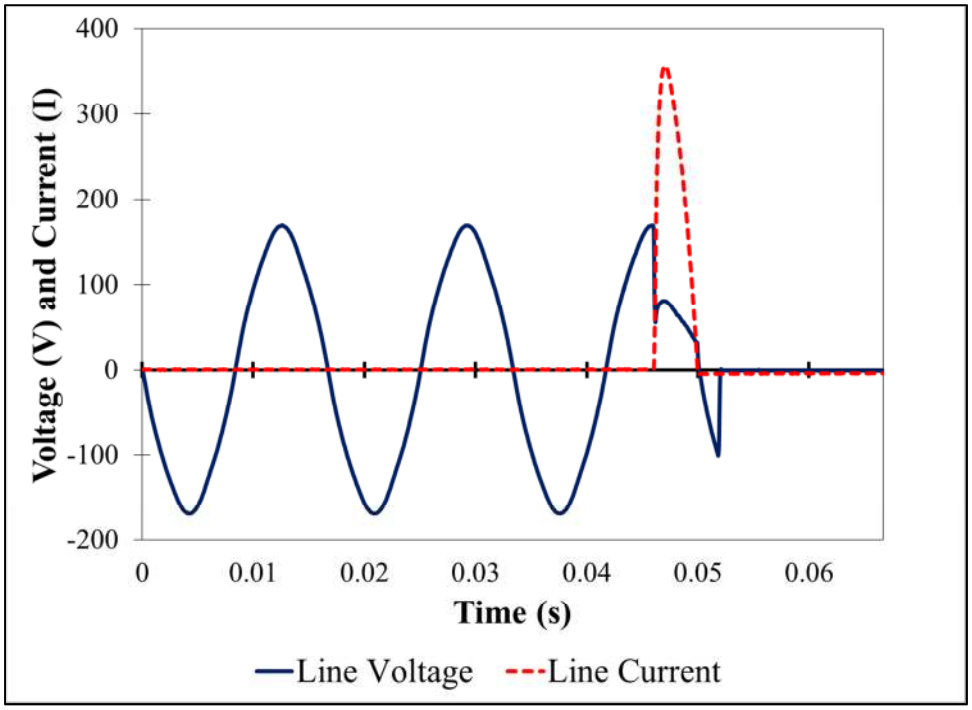

Figure 182 - Voltage and current waveforms produced in test 2-45 (31 kW/m^2). A total of 4 cycles (1/15 of a second) is shown.

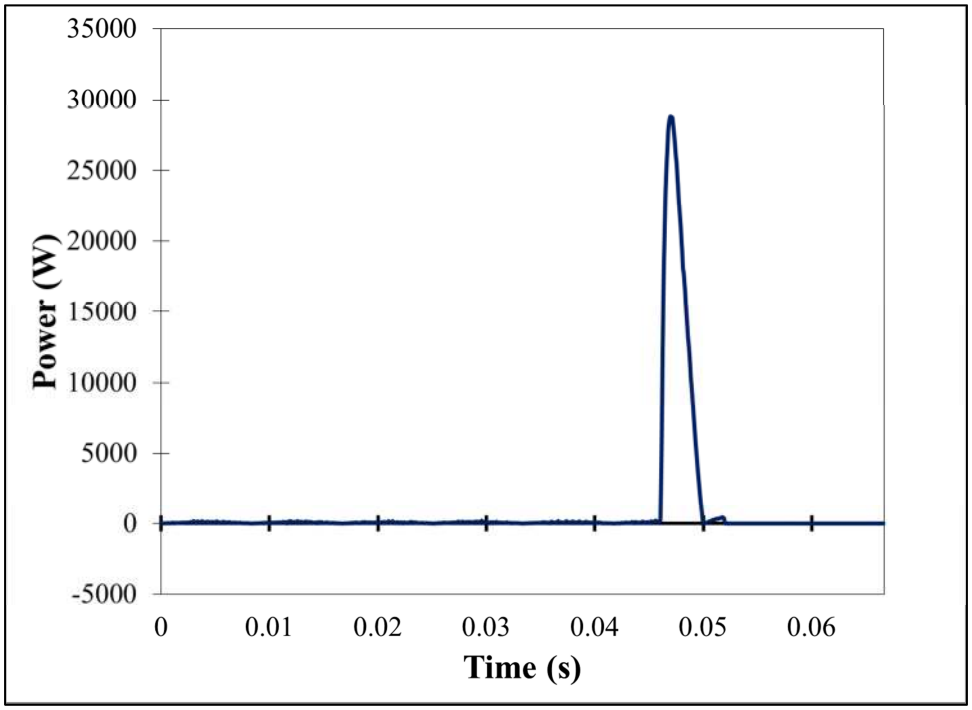

Figure 183 - Waveform of the instantaneous power produced in test 2-45 (31 kW/m^2). A total of 4 cycles (1/15 of a second) is shown.

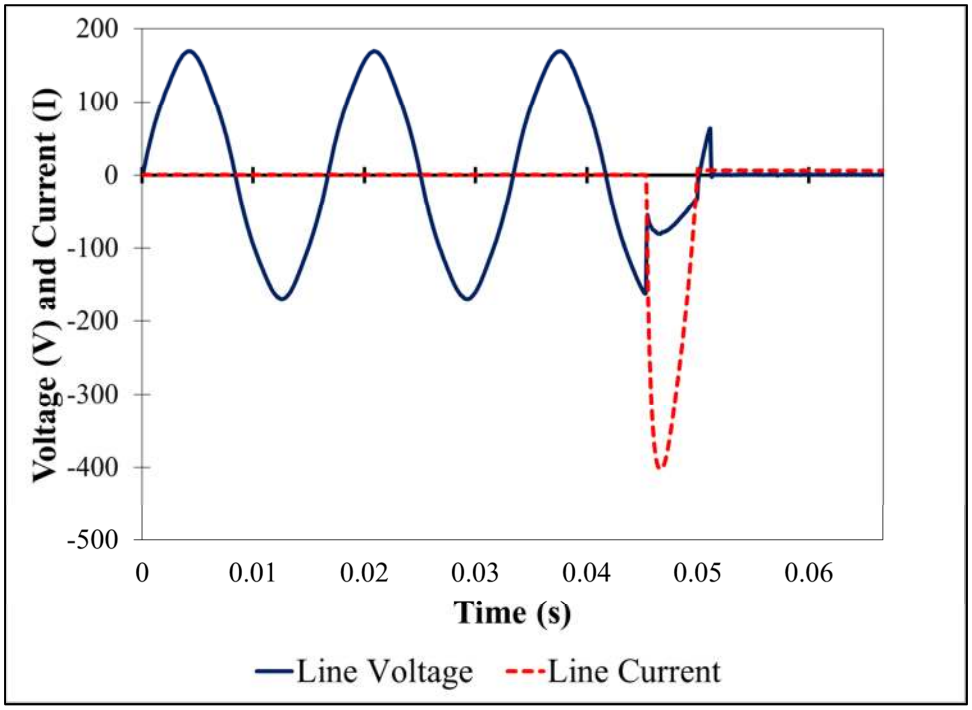

Figure 184 - Voltage and current waveforms produced in test 2-46 (29 kW/m^2). A total of 4 cycles (1/15 of a second) is shown.

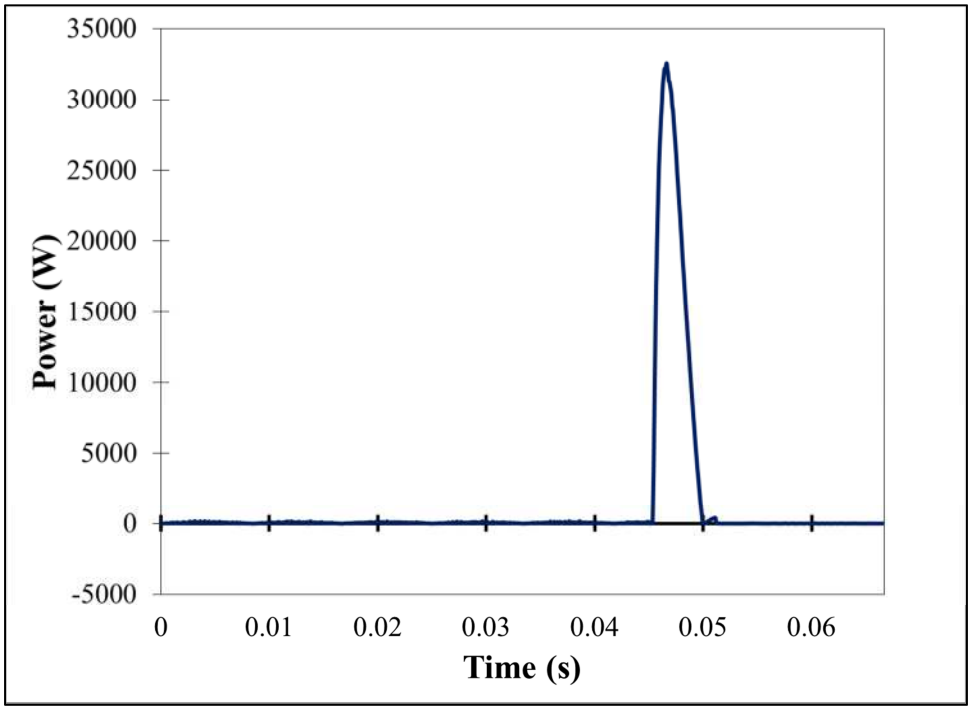

Figure 185 - Waveform of the instantaneous power produced in test 2-46 (29 kW/m^2). A total of 4 cycles (1/15 of a second) is shown.

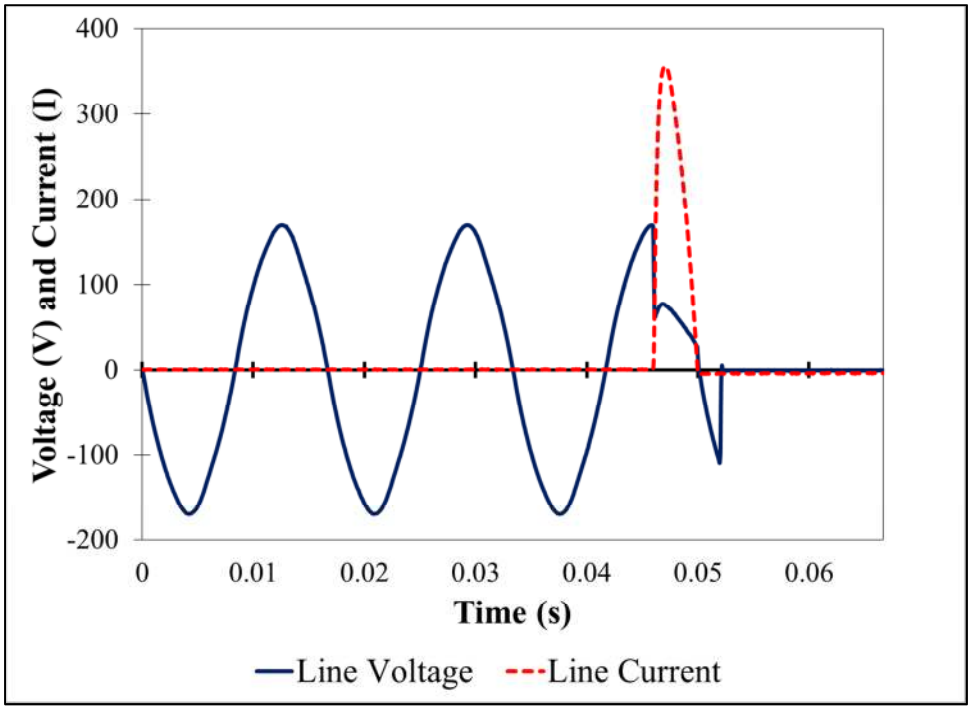

Figure 186 - Voltage and current waveforms produced in test 2-47 (27 kW/m^2). A total of 4 cycles (1/15 of a second) is shown.

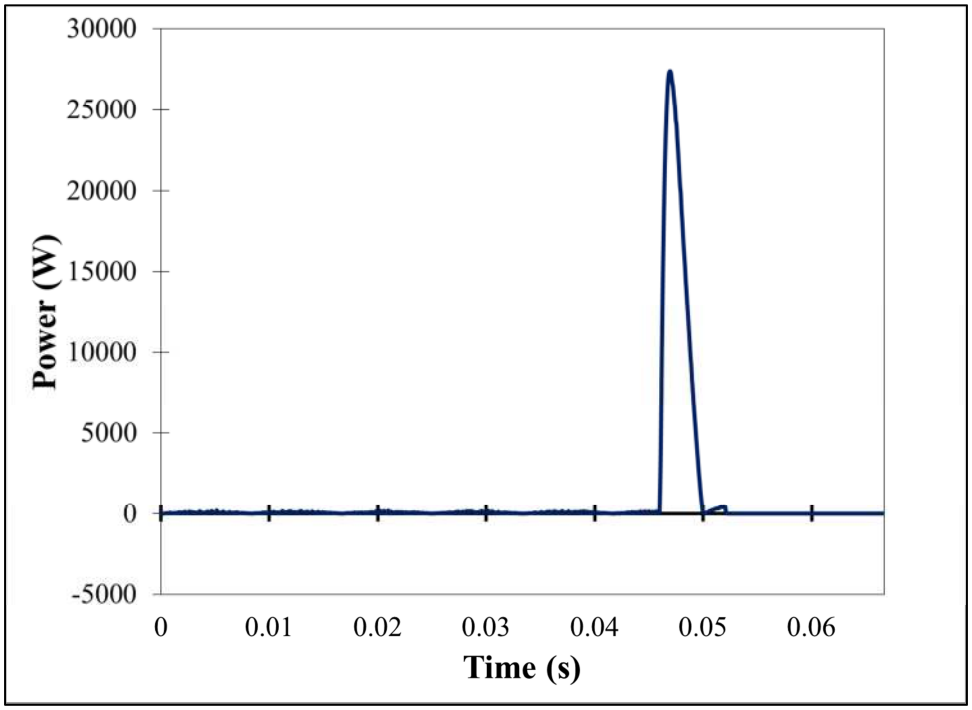

Figure 187 - Waveform of the instantaneous power produced in test 2-47 (27 kW/m^2). A total of 4 cycles (1/15 of a second) is shown.

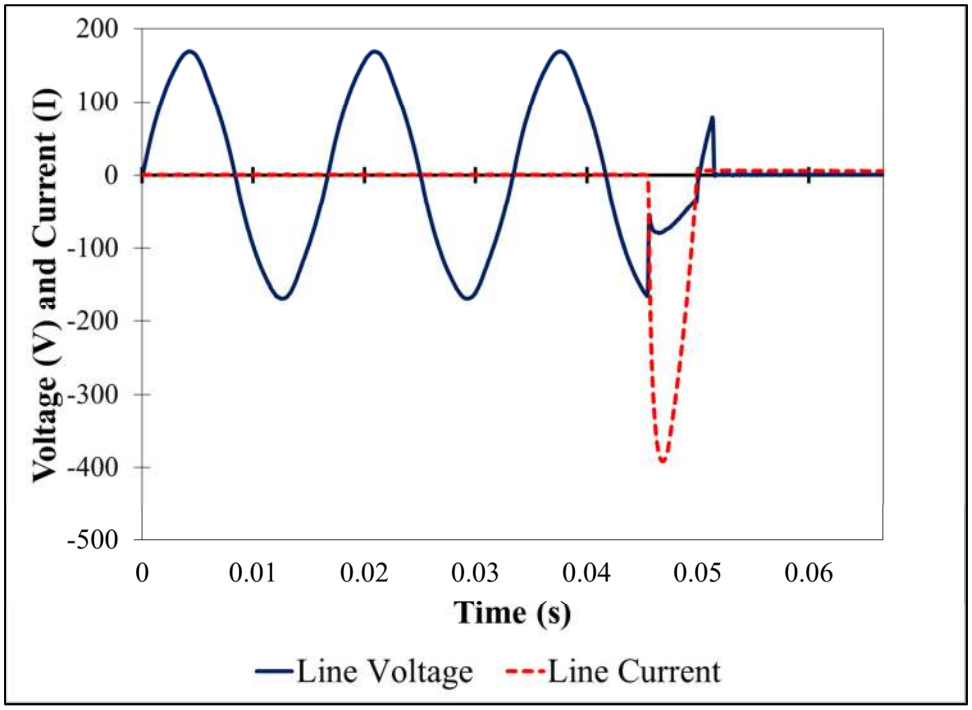

Figure 188 - Voltage and current waveforms produced in test 2-48 (27 kW/m^2). A total of 4 cycles (1/15 of a second) is shown.

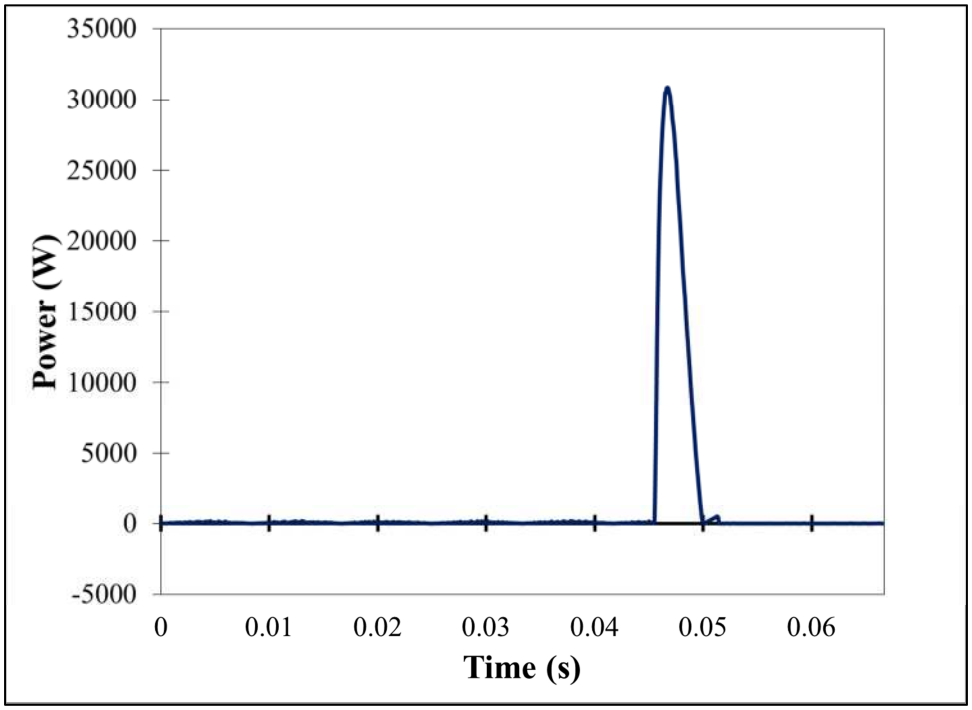

Figure 189 - Waveform of the instantaneous power produced in test 2-48 (27 kW/m^2). A total of 4 cycles (1/15 of a second) is shown.

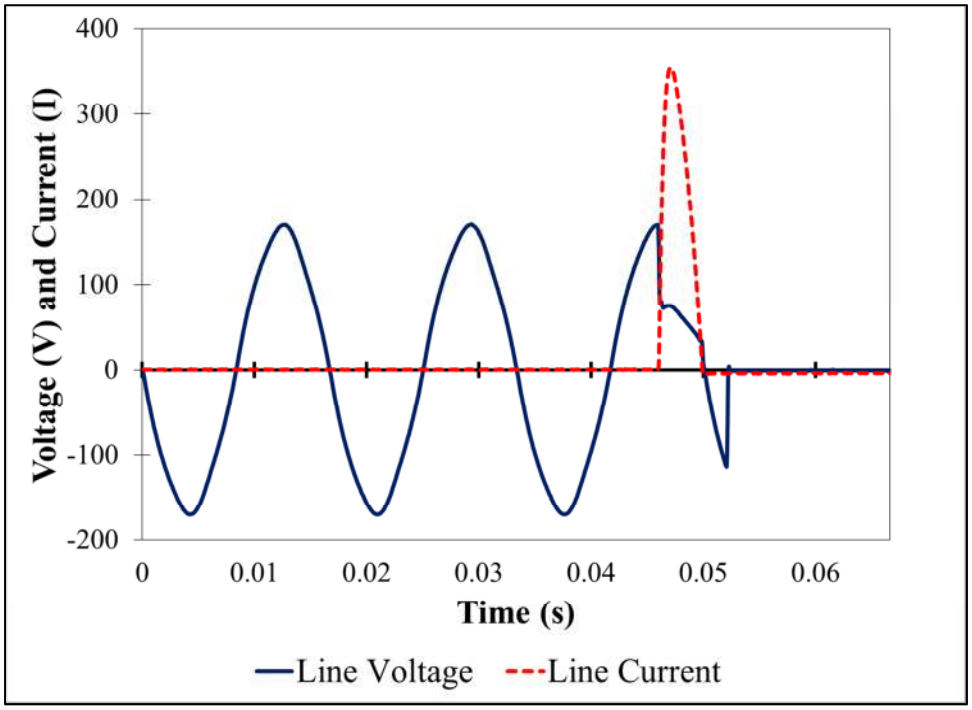

Figure 190 - Voltage and current waveforms produced in test 2-49 (25 kW/m^2). A total of 4 cycles (1/15 of a second) is shown.

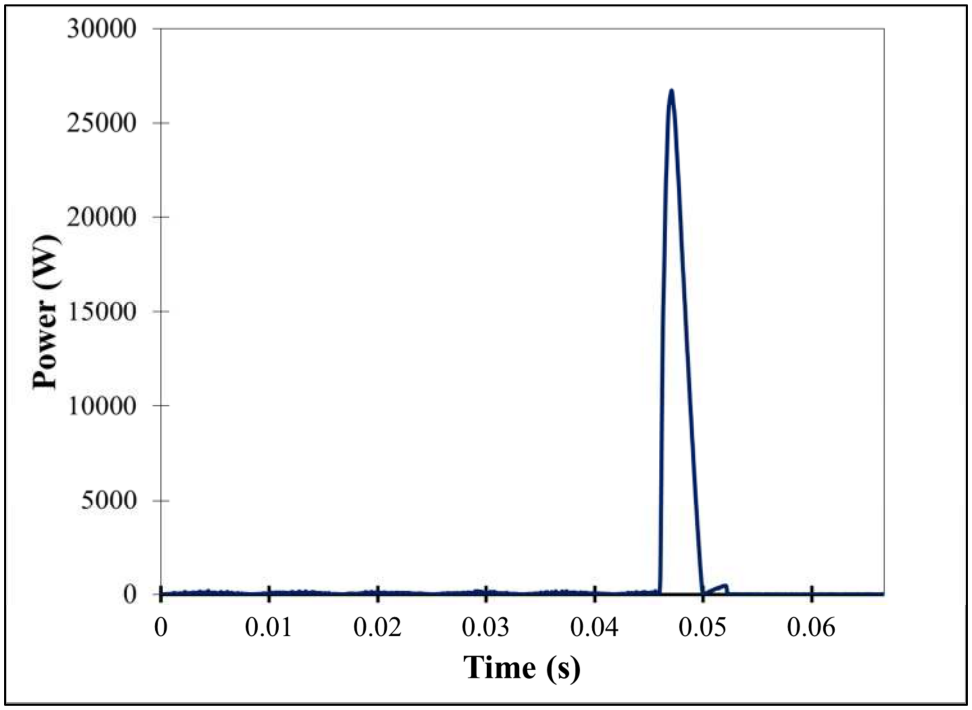

Figure 191 - Waveform of the instantaneous power produced in test 2-49 (25 kW/m^2). A total of 4 cycles (1/15 of a second) is shown.

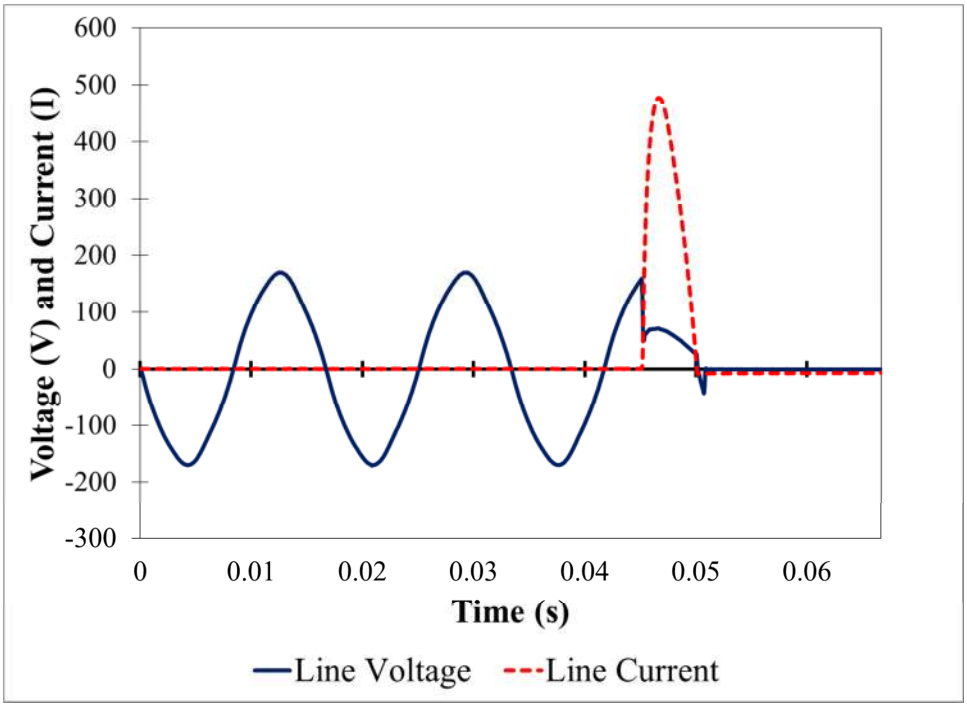

Figure 192 - Voltage and current waveforms produced in test 2-50 (52 kW/m^2). A total of 4 cycles (1/15 of a second) is shown.

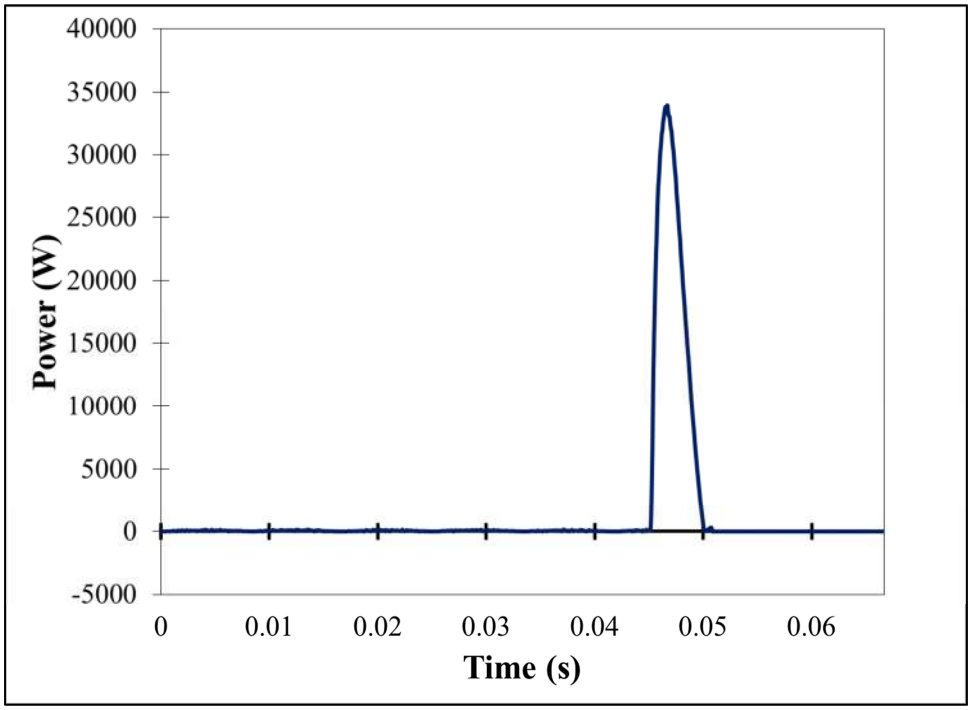

Figure 193 - Waveform of the instantaneous power produced in test 2-50 (52 kW/m^2). A total of 4 cycles (1/15 of a second) is shown.

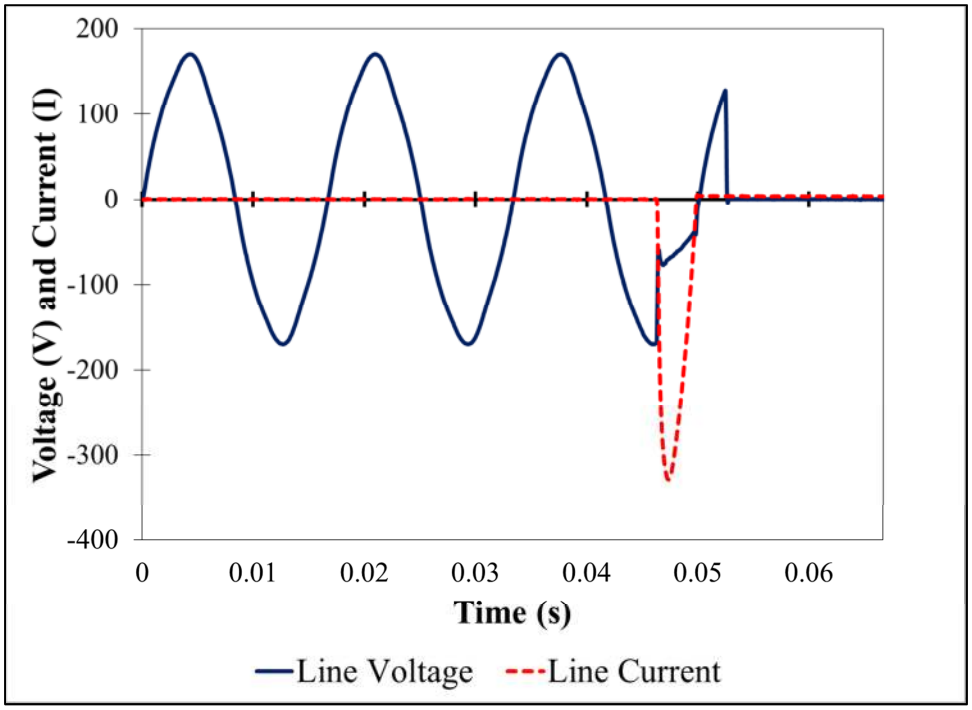

Figure 194 - Voltage and current waveforms produced in test 2-51 (25 kW/m^2). A total of 4 cycles (1/15 of a second) is shown.

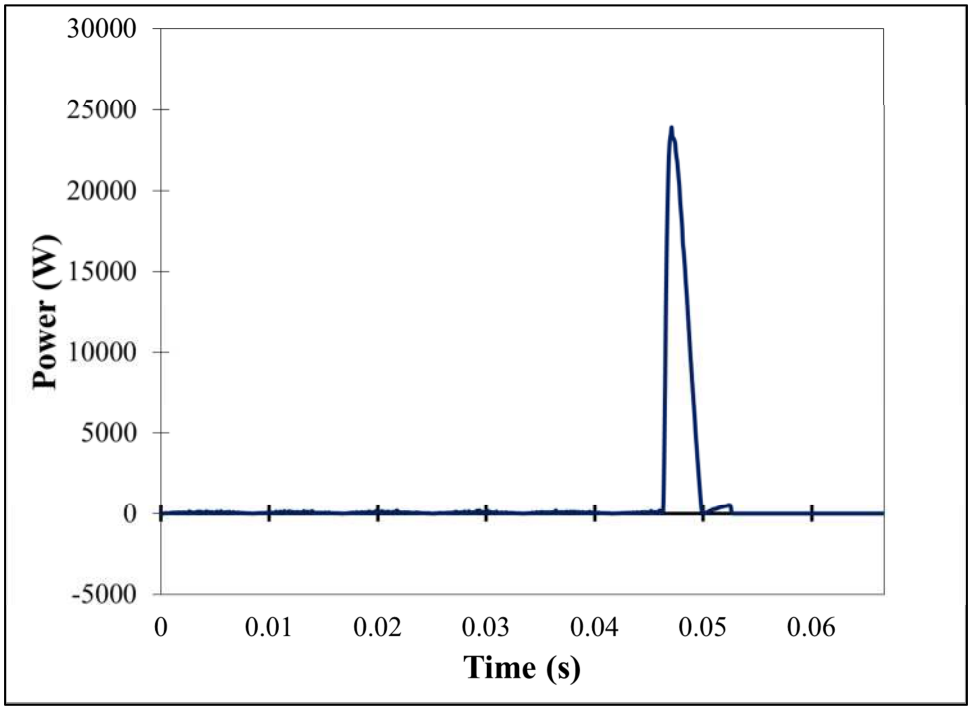

Figure 195 - Waveform of the instantaneous power produced in test 2-51 (25 kW/m^2). A total of 4 cycles (1/15 of a second) is shown.

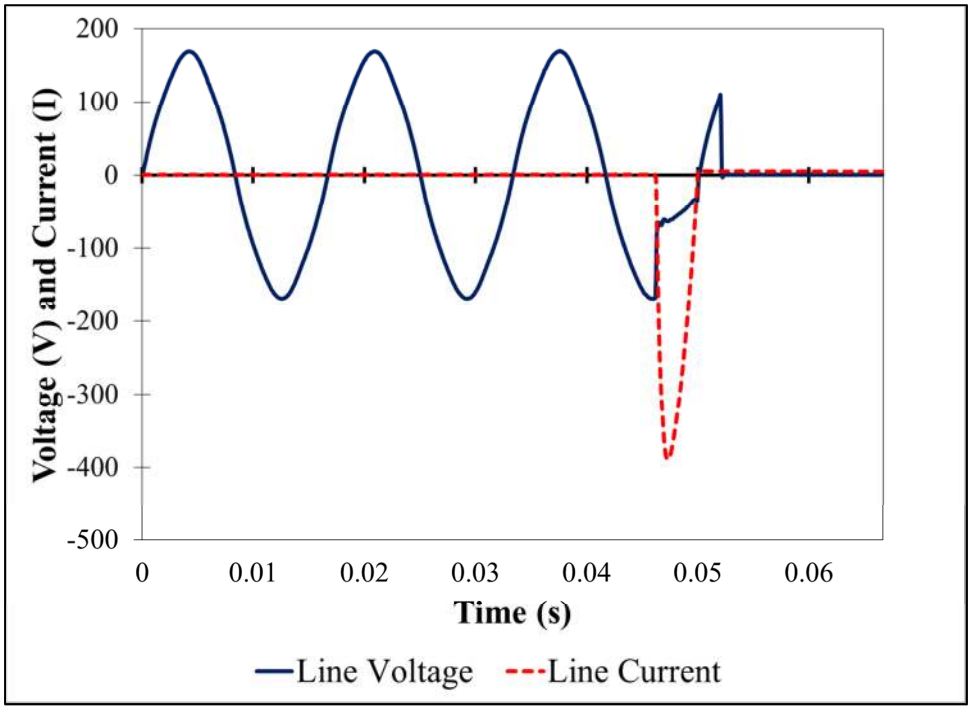

Figure 196 - Voltage and current waveforms produced in test 2-54 (25 kW/m^2). A total of 4 cycles (1/15 of a second) is shown.

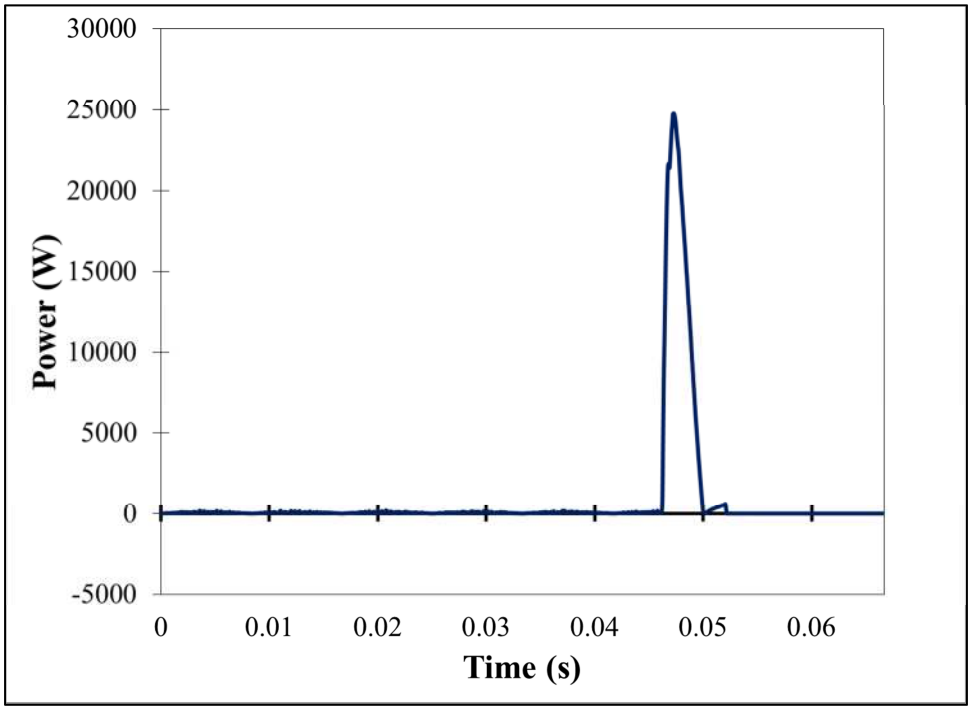

Figure 197 - Waveform of the instantaneous power produced in test 2-54 (25 kW/m^2). A total of 4 cycles (1/15 of a second) is shown.

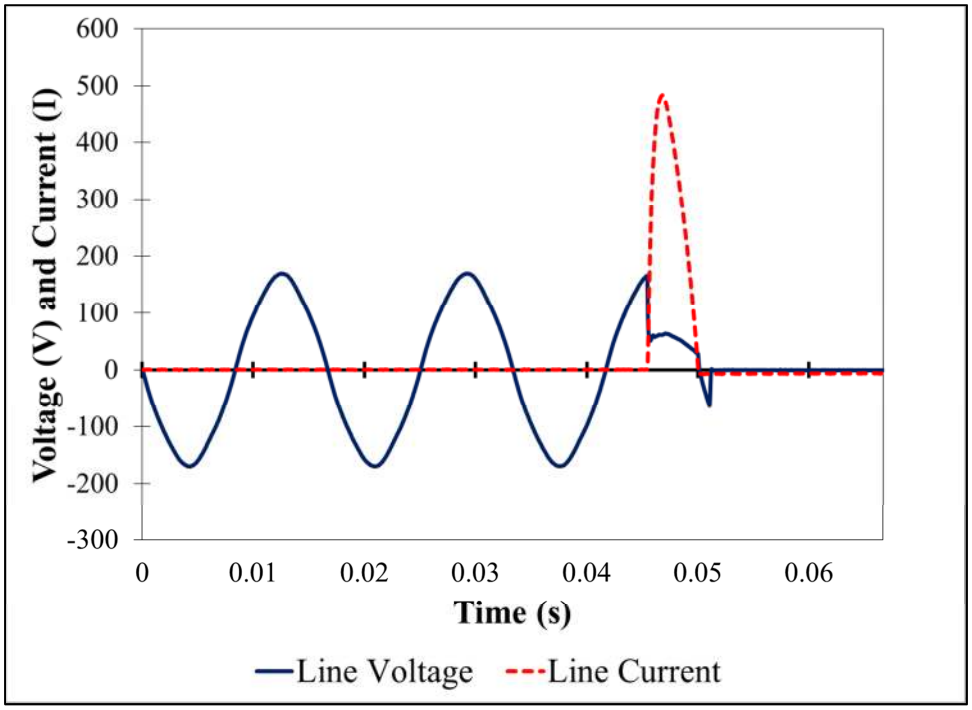

Figure 198 - Voltage and current waveforms produced in test 2-55 (25 kW/m^2). A total of 4 cycles (1/15 of a second) is shown.

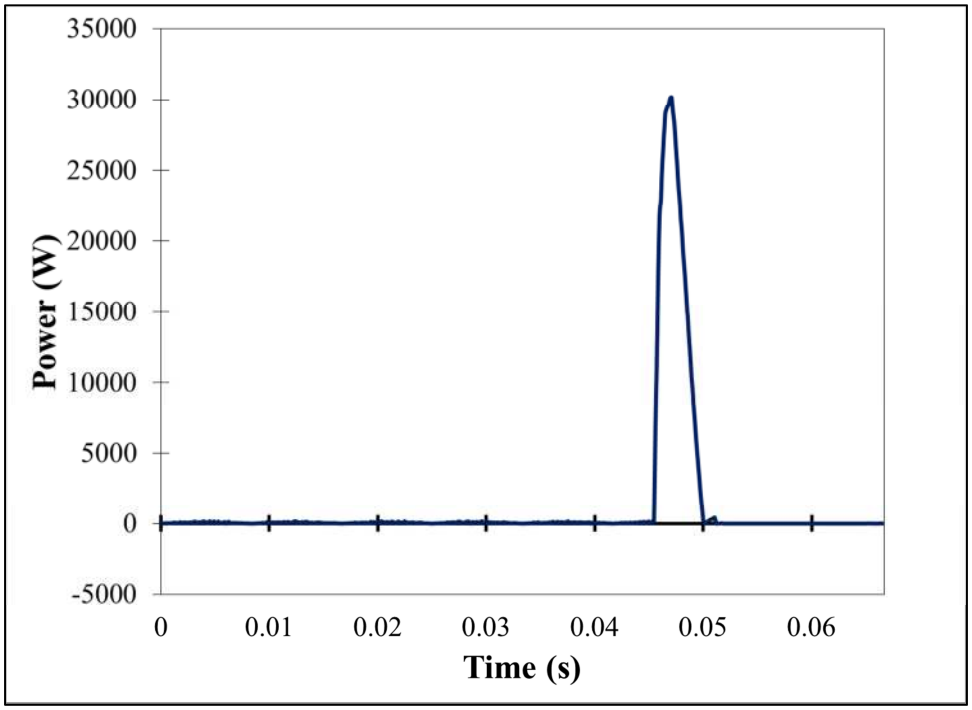

Figure 199 - Waveform of the instantaneous power produced in test 2-55 (25 kW/m^2). A total of 4 cycles (1/15 of a second) is shown.

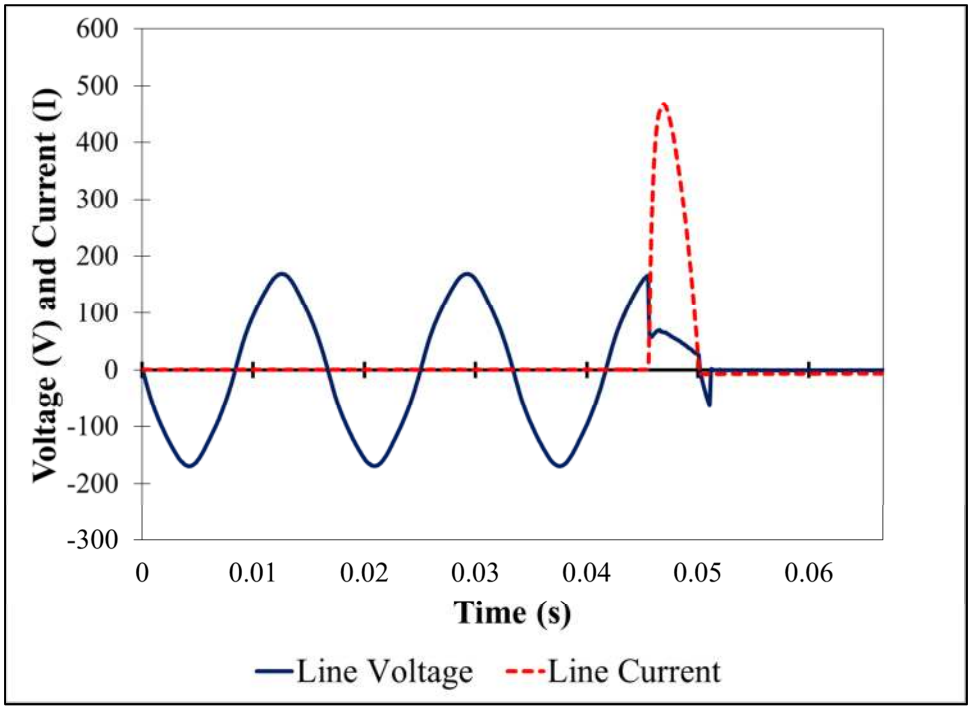

Figure 200 - Voltage and current waveforms produced in test 2-56 (25 kW/m^2). A total of 4 cycles (1/15 of a second) is shown.

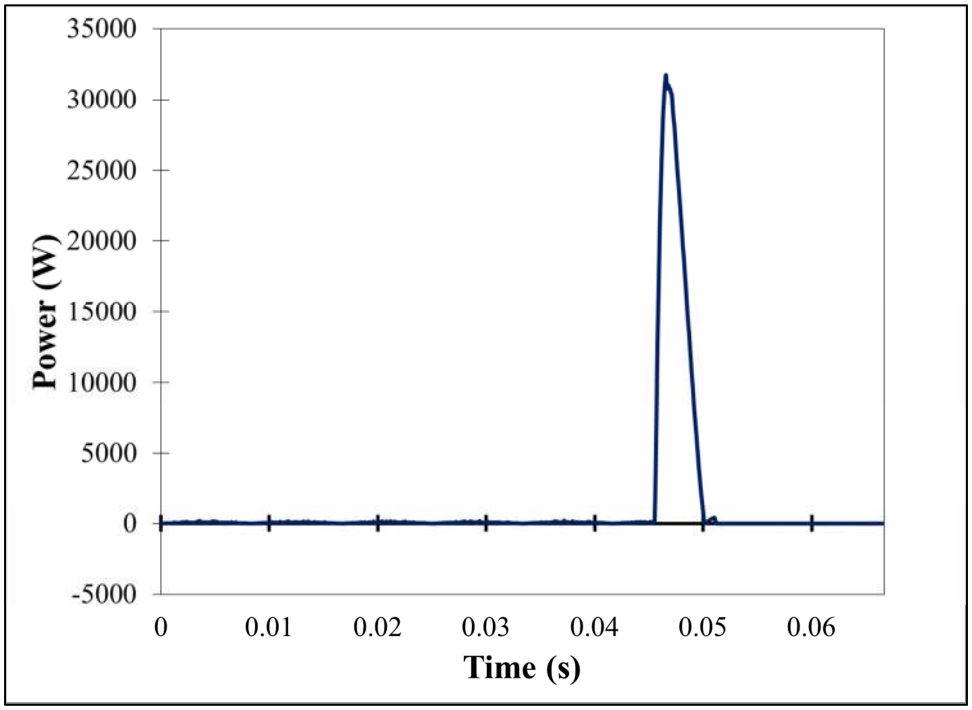

Figure 201 - Waveform of the instantaneous power produced in test 2-56 (25 kW/m^2). A total of 4 cycles (1/15 of a second) is shown.

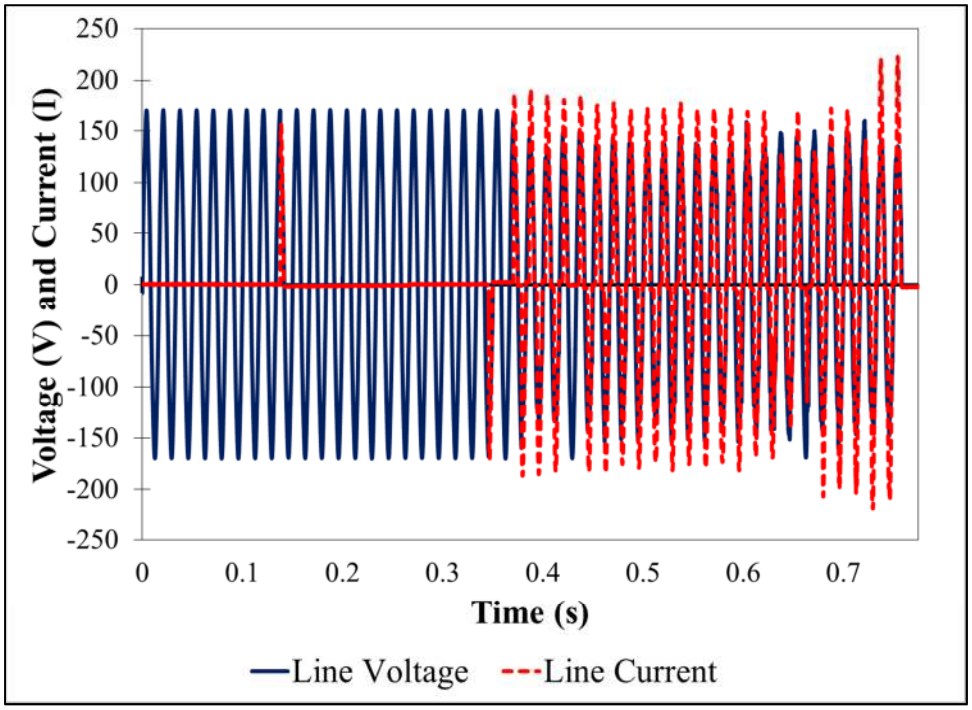

Figure 202 - Voltage and current waveforms produced in test 2-57 (25 kW/m^2). A total of 45 cycles (3/4 of a second) is shown.

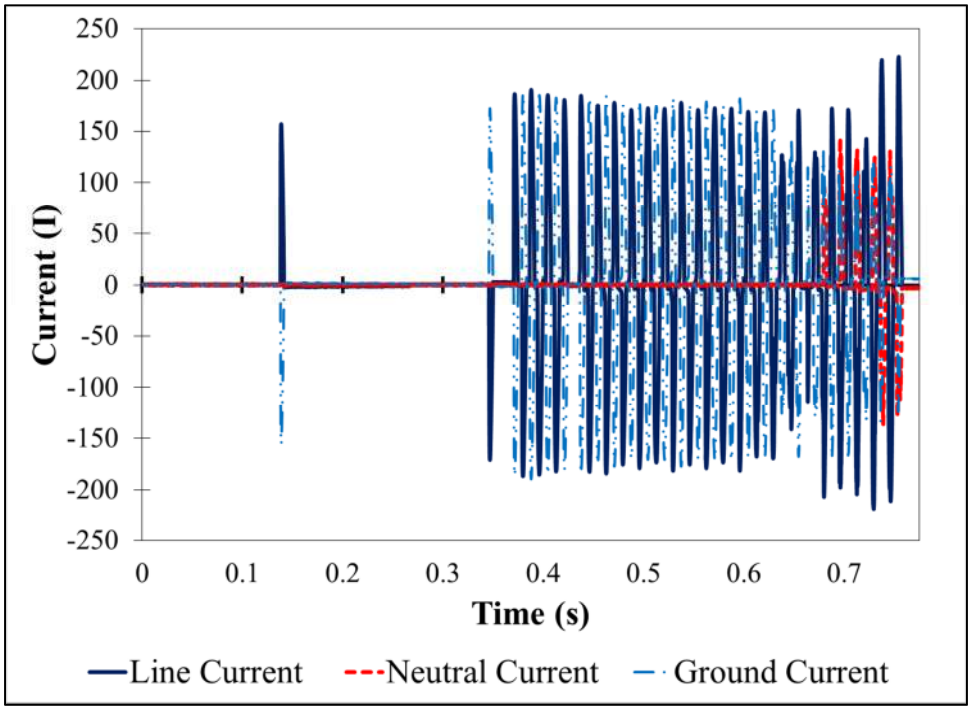

Figure 203 - Current waveforms produced in test 2-57 (25 kW/m^2). A total of 45 cycles (3/4 of a second) is shown.

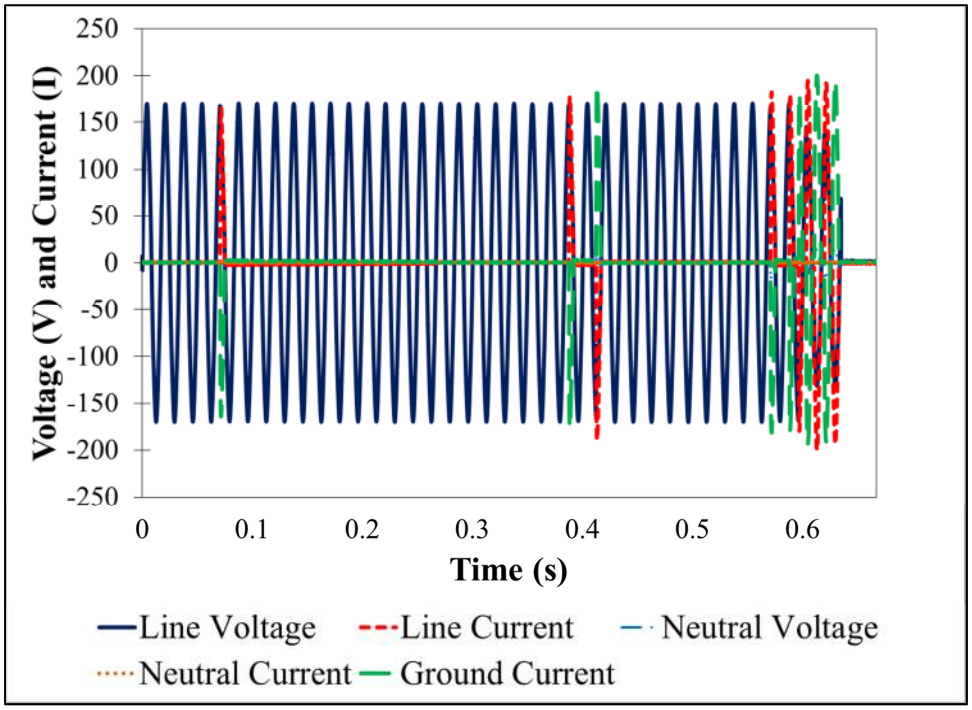

Figure 204 - Voltage and current waveforms produced in test 2-58 (24 kW/m^2). A total of 40 cycles (2/3 of a second) is shown.

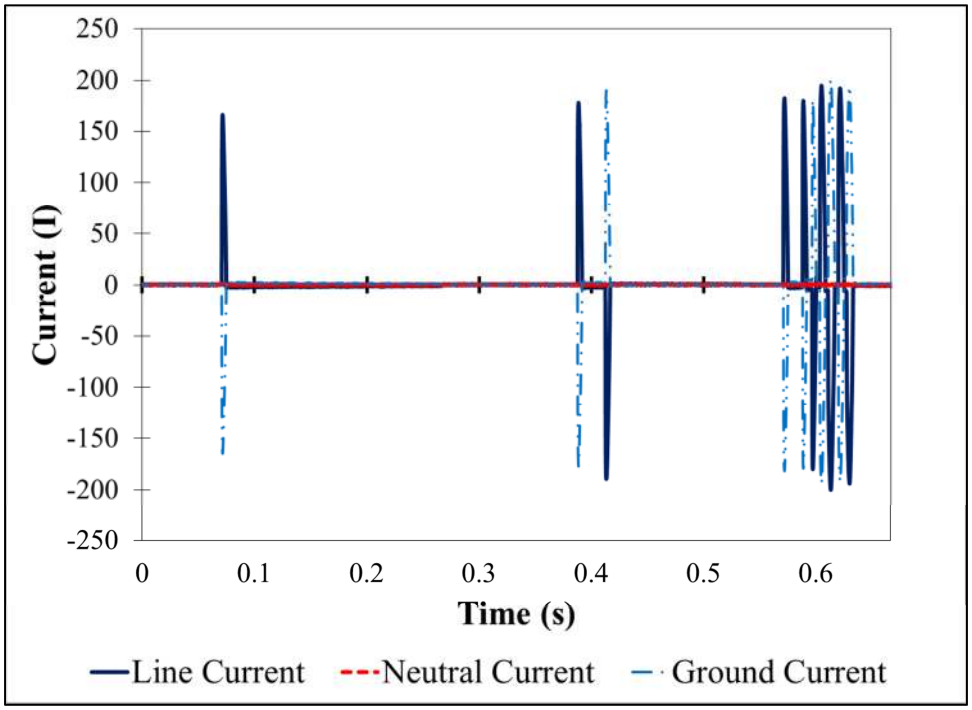

Figure 205 - Current Waveforms produced in test 2-58 (24 kW/m^2). A total of 40 cycles (2/3 of a second) is shown.

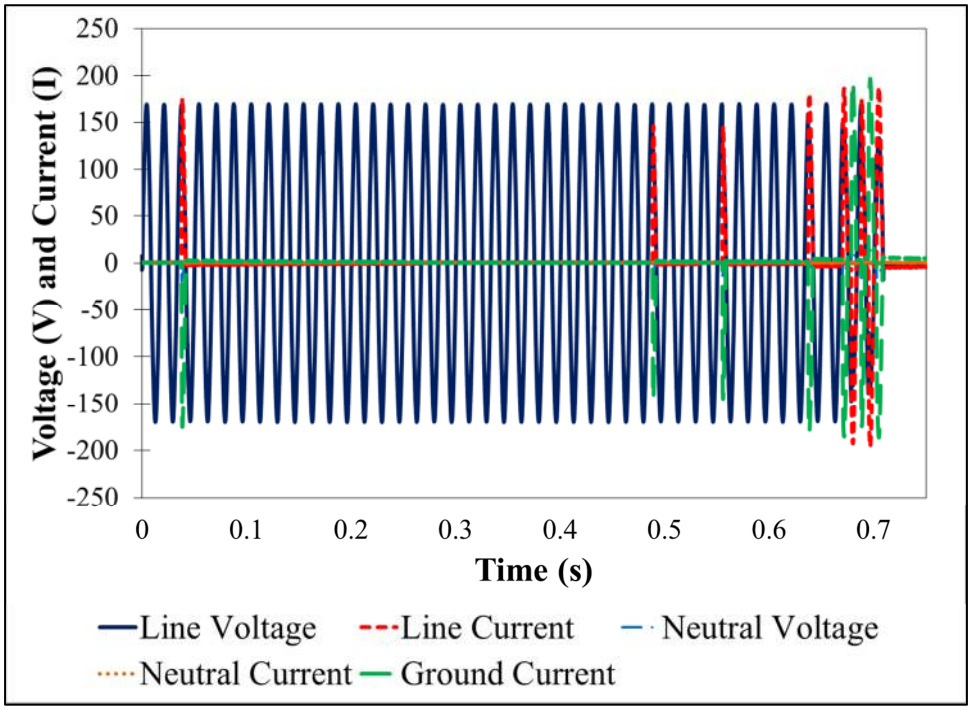

Figure 206 - Voltage and current waveforms produced in test 2-60 (25 kW/m^2). A total of 45 cycles (3/4 of a second) is shown.

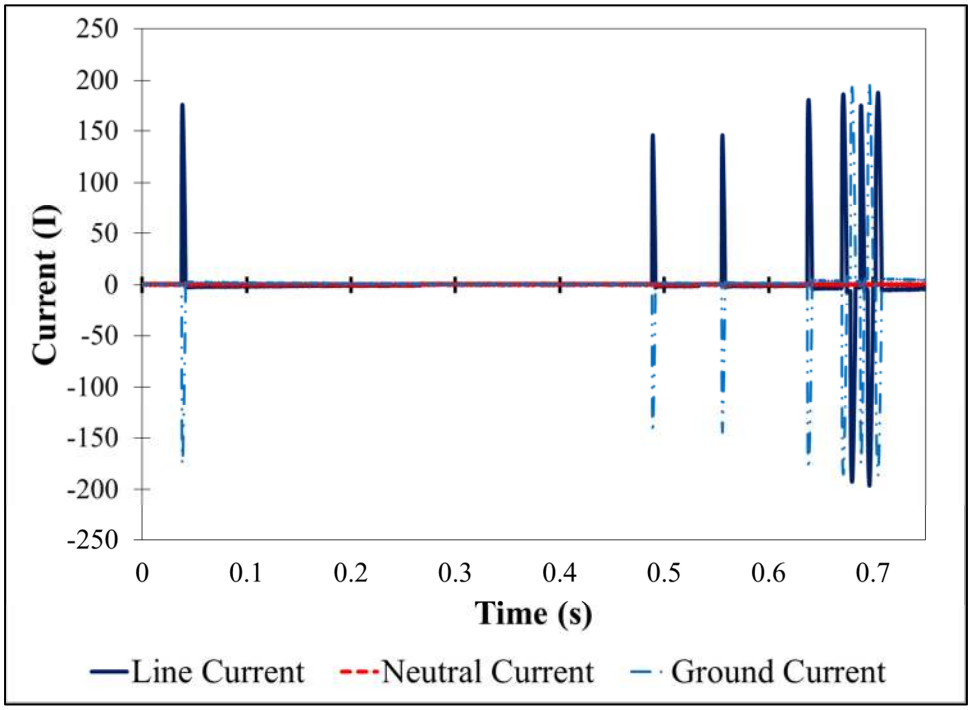

Figure 207 - Current waveforms produced in test 2-60 (25 kW/m^2). A total of 45 cycles (3/4 of a second) is shown.

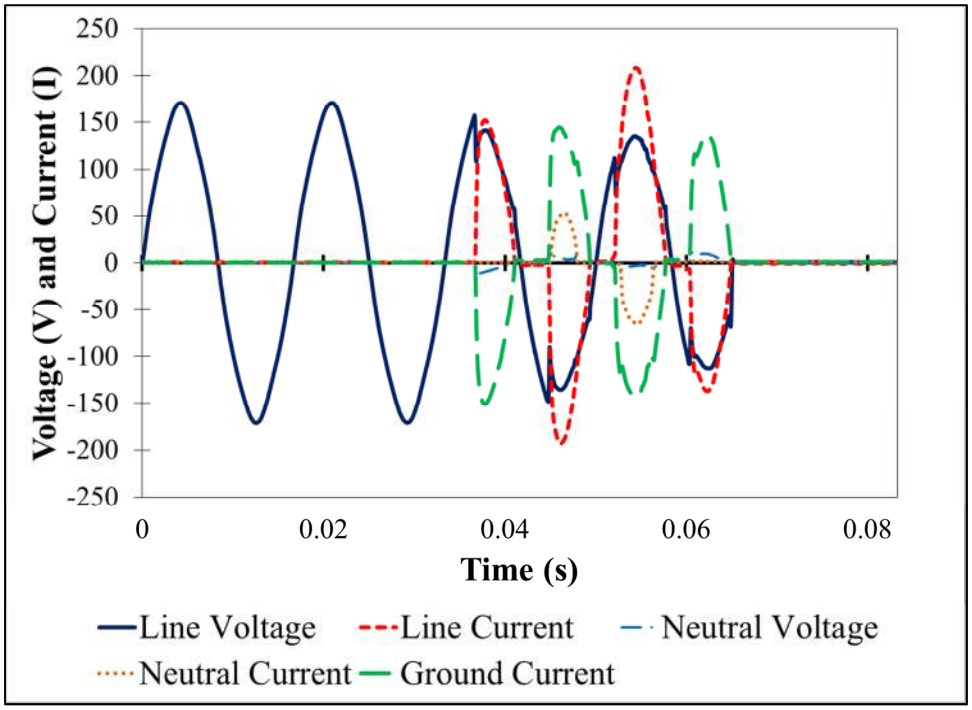

Figure 208 - Voltage and current waveforms produced during test 2-61 (25 kW/m^2). A total of 5 cycles (1/12 of a second) is shown.

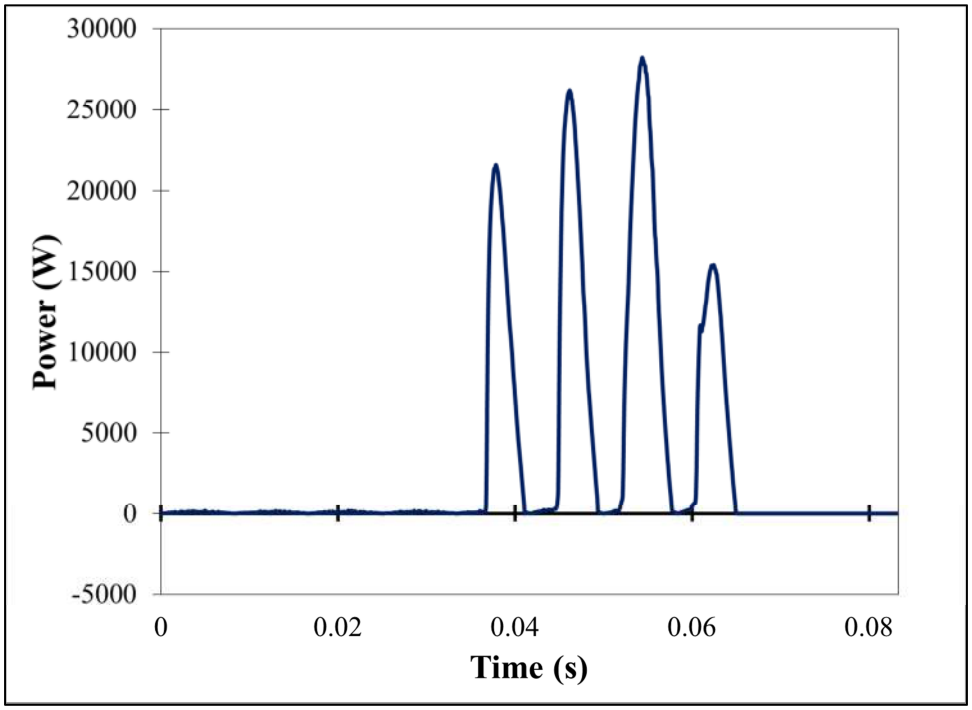

Figure 209 - Waveform of the instantaneous power produced during test 2-61 (25 kW/m^2). A total of 5 cycles (1/12 of a second) is shown.

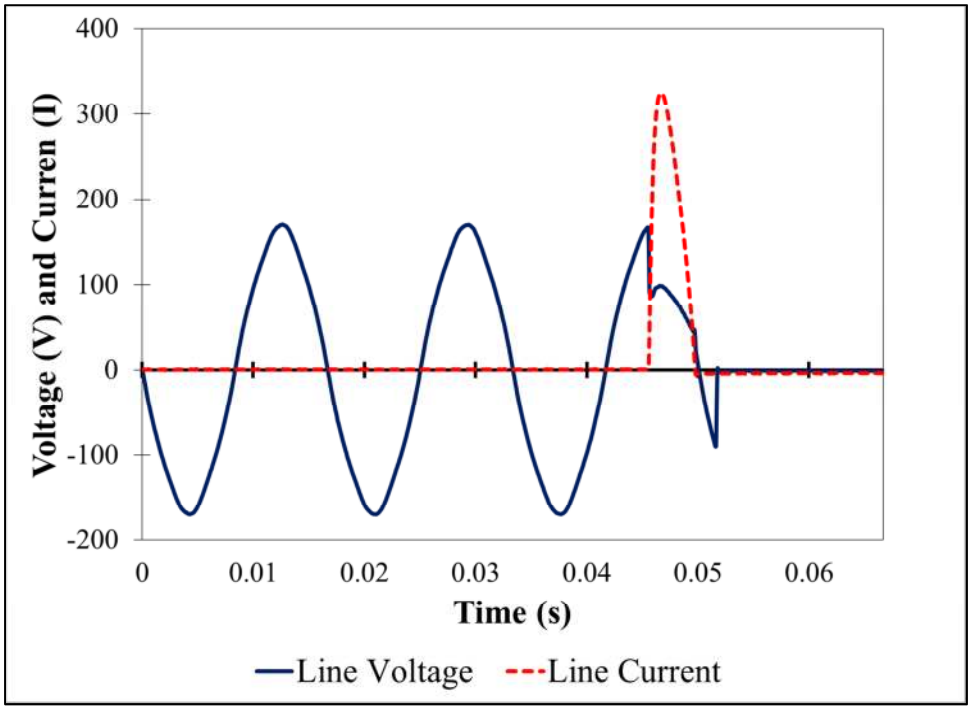

Figure 210 - Voltage and current waveforms produced in test 2-63 (25 kW/m^2). A total of 4 cycles (1/15 of a second) is shown.

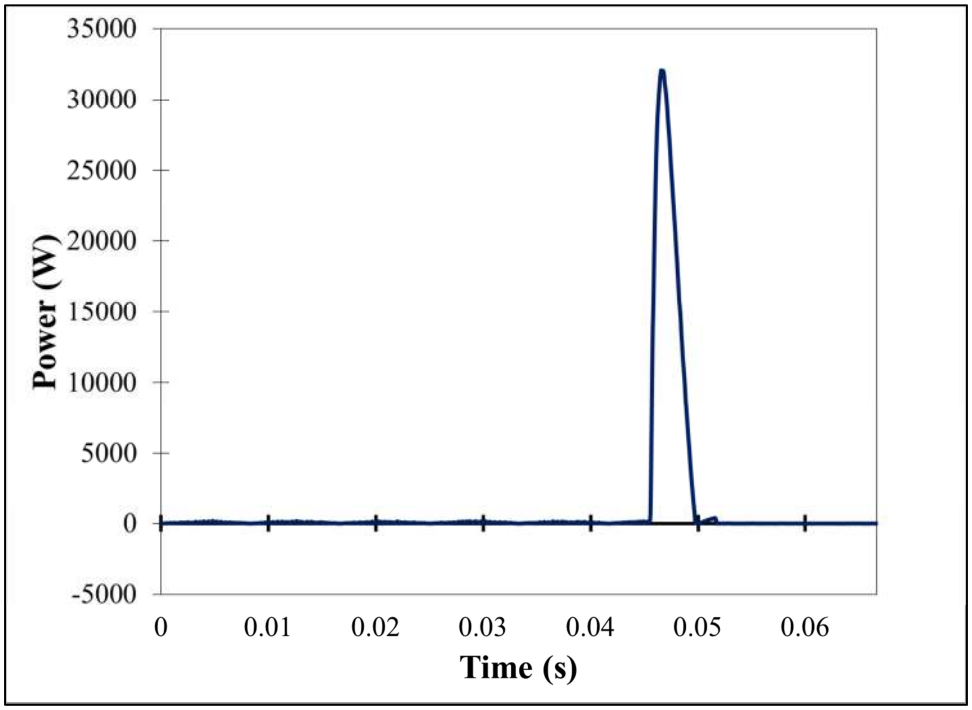

Figure 211 - Waveform of the instantaneous power produced in test 2-63 (25 kW/m^2). A total of 4 cycles (1/15 of a second) is shown.

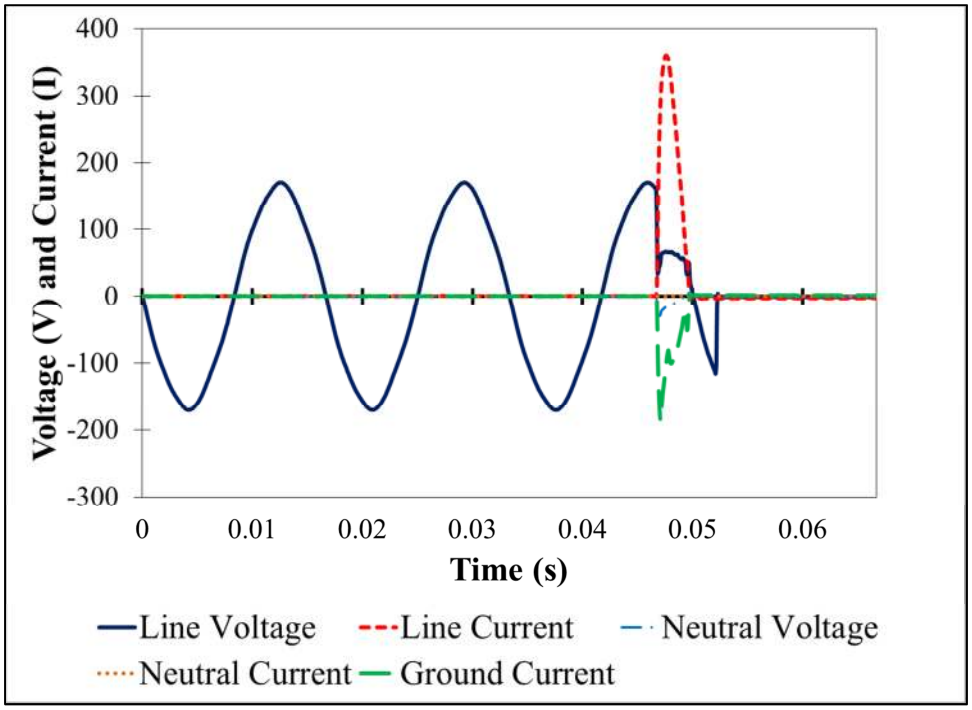

Figure 212 - Voltage and current waveforms produced in test 2-67 (55 kW/m^2). A total of 4 cycles (1/15 of a second) is shown.

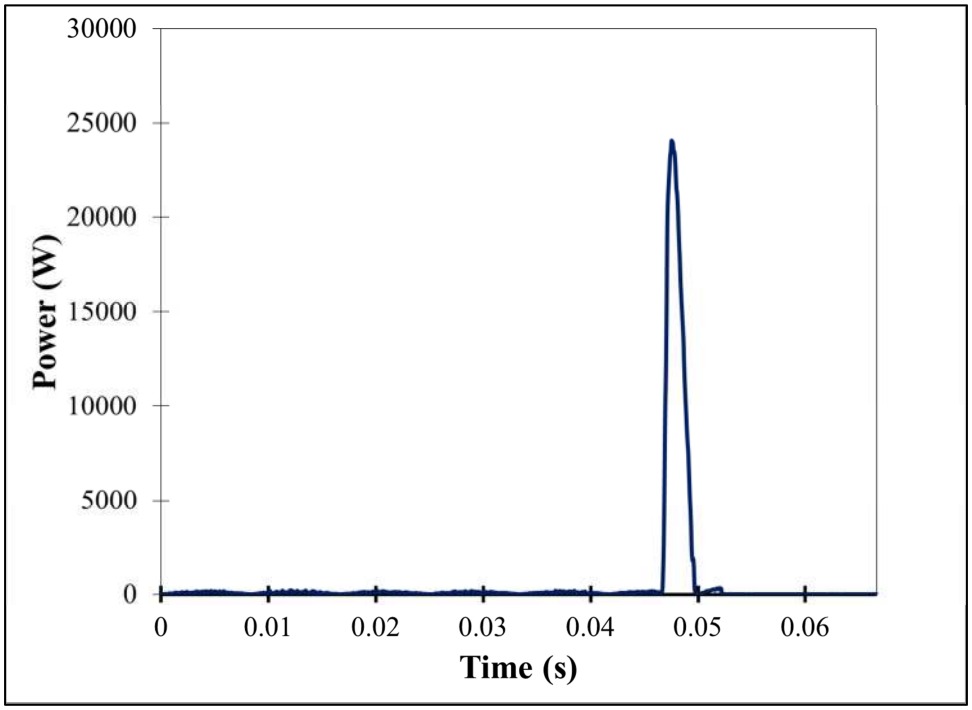

Figure 213 - Waveform of the instantaneous power produced in test 2-67 (55 kW/m^2). A total of 4 cycles (1/15 of a second) is shown.

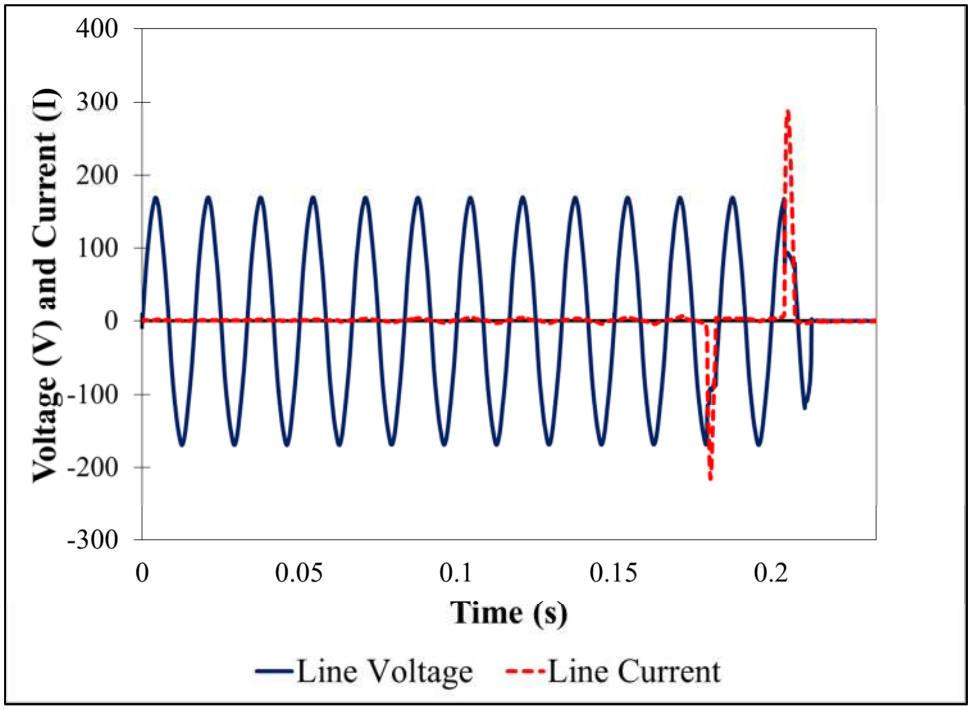

Figure 214 - Voltage and current waveforms produced in test 2-68 (55 kW/m^2). A total of 14 cycles (7/30 of a second) is shown.

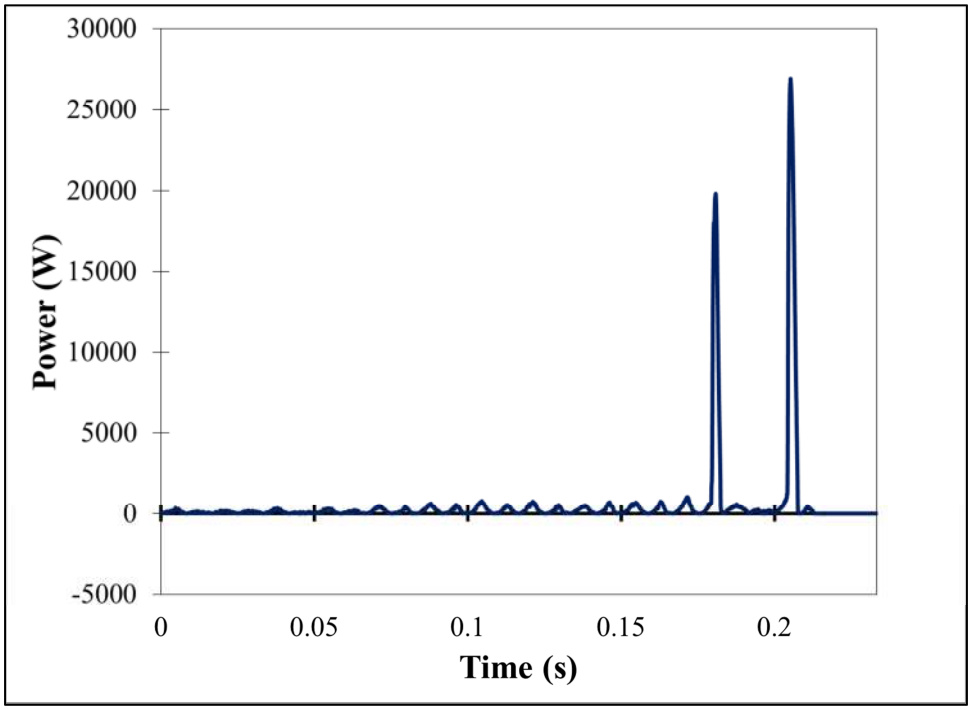

Figure 215 - Waveform of the instantaneous power produced in test 2-68 (55 kW/m^2). A total of 14 cycles (7/30 of a second) is shown.

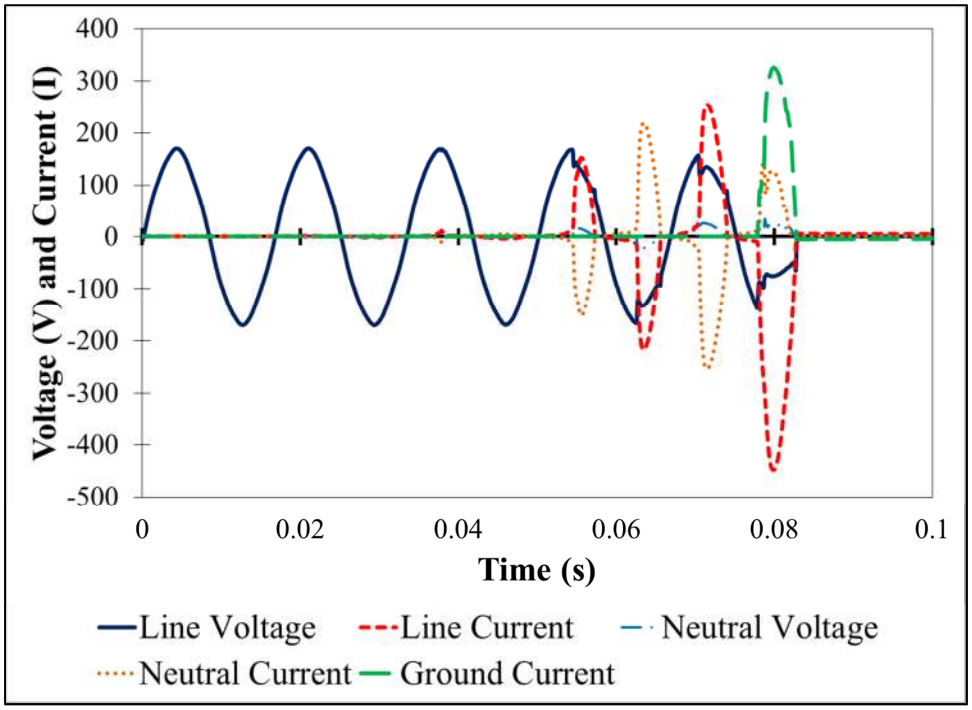

Figure 216 - Voltage and current waveforms produced in test 2-69 (55 kW/m^2). A total of 6 cycles (1/10th of a second) is shown.

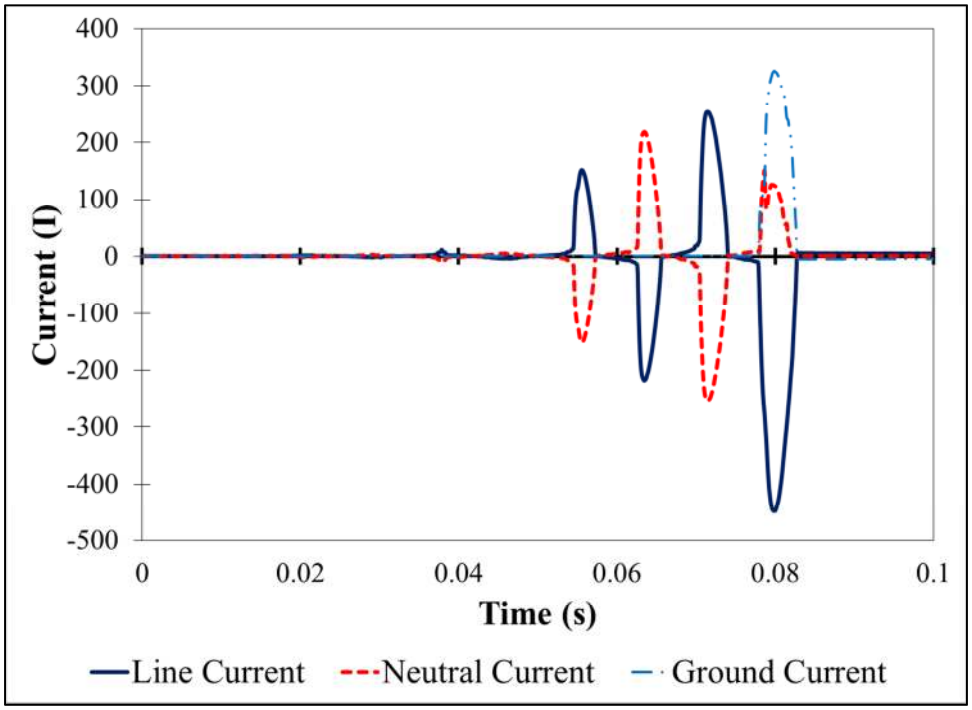

Figure 217 - Currents waveforms produced in test 2-69 (55 kW/m^2). A total of 6 cycles (1/10 of a second) is shown.

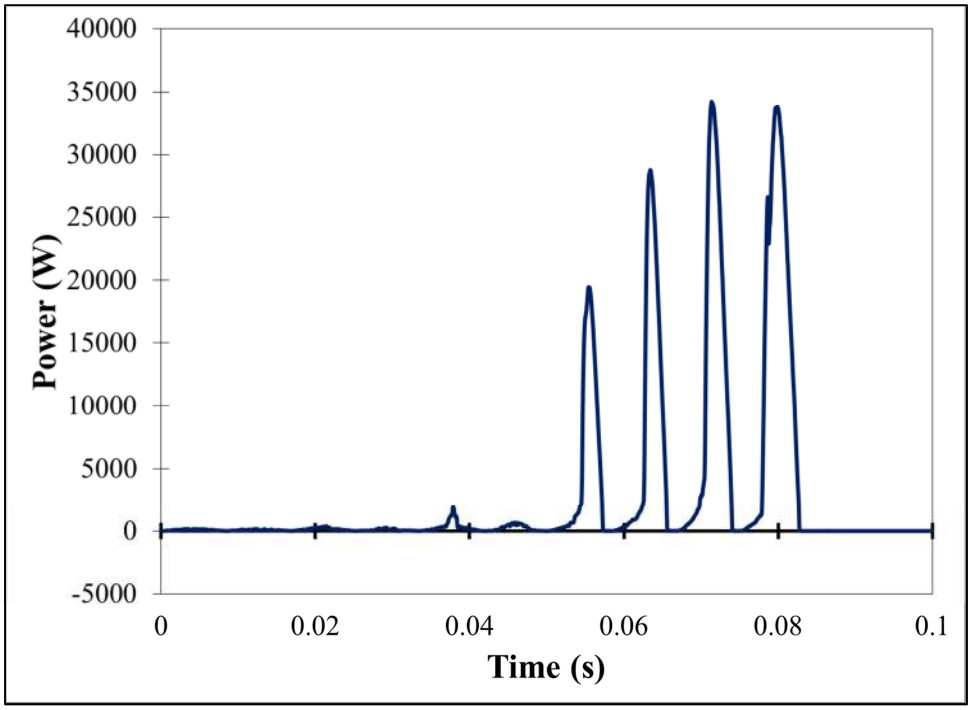

Figure 218 - Waveform of the instantaneous power produced in test 2-69 (55 kW/m^2). A total of 6 cycles (1/10 of a second) is shown.

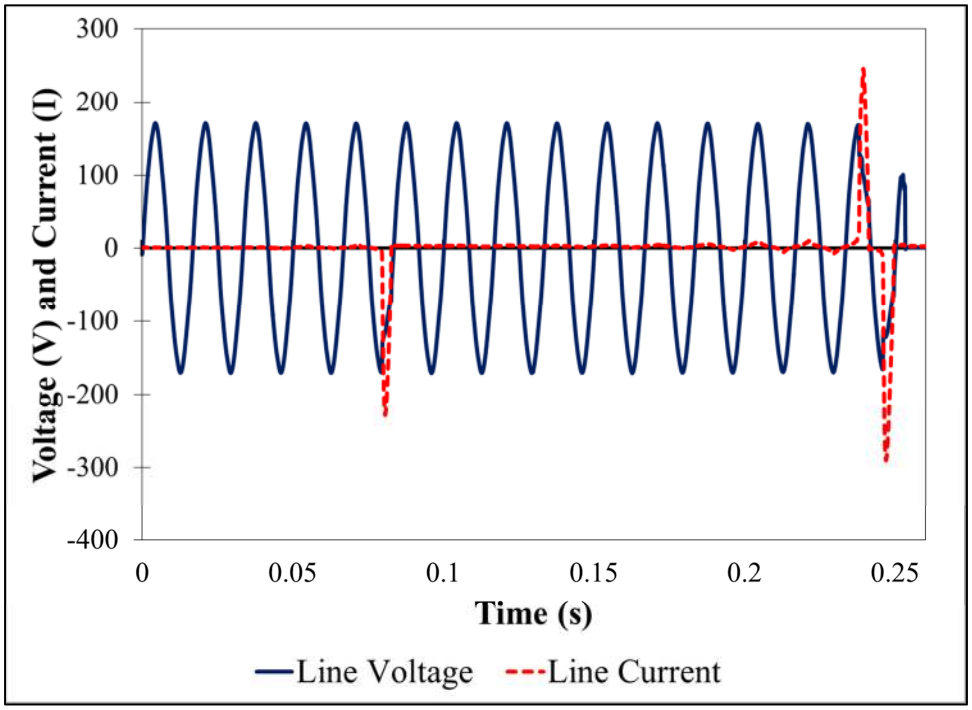

Figure 219 - Voltage and current waveforms produced in test 2-70 (50 kW/m^2). A total of 16 cycles (4/15 of a second) is shown.

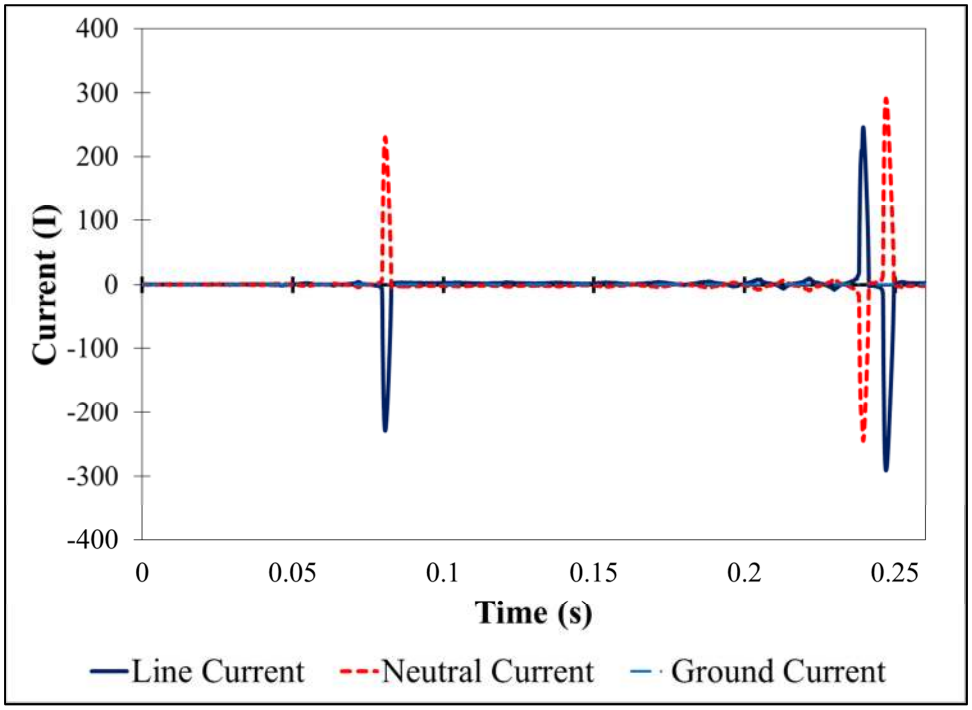

Figure 220 - Current waveforms produced in test 2-70 (50 kW/m^2). A total of 16 cycles (4/15 of a second) is shown.

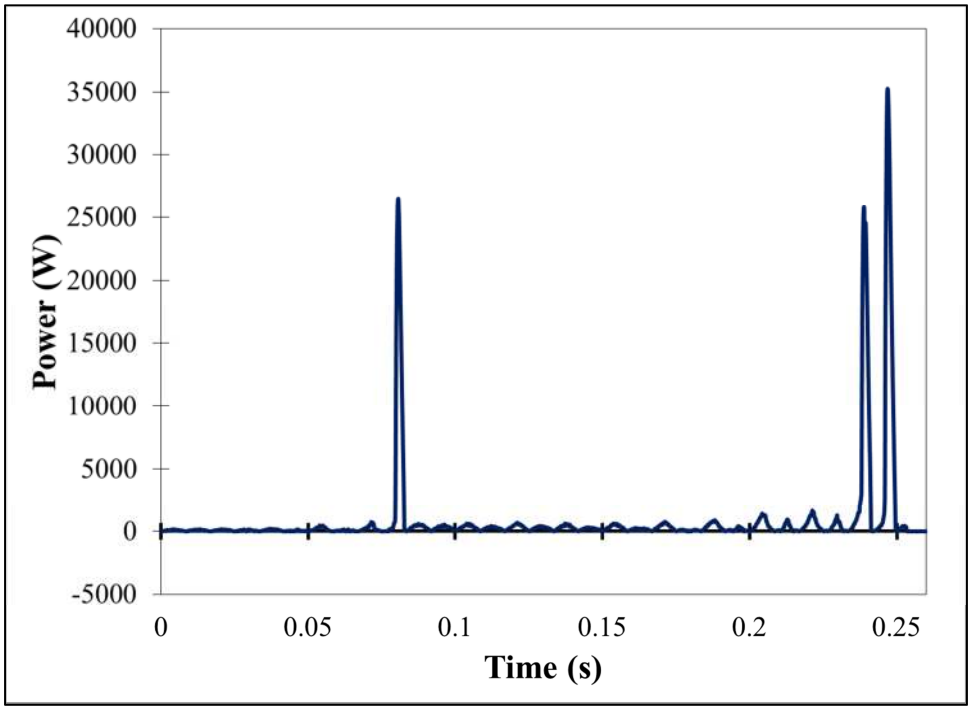

Figure 221 - Waveform of instantaneous power produced in test 2-70 (50 kW/m^2). A total of 16 cycles (4/15 of a second) is shown.

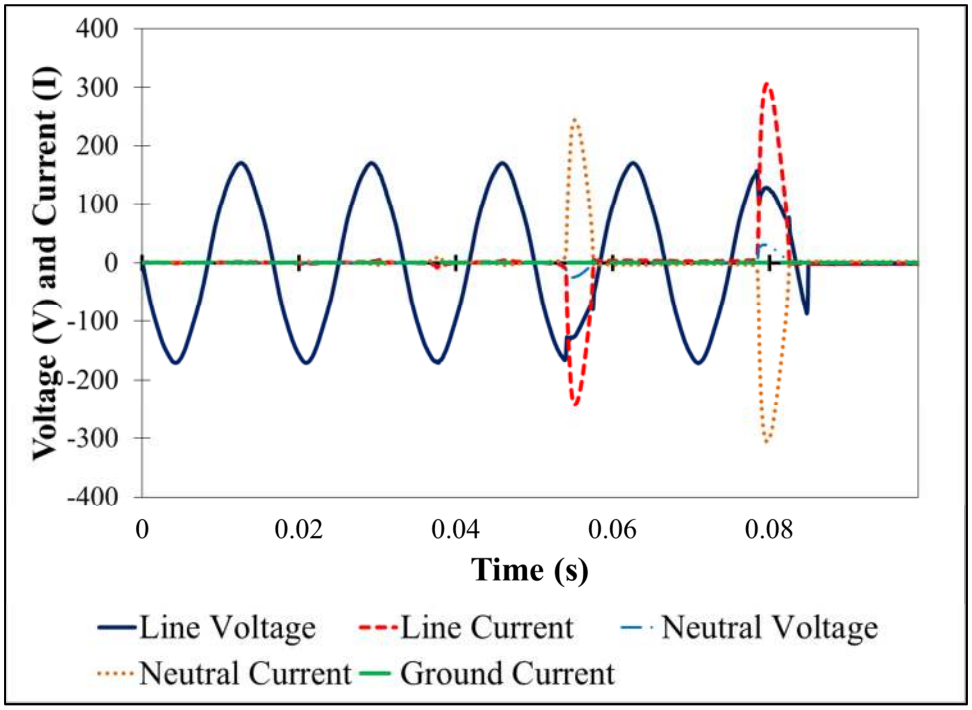

Figure 222 - Voltage and current waveforms produced in test 2-71 (50 kW/m^2). A total of 6 cycles (1/10 of a second) is shown.

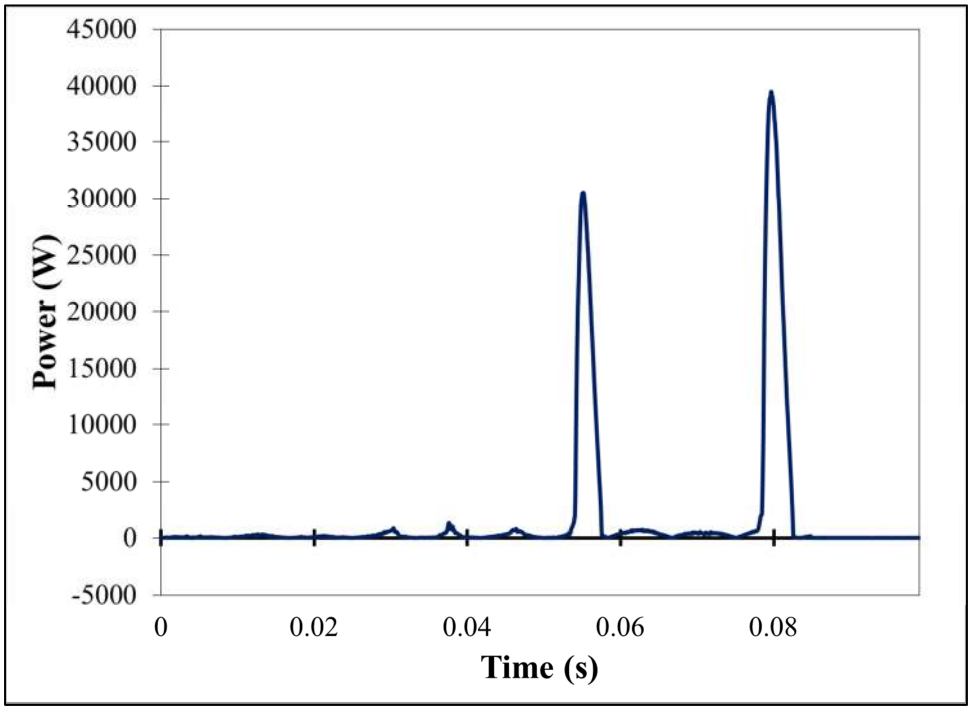

Figure 223 - Waveform of the instantaneous power produced in test 2-71 (50 kW/m^2). A total of 6 cycles (1/10 of a second) is shown.

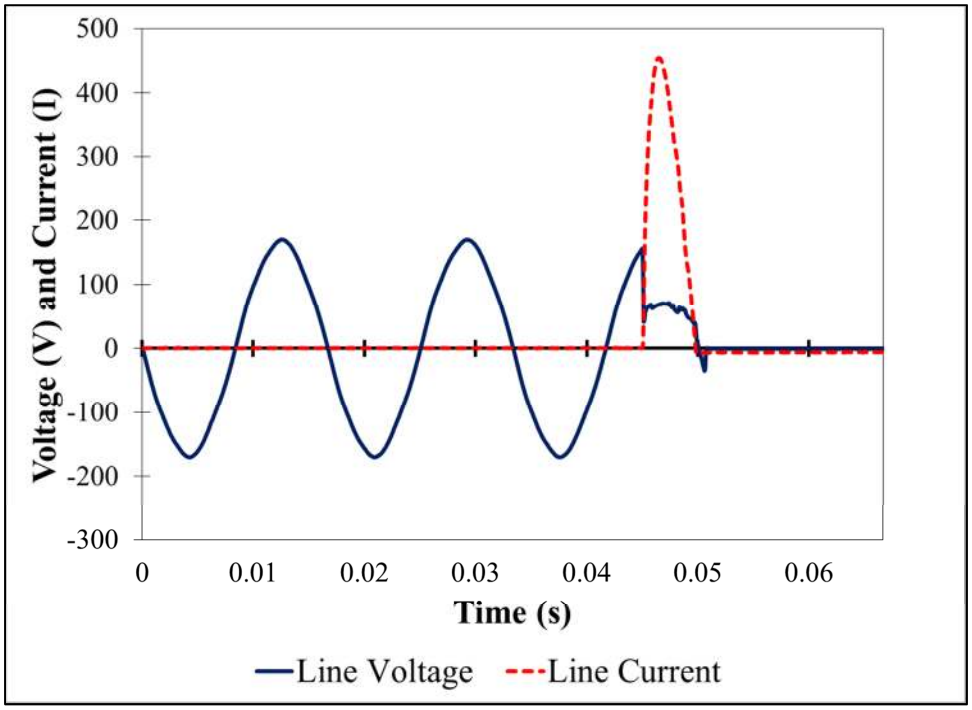

Figure 224 - Voltage and current waveforms produced in test 2-72 (45 kW/m^2). A total of 4 cycles (1/15th of a second) is shown.

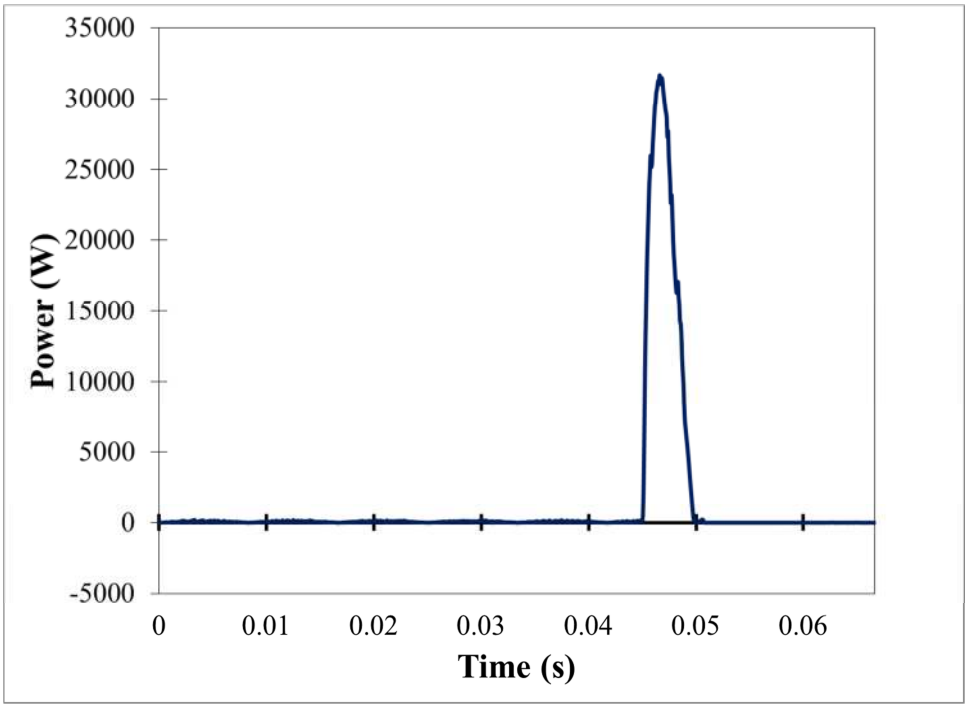

Figure 225 - Waveform of the instantaneous power produced in test 2-72 (45 kW/m^2). A total of 4 cycles (1/15th of a second) is shown.

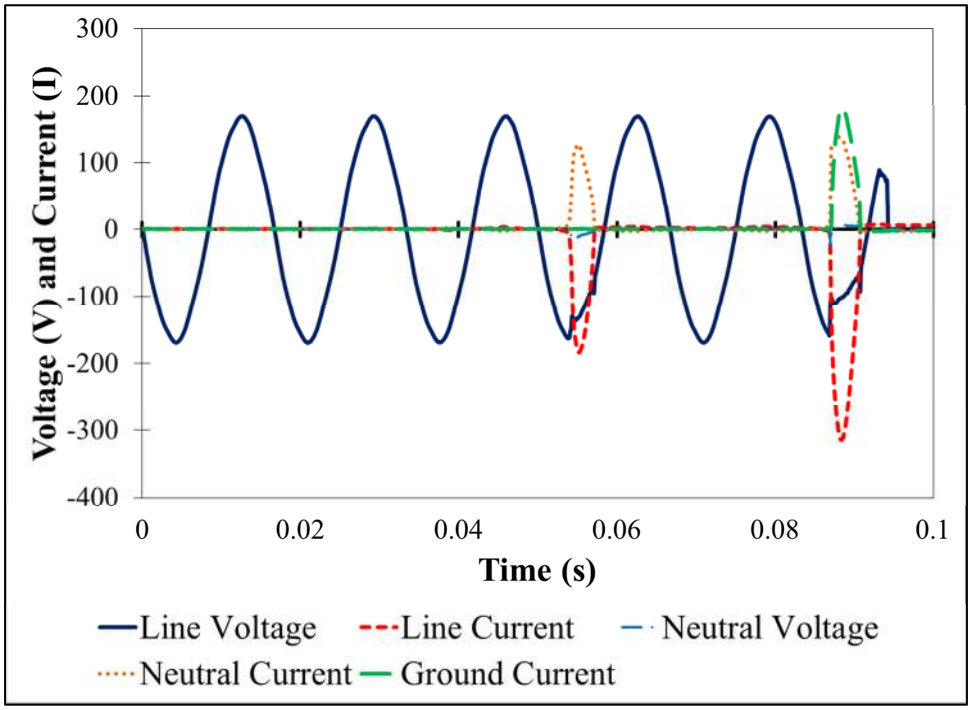

Figure 226 - Voltage and current waveforms produced in test 2-74 (45 kW/m^2). A total of 6 cycles (1/10 of a second) is shown.

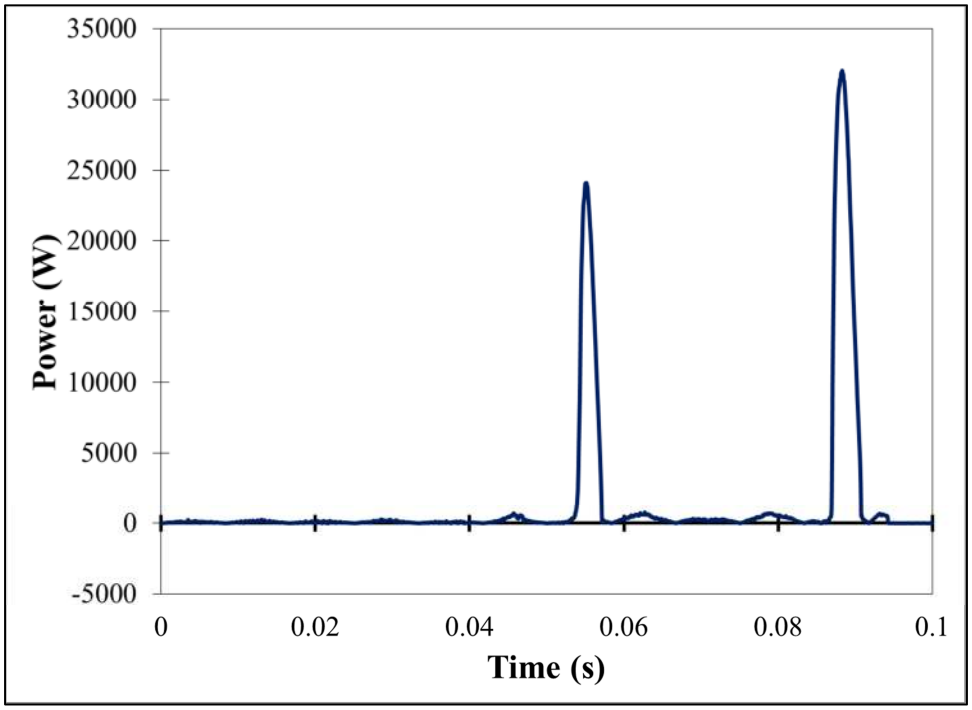

Figure 227 - Waveform of the instantaneous power produced in test 2-74 (45 kW/m^2). A total of 6 cycles (1/10 of a second) is shown.

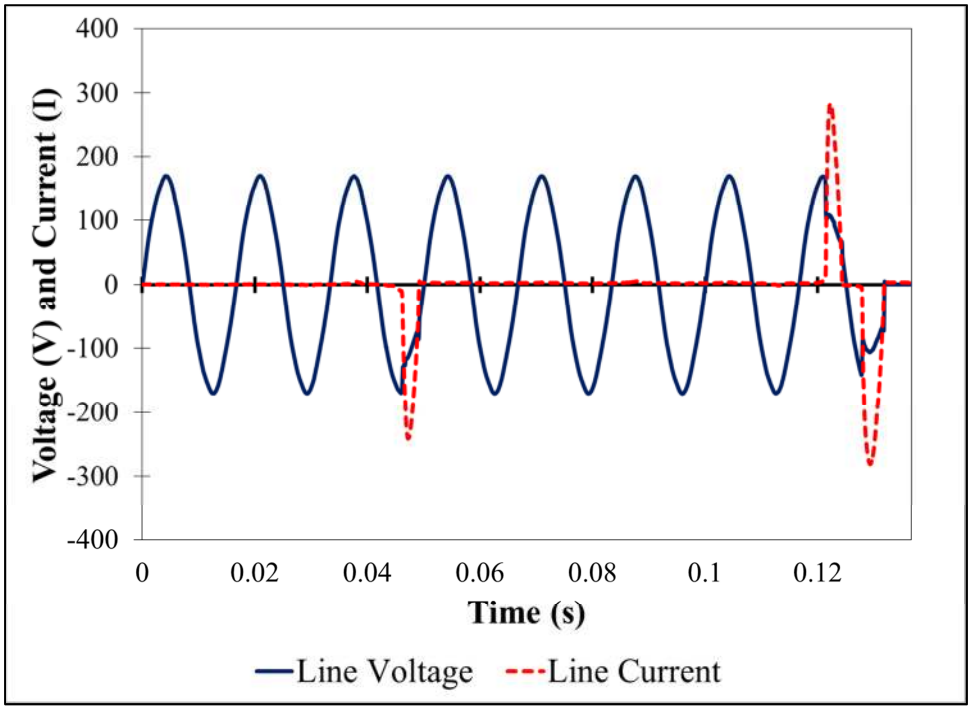

Figure 228 - Voltage and current waveforms produced in test 2-76 (45 kW/m^2). A total of 9 cycles (3/20 of a second) is shown.

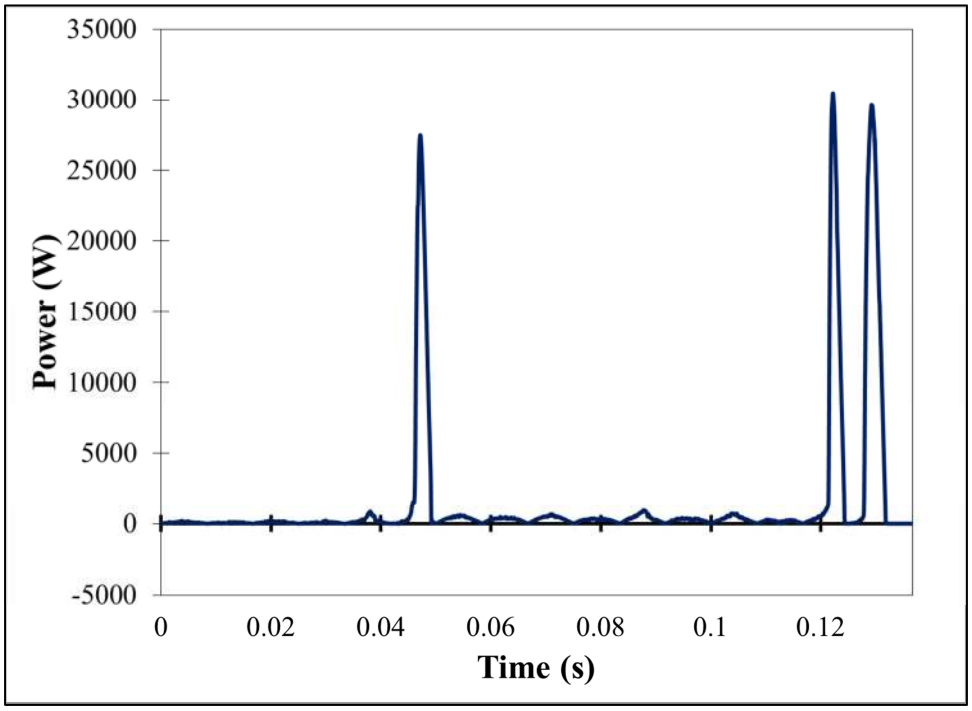

Figure 229 - Waveform of the instantaneous power produced in test 2-76 (45 kW/m^2). A total of 9 cycles (3/20 of a second) is shown.

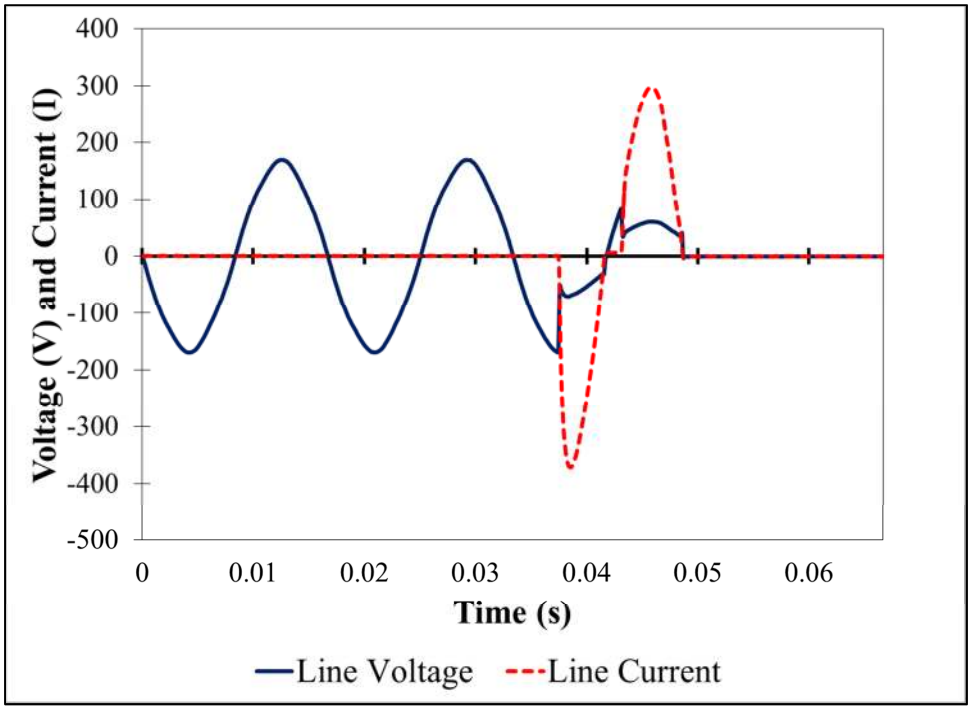

Figure 230 - Voltage and current waveforms produced in test 2-81 (45 kW/m^2). A total of 4 cycles (1/15 of a second) is shown.

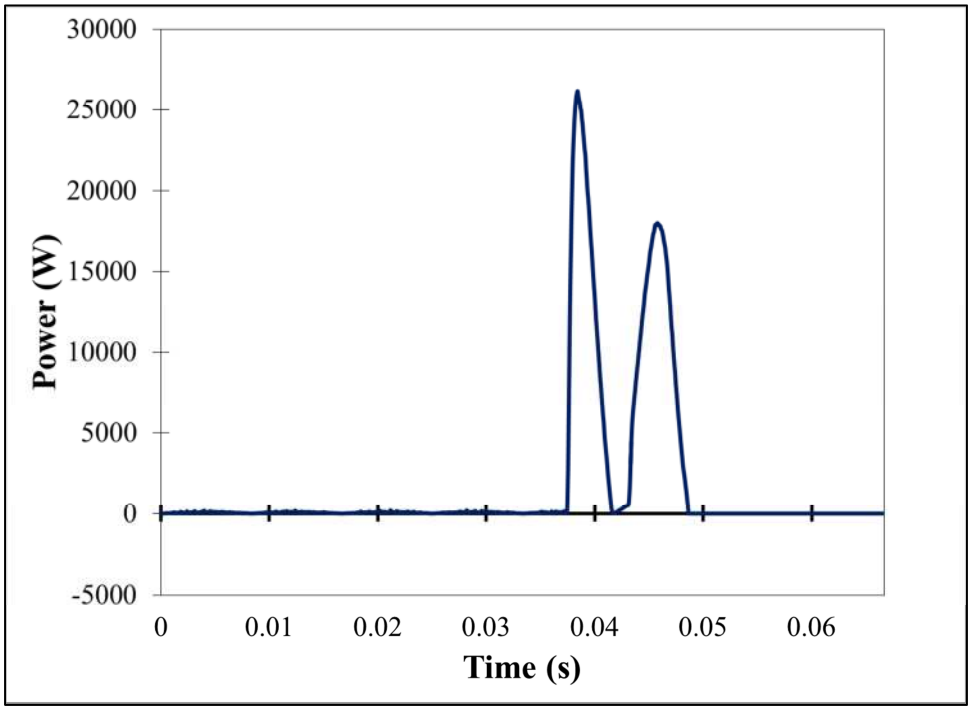

Figure 231 - Waveform of the instantaneous power produced in test 2-81 (45 kW/m^2). A total of 4 cycles (1/15 of a second) is shown.

7.4 Arcing Artifacts – Energized Cables in a Nitrogen Environment

Figure 232 - Arc 3-1 (16x magnification)

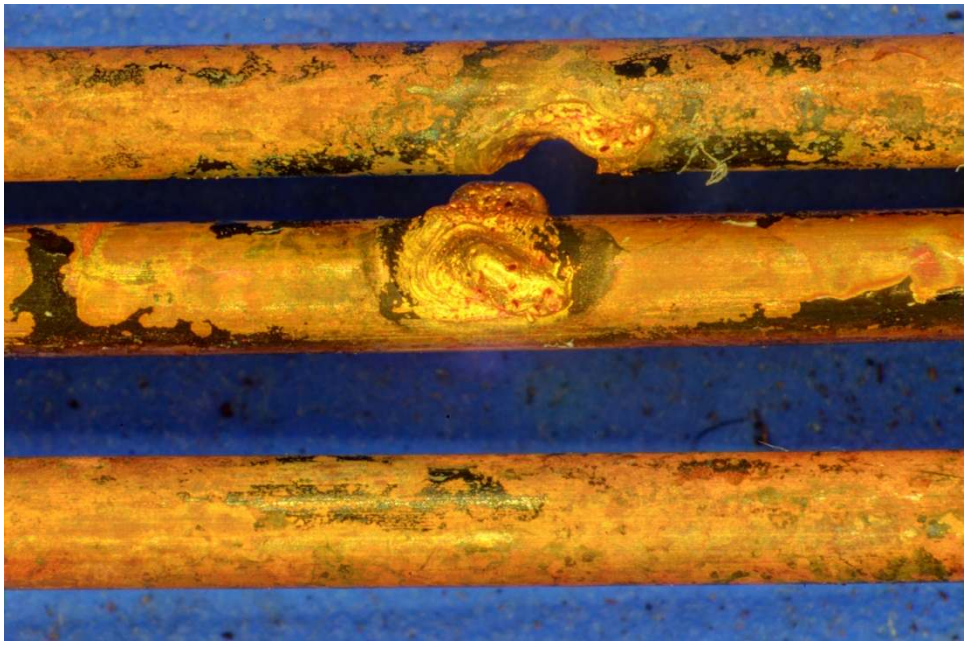

Figure 233 – Arc 3-2 (16x magnification)

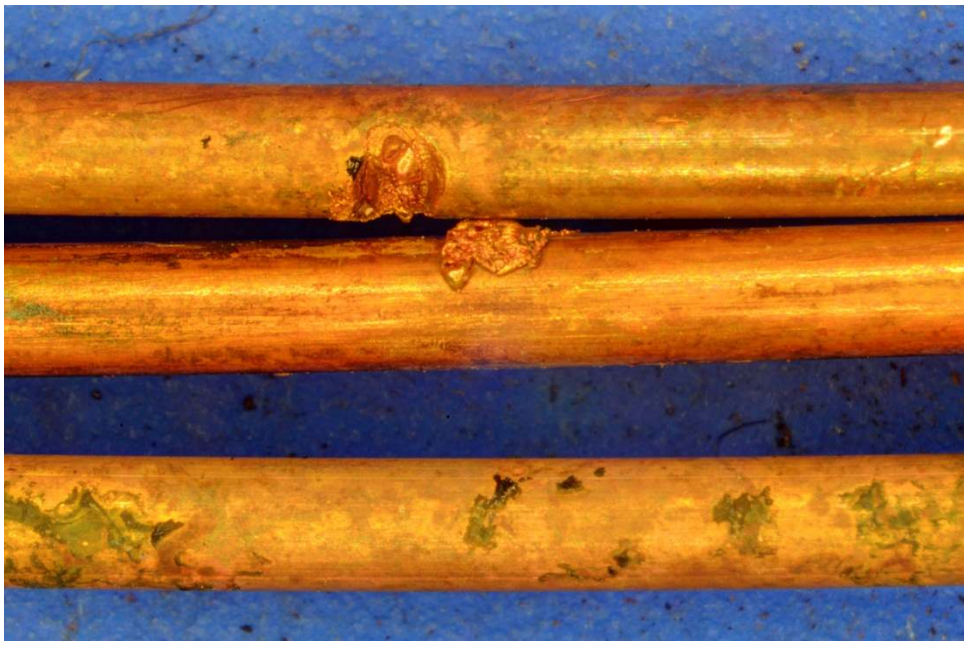

Figure 234 – Arc 3-3 (16x magnification)

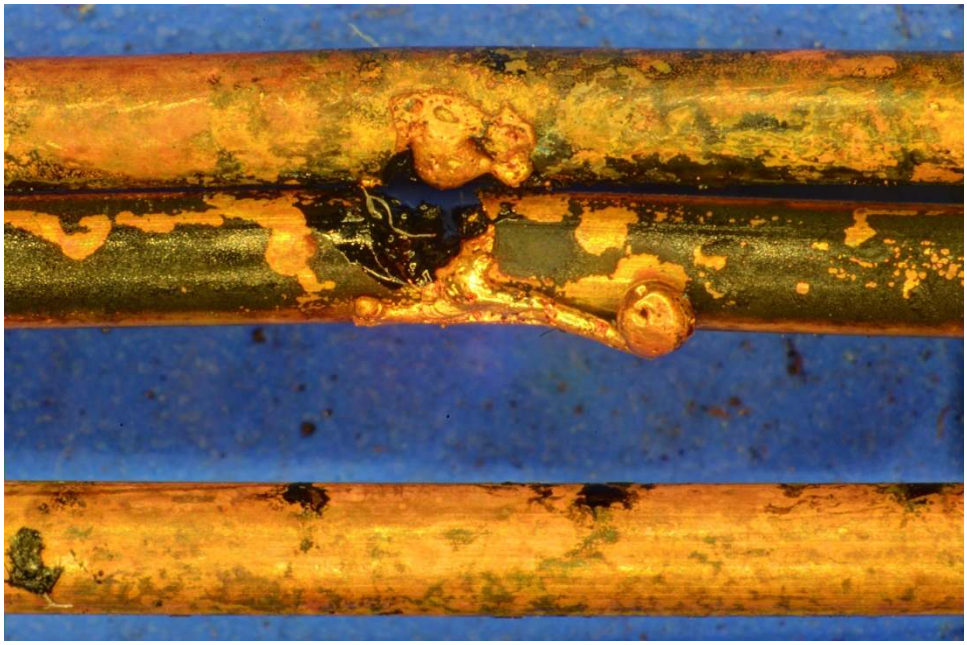

Figure 235 – Arc 3-4 (16x magnification)

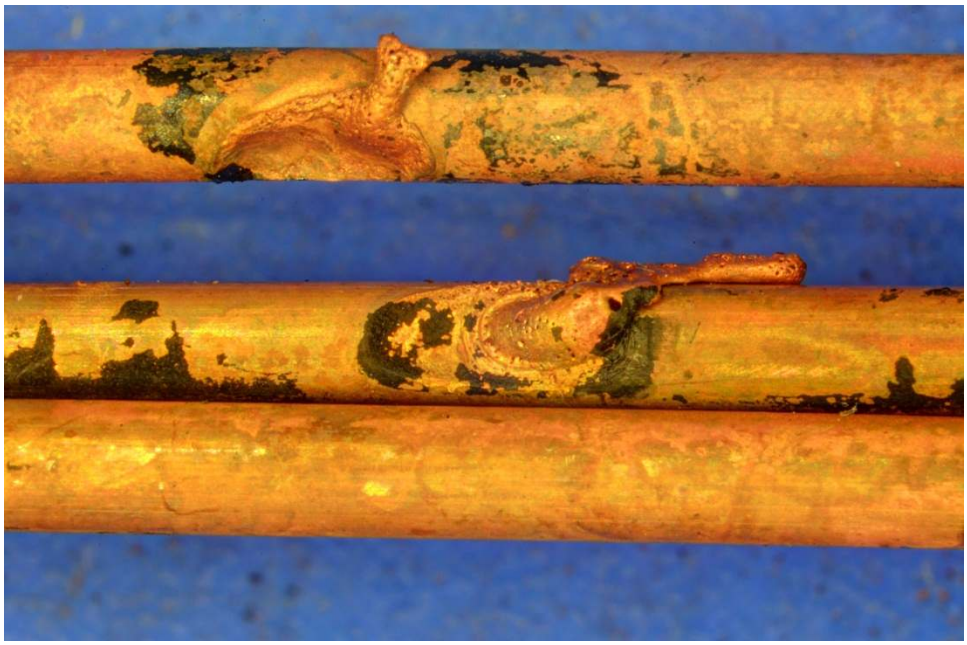

Figure 236 – Arc 3-6 (16x magnification)

7.5 Enhanced and SEM Photographs – Energized Cables in a Nitrogen Environment

Figure 237 - Arc 3-1 (16x magnification)

Figure 238 - Arc 3-2 (16x magnification)

Figure 239 - Arc 3-3 (16x magnification)

Figure 240 - Arc 3-4 (16x magnification)

Figure 241 - Arc 3-6 (16x magnification)

7.6 Arcing Waveforms – Energized Cables in a Nitrogen Environment

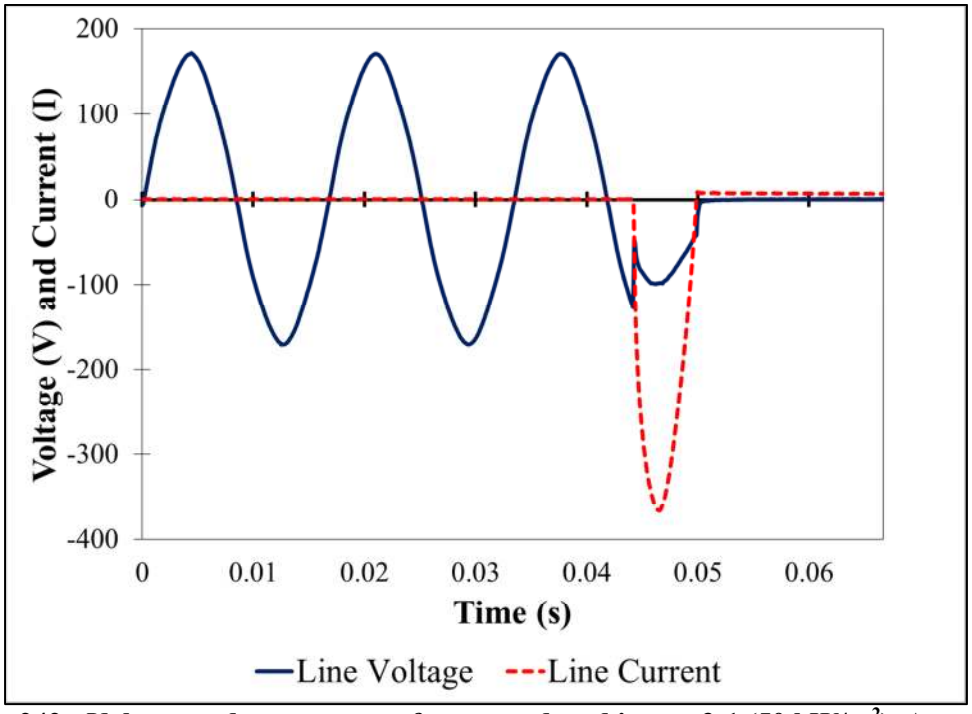

Figure 242 - Voltage and current waveforms produced in test 3-1 (50 kW/m^2). A total of 4 cycles (1/15 of a second) is shown.

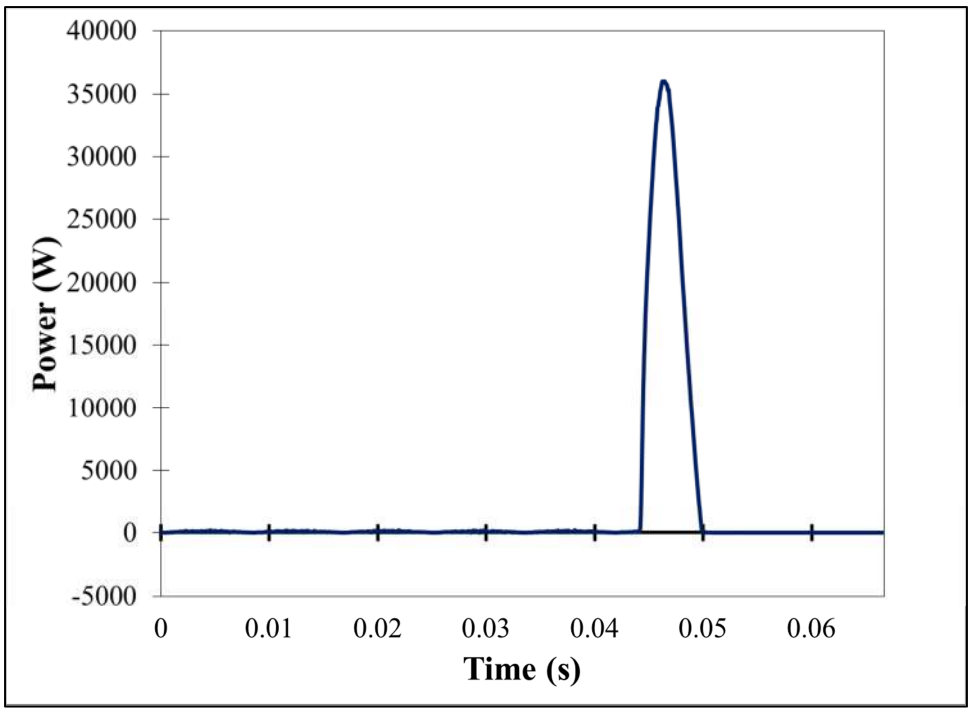

Figure 243 - Waveform of the instantaneous power produced in test 3-1 (50 kW/m^2). A total of 4 cycles (1/15 of a second) is shown.

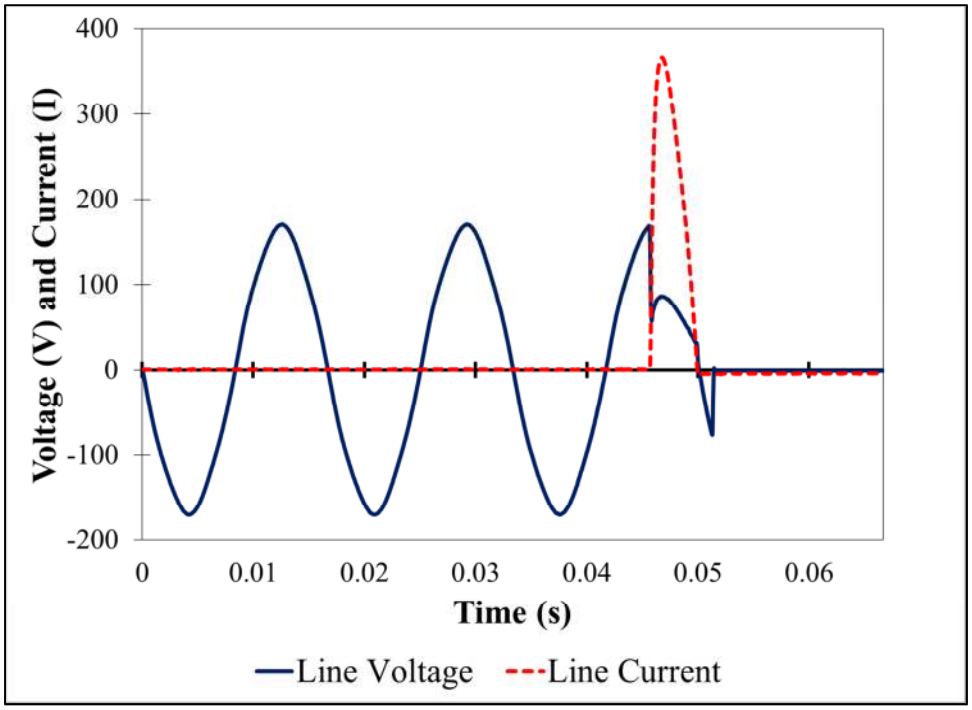

Figure 244 - Voltage and current waveforms produced in test 3-2 (50 kW/m^2). A total of 4 cycles (1/15 of a second) is shown.

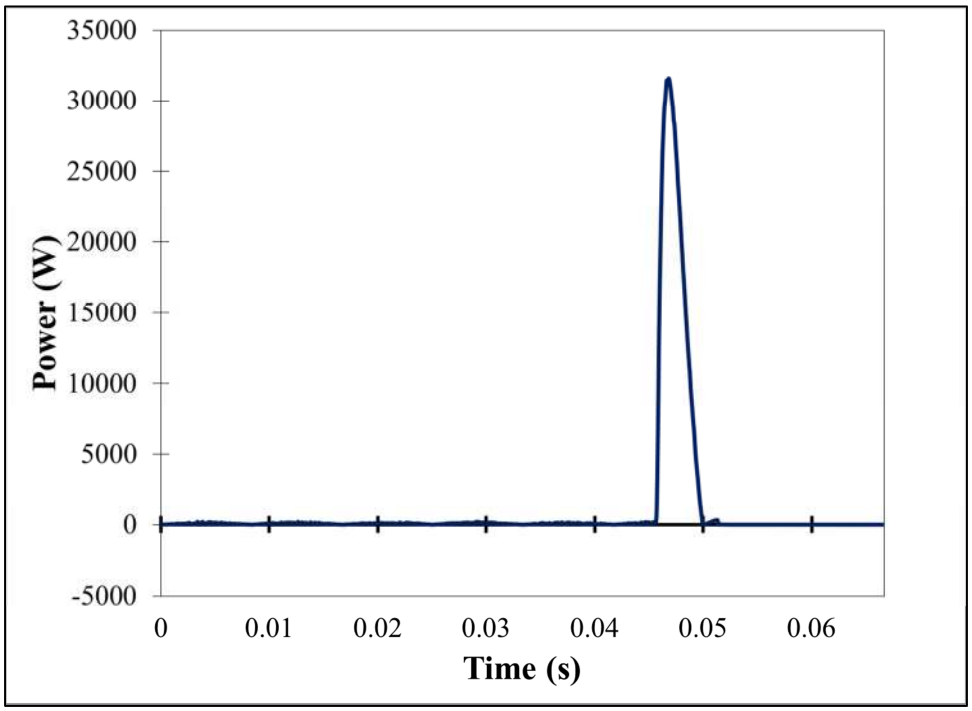

Figure 245 - Waveform of the instantaneous power produced in test 3-2 (50 kW/m^2). A total of 4 cycles (1/15 of a second) is shown.

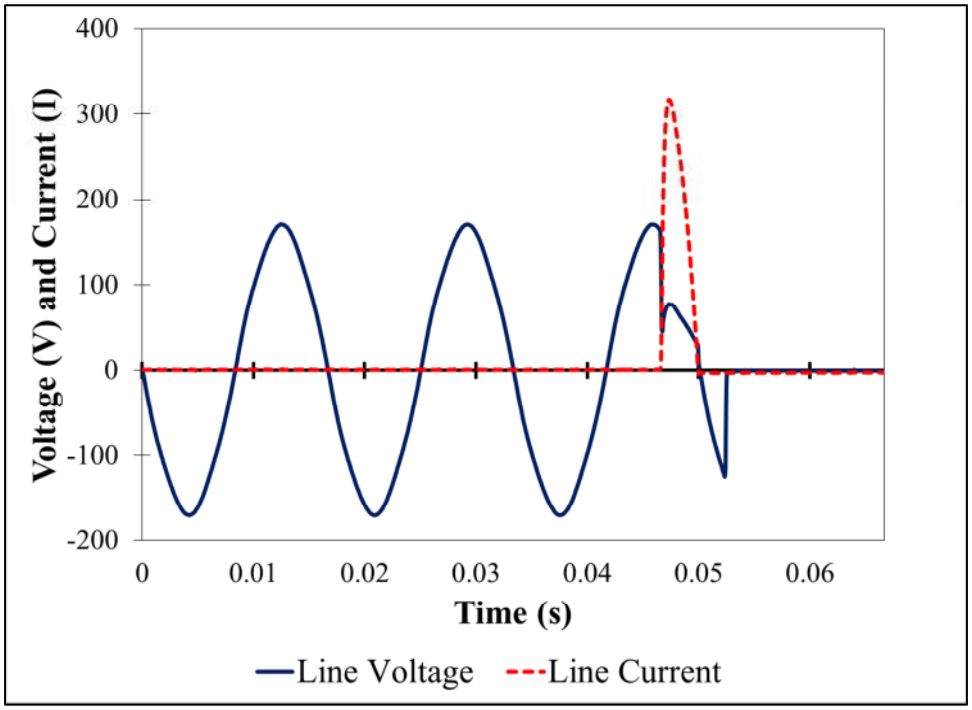

Figure 246 - Voltage and current waveforms produced in test 3-3 (54 kW/m^2). A total of 4 cycles (1/15 of a second) is shown.

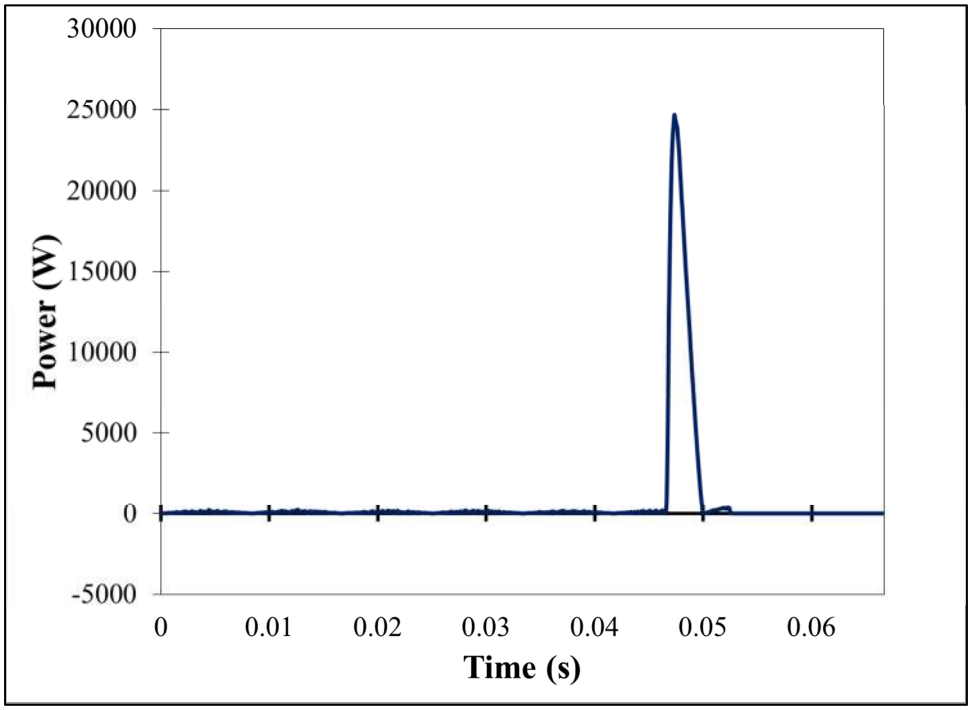

Figure 247 - Waveform of the instantaneous power produced in test 3-3 (54 kW/m^2). A total of 4 cycles (1/15 of a second) is shown.

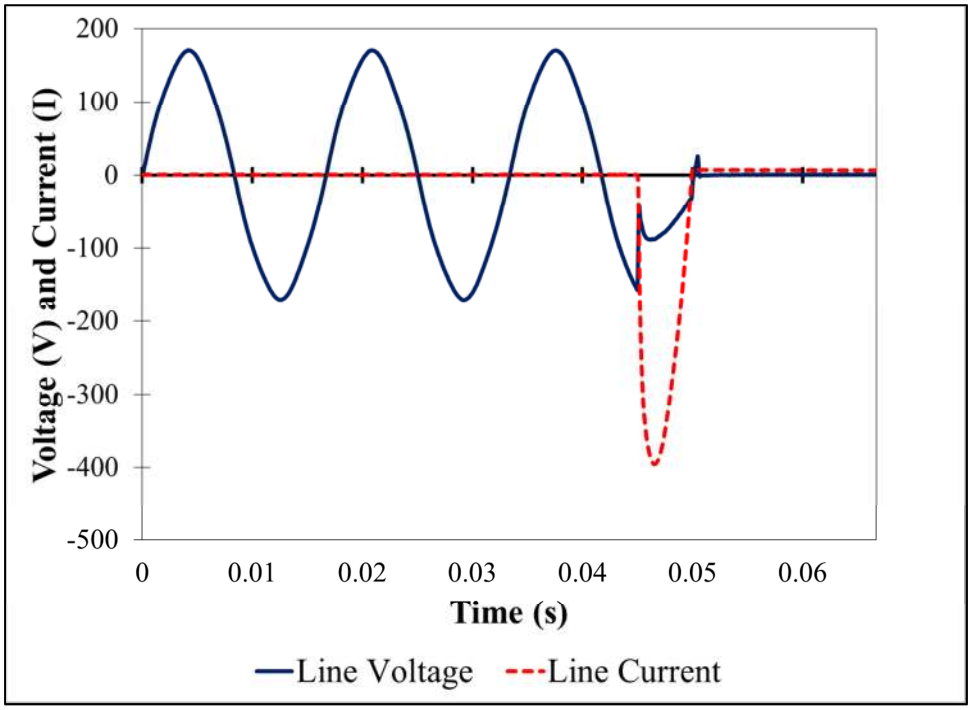

Figure 248 - Voltage and current waveforms produced in test 3-4 (54 kW/m^2). A total of 4 cycles (1/15 of a second) is shown.

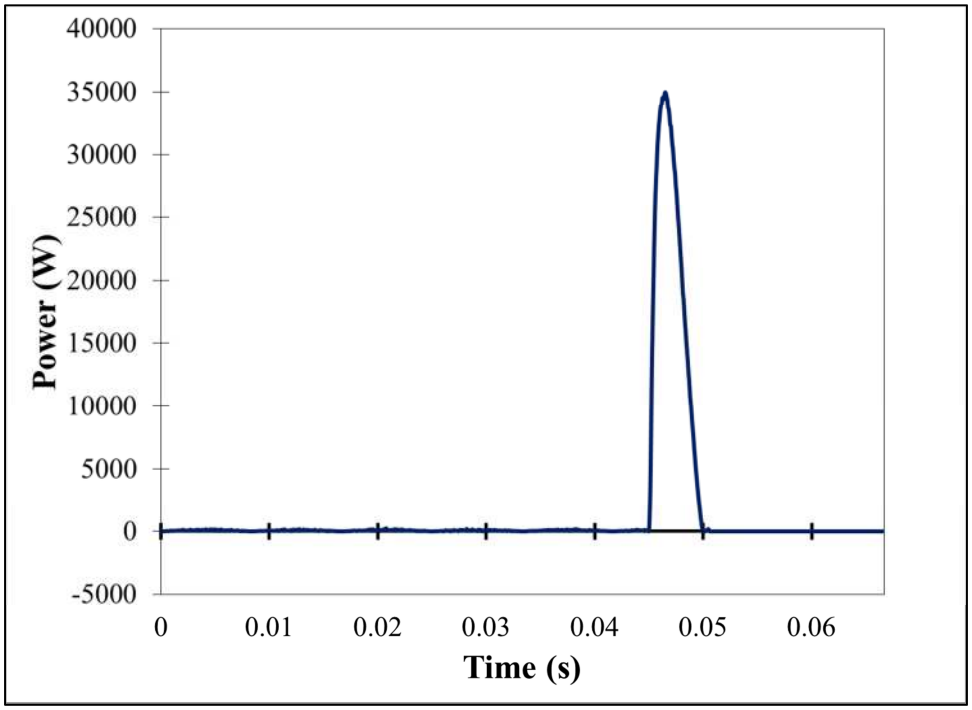

Figure 249 - Waveform of the instantaneous power produced in test 3-4 (54 kW/m^2). A total of 4 cycles (1/15 of a second) is shown.

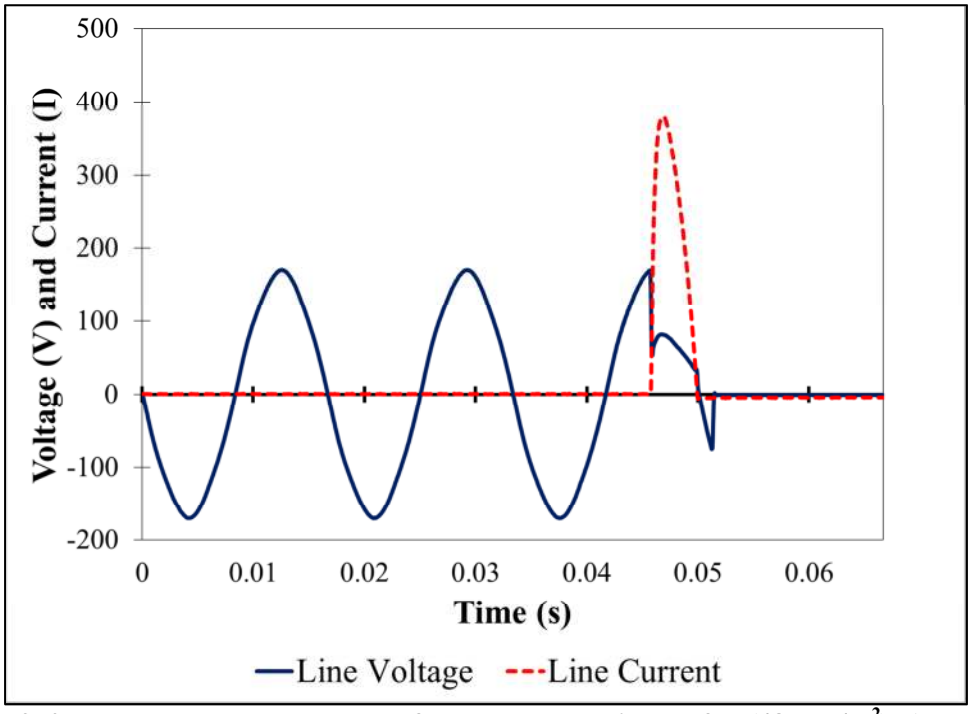

Figure 250 - Voltage and current waveforms produced in test 3-5 (48 kW/m^2). A total of 4 cycles (1/15 of a second) is shown.

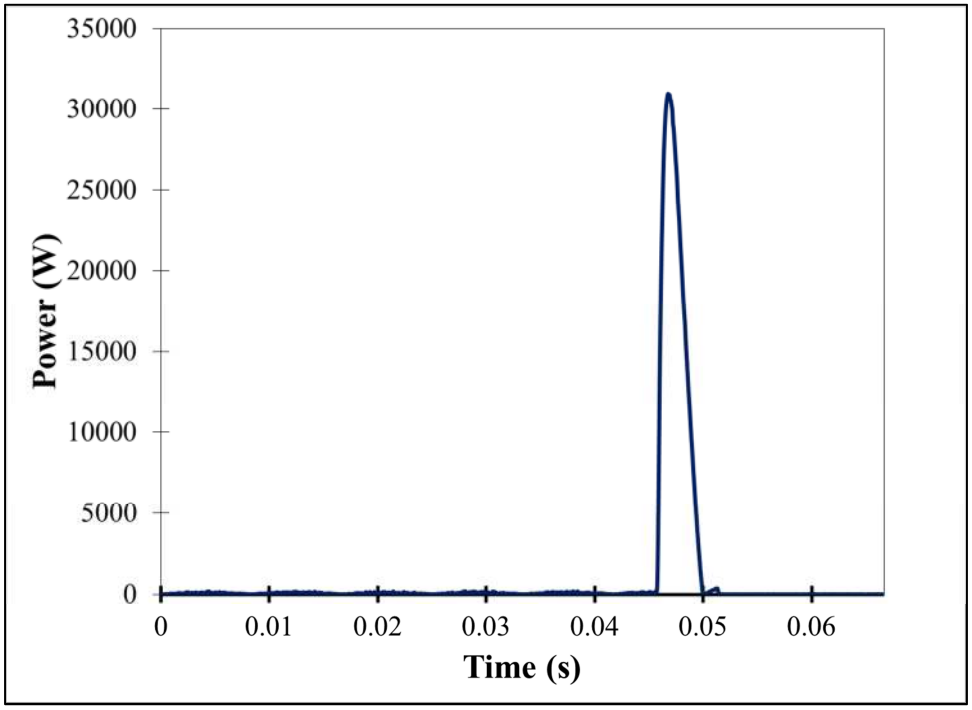

Figure 251 - Waveform of the instantaneous power produced in test 3-5 (48 kW/m^2). A total of 4 cycles (1/15 of a second) is shown.

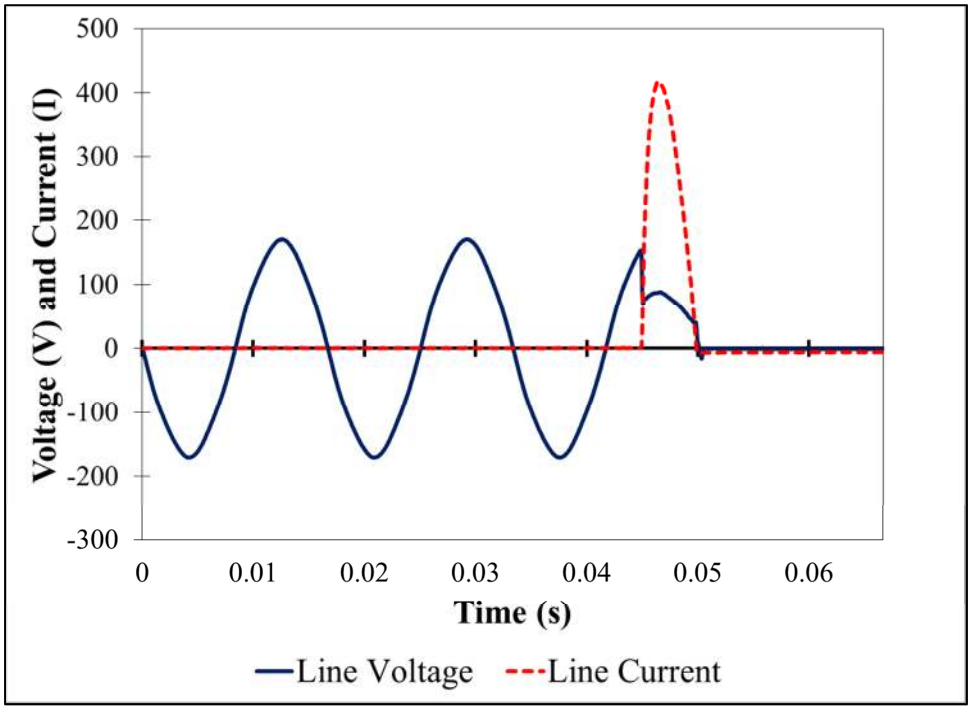

Figure 252 - Voltage and current waveforms produced in test 3-6 (48 kW/m^2). A total of 4 cycles (1/15 of a second) is shown.

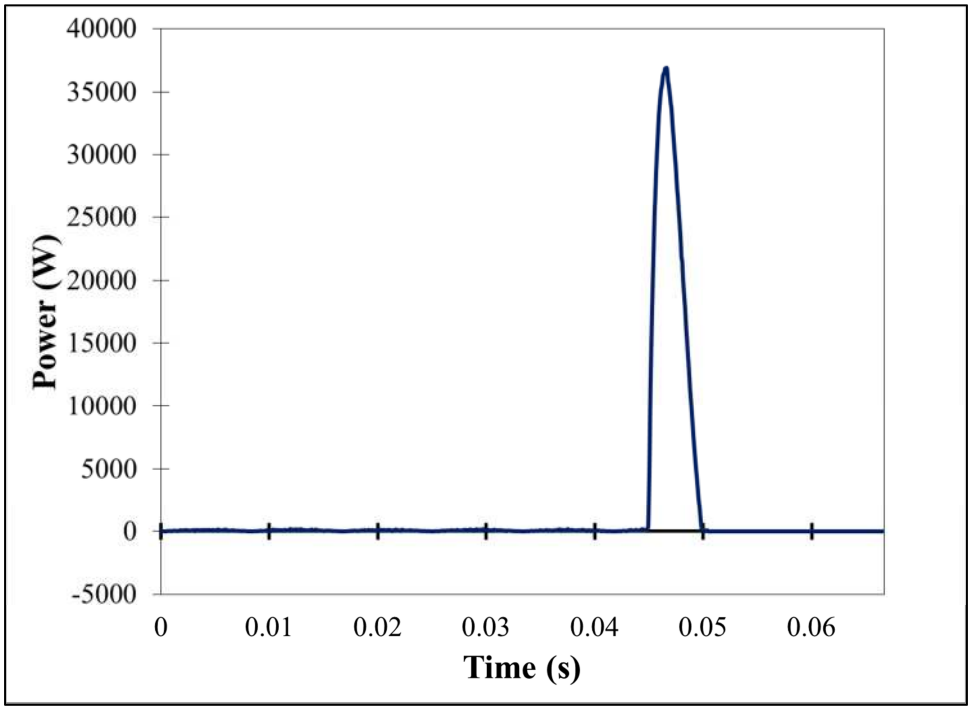

Figure 253 - Waveform of the instantaneous power produced in test 3-6 (48 kW/m^2). A total of 4 cycles (1/15 of a second) is shown.

7.7 Arcing Artifacts – Energized Cables under Variable Voltages

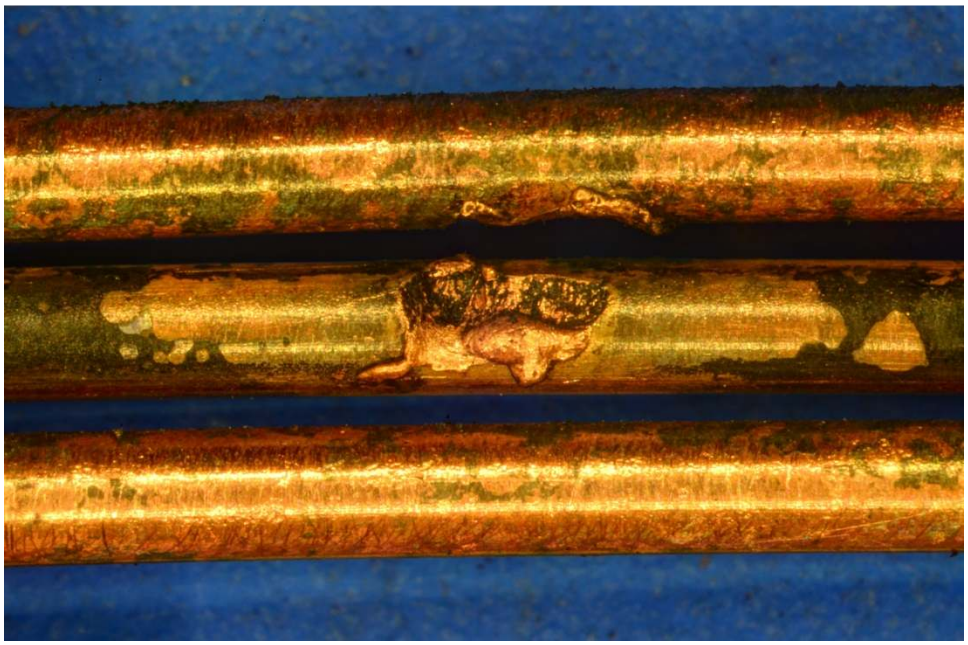

Figure 254 – Arc 140-1 (16x magnification)

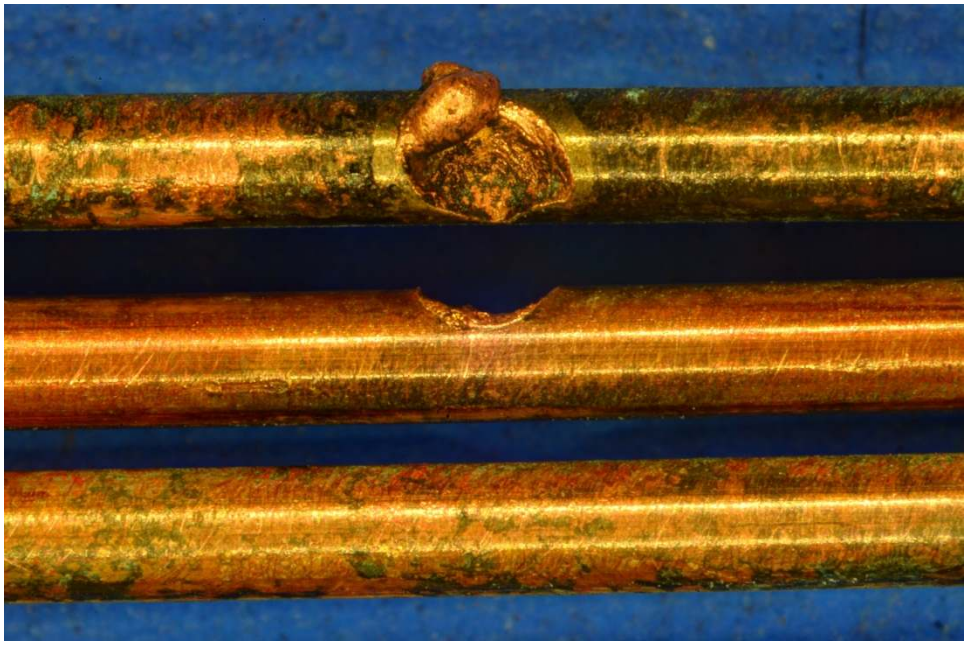

Figure 255 – Arc 140-2 (16x magnification)

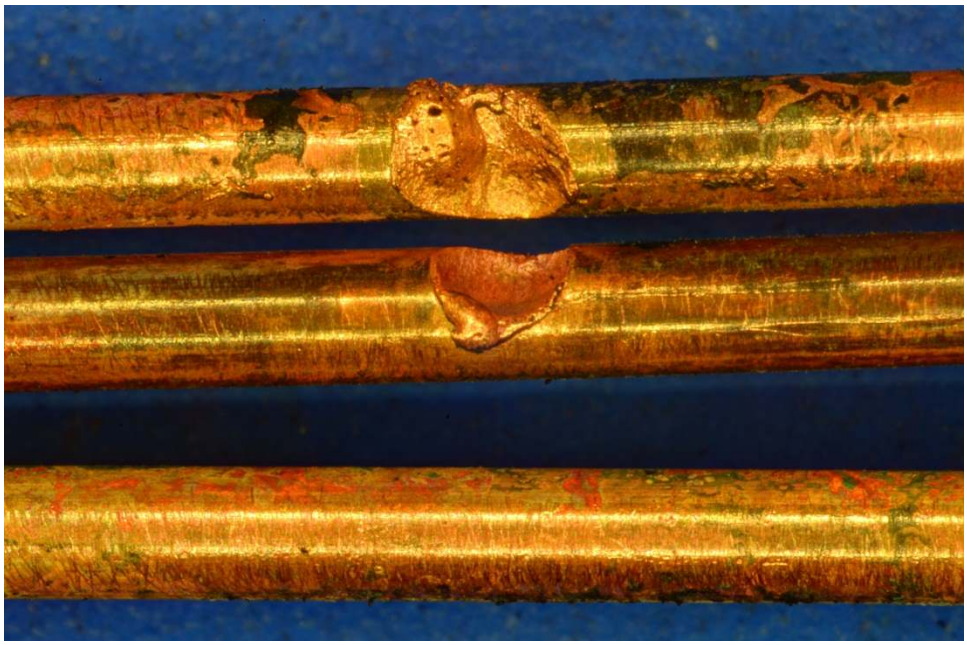

Figure 256 - Arc 140-3 (16x magnification)

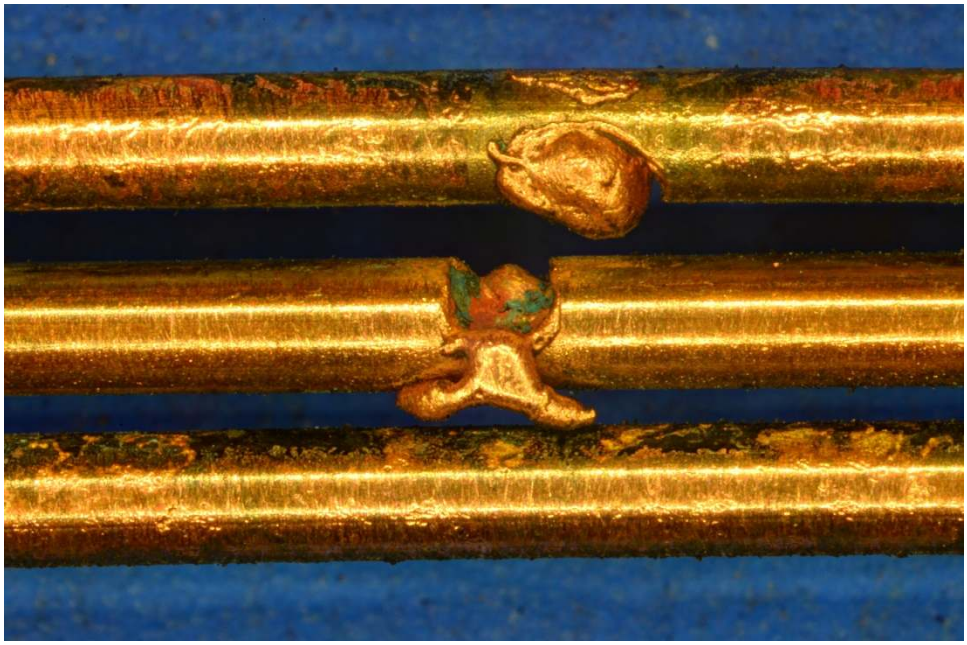

Figure 257 - Arc 100-1 (16x magnification)

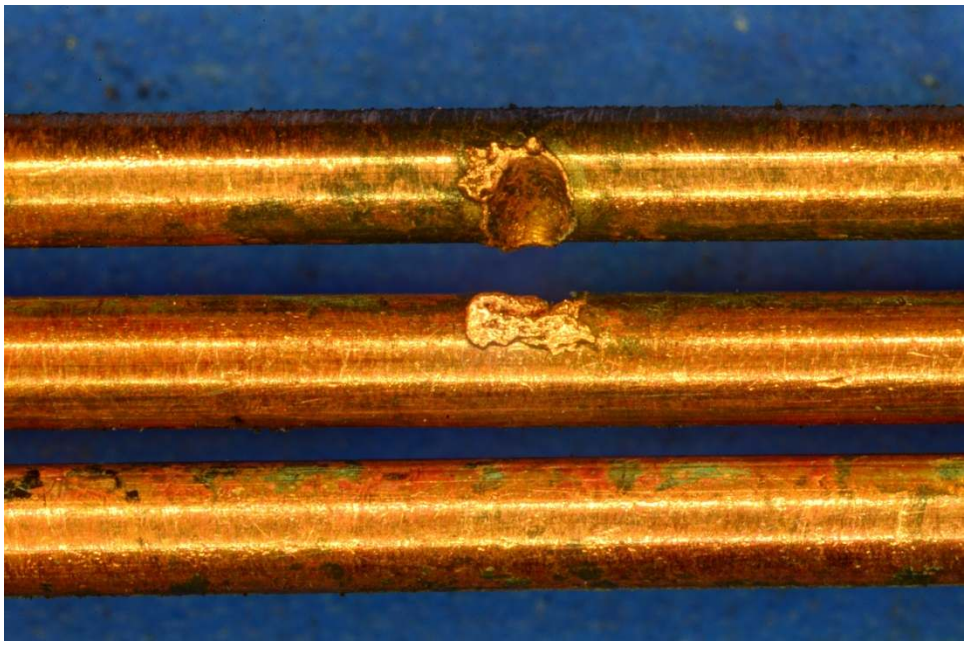

Figure 258 - Arc 100-2 (16x magnification)

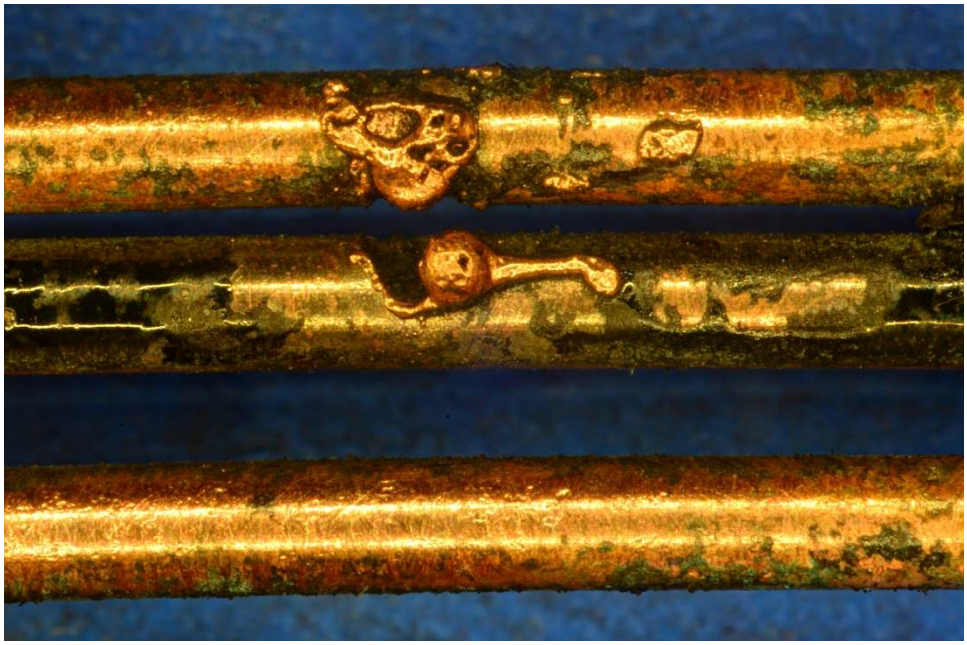

Figure 259 - Arc 100-3 (16x magnification)

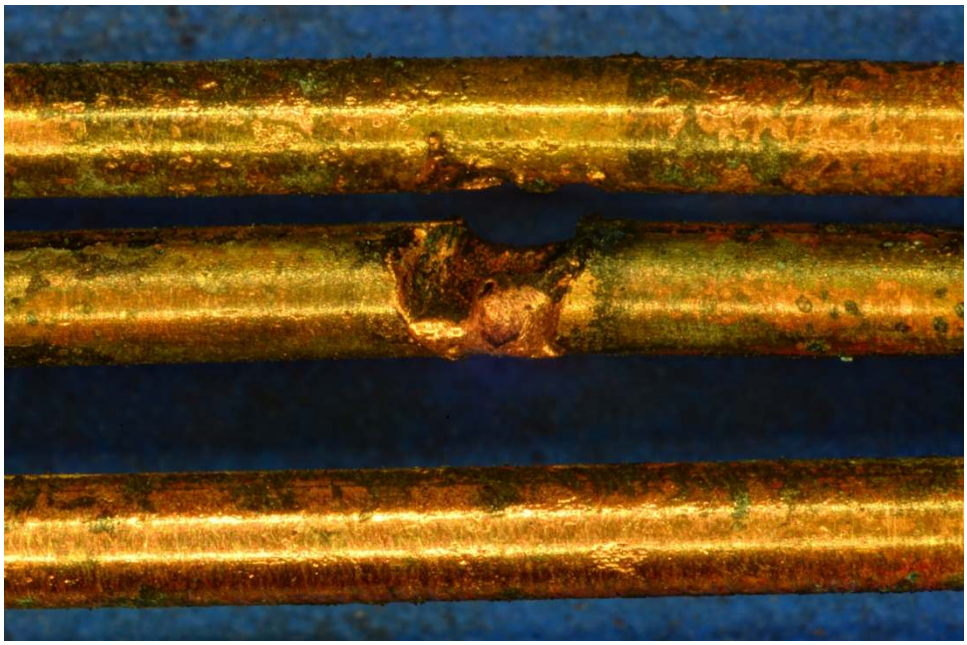

Figure 260 - Arc 100-3 (16x magnification)

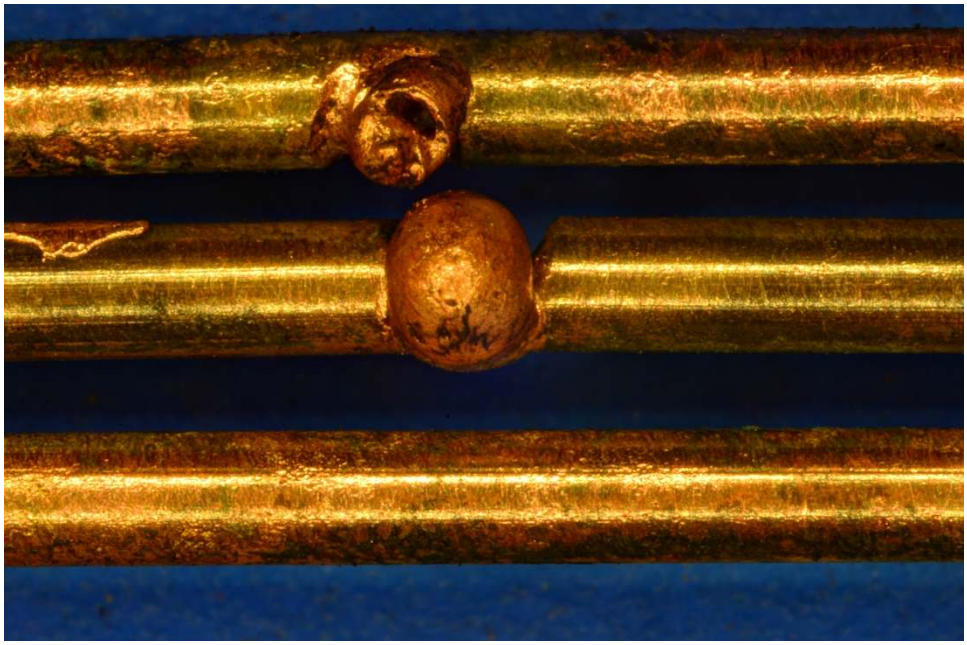

Figure 261 - Arc 100-4 (16x magnification)

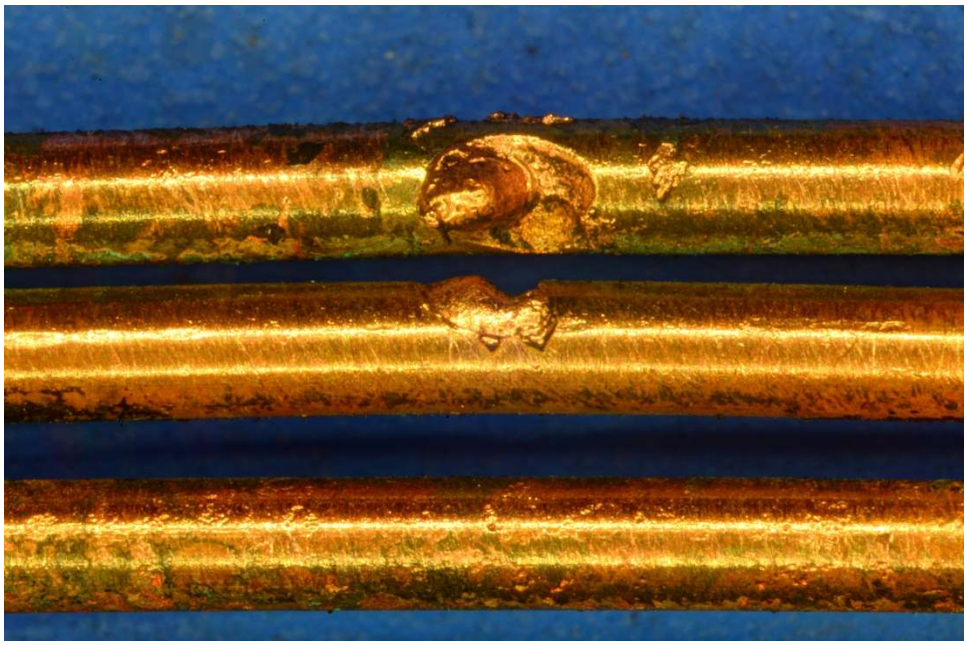

Figure 262 - Arc 80-2 (16x magnification)

Figure 263 - Arc 80-3 (16x magnification)

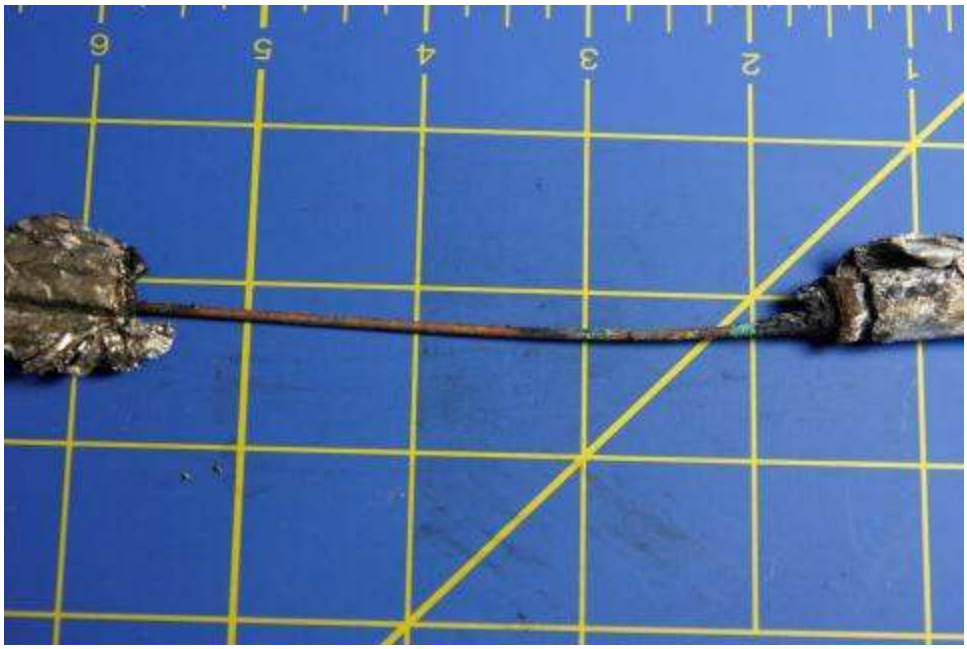

Figure 264 - Arc 60-1. One square equals one inch.

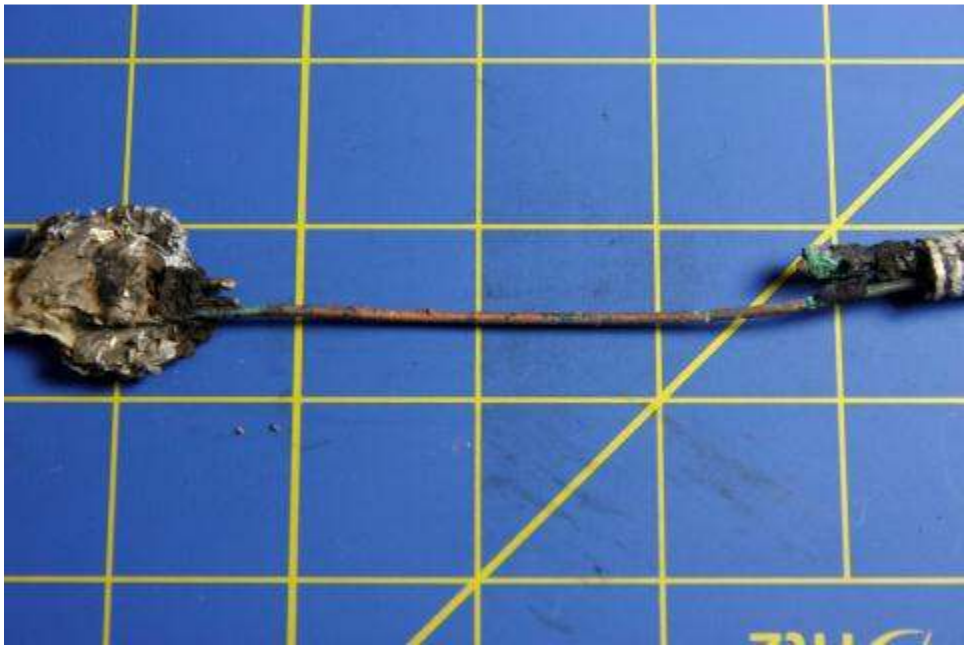

Figure 265 - Arc 60-2. One square equals one inch.

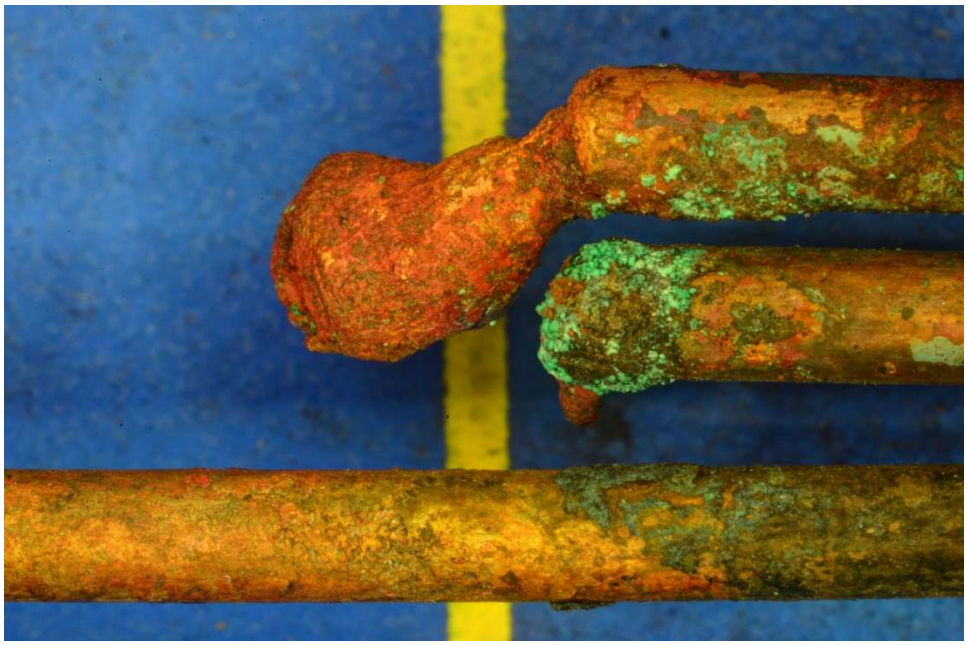

Figure 266 - Arc 60-4 (16x magnification)

Figure 267 - Arc 60-3 (12.5x magnification)

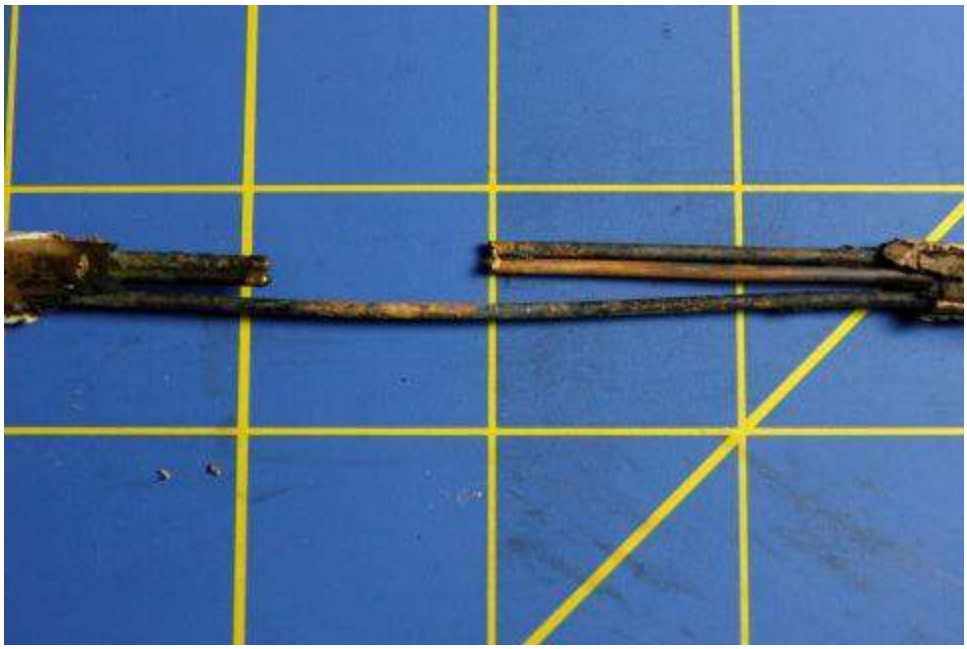

Figure 268 - Arc 60-6. One square equals one inch.

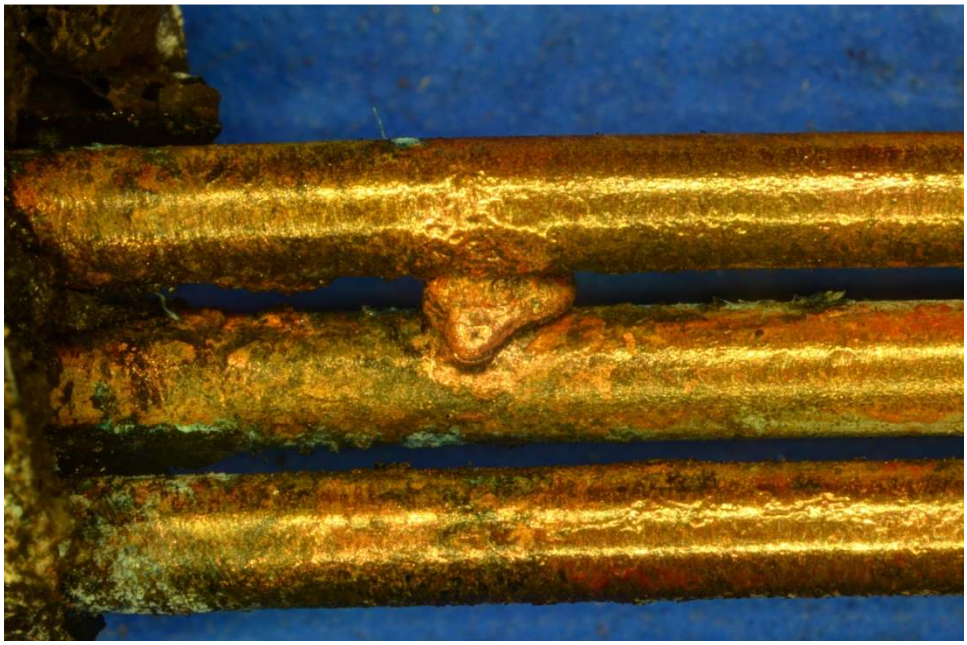

Figure 269 - Arc 40-1 (16 magnification)

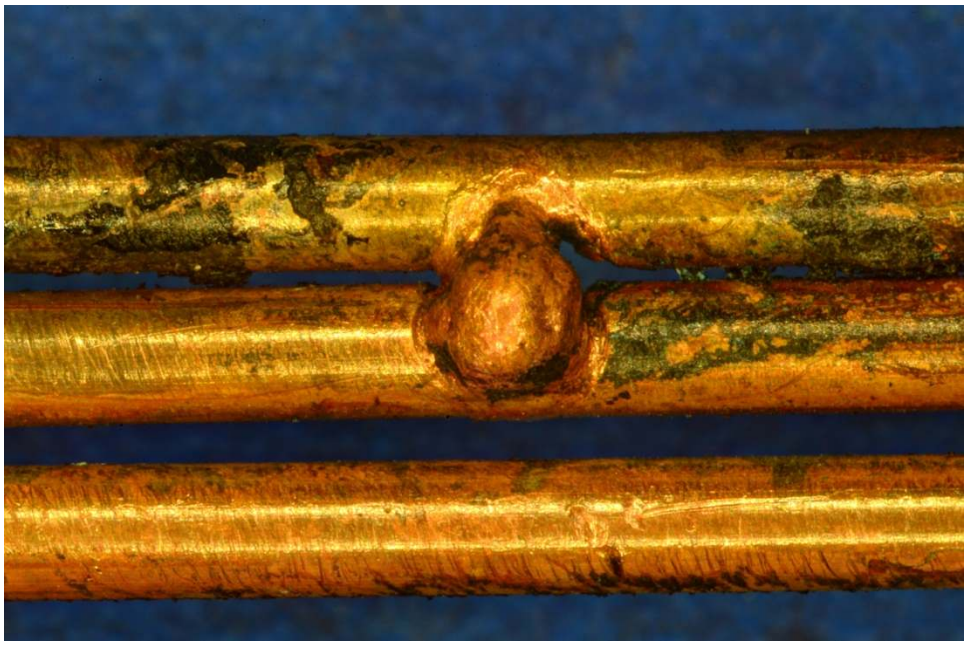

Figure 270 - Arc 40-2 (16x magnification)

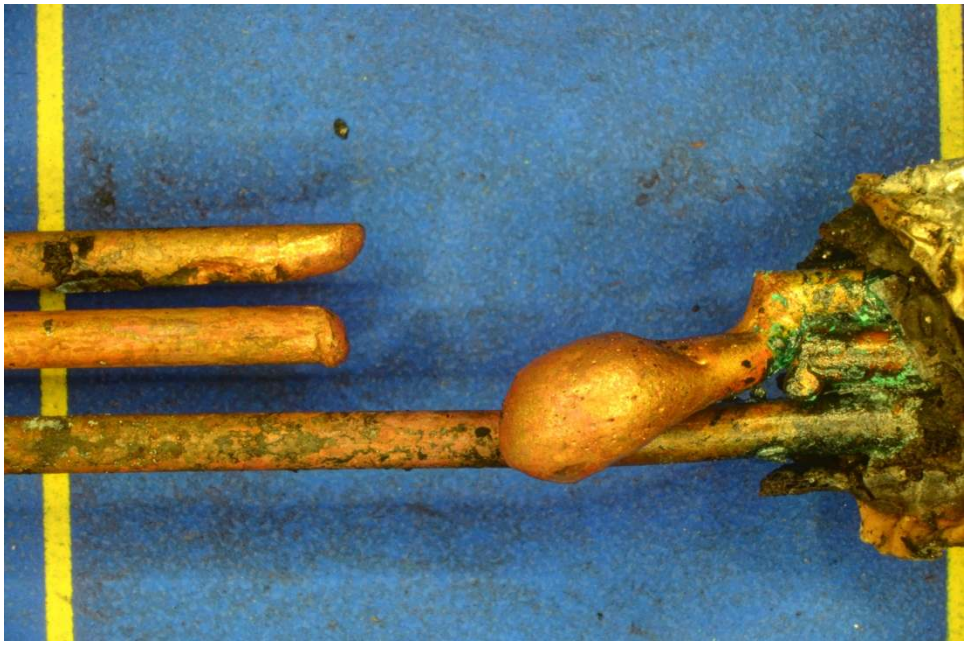

Figure 271 - Arc 40-3 (10x magnification)

Figure 272 - Arc 40-4 (16x magnification)

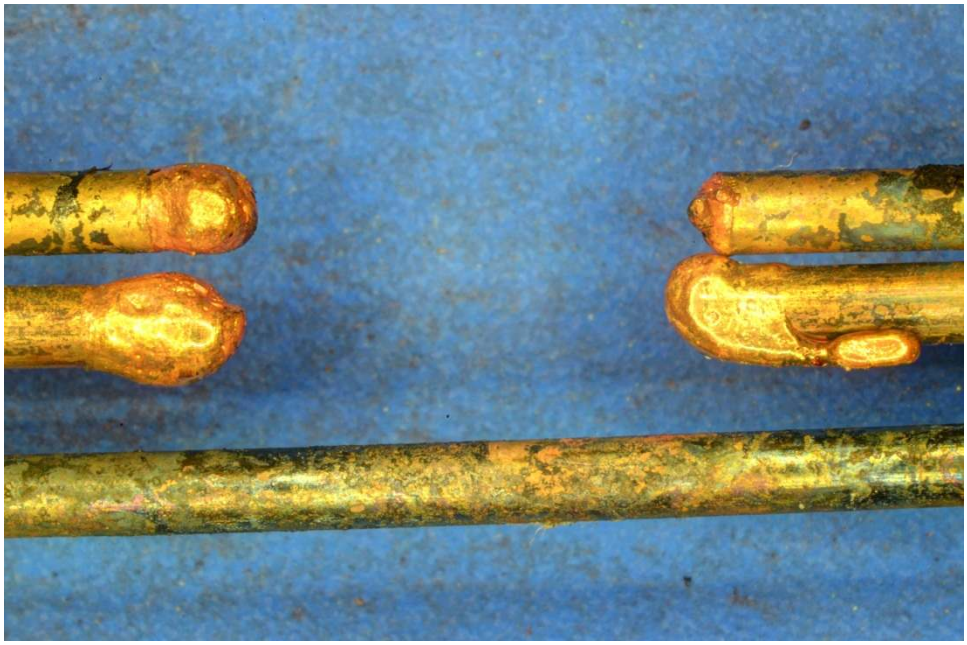

Figure 273 - Arc 50-5 (16x magnification)

Figure 274 - Arc 50-4 (12.5x magnification)

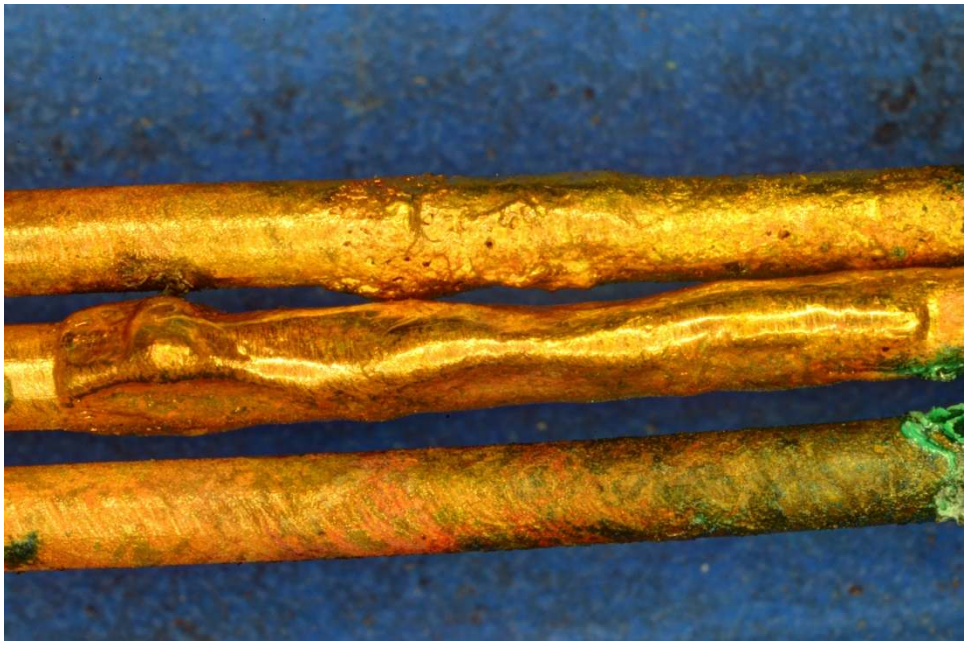

Figure 275 – Arc 20-1 (12.5x magnification)

7.8 Arcing Waveforms – Energized Cables under Variable Voltages

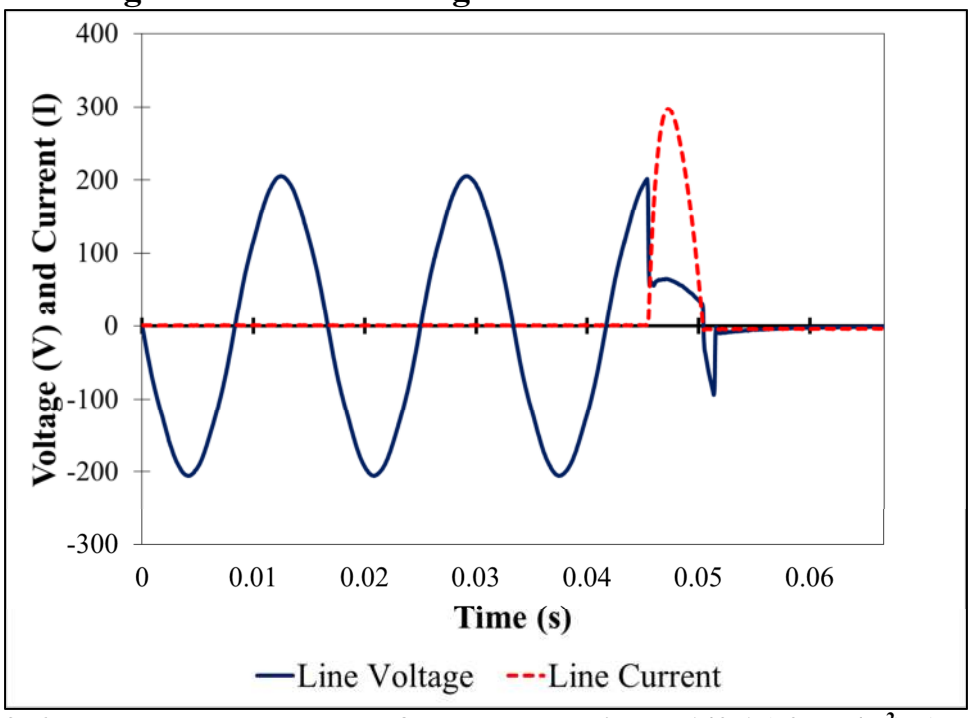

Figure 276 - Voltage and current waveforms produced in test 140-1 (50 kW/m^2). A total of 4 cycles (1/15 of a second) is shown.

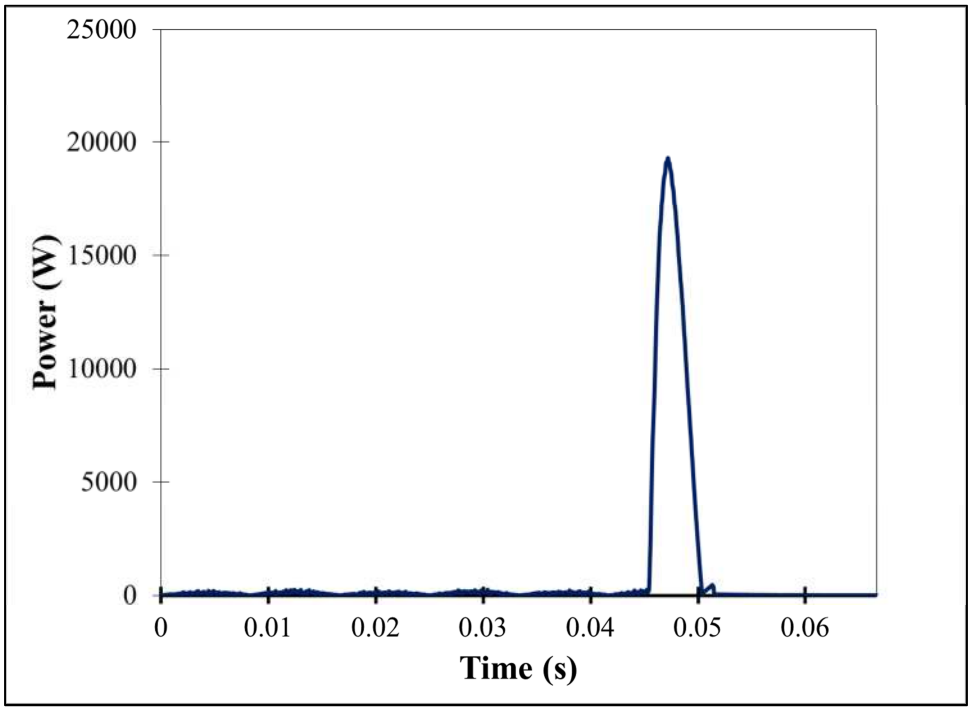

Figure 277 - Waveform of the instantaneous power produced in test 140-1. A total of 4 cycles (1/15 of a second) is shown.

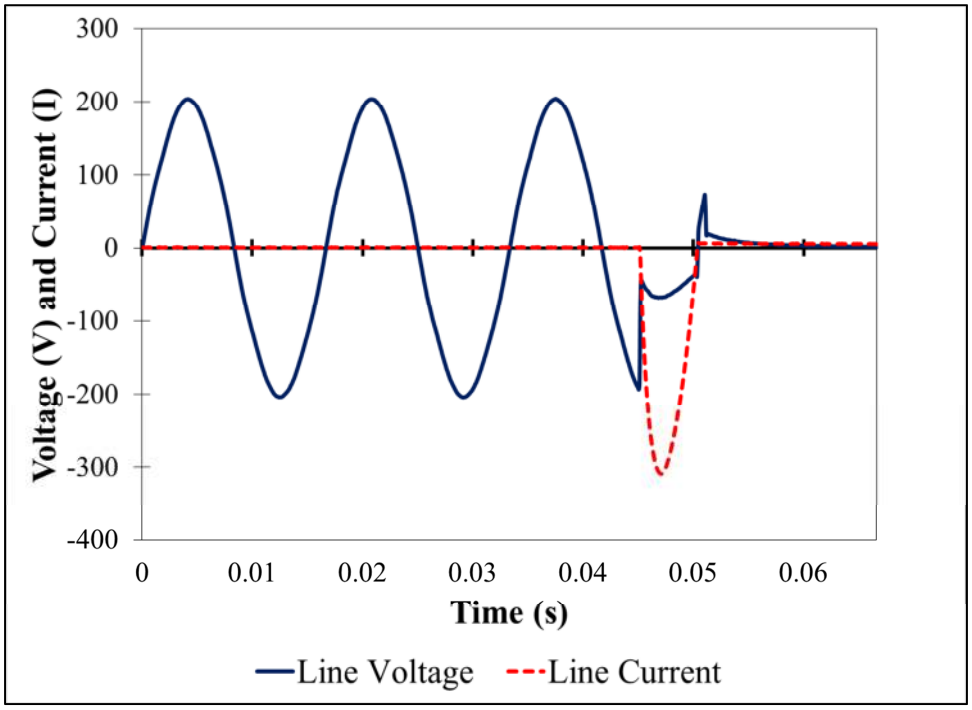

Figure 278 - Voltage and current waveforms produced in test 140-2. A total of 4 cycles (1/15 of a second) is shown.

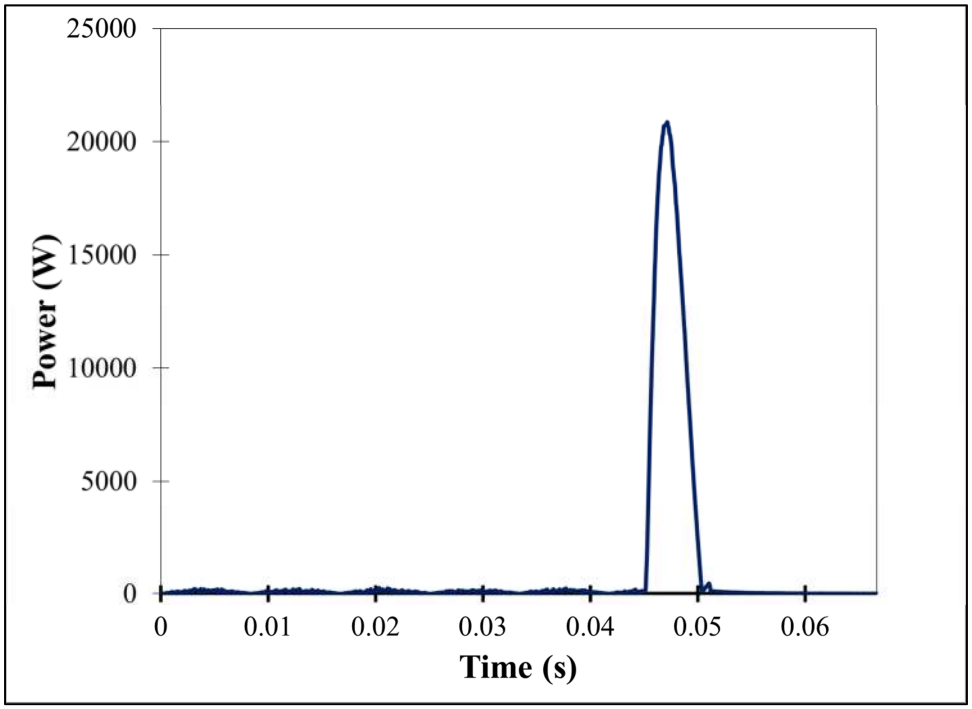

Figure 279 - Waveform of the instantaneous power produced in test 140-2. A total of 4 cycles (1/15 of a second) is shown.

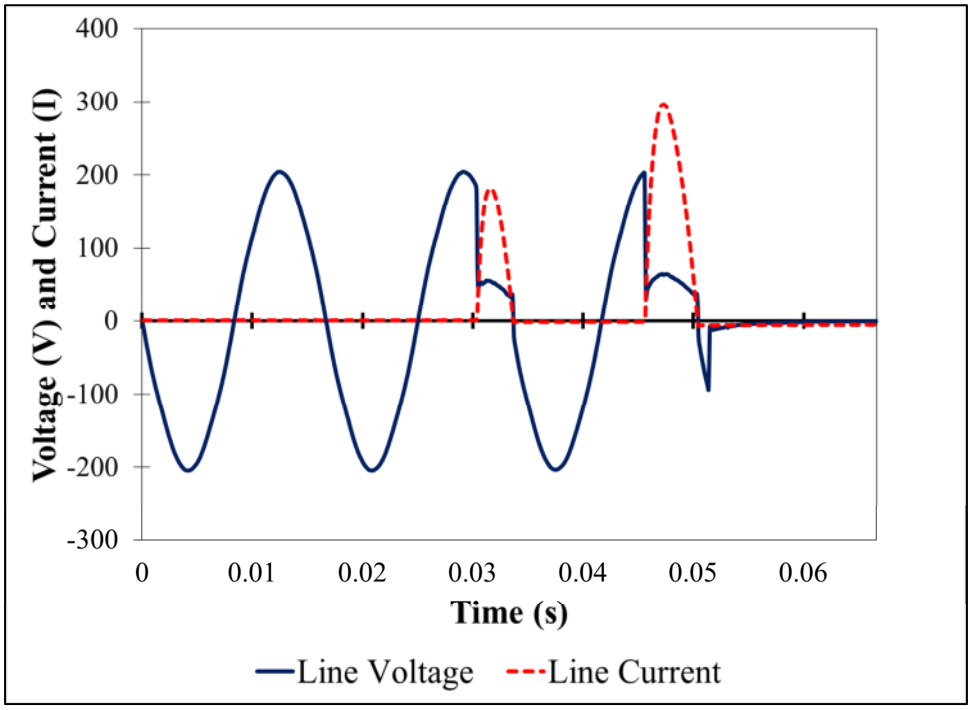

Figure 280 - Voltage and current waveforms produced in test 140-3. A total of 4 cycles (1/15 of a second) is shown.

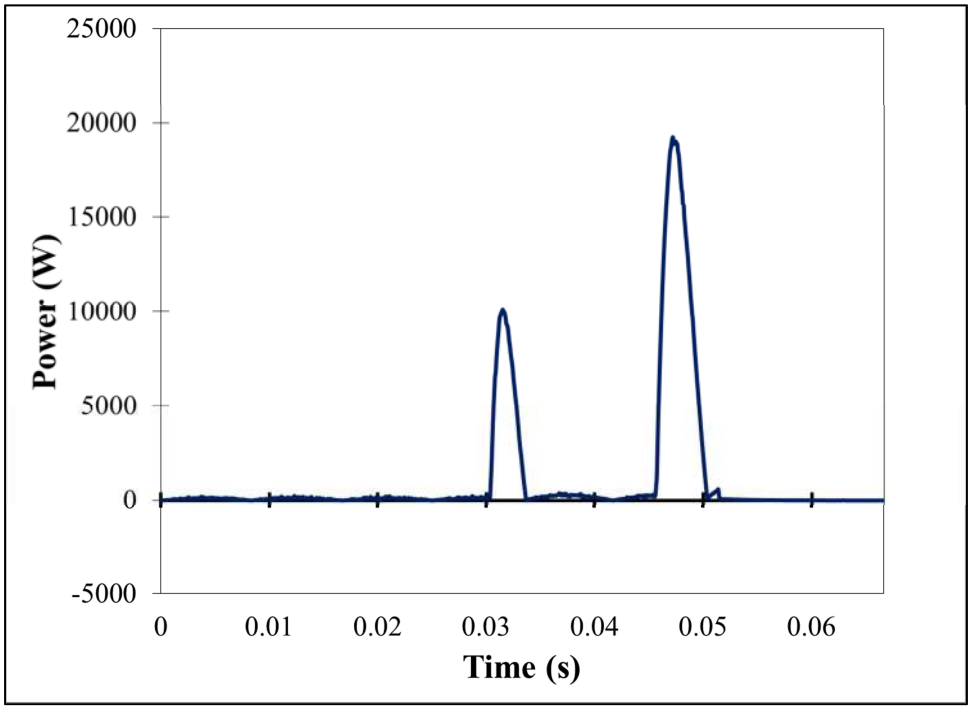

Figure 281 - Waveform of the instantaneous power produced in test 140-3. A total of 4 cycles (1/15 of a second) is shown.

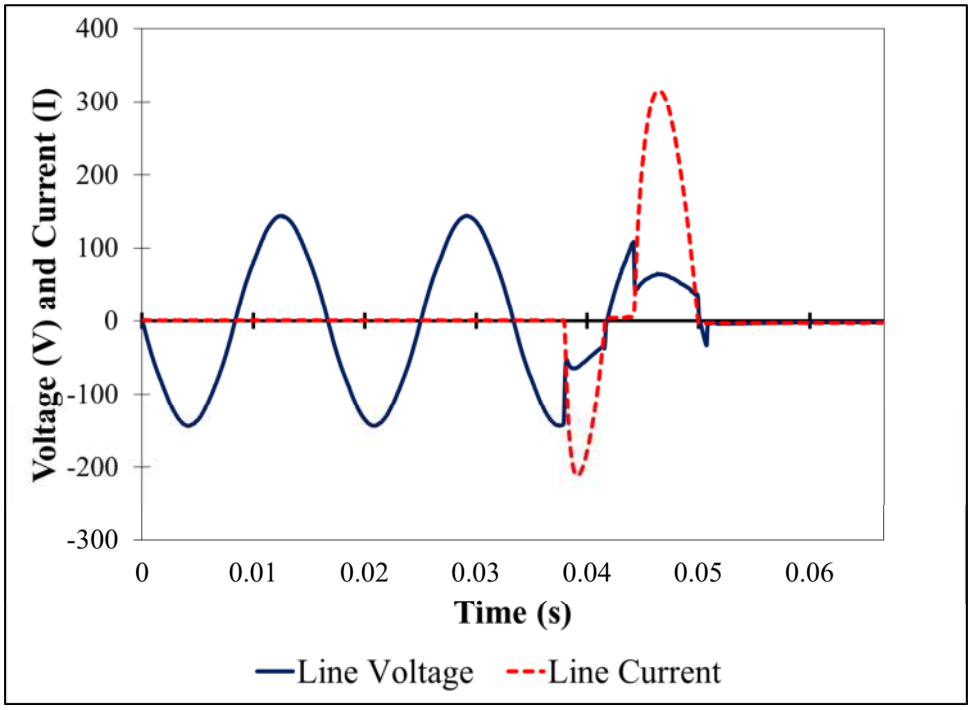

Figure 282 - Voltage and current waveforms produced in test 100-1. A total of 4 cycles (1/15 of a second) is shown.

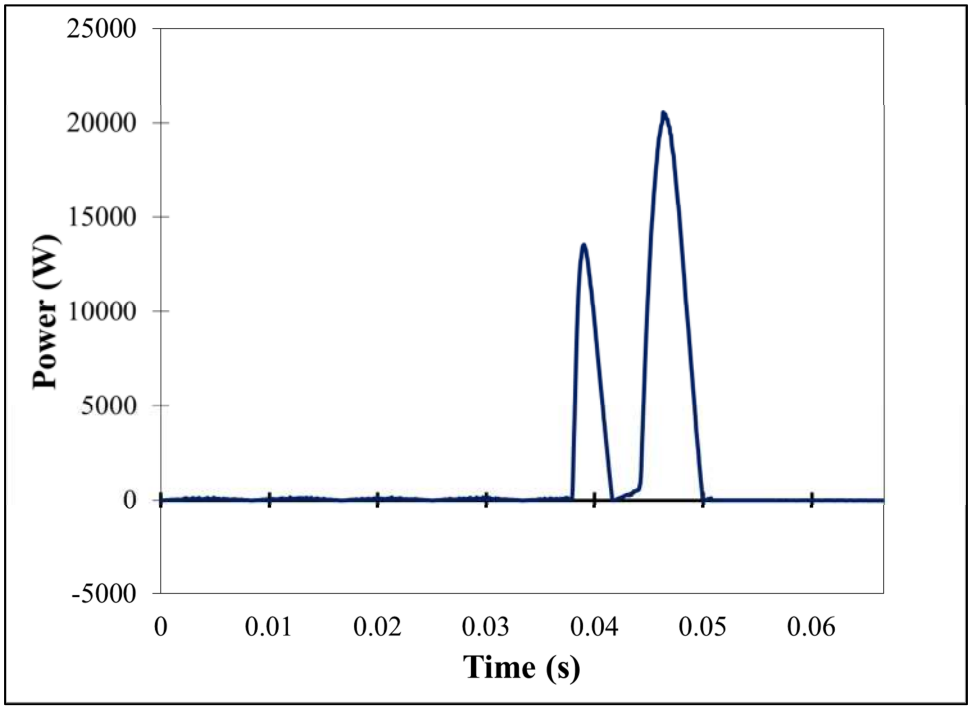

Figure 283 - Waveform of the instantaneous power produced in test 100-1. A total of 4 cycles (1/15 of a second) is shown.

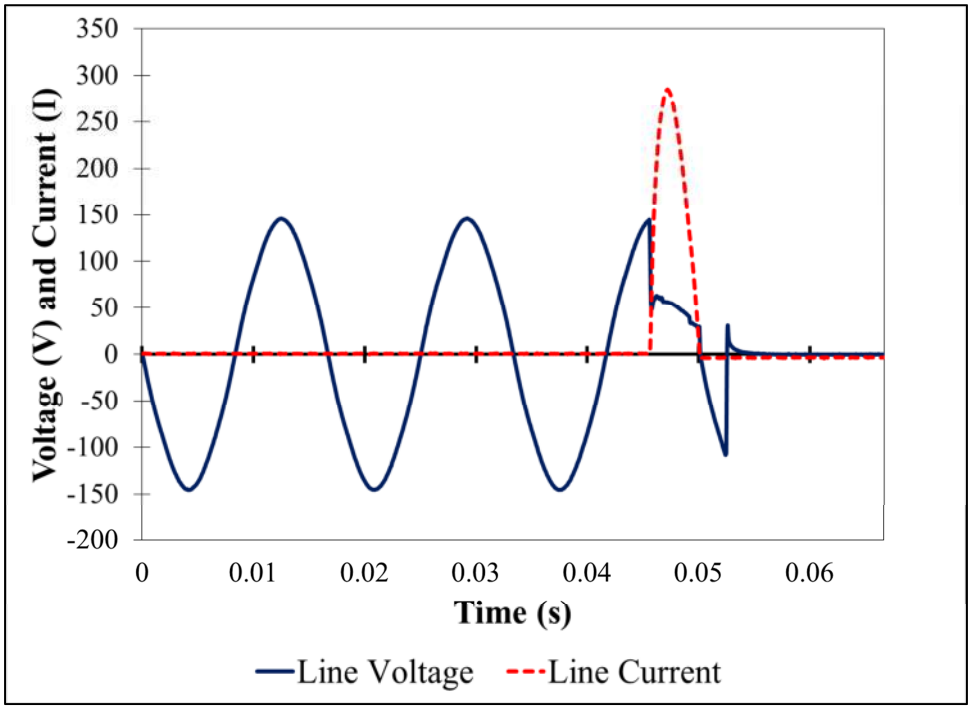

Figure 284 - Voltage and current waveforms produced in test 100-3. A total of 4 cycles (1/15 of a second) is shown.

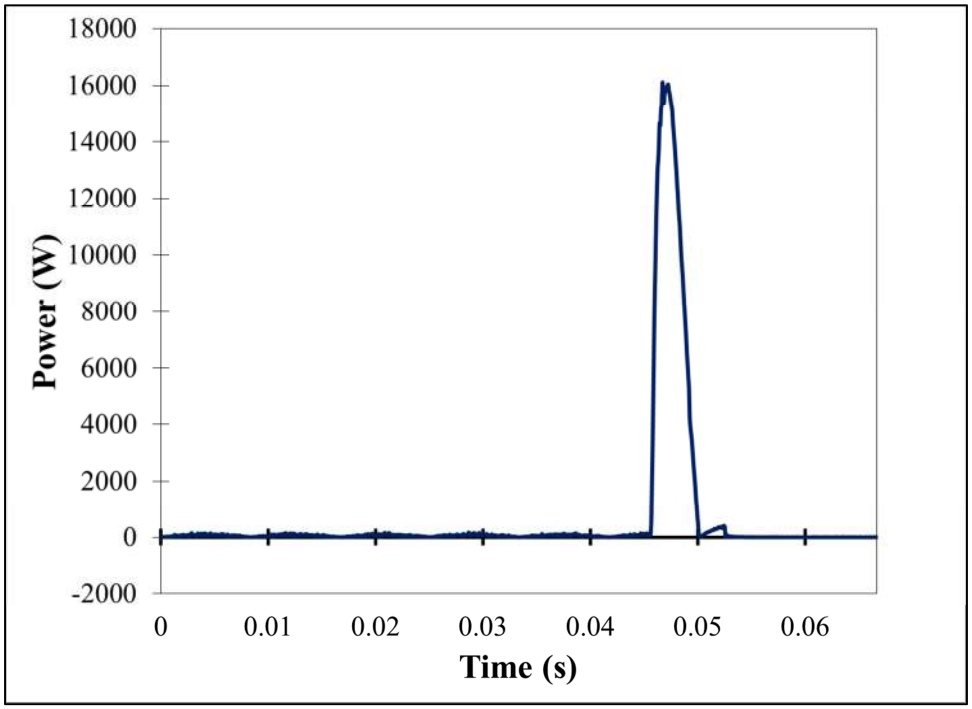

Figure 285 - Waveform of the instantaneous power produced in test 100-3. A total of 4 cycles (1/15 of a second) is shown.

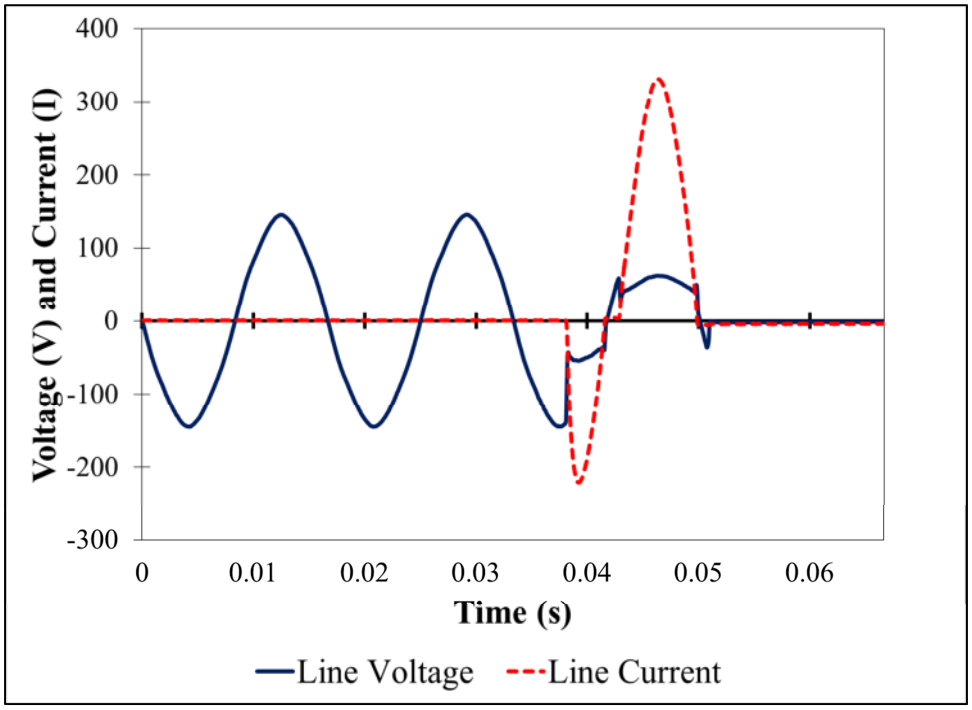

Figure 286 - Voltage and current waveforms produced in test 100-4. A total of 4 cycles (1/15 of a second) is shown.

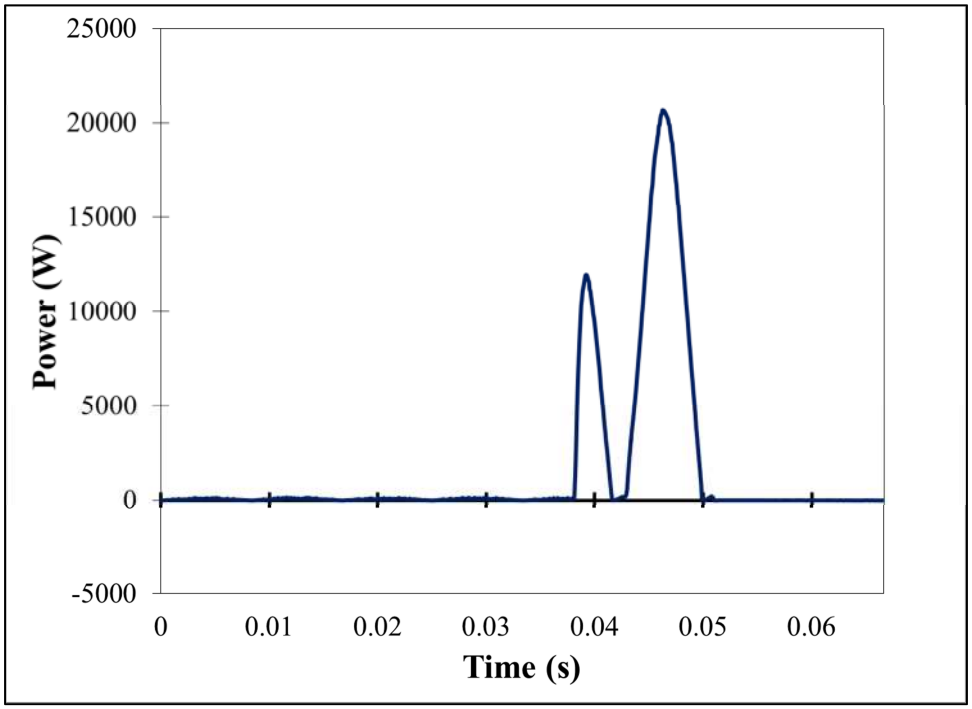

Figure 287 - Waveform of the instantaneous power produced in test 100-4. A total of 4 cycles (1/15 of a second) is shown.

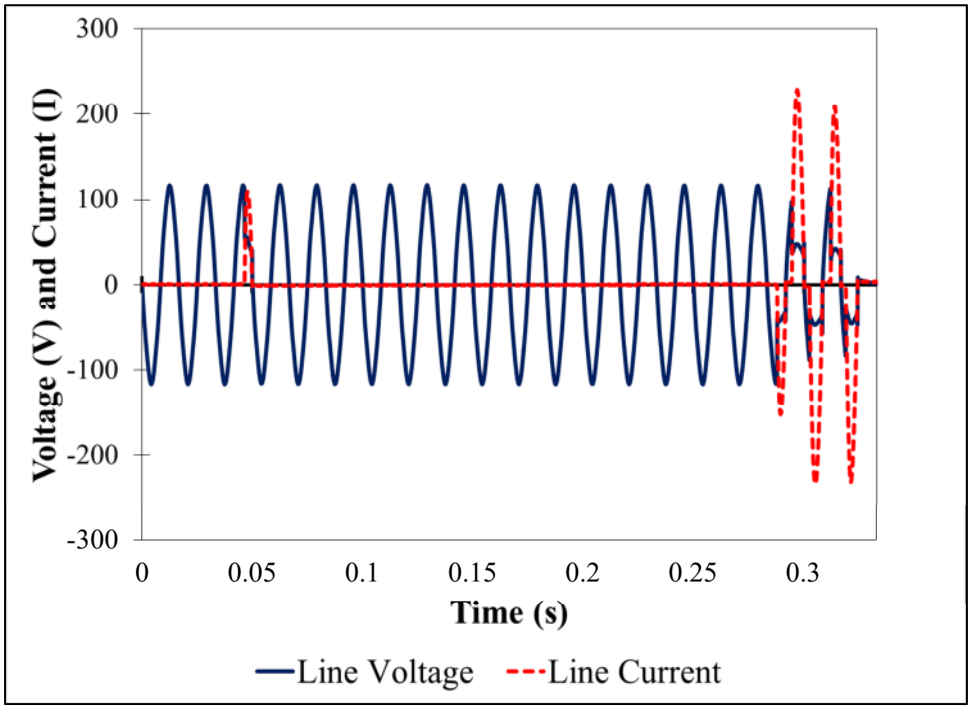

Figure 288 - Voltage and current waveforms produced in test 80-2. A total of 20 cycles (1/3 of a second) is shown.

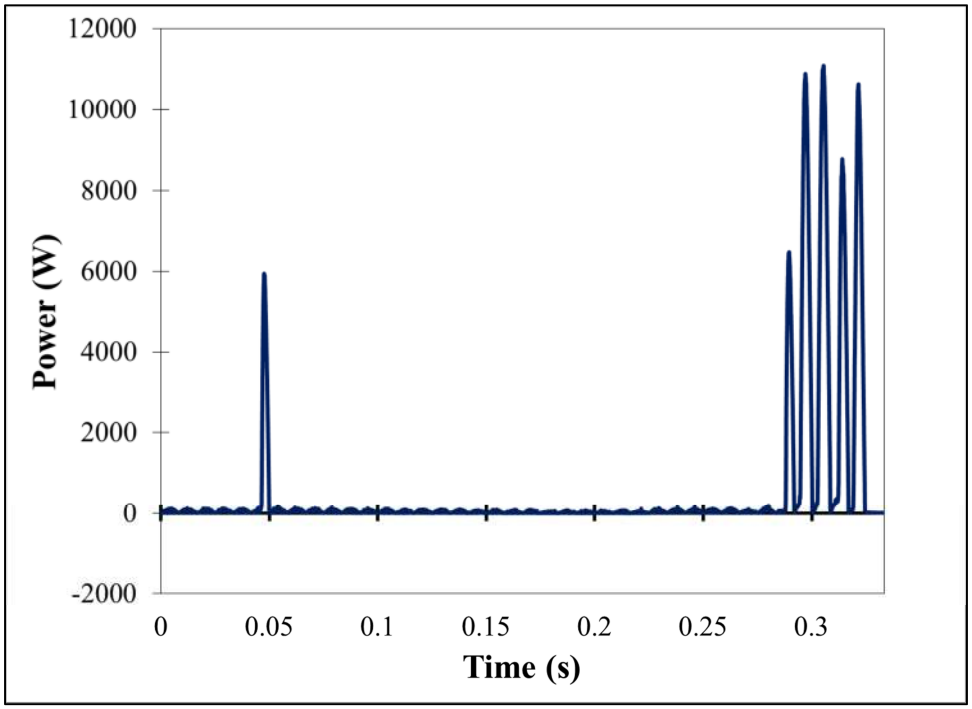

Figure 289 - Waveform of the instantaneous power produced in test 80-2. A total of 20 cycles (1/3 of a second) is shown.

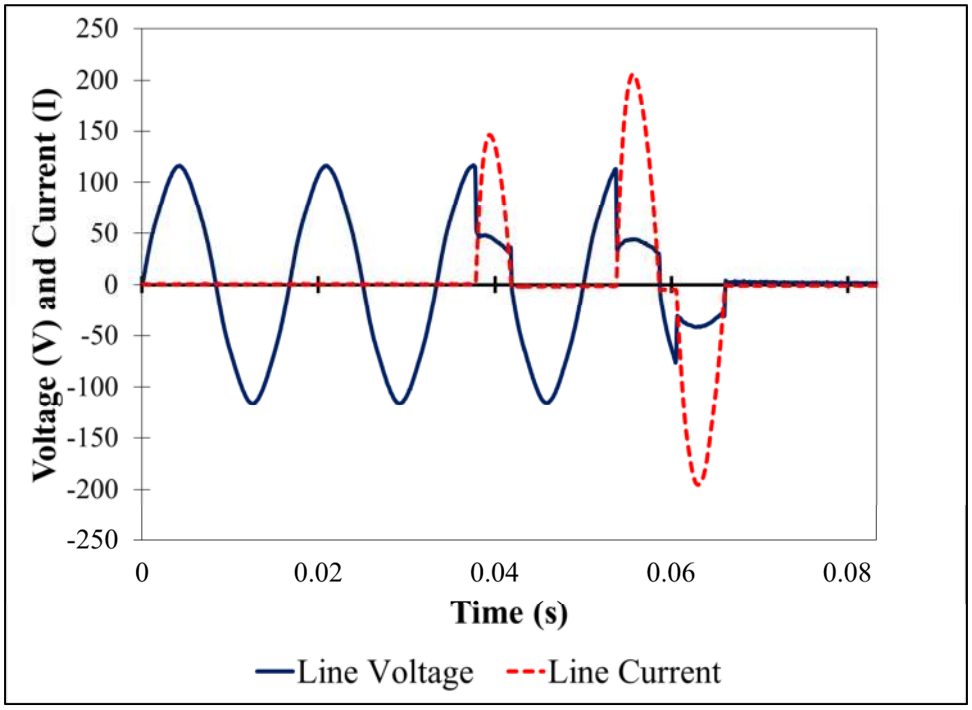

Figure 290 - Voltage and current waveforms produced in test 80-3. A total of 5 cycles (1/12 of a second) is shown.

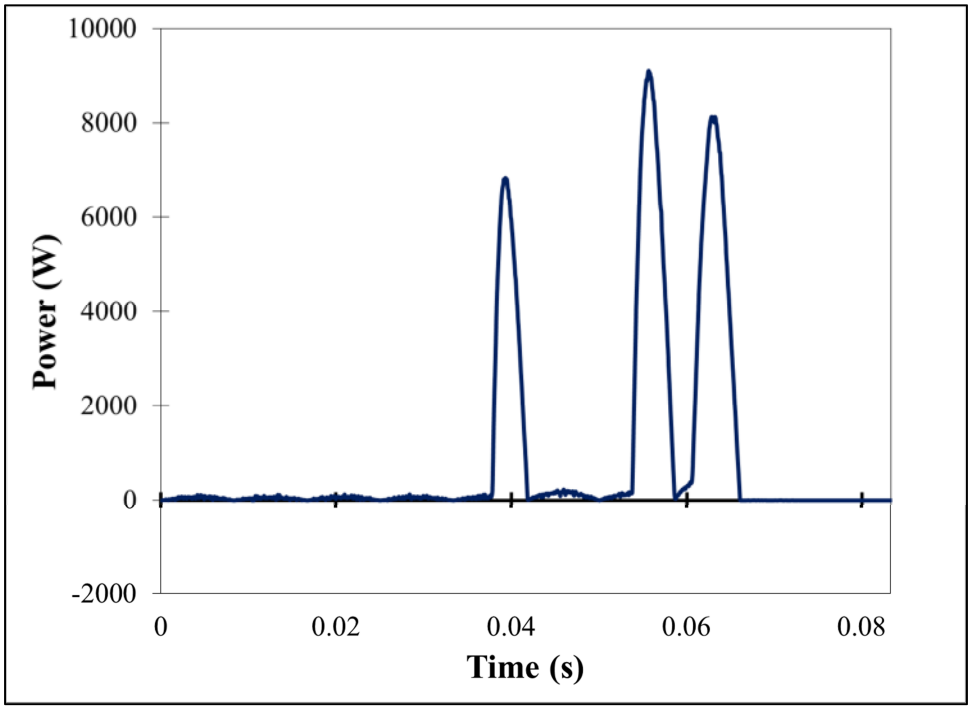

Figure 291 - Waveform of the instantaneous power produced in test 80-3. A total of 5 cycles (1/12 of a second) is shown.

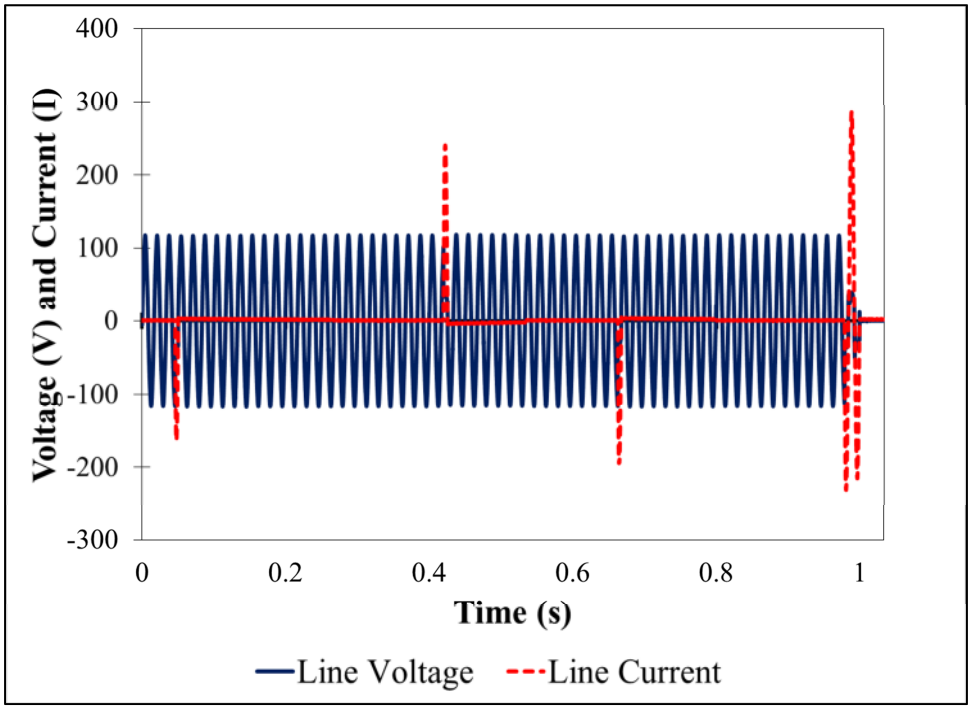

Figure 292 - Voltage and current waveforms produced in test 80-4. A total of 62 cycles (1.03 seconds) is shown.

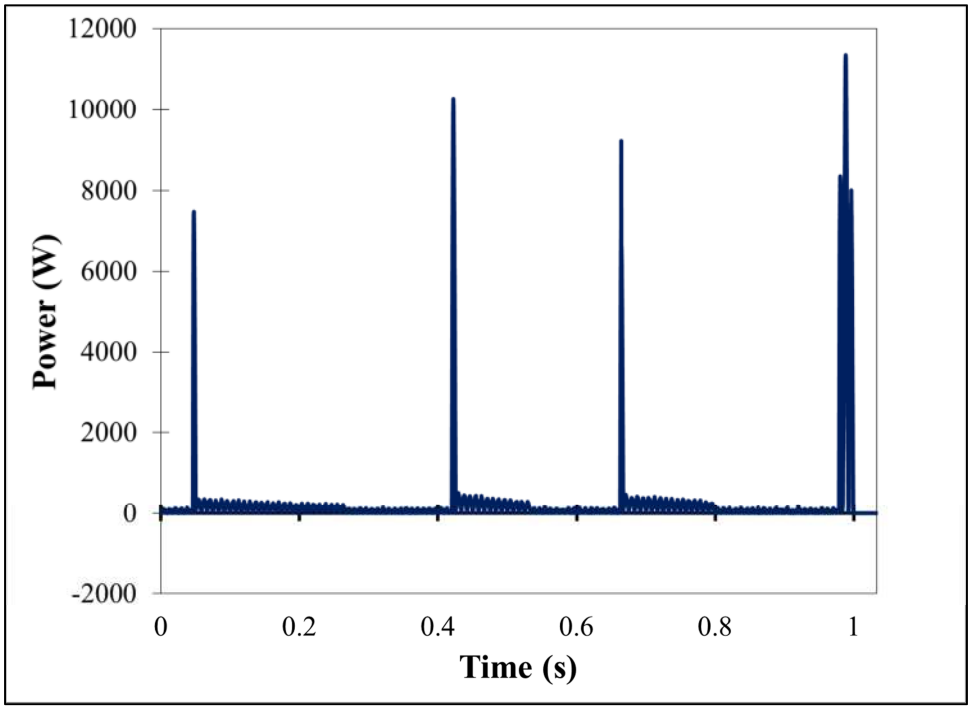

Figure 293 - Waveform of the instantaneous power produced in test 80-4. A total of 62 cycles (1.03 seconds) is shown.

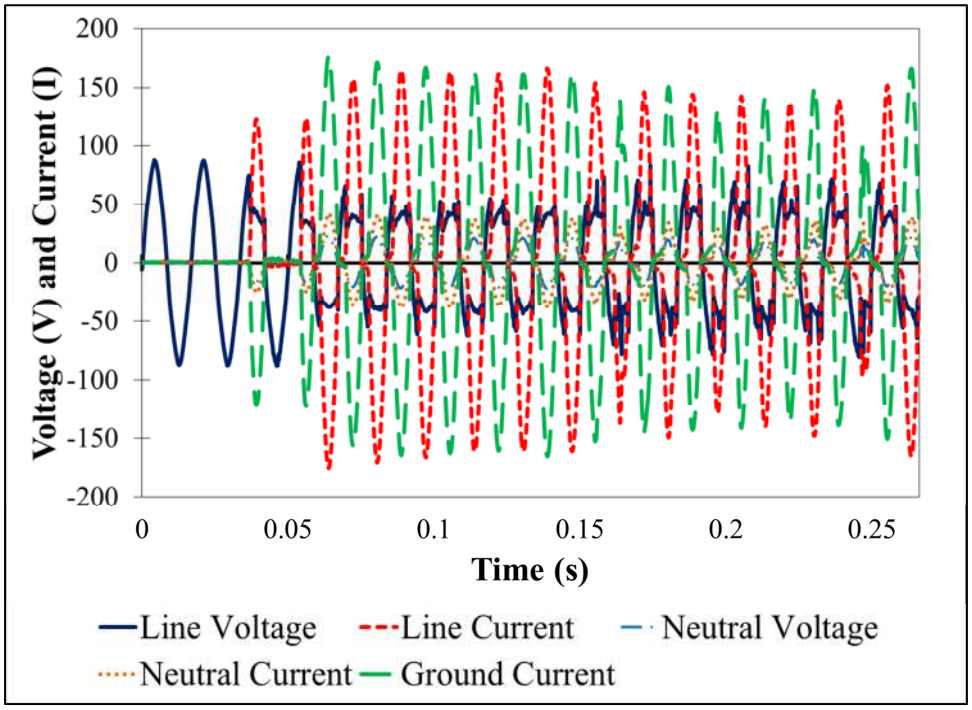

Figure 294 - Voltage and current waveforms produced in test 60-1. A total of 16 cycles (4/15 of a second) is shown.

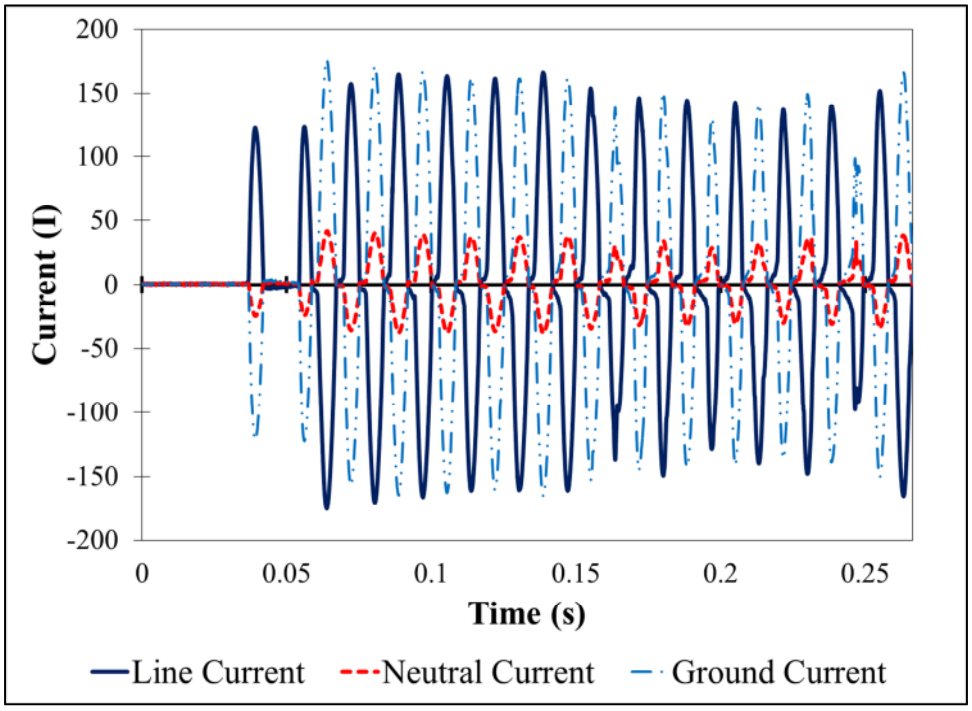

Figure 295 - Current waveforms produced in test 60-1. A total of 16 cycles (4/15 of a second) is shown.

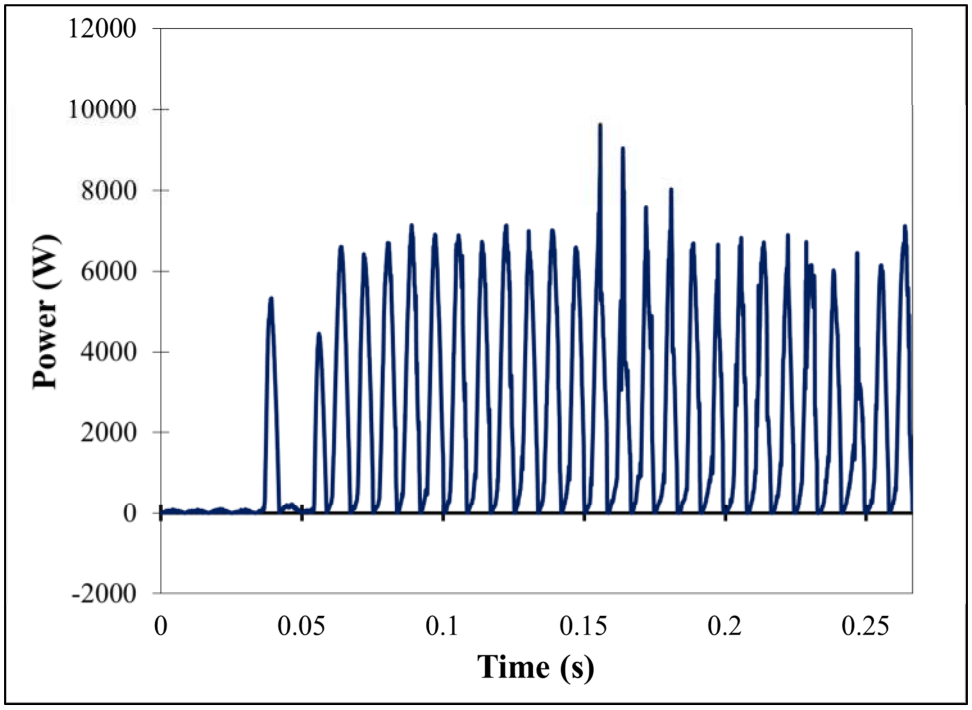

Figure 296 - Waveform of the instantaneous power produced in test 60-1. A total of 16 cycles (4/15 of a second) is shown.

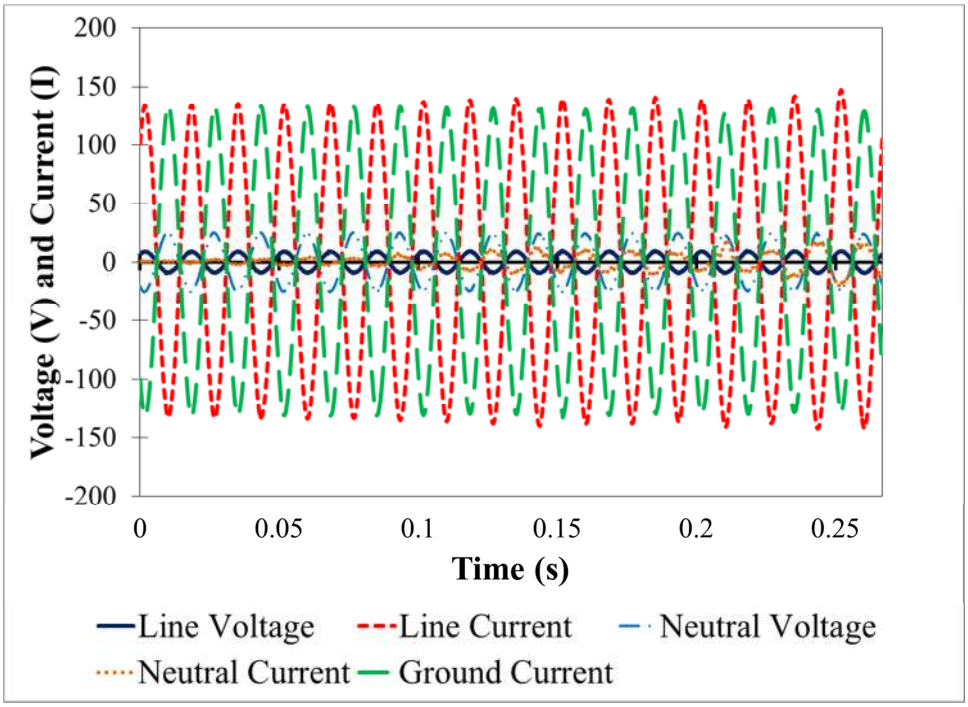

Figure 297 - Voltage and current waveforms produced in test 30-1. A total of 16 cycles (4/15 of a second) is shown.

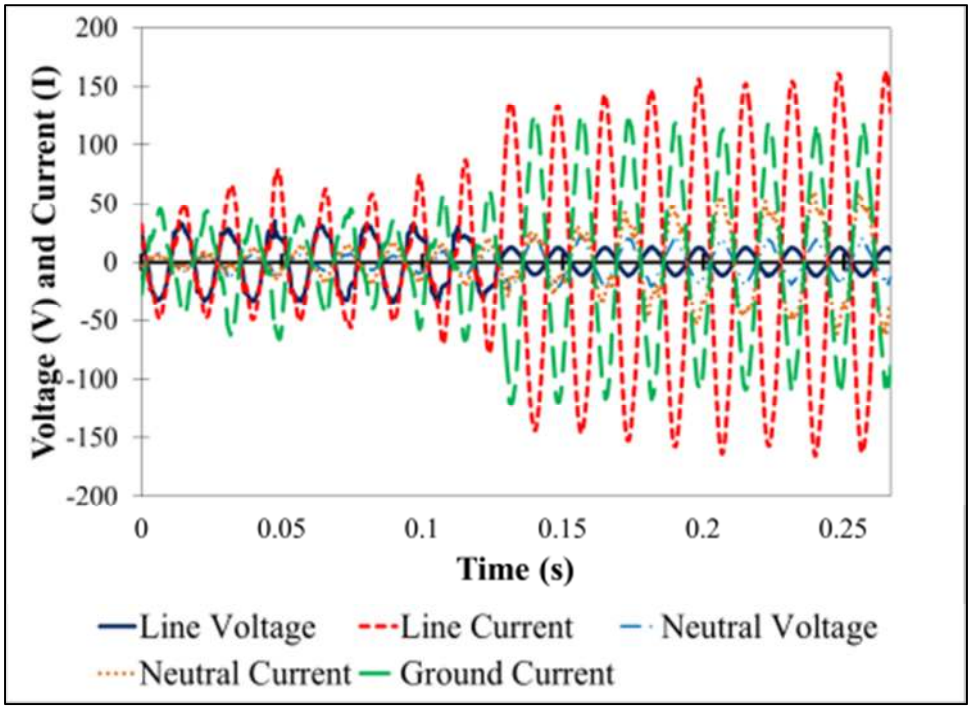

Figure 298 - Voltage and current waveforms produced in test 30-6. A total of 16 cycles (4/15 of a second) is shown.

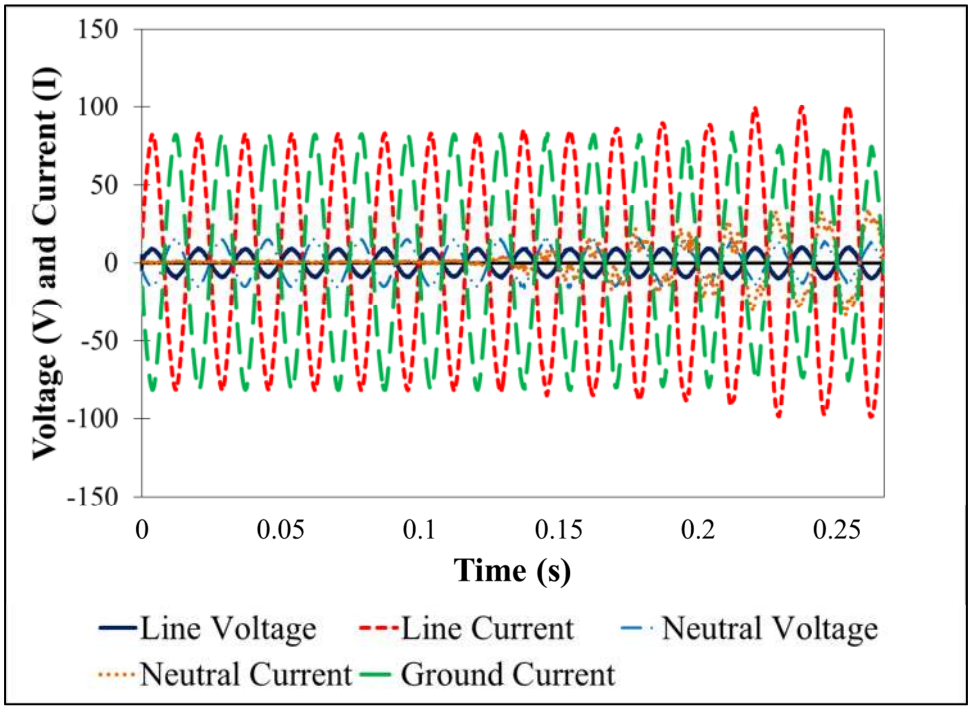

Figure 299 - Voltage and current waveforms produced in test 20-1. A total of 16 cycles (4/15 of a second) is shown.

7.9 Thermakin Code

7.9.1 Components File for Cone Calorimeter Simulations

```
OBJECT TYPE:  1D

OBJECT STRUCTURE
**********
THICKNESS:  .004
TEMPERATURE:  300
MASS FRACTIONS:
PVC  1

OBJECT BOUNDARIES
**********
TOP BOUNDARY
MASS TRANSPORT:  YES
PVC_g1  LIN  0.05  0
PVC_g2  LIN  0.05  0
OUTSIDE TEMP TIME PROG:  300  0
CONVECTION COEFF:  10
EXTERNAL RADIATION:  YES
TIME PROG1:  5.50e4  0  100000
TIME PROG2:  0   0   0
REPEAT:  NO
ABSORPTION MODE:  RAND
FLAME:  NO

BOTTOM BOUNDARY
MASS TRANSPORT:  NO
OUTSIDE TEMP TIME PROG:  300  0
CONVECTION COEFF:  10
EXTERNAL RADIATION:  YES
TIME PROG1:  4.10e2  0  100000
TIME PROG2:  0   0   0
REPEAT:  NO
ABSORPTION MODE:  RAND
FLAME:  NO

INTEGRATION PARAMETERS
**********
ELEMENT SIZE:  5e-5
TIME STEP:     0.005
DURATION:      3600
OUTPUT FREQUENCY:
ELEMENTS:    4
TIME STEPS:  200
```

7.9.2 Conditions File for Cone Calorimeter Simulations

```
COMPONENT:      PVC
STATE:          S
DENSITY:        1430  0  0  0
HEAT CAPACITY:  1550  0  0  0
CONDUCTIVITY:   0.17  0  0  0
TRANSPORT:      2e-5  0  0  0
EMISSIVITY & ABSORPTION:  0.9  1.5

COMPONENT:      PVC_in
STATE:          S
DENSITY:        629.2  0  0  0
HEAT CAPACITY:  1550  0  0  0
CONDUCTIVITY:   0.17  0  0  0
TRANSPORT:      2e-5  0  0  0
EMISSIVITY & ABSORPTION:  0.9  3.9

COMPONENT:      PVC_ch
STATE:          S
DENSITY:        295.724  0  0  0
HEAT CAPACITY:  1720  0  0  0
CONDUCTIVITY:   0  0  3.5e-10  3
TRANSPORT:      2e-5  0  0  0
EMISSIVITY & ABSORPTION:  0.85  100

COMPONENT:      PVC_g1
STATE:          G
DENSITY:        1430  0  0  0
HEAT CAPACITY:  840  0  0  0
CONDUCTIVITY:   0.17  0  0  0
TRANSPORT:      2e-5  0  0  0
EMISSIVITY & ABSORPTION:  0.9  1.5

COMPONENT:      PVC_g2
STATE:          G
DENSITY:        1430  0  0  0
HEAT CAPACITY:  1000  0  0  0
CONDUCTIVITY:   0.17  0  0  0
TRANSPORT:      2e-5  0  0  0
EMISSIVITY & ABSORPTION:  0.9  1.5

COMPONENT:      KAOWOOL
STATE:          S
DENSITY:        48  0  0  0
HEAT CAPACITY:  800  0  0  0
CONDUCTIVITY:   0.08  0  0  0
TRANSPORT:      1e-30  0  0  0
EMISSIVITY & ABSORPTION:  0  1000
```

```
MIXTURES
S SWELLING:          0
L SWELLING:          0
G SWELLING LIMIT:    1e-30
PARALL CONDUCTIVITY:  0.5
PARALL TRANSPORT:    0.5

REACTION:       PVC + NOCOMP -> PVC_in + PVC_g1
STOICHIOMETRY:  1     0        0.44     0.56
ARRHENIUS:      1.4e33  3.67e5
HEAT:           -1.7e5  0  0  0
TEMP LIMIT:     L  400

REACTION:       PVC_in + NOCOMP -> PVC_ch + PVC_g2
STOICHIOMETRY:  1       0        0.47     0.53
ARRHENIUS:      3.5e12  2.07e5
HEAT:           -1.23e6  0  0  0
TEMP LIMIT:     L  400
```

7.9.3 Conditions File for Fire Test Simulations

```
OBJECT TYPE:  1D

OBJECT STRUCTURE

***************

THICKNESS: .0095
TEMPERATURE: 300
MASS FRACTIONS:
GYPSUM  1

THICKNESS:  .004
TEMPERATURE:  300
MASS FRACTIONS:
OBJECT BOUNDARIES
***************

TOP BOUNDARY

MASS TRANSPORT:  YES
PVC_g1  LIN  0.05  0
PVC_g2  LIN  0.05  0

OUTSIDE TEMP TIME PROG:  300  0
CONVECTION COEFF:  0

EXTERNAL RADIATION:  YES
TIME PROG1:  1.50e5  0  100000
```

TIME PROG2: 0 0 0
REPEAT: NO
ABSORPTION MODE: RAND

FLAME: NO

BOTTOM BOUNDARY

MASS TRANSPORT: NO

OUTSIDE TEMP TIME PROG: 300 0
CONVECTION COEFF: 10

EXTERNAL RADIATION: YES
TIME PROG1: 4.10e2 0 100000
TIME PROG2: 0 0 0
REPEAT: NO
ABSORPTION MODE: RAND

FLAME: NO

INTEGRATION PARAMETERS
****

ELEMENT SIZE: 5e-5
TIME STEP: 0.005
DURATION: 3600

OUTPUT FREQUENCY:
ELEMENTS: 4
TIME STEPS: 200

7.9.4 Components File for Fire Test Simulations

COMPONENT: PVC
STATE: S
DENSITY: 1430 0 0 0
HEAT CAPACITY: 1550 0 0 0
CONDUCTIVITY: 0.17 0 0 0
TRANSPORT: 2e-5 0 0 0
EMISSIVITY & ABSORPTION: 0.9 1.5

COMPONENT: PVC_in
STATE: S
DENSITY: 629.2 0 0 0
HEAT CAPACITY: 1550 0 0 0
CONDUCTIVITY: 0.17 0 0 0
TRANSPORT: 2e-5 0 0 0
EMISSIVITY & ABSORPTION: 0.9 3.9

```
COMPONENT:      PVC_ch
STATE:          S
DENSITY:        295.724  0  0  0
HEAT CAPACITY:  1720  0  0  0
CONDUCTIVITY:   0  0  3.5e-10  3
TRANSPORT:      2e-5  0  0  0
EMISSIVITY & ABSORPTION:  0.85  100

COMPONENT:      PVC_g1
STATE:          G
DENSITY:        1430  0  0  0
HEAT CAPACITY:  840  0  0  0
CONDUCTIVITY:   0.17  0  0  0
TRANSPORT:      2e-5  0  0  0
EMISSIVITY & ABSORPTION:  0.9  1.5

COMPONENT:      PVC_g2
STATE:          G
DENSITY:        1430  0  0  0
HEAT CAPACITY:  1000  0  0  0
CONDUCTIVITY:   0.17  0  0  0
TRANSPORT:      2e-5  0  0  0
EMISSIVITY & ABSORPTION:  0.9  1.5

COMPONENT:      GYPSUM
STATE:          S
DENSITY:        1440  0  0  0
HEAT CAPACITY:  840  0  0  0
CONDUCTIVITY:   0.48  0  0  0
TRANSPORT:      2e-5  0  0  0
EMISSIVITY & ABSORPTION:  .9  1000

MIXTURES
S SWELLING:          0
L SWELLING:          0
G SWELLING LIMIT:    1e-30
PARALL CONDUCTIVITY:  0.5
PARALL TRANSPORT:    0.5

REACTION:       PVC + NOCOMP -> PVC_in + PVC_g1
STOICHIOMETRY:  1     0        0.44     0.56
ARRHENIUS:      1.4e33  3.67e5
HEAT:           -1.7e5  0  0  0
TEMP LIMIT:     L  400

REACTION:       PVC_in + NOCOMP -> PVC_ch + PVC_g2
STOICHIOMETRY:  1       0        0.47     0.53
ARRHENIUS:      3.5e12  2.07e5
HEAT:           -1.23e6  0  0  0
TEMP LIMIT:     L  400
```

7.10 PVC Properties [56]

Decomposition mechanism: R1: Polymer → Char1 + Gas1; R2: Char1 → Char2 + Gas2

Property	Value±2σ	Method
Polymer Density (kg m^{-3})	1430±70	Volume and mass measurement
Polymer Heat Capacity (J kg^{-1} K)	1550±250	Differential scanning calorimetry
Polymer Thermal Conductivity (W m^{-1} K^{-1})	0.17±0.01	Literature review
Polymer Surface Reflectivity	0.10±0.05	Integrating sphere reflectometry
Polymer Absorption Coefficient (m^2 kg^{-1})	1.5±0.5	Analysis of transmission spectra
Char1 Density (kg m^{-3})	629	From assumed constant volume
Char1 Heat Capacity (J kg^{-1} K)	1550	Assumed the same as for Polymer
Char1 Thermal Conductivity (W m^{-1} K^{-1})	0.17	Assumed the same as for Polymer
Char1 Surface Reflectivity	0.10	Assumed the same as for Polymer
Char1 Absorption Coefficient (m^2 kg^{-1})	3.9	Fit to cone calorimetry data
Char2 Density (kg m^{-3})	296	From assumed constant volume
Char2 Heat Capacity (J kg^{-1} K)	1720±170	Pulsed current heating
Char2 Thermal Conductivity (W m^{-1} K^{-1})	0.26	Fit to cone calorimetry data
Char2 Surface Reflectivity	0.15±0.05	Pulsed current heating
Char2 Absorption Coefficient (m^2 kg^{-1})	100	Assumed opaque
R1 Decomp. Pre-exponential Factor (s^{-1})	$(1.4\pm0.8)\times10^{33}$	Thermogravimetric analysis
R1 Decomp. Activation Energy (J mol^{-1})	$(3.67\pm0.07)\times10^{5}$	Thermogravimetric analysis
R1 Decomp. Char Yield (mass fraction)	0.44±0.01	Thermogravimetric analysis
R1 Heat of Decomp. (J kg^{-1})	$-(1.7\pm1.7)\times10^{5}$	Differential scanning calorimetry
Gas1 Heat of Combustion (J kg^{-1})	$(2.7\pm0.3)\times10^{6}$	Microscale combustion calorimetry
Gas1Combustion Efficiency	0.75±0.03	Cone calorimetry
R2 Decomp. Pre-exponential Factor (s^{-1})	$(3.5\pm2.1)\times10^{12}$	Thermogravimetric analysis
R2 Decomp. Activation Energy (J mol^{-1})	$(2.07\pm0.04)\times10^{5}$	Thermogravimetric analysis
R2 Decomp. Char Yield (mass fraction)	0.47±0.01	Thermogravimetric analysis
R2 Heat of Decomp. (J kg^{-1})	$-(1.2\pm0.9)\times10^{6}$	Differential scanning calorimetry
Gas2 Heat of Combustion (J kg^{-1})	$(3.65\pm0.18)\times10^{7}$	Microscale combustion calorimetry
Gas2 Combustion Efficiency	0.75±0.03	Cone calorimetry

Works Cited

[1] United States Fire Administration, "Residential Building Electrical Fires," U.S. Department of Homeland Security - U.S. Fire Administration, Emmitsburg, 2008.

[2] V. Babrauskas, "Electrical Fires: Research Needed to Improve Safety," *Fire Protection Engineering,* pp. 20-30, 2010.

[3] L. Smith and D. McCoskrie, "What Causes Wiring Fires in Residences?," *Fire Journal,* vol. 84, no. 1, pp. 18-24, 69, 1990.

[4] J. J. Shea, "Conditions for Series Arcing Phenomena in PVC Wiring," IEEE Xplore, 2005.

[5] B. Ettling, "Electrical Wiring in Building Fires," *Fire Technology,* vol. 14, no. 4, pp. 317-325, 1978.

[6] J. J. Shea, "Identifying Causes for Certain Types of Electrically Initiated Fires in Residential Circuits," in *Fire and Materials*, 2010.

[7] Consumer Product Safety Commission, "Residential Electrical Distribution System Fires," U.S. Consumer Product Safety Commission, Washington, D.C., 1988.

[8] J. Prusaczyk and R. Boardway, "The Effect of Thermal Insulation on the Fire Hazards of Electrical Wiring," *Fire Technology,* vol. 18, no. 2, pp. 162-173, 1982.

[9] S. Davis, J. Wise, D. Engel and V. Somandepalli, "Crimp Connector Failures: Quantifying Copper Oxide Layer Growth," in *International Symposium on Fire Investigation Science and Technology*, Sarasota, 2008.

[10] V. Somandepalli, J. Wise, B. Arena and S. Davis, "Crimp Connector Failures: Quantifying the Cause of Resistive Heating," in *International Symposium on Fire Investigation Science and Technology*, Sarasota, 2010.

[11] J. Sletbak, R. Kristensen, H. Sundklakk, G. Navik and M. Runde, "Glowing Contact Areas in Loose Copper Wire Connections," IEEE Transactions on Components, Hybrids, and Manufacturing Technology, 1992.

[12] J. J. Shea, "Glowing Contact Physics," in *IEEE Holm Conference On Electrical Contacts*, Montreal, 2006.

[13] J. Ferrino-McAllister, R. Roby and J. Milke, "Heating at Electrical Contacts: Characterizing the Effects of Torque, Contact Area, and movement on the Temperature of Residential Receptacles," *Fire Technology,* vol. 42, no. 1, pp. 49-74, 2006.

[14] M. Mitolo, "Short-Circuit Calculation Methods," Electrical Construction and Maintenence, 1 October 2004. [Online]. Available: http://ecmweb.com/mag/electric_shortcircuit_calculation_methods/index.html. [Accessed 30 October 2011].

[15] V. Babrauskas, "Mechanisms and modes for Ignition of Low-Voltage PVC Wires, Cables, and Cords," in *Fire & Materials 2005*, London, 2005.

[16] V. Babrauskas, "Electrical Fires," in *SFPE Handbook of Fire Protection Engineering*, Quincy, National Fire Protection Association, 2008, pp. 479 - 498.

[17] National Fire Protection Association, NFPA 921: Guide for Fire and Explosion Investigations, Quincy: National Fire Protection Association, 2011.

[18] E. Greenwald, Electrical Hazards and Accidents: Their Cause and Prevention, Wiley-Interscience, 1991.

[19] V. Babrauskas, Ignition Handbook: Principles and Applications to Fire Safety Engineering, Fire Investigation, Risk Management and Forensic Science, Issaquah: Fire Science Publishers, 2003.

[20] F. L. Fire, Combustibility of Plastics, New York: Van Nostrand Reinhold, 1991.

[21] V. Babrauskas, "Research on Electrical Fires: The State of the Art," in *International Symposium for Fire Safety Science*, 2009.

[22] V. Babrauskas, "How Do Electrical Wiring Faults Lead to Structure Ignitions," in *Fire and Materials*, London, 2001.

[23] V. Babrauskas, "Fires Due to Electric Arcing: Can 'Cause' Beads Be Distinguished from 'Victim' Beads by Physical or Chemical Testing?," in *Fire and Materials*, London, 2003.

[24] H. Otani and K. Kawamura, "An Experimental Study on Thermal Deterioration of Electric Insulation of a PVC Attachment Plug," *Japan Society for Safety Engineering,* vol. 42, no. 4, pp. 216-221, 2003.

[25] A. Kemal, D. Mattison, S. Murray and M. Loose, "Degradation and Ignition of Polyvinyl Chloried Wire Insulation," in *Fire and Materials*, London, 2007.

[26] M. Benes, N. Milanov, G. K. A. Matuschek and V. B. V. Placek, "Thermal Degradation of PVC Cable Insulation Studied by Simultaneous TG-FTIR and TG-EGA Methods," *Thermal Analysis and Calorimetry,* vol. 78, pp. 621-630, 2004.

[27] R. Armstrong, J. Mason and A. Kumar, "Thermally Induced Failure of Low-Voltage Electrical Nonmentallic-Sheated Cable Insulation," *Fire Technology,* vol. 35, no. 3, 1999.

[28] B. Beland, "Examination of Electrical Conductors Following a Fire," *Fire Technology,* vol. 16, no. 4, pp. 252-258, 1980.

[29] B. Beland, "Arcing Phenomenon as Related to Fire Investigation," *Fire Technology,* vol. 17, no. 3, pp. 189-201, 1981.

[30] B. Beland, "Considerations on Arcing as a Fire Cause," *Fire Technology,* vol. 18, no. 2, pp. 188-202, 1982.

[31] B. Beland, "Heating of Damaged Conductors," *Fire Technology,* vol. 18, no. 3, pp. 229-236, 1982.

[32] C. E. Wilkes, J. W. Summers, A. D. Daniels and M. T. Berard, PVC Handbook, Munich: Hanswer, 2005.

[33] D. Dini, "Residential Electrical System Aging Research Project," The Fire Protection Reseach Foundatioin, Quincy, 2008.

[34] J. Hoffmann, D. Hoffmann, E. Kroll and M. Kroll, "Electrical Power Cord Damage from Radiant Heat and Fire Exposure," *Fire Technology,* vol. 37, no. 2, pp. 129-141, 2001.

[35] L. Dissado and J. Fothergill, Electrical Degradation and Breakdown in Polymers, 1992.

[36] T. Karayildirim, J. Yanik, M. S. M. Yuksel and C. B. H. Vasile, "The Effect of Some Fillers on PVC Degradation," *Journal of Analytical and Applied Pyrolysis,* vol. 75, no. 2, pp. 112-119, 2006.

[37] Y. Hagimoto and N. O. K. Watanabe, "Short Circuit Faults in Electrical Cables Exposed to Radiant Heat," in *Fire and Materials*, London, 2003.

[38] J. L. Ferrino-McAllister, "An Investigation of Fire Phenomena in Residential Electrical Wiring and Connections," University of Maryland, College Park, College Park, 2002.

[39] T. Osswald, International Plastics Handbook, Munich: Hanswer, 2006.

[40] R. Grossmann, Handbook of Vinyl Formulating, Hoboken: Wiley-Interscience, 2008.

[41] C. Harper, Handbook of Plastics, Elastomers, and Composites, New York: McGraw-Hill, 2002.

[42] W. Johnson and L. Rich, "Arc Fault Analysis: Post Flashover Studies of the Power Cord".

[43] D. Churchward, R. Cox and D. Reiter, "Arc Surveys as a Means to Determine Fire Origin in Residential Structurs".

[44] National Fire Protection Agency, "NFPA 70: National Electrical Code," Quincy, MA, National Fire Protection Agency, 2011.

[45] M. Goodson, T. Perryman and K. Colwell, "Effects of Polyurethane Foam Systems on Wiring Ampacity".*Fire and Arson Investigator*.

[46] R. Powell and F. Schofield, "The Thermal and Electrical Conductivities of Carbon and Graphite to High Temperatures," *Proceedings of the Physical Society,* 1938.

[47] J. Reynolds, H. Hemstreet and T. Leinhardt, "The Electrical Resistance of Graphite at Low Temperatures," *Physical Review,* vol. 91, no. 5, pp. 1152-1155, 1953.

[48] "HDRsoft - Photomatix," Photomatix, [Online]. Available: www.hdrsoft.com. [Accessed 31 October 2011].

[49] V. Babrauskas, W. Twilley, M. Jannssens and S. Yusa, "A Cone Calorimeter for Controlled-Atmosphere Studies," in *Fire and Materials*, 1992.

[50] M. Janssens and C. Gomez, "Enclosure Effects on Burning Behavior in the Cone Calorimeter," in *21st Annual Conference on Recent Advances on Flame Retardancy of Polymeric Materials*, 2010.

[51] F. T. T. Limited, *Users' Guide for the Low Oxygen Cone Calorimeter Attachment,* West Sussex: Fire Testing Technology Limited, 2006.

[52] M. Keller, J. Ouellette and J. Rowe, Ammendale: Bureau of Alcohol, Tobacco, Firearms, and Explosives, 2009.

[53] ASTM International, *ASTM D149 - 09 Standard Test Method for Dielectric Breakdown Voltage and Dielectric Strength of Solid Electrical Insulating Materials at Commercial Power Frequencies,* West Conshohocken: ASTM International, 2009.

[54] S. I. Stoliarov and R. E. Lyon, "Technical Note: Thermo-Kinetic Model of Burning," U.S. Department of Transportation - Federal Aviation Administration, Springfield, 2008.

[55] S. Stoliarov, S. Crowley, R. Walters and R. Lyon, "Prediction of the Burning Rates of Charring Polymers," *Combustion and Flame,* vol. 157, no. 11, pp. 2024-2034, 2010.

[56] S. Stoliarov, *Poly(vinyl chloride) (trade name: Versadur 150),* 7/27/2011.

[57] B. Karlsson and J. Quintiere, Enclosure Fire Dynamics, Boca Raton: CRC Press, 2000.

[58] N. J. Carey, "Developing a Reliable Systematic Analysis for Arc Fault Mapping," University of Strathclyde - Department of Pure and Applied Chemistry: Centre for Forensic Science, 2009.

[59] W. Rieder and A. Neuhaus, "Short Arc modes Determining both Contact Welding and Material Transfer," *IEEE Transactions on Components and Packaging Technologies,* no. 30, pp. 9-14, 2007.

[60] Z. Chen and K. Sawa, "Effect of Arc Behavior on Material Transfer: A Review," *IEEE Transactions on Components, Packaging, and Manufacturing Technology,* no. 21, pp. 310-322, 1998.

[61] G. Slenski and D. Galler, "Wires and Cables," in *Electronic Failure Analysis Handbook*, New York, McGraw-Hill, 1999.